Enclosure (1)

Responses to Request for Additional Information
Model No. WE-1 Package
Docket No. 71-9289

1.0 GENERAL INFORMATION

General:

The WE-1 Shipping Container is a descendent of container 51032-1 (Docket 71-6581) and 51032-2 (Docket 71-9252). The major components and dimensions of the WE-1 container are the same as those of containers 51032-1 and 51032-2.

Information requested for the previously certified package is omitted here unless the design has changed to accommodate the Pathfinder Canister. All the requested data for the 'Pathfinder Canister amendment' is provided

1-1 *Revise drawings to include a description of the proposed package in sufficient detail to identify the package accurately and provide a sufficient basis for evaluation of the package. The information must include specific materials of construction, weights, dimensions, design codes and standards proposed for use in package design, fabrication, assembly, testing, maintenance and use, bill of materials, etc. For example:*

Drawing No. 1273964, Rev. 0

- *Dimensions of the skid.*

Response:

Dimension of skid: The WE-1 Shipping Container is a descendent of container 51032-1 (Docket 71-6581) and 51032-2 (Docket 71-9252). The dimensions of the skid are the same as those of 51032-1 and 51032-2. There will be only one package per shipment. The skid dimension has not changed from the certified WE-1.

Drawing No. 1273965, Rev.1

- *Material specification for Aluminum.*
- *Material specification for wood wedge filler blocks.*
- *Details of the Base Assembly supporting the Strongback.*

Response:

These hardware items are the same as that of the previously certified container.

Drawing No. 1273966, Rev. 0

- *Dimensions of the skid.*

Response:

This drawing provides the metal gauges and weld specification. The skid is 7 GA steel, and is specified on the drawing.

Drawing No. 1273968, Rev. 0

- *Specification for the Shock Mount assembly.*

Response:

The WE-1 shipping container is a descendent of shipping containers 51032-1 (Docket 71-6581) and 51032-2 (Docket 71-9252) with the same shock mount. This hardware is the same as the previously certified container. The shock mounts have not changed from the certified WE-1.

Drawing No. 5016270, Rev. 0

- *Details of the O-rings, material specifications, and manufacturer, including the O-rings grooves dimensions and locations.*
- *Canister closure bolts size and materials.*
- *Grades and Crushing strengths of the Pine Spacer and Oak Spacer wood materials.*
- *Size of the weld between the spacer tube and the spacer tube end plate.*
- *Details of the positioning clamp blocks and Rubber Material Specification.*
- *Weights of various components.*
- *Size of the weld between the Flat Cap and Pathfinder Canister.*
- *Clamp locations.*
- *Weight and Center of gravity of the WE-1 package with the Pathfinder Fuel Canister.*
- *Material specifications for the "Fill Material" at the top end of the canister.*
- *Parts List or other appropriate list to identify materials of construction, and quantity required for each design feature, component, or part, as applicable.*
- *Details of the test port.*
- *Torque requirements for closure bolts for the lids.*

- *Manufacturer's name/specification of the insulating material(s) for the package.*
- *Details of the containment system, closure and seal regions, including notes, material parts lists, specifications, and codes or standards for fabrication:*
  - *Flange design (weld neck flange, blind flange)*
  - *Lid*
  - *Closure bolts*
  - *Seals, include type, dimension, and materials*
  - *Seal grooves*
  - *Seal test port and plug*

Response:

The following was added to Drawing No. 5016270

- Wood spacer material specification. Wood crushing strength is discussed in responses to RAI 2-4 and 2-5.
- Weld size for the weld between the spacer tube and the end plates.
- Support spacer (clamp block) detail. The rubber material is commercial Nitrile Duro 60.
- Clamp location dimensions.
- Weight and center of gravity of the WE-1 package with the Pathfinder Canister.
- Wood as a fill material.
- Insulating material manufacture and specification number.
- Quantity of each design feature.

All other requested information is provided in a new drawing No. 5021426

The following is included in the new drawing, Drawing No. 5021426

- Parts list for the Pathfinder Canister to identify materials of construction and quantity required.
- A detail of O-rings, grooves and dimensions.
- Canister closure bolt size, materials and bolt torque (Note 7).
- Weight of the Pathfinder Canister.
- Welds of the Pathfinder Canister (full penetration weld).
- Details of the containment system, closure and seal regions to identify the seal type, material, groove dimension and details of the seal test port and plug.
- Weld neck and blind flange design specification.
- Fabrication, examination codes and standards.

For applicable drawings:

- *Codes, standards, or other similar specification documents for fabrication, examination, assembly, and testing*

For all drawings:

- *Parts list or other appropriate list to identify materials of construction, and quantity required for each design feature, component, or part, as applicable.*

This information is required to comply with 10 CFR 71.31(c), and 10 CFR 71.33 requirements. NUREG/CR-5502 may be used as a guide for compliance to the 10 CFR 71.31(c) and 10 CFR 71.33 requirements.

Response:

The WE-1 Shipping Container is a descendent of container 51032-1 (Docket 71-6581) and 51032-2 (Docket 71-9252). Container 51032-1 has been in use since 1990 and container 51032-2 has been in use since 1994. The major components and dimensions of the WE-1 container are the same as those of 51032-1 and 51032-2 containers.

Information requested for the previously certified package is omitted here unless the design has changed to accommodate the Pathfinder Canister. All the requested data for the 'Pathfinder Canister amendment' is provided

1-2 *Provide a design drawing of the Pathfinder fuel assembly.*

The drawing should identify (at a minimum) the relevant dimensions and materials that were used in the criticality analysis.

Response:

We have added Appendix 1-2 "Pathfinder Historical Information", which includes a drawing, a sketch, and some measured information. The drawing included in Appendix 1-2 is the best-available drawing of the Pathfinder (Superheater) Fuel Assembly.

1-3 *Provide the manufacture data sheet for the thermal insulation.*

Staff needs to verify the compatibility of insulation material(s) with the carbon and stainless steel components of the canister, inner container, and the strongback.

Response:

The manufacture data sheets for Zircar Alumina-Silica Blanket type ASB-2300 are attached. Note that the insulation properties given in the SI units with proper unit conversion are used in the thermal analysis.

1-4 *Clarify the statement that the Pathfinder fuel canister is "leaktight."*

Page 1 of the SAR indicates that the package is "leaktight." ANSI-N14.5 defines "leaktight" as testing a containment boundary with a minimum sensitivity of 10^{-7} cm^3/s.

Response:

Because this level of detail is not considered appropriate for Chapter 1, we changed "leaktight" to "Pathfinder Canister", leaving the leaktight discussion for Chapters 4, 7 and 8. The leak tightness is defined in Chapter 4: Containment, Section 4.1.3 of the SARP as 1×10^{-7} cm^3/s of air.

1-5 *Specify in Section 1.2 the transportation index that is determined for the WE-1 package.*

Response:

We added "Transport Index - 100" to section 1.2.3.1, below "Maximum Decay Heat"

1-6 *Revise Table 1-3, in Section 1.2.3.3, to include the following:*

- *Tolerances for nominal dimensions;*
- *Triangular pitch of the Pathfinder fuel pins; and,*
- *UO_2 density.*

Response:

Framatome ANP revised Table 1-3 as requested.

1-7 *Clarify the value listed for maxi um k_{eff} in Table 1-3, found in Section 1.2.3.3 (note this value is inconsistent with the value listed in Table 6-16).*

Response:

We corrected the value in Table 1-3. It should have been 0.82126.

2.0 STRUCTURAL

2-1 *Demonstrate by analysis or testing that the WE-1 package with the Pathfinder canister maintains structural integrity during a Hypothetical Accident Condition (HAC) free drop through a distance of 30 ft.*

The WE-1 package with the Pathfinder fuel canister is not tested or analyzed to verify that the Pathfinder fuel canister will maintain a structural integrity during a HAC free drop through a distance of 30 ft. and comply with the 10 CFR 71.73(c)(1) requirements. Test results of the WE-1 package with the BW 17x17 fuel assembly are not appropriate for qualification of the WE-1 package with the Pathfinder fuel canister, because the dynamic characteristics of the tested fuel assembly and the Pathfinder fuel canister are different. Since the Pathfinder fuel canister could be higher and may affect adversely the canister and other structural components, such as the Inner Canister, the Strongback, and bolted connections.

Additionally, the tested package was not instrumented for forces/accelerations in the package. Instead, a limit analysis of a fuel rod in bending was performed to predict analytically the accelerations in the fuel rod, which are then used for qualification of the Pathfinder fuel canister. This is not appropriate because the dynamic characteristics of the fuel assembly in a canister would be different than the tested fuel assembly. The prediction of accelerations based on the behavior of a single component does not address the damage experienced by other components, such as the failure of bolts in the inner canister. Analytical modeling of the package may be performed to relate the test results to the analysis, and then the analytical model with the Pathfinder fuel canister may be used to qualify all components of the package.

This information is required to comply with the 10 CFR 71.73(c)(1) requirements.

Response:

The WE-1 shipping container was drop tested from a height of 30 feet per 10CFR71.73 (c) (1) requirement. For the 30-foot drop test, the WE-1 package was loaded with a dummy BW17x17 fuel assembly. The WE-1 package will be used with the Pathfinder Canister to ship Pathfinder fuel assemblies. The Pathfinder Canister is stiffer than the

BW17x17 fuel assembly. The WE-1 shipping container with a fully-loaded Pathfinder Canister weighs 8500 lb versus 9,090 lb with the BW17x17 fuel.

Parametric studies were performed using the Shipping Cask ANalysis System (SCANS) computer program to investigate the performance of the WE-1 package with the Pathfinder Canister during a 30-foot drop hypothetical accident event. Studies were performed to compare the dynamic response of the WE-1 package with BW17x17 fuel package to that of the WE-1 with the Pathfinder Canister. These dynamic drop studies evaluate the effects of the stiffer Pathfinder Canister and lighter weight of the package during 30-foot drops. These studies were performed for various drop orientations. Additionally, these studies evaluate the loading on strongback, HY-80 inner container and internal connections. Results of these parametric studies are summarized below. This information was added to the SAR.

Table RAI 2-1a Summary of SCANS 30-foot Drop Analysis

	Drop Angle	Primary Impact Acceleration in g's	Secondary Impact Acceleration in g's
WE-1 BW17x17 Fuel	15	83.9	126.5
	30	97.4	123.7
	45	116	99.9
WE-1 Pathfinder Fuel	15	87.6	131.2
	30	101.5	127.8
	45	121.1	100.4

(See also responses to RAIs 2-6 and 2-7)

The peak acceleration for WE-1 shipping container with BW17x17 fuel is 126.5 g's. The results based on the WE-1 drop test in conjunction with fuel rod deformation provide a calculated acceleration of 135 g's. This indicates conservatism in the calculated number (used in the original Pathfinder Canister Analysis). The peak acceleration for the WE-1 with the Pathfinder Canister is 131.2 g's compared against 126.5 g's of WE-1 with the BW17x17 fuel. The acceleration increased by 3.7% due to the stiffer Pathfinder Canister and lighter weight. An increase of 5% in g's was used for the revised Pathfinder Canister analysis.

Table RAI 2-1b summarizes the loads on the strongback and HY-80 inner container for these two configurations.

Table RAI 2-1b Strongback and HY-80 Inner Container Load Summary
15 Degree, 30 foot Drop - Loads due to Secondary Impact

Node No. (Location)	Axial Position - inch	WE-1 with BW17x17 Fuel			WE-1 with Pathfinder Canister		
		Maximum Axial Force (kips)	Maximum Shear Force (kips)	Maximum Moment (In-Kips)	Maximum Axial Force (kips)	Maximum Shear Force (kips)	Maximum Moment (In-Kips)
Primary	End	.0	.0	.0	.0	.0	.0
1	.0	-43.7	334.5	1249.4	-38.8	317.8	1176.3
2	18.9	-52.4	366.0	7657.4	-46.0	345.7	7228.8
3	37.8	-69.2	395.2	15455.3	-60.4	370.2	14575.1
4	56.7	-85.2	359.5	23182.6	-74.6	330.5	21764.2
5	75.6	-99.8	257.9	29508.3	-87.8	236.2	27565.4
6	94.5	-111.9	120.5	33252.8	-98.8	102.4	31066.5
7	113.4	-120.2	-97.6	33636.0	-106.5	-91.2	31488.1
8	132.3	-124.2	-280.0	30268.7	-110.2	-262.1	28297.8
9	151.2	-124.5	-466.6	23075.2	-110.3	-436.2	21587.4
10	170.1	-122.4	-629.8	12430.9	-111.6	-593.7	11672.1
11	189.0	-120.9	-706.8	-2362.3	-113.3	-670.0	-2374.8
Secondary	End	-125.1	-1152.4	-1923.1	-125.2	-1116.7	-1910.8

The strongback and HY-80 inner container loading were compared for the two configurations. The peak axial force is approximately the same for both configurations. The maximum shear force decreased from 1,152.4 kips to 1,116.7 kips. The maximum bending moment was reduced from 33,636 in-kips to 31,488.1 in-kips for the WE-1 with the Pathfinder Canister configuration. Even though the acceleration was increased by 3.7%, the loads were reduced due to lighter weight of the WE-1 with the Pathfinder fuel. This comparison shows that the strongback, HY-80 inner container, and bolt connection qualification performed for the WE-1 with the BW17x17 is also applicable for the WE-1 with the Pathfinder. The WE-1 with the stiffer Pathfinder Canister does not impose any additional loading to the internal hardware. Therefore, only the changed hardware needs to be analyzed with the new acceleration loading.

Benchmarking Analysis against Drop Test: The WE-1 package 30-foot drop test was not instrumented. No measured drop accelerations are available for the WE-1. The shipping package 51032-1 (docket 71-6581) was drop tested from a height of 30 ft. This package was instrumented during the drop tests. The outer container, shock mount and the strongback are the same for the 51032-1 and the WE-1 packages. Due to the similarities between the two packages, and the availability of drop acceleration data, a SCANS benchmark was performed for the 51032-1 package. For this benchmark, the impact stiffness of the outer container for the WE-1 and 51032-1 were kept the same. The drop test weight of the 51032-1 package with two fuel assembly was 7,486 lb. This weight was used in the SCANS analysis. The SCANS analysis result is summarized in the Table RAI 2-1c.

Table RAI 2-1c SCANS 30-foot Drop Analysis for 51032-1 Package

	Drop Angle	Primary Impact Acceleration in g's	Secondary Impact Acceleration in g's
51032-1 Container	0	146.7	146.7

For the 51032-1 package drop test, the accelerometer was mounted on the strongback. The measured peak acceleration for the 30-foot drop test was 125 g's (Appendix IV of docket 71-6581). The peak acceleration calculated by SCANS is 146.7 g's (Table RAI 2-1c). The SCANS calculated number is conservative as compared to the measured acceleration. One of the reasons the SCANS acceleration is higher is due to the fact that, in an actual drop test, several pieces of the inside hardware deformed and the outer container buckled. The SCANS analysis does not account for the energy absorbed in internal hardware deformation, nor energy absorbed in the buckling of the outer container. For this reason, the SCANS calculated number is conservative. This is an adequate benchmark of test versus analysis.

2-2 *Provide the basis for using the 1992 edition of the ASME Code, Section III, for the design of the Pathfinder fuel canister, instead of the latest edition of the ASME code.*

Basis for using the 1992 edition of the ASME III Code is not explained in the SAR. This information is required to meet the 10 CFR 71.31 requirements.

Response:

The Pathfinder canister is not an ASME Code component and will not have a Code stamp. The ASME Section III code is used to facilitate design and fabrication as a good industrial practice.

The SAR has been updated to reference the ASME Section III 1995 edition and addenda through the 1996 addenda. Per 10 CFR 50.55a, the most current NRC-approved edition of the ASME Section III is the 1995 Edition and addenda through the 1996 addenda. The 1992 edition of the Code was used to maintain consistency with the earlier submittal. However, the differences between the 1992 and 1995 Editions is not significant in the areas applicable to this design.

2-3 *Revise Chapter 2 to include Appendix 2-2 as a part of Chapter 2, and not as an Appendix.*

Reference to Section 2.10 in Appendix 2-2 is confusing. Since this is a part of the Chapter 2 and includes references for the Chapter 2. It would be easier to follow if the information is included in the Chapter 2. This information is required to meet 10 CFR 71.33 requirements.

Response:

The entire Appendix 2-2 is now moved behind Section 2.9.

2-4 *Provide bases for the selection of wood materials (Eastern White Pine and White Oak), including thickness values and maximum crushing strengths, and demonstrate that the package meets the 10 CFR 71.73 requirements for a Hypothetical Accident Condition free end-drop of 30 ft.*

Bases for selections of the wood materials including the type of wood, thickness values, the maximum crushing strengths, and orientation of the wood grains, are not discussed. Structural adequacy of the selected wood materials to absorb impact energy and reduce the forces on the Pathfinder fuel canister to meet the 10 CFR 71.73 requirements must be demonstrated either by analysis or testing. This information is required to meet 10 CFR 71.73 requirements.

Response:

Wood is an excellent energy absorber. Pine and oak are selected (for end spacer) based on easily and commercially available lumber. The wood crush strength is a function of grain orientation with respect to crush direction. The grains are oriented to get maximum benefit of the wood properties.

Section 2.3 and 2.10.3.2 discuss the type of wood, wood properties, thickness, crushing strength and grain orientation.

The outer cylindrical container and the strongback are the main energy absorbers in the event of hypothetical accidental drops. For the Pathfinder end drop qualifications, no benefit is taken for energy absorbed in the outer cylinder or the strongback. Conservatively, all energy is absorbed in the end wood spacers. The Pathfinder canister has a very robust design and can withstand these highly conservative deceleration values.

An instrumented 30-foot end drop test was performed on the 51032-1 package. The peak acceleration of the strongback was 110 g's (Appendix IV, docket 71-6581). The outer container and the strongback for the 51032-1 package are the same as that for WE-1 package. For the WE-1 shipping container with the Pathfinder Canister and the pine wood energy absorber, an axial acceleration of 1,037 g's is used for the qualification. No

credit is taken for the energy absorbed in the outer container or the deformation of the strongback. This is a very conservative end drop acceleration value.

The wood properties used, in addition to Marks Handbook, 10th Edition, are also from Wood Handbook, Forest Products Laboratory, 1999 – Wood as an Engineering Material, General Technical Report, FPL-GTR-113, Madison, WI; U.S. Department of Agriculture, Forest Service, Forest Products Laboratory. These properties have been used as engineering material for decades.

Wood properties vary with wood density and moisture content. The wood we will use is S-dry or moisture content <12%. The wood density will be measured before its use.

In summary: The wood will be tested for density. The wood will be S-dry. Since the wood is a second level energy absorber and we are not taking credit for the energy absorbed in the outer container and the strongback, there is sufficient conservatism in the acceleration values used for the structural qualification. The wood properties used are from U.S. Department of Agriculture, Forest Service, Forest Product Laboratory and used as engineering material for decades. The analysis uses the wood crush strength within the minimum and maximum tolerances. Additional crush testing of this wood would not provide any additional level of safety.

2-5 *Verify the variation in wood maximum crushing strength parallel and perpendicular to grain as ± 15% (Reference: Chapter 2, page 9 of 28).*

The variation in the Eastern White Pine maximum crushing strength parallel to grain, and the White Oak maximum crushing strength perpendicular to grain, is used as ± 15%, based on Mark's Handbook for Mechanical Engineers, eighth edition. This is not consistent with ± 18% for maximum crushing strength parallel to grain, and ± 14% in tenth edition of the Mark's Handbook, page 6-113. The strength is also dependent on the moisture content. The higher strength may affect the impact properties adversely, and thus must be considered. This information is required to verify that the package meets 10 CFR 71.73 requirements.

Response:

The wood crush strength depends upon the type, density, and moisture content of the wood. The wood to be used will be S-dry, i.e., the moisture content will be less than 12%. Per Mark's Handbook, Tenth Edition, page 6-113, the wood crush strength tolerance is ±18% parallel to the grain and ±14% perpendicular to the grain. The analysis has been revised to use ±18% tolerance for the wood crush strength parallel to grain. The tolerance of ±15% was kept the same for crush strength perpendicular to the grain, because it envelops the ±14% specified in the Mark's Handbook.

2-6 *Revise the fuel assembly SCANS analyses for free drops at various angles, for the Pathfinder fuel canister, and verify that the free drop at 15° angle to the horizontal is a bounding case for the WE-1 package with the Pathfinder fuel canister.*

To determine a bounding case for a free drop of the WE-1 package with the fuel assembly, a simplistic model of the WE-1 container/fuel assembly was developed for running the Shipping Cask Analysis System (SCAN) computer program at various angles of free drops. Based on the results of the SCANS analyses, it was concluded that the impact accelerations (the primary and secondary impacts) of the inner canister for a free drop at 15° angle to the horizontal, would bound the accelerations at other free drop angles. Since the dynamic characteristics of he Pathfinder fuel canister is different from the fuel assembly, the response of the WE-1 package with the Pathfinder fuel canister would be difference than the WE-1 package with the fuel assembly, and must be evaluated. This information is required to verify that the package meets 10 CFR 71.73 requirements.

Response:

To determine a bounding case for a 30-foot drop of the WE-1 package containing a BW17x17 fuel assembly, an analysis was performed using the SCANS computer program. The analytical results presented in the earlier revision of the SAR were calculated prior to the drop test. After the drop tests, the package's permanent deformations were available. Based on the test results, the SCANS analysis was performed using a revised stiffness and the results are provided in Table RAI 2-1a, and in the revised Table 2.7-1 of SAR. The revised results confirm that the 15-degree drop is still the worst-case drop angle for the slapdown drop.

Due to the geometrical configurations, the Pathfinder Canister is stiffer than the BW17x17 fuel assembly. The WE-1 package with the Pathfinder Canister is approximately 590 lb lighter than the WE-1 package with the BW17x17 fuel assembly. Similar studies were performed for the WE-1 with the Pathfinder Canister to determine the worst-case drop angle for the slapdown drop. The results indicate that the 15-degree drop is also the worst-case for the WE-1 with the Pathfinder Canister. The results are summarized in Table RAI 2-1a and are also included in the revised Table 2.7-1 of the SAR.

2-7 *Verify that the SCAN analyses impact accelerations of approximately 66g (Table 2.7-1) for the free drop at 15° angle to the horizontal are consistent with the Case 1 results of approximately 135g in Section 2.10.3.1.*

The SCAN analyses accelerations of 65.8g for a secondary impact in a free drop at 15° angle to the horizontal appear inconsistent with the evaluation in Section 2.10.3.1 that the fuel assembly would have experienced approximately 135g based on the permanent damage in fuel rods. This information is required to verify that the package meets 10 CFR 71.73 requirements.

Response:

The SCANS analysis results presented in the earlier revision of SAR Table 2.7-1 were based on parametric studies performed prior to the WE-1 package drop tests. The intent of these studies was to calculate the worst-case drop angle. Various stiffness parameters were used for the studies. After the WE-1 package drop tests, the deformations of the outer container were measured. A revised SCANS analysis was performed using these test results. The results are summarized in Table RAI 2-1a. For the WE-1 package with the BW17x17 fuel, the SCANS program calculated 126.5 g's for the impact acceleration. This is for a secondary impact from a 30-foot drop for package oriented at a 15° angle to the horizontal. Based on fuel rod deformation (Section 2.10.3.1), the calculated drop acceleration for this case is 135 g's. The calculation is based on conservative methods and predicts higher acceleration than actually experienced by the package. This conservative acceleration with an additional factor of 1.05 is used for the Pathfinder Canister qualification.

2-8 *Provide labels and explanation for the WE-1 package test photographs included in Appendix 2-1.*

This information is required to verify that the package meets 10 CFR 71.33 requirements.

Response:

Descriptive labels were added to the test photographs in Appendix 2-1.

2-9 *Describe the Quality Assurance Program, as required by 10 CFR 71.37, or a reference to a previously approved quality assurance program.*

This information is required to verify that the package meets 10 CFR 71.31 requirements.

Response:

All of the activities for design, fabrication, and testing of the revised package submittal were performed in accordance with the Framatome ANP Quality Assurance Program, document NFQM, titled "Nuclear Fuel Business Group Quality Management Manual," (US Version) Rev 0 dated June 2002. The NRC has reviewed the Quality Assurance Manual under 10 CFR 71.12(b). The NRC approval is documented in docket #71-0003, Revision 21, dated June 14, 2002. This information was added to Section 1.3.

2-10 *Provide the bases of the statements in Section 2.10.2.8, regarding the adverse effects of the removal of one clamp in the Pathfinder fuel canister arrangement. The statements relate to the effects on the stiffness and resulting impact accelerations, and the adequacy of the high strength bolts in the new configuration.*

Section 2.10.2.8 discusses the effects of removing one clamp at the end, but does not provide any bases to support the statements related to the effects on the stiffness and the g-level, and the replacement of the low-strength bolts with the high-strength bolts. This information is required to verify that the package meets 10 CFR 71.33 requirements.

Response:

A finite-element stiffness analysis (ANSYS) was performed for the HY-80 armor plate inner container with and without the end clamp. The inner container stiffness in the diagonal direction was calculated. Due to structural symmetry, half of the box is analyzed. The results of the analysis are:

Inner Container local stiffness (half of the symmetrical box)	
With all clamps	5,348,200 lb/inch
With last clamp removed	5,084,300 lb/inch

The inner container stiffness in the diagonal direction was calculated. Due to the symmetry of the inner container, only one-half of the containers was modeled in the computer analysis.

The localized stiffness is reduced by 4.9% after removing the end clamp. This is within the accuracy of the impact analysis. The end spacer, end plate and two end clamp are closely spaced. Therefore, removal of one end clamp did not compromised stiffness of

the inner container. This was verified by the computer analysis. There is no change in the beam bending stiffness with or without the end clamp. Also, when one considers, all of the other structural members, the change in the overall stiffness is insignificant. The stiffness calculation methods, analysis, and result are included in Section 2.10.2.8 of the SAR.

The end plate bolts will remain stainless steel, the same as the previous revision of the WE-1 package, i.e., ½-13NC SST Hex HCS (Drawing 02-1273965, view "Y"). These stainless steel bolts were qualified during the WE-1 package drop tests.

2-11 *Provide dimensions and material specifications for the Rubber between the Aluminum Clamp Blocks and the Pathfinder fuel canister, and provide methods of attachment to the blocks, if any.*

This information is required to 10 CFR 71.33 requirements.

Response:

Commercial Nitrile Duro 60 rubber will be used between the aluminum support spacer and the Pathfinder canister. The rubber strip, minimum 1/8-inch thick, will be attached to the clamp blocks by either glue or double-sided tape. A note was added to drawing #5016270 specifying the rubber specification and method of attachment. The clamps will compress the rubber to keep it in place. The rubber will prevent gouging of the metal and also will provide separation between the aluminum support spacer and the stainless steel Pathfinder Canister. During the WE-1 30-foot drop test with the dummy BW17x17 fuel, the rubber pieces remained attached to the clamps. Commercial Nitrile Duro 60 rubber has an excellent weather resistance between -67 °F and +275 °F.

2-12 *Verify that the rubber pads between the Aluminum blocks and the stainless steel canister will remain in place and will not degrade at service temperatures (ambient temperatures from -40° F to 100° F), and keep the two materials separate during the transportation of the package to preclude the galvanic reactions.*

This information is required to meet 10 CFR 71.43(d) and 10 CFR 71.71(c)(1) and 10 CFR 71.71(c)(2) requirements.

Response:

Commercial Nitrile Duro 60 rubber has an excellent weather resistance between -67 °F and +275 °F. The rubber will not degrade at service temperature. Due to the clamp force of the bolted clamps, and easy compression of the rubber, the rubber will remain in place under normal conditions of transport. The rubber provides separation between the

aluminum spacers and the stainless steel Pathfinder canister; this will prevent galvanic reaction between them.

2-13 *Verify that the available closure bolt engagement length state on page 38 of Appendix 2-2 is provided.*

The thread engagement length available to resist the forces in the bolts is stated as 0.9475 inches on page 38 of Appendix 2-2. Since the drawings do not provide information regarding the bolts, the calculations cannot be verified. This information is required to verify that the 10 CFR 71.71 and 10CFR 71.73 requirements.

Response:

A drawing #5021426 was added to the report showing the depth of thread (thread engagement) in the weld neck flange. The nominal thickness of the weld-neck flange is 1.06 inch, and the thread length used in the analysis is 0.9475 inch, which is more than the minimum thread engagement requirement of 0.55 inch.

2-14 *Verify the structural integrity of the fuel assembly to meet the requirements of 10 CFR 71.71 Normal conditions of Transport, and 10 CFR 10.73 Hypothetical Accident Conditions requirements.*

The criticality analysis assumes that the fuel assembly will maintain its configuration during the test conditions of 10 CFR 71.71 and 10 CFR 71.73. However, the fuel assembly is not evaluated for structural integrity. This information is required to meet 10 CFR 71.71 and 10 CFR 71.73 requirements.

Response:

The structural analysis assumes no cladding integrity (for maximum pressure calculations). The canister will be filled with filler material during transport. Due to the space limitations, the fuel will remain within Pathfinder Canister space.

The criticality analysis evaluates the most reactive accident scenario. This included a variety of cladding and fuel configurations, and water intrusion. The following will be added to Chapter 6, Section 6.4, under Table 6-14.

> "The data shows that the fuel is more reactive when it is intact and optimally moderated, than when the assemblies do not remain intact and when the pellets are allowed to move freely in the container. This is demonstrated by comparing the calculated k_{eff} for the homogeneous case, with no Incoloy removed (0.68008 $\pm$ 0.00073), from Table 6-14, to that for the comparable heterogeneous case (0.68898 $\pm$ 0.00078), from Table

6-10. Even when half of the Incoloy clad material is removed from the canister, k_{eff} is less than when the assemblies are allowed to spread apart into an optimally moderated configuration. As such, the worst case situation for criticality is when the fuel remains intact, and is allowed to spread apart rather than collapse together. This is clearly demonstrated by comparing the k_{eff} values presented in Table 6-10 with those presented in Table 6-14."

3.0 THERMAL

3-1 *Correct pages 4, 5, and 9, to correctly reference Section 10 CFR 71.73(c)® (Thermal), rather than 10 CFR 71.73(c)(3) (Puncture).*

This information is needed to assure compliance with 10 CFR 71.7.

Response:

Framatome ANP, will correct the subject reference sections on pages 4, 5, and 9.

3-2 *Correct the thermal conditions for the fire accident analysis to properly reflect the conditions mandated on 10 CFR 71.73(c)(4) (Thermal).*

On page 5 of Chapter 3, it is stated that an emissivity of 0.8 was applied for the Hypothetical accident conditions of the fire. 10 CFR 71.73(c)(4) (thermal) states that for the purpose of the calculation, the surface absortivity coefficient must be either that value which the package may be expected to possess if exposed to the fire specified or 0.8, whichever is greater. This information is needed to assure compliance with 10 CFR 71.7 and 10 CFR 71.73.

Response:

Conservative fire accident analysis is performed. As stated in Section 3.5.1, for the fire accident analysis, the outer container is assumed to be totally compromised. The outer surface of the inner container is fully exposed to the fire event. The emissivity of the inner container is 0.5 (Table 3.2-3). Per requirement of 10CFR71.73 (c) (4), the higher of 0.5 and 0.8, i.e., emissivity of 0.8 is used in the analysis.

Note that absorptivity is equal to emissivity for systems in thermal equilibrium and are approximately equal for nonequilibrium systems.

3-3 *Provide thermal properties for stainless steel and Alloy 600 O-rings. Provide also the type of stainless steel used on this package.*

On page 5 of Chapter 3, it is stated that the Pathfinder canister is entirely of stainless steel construction except for the Alloy 600 O-rings and that these materials are not sensitive to temperatures within the range of -40° F to 800° F. This information is needed to assure compliance with 10 CFR 71.7 and 10 CFR 71.39.

Response:

The Pathfinder Canister is fabricated from type 304 stainless steel. The material properties for the 304 stainless steel and Alloy 600 are provided in Table 3.2-1. The 304 stainless steel and Alloy 600 are not subject to ductile-to-brittle transition above -40° F, therefore they are safe from brittle fracture. This information is added to Section 3.2.

3-4 *Verify that the thermal property tables are properly covering the range of temperatures expected for normal condition of transport and for hypothetical accident conditions.*

The thermal analysis performed on this package uses thermal properties interpolated at temperatures that are not covered by the property tables provided on the SAR. This information is needed to assure compliance with 10 CFR 71.7.

Response:

Table 3.2-1 is revised to include properties at -40° F. The thermal properties at -20 °F and -40 °F are extrapolated values from the ASME Code for HY-80, 304 SS and Alloy 600. A review of the Metals Handbook indicates that the thermal properties follow smooth curves in the temperature range of -40 °F to 1500 °F and the extrapolations at -20 °F and -40 °F are justified.

3-5 *Modify Table 3.2-4 to reference note 1.*

Response:

Reference to note 1 is identified in the Table 3.2-4.

3-6 *Verify that the heat balance calculation shown on page 7 of Chapter 3 of the SAR uses a Stefan-Boltzman constant that is consistent with your system of units.*

According to the above calculation, the Stefan-Boltzman constant should be expressed as Btu/hr-ft^2-R^4. This information is needed to assure compliance with 10 CFR 71.7.

Response:

The Stefan-Boltzman constant used is:

$$\sigma = 1.714\ (10)^{-9}\ \text{BTU/hr} - \text{ft}^2 - {}^{\circ}\text{R}^4$$

This will be corrected in the report.

3-7 *Explain or justify why this transportation package can perform safely without any material concern for operating conditions at -40° F.*

On page 5 of the SAR it is stated that the operating conditions of the package include -40° F. This information is needed to assure compliance with 10 CFR 71.41.

Response:

The Pathfinder Canister is fabricated from type 304 stainless steel. The closure system includes two Alloy 600 metallic O-rings. The 304 stainless steel and Alloy 600 are not subject to ductile-to-brittle transition above -40° F, therefore they are safe from brittle fracture. There is no other material safety concern for the Pathfinder Canister at -40 ° F.

3-8 *Provide Appendix 3-2, ANSYS Input files.*

On page 9 of the SAR, Appendix 3-2 is mentioned but this appendix was not included in the SAR. This information is needed to assure compliance with 10 CFR 71.7.

Response:

The Appendix 3-2, ANSYS input files were included in earlier submittals. However, by mistake it was omitted in the last submittal (May 2002). The Appendix 3-2 is now included.

3-9 *Verify that the convection heat transfer coefficient used on the thermal evaluation of the fire has the correct units.*

The heat transfer coefficient presented in Section 3.2.5 has incomplete units. This information is needed to assure compliance with 10 CFR 71.7.

Response:

The missing units, "°F", is added after "ft^2," to identify the convection units as Btu/hr-ft^2-°F.

3-10 *Provide the detailed calculation of the maximum internal pressure, as summarily described in Section 3.5.4. Also state the design pressure of the Pathfinder canister for normal condition of transport and for hypothetical accident conditions.*

This information is needed to assure compliance with 10 CFR 71.7.

Response:

Section 2.10.1.1 provides the calculation of the Pathfinder Canister pressures during normal and accidental conditions. Reference to Section 2.10.1.1 was added to Section 3.5.4.

3-11 *Correct the first paragraph of Page 1 of Appendix 3-1 to address the correct reference.*

Reference 7 should be changed to Reference 3 (see foot notes on page 1 of Appendix 3). This information is needed to assure compliance with 10 CFR 71.7.

Response:

Reference call out was changed from 7 to 1 on Page 1 of Appendix 3-1.

3-12 *A copy of References 1 and 2 of Appendix 3-1 will be provided as an attachment to the RAI response letter.*

Response:

References 1 and 2 of Appendix 3-1 are provided as attachments to the accompanying cover letter.

4.0 CONTAINMENT

4-1 *Provide a sketch of the containment system for the package that illustrates the containment boundary. Include which seal is the containment boundary and show any penetrations into the containment system.*

The application must define the containment boundary penetrations and their method of closure must be adequately described. This information is needed to assure compliance with 10 CFR 71.31(c), and 10 CFR 71.33 requirements

Response:

Drawing #5021426 and Figure 4.5-1 are added to the report. The drawing and figure provide the details of the seal and groove. The drawing also provides the closure bolt specification. There are no penetrations into the containment system.

4-2 *In Paragraph 4.2.2, the viscosity of air at 298K is incorrectly stated as 0.00185 cP. The correct value of the viscosity of air at 298K and 1 atm abs is 0.01185 cP.*

This information is needed to assure compliance with 10 CFR 71.7.

Response:

The viscosity of air at 298K and 1 atm abs has been corrected. The correct value, and that used in the calculations is 0.0185 cP.

6.0 CRITICALITY

Section 6.2 – Package Fuel Loading

6-1 *Clarify the statement that the dimensions in Table 6-2B "represent nominal values."*

It appears that some of these values may be based on tolerance values for the Pathfinder fuel element specifications.

Response:

Table 6-2b has been revised to show Fabrication Specifications with dimensional tolerances and KENO model values.

6-2 a. *Add the triangular pitch of the Pathfinder pins and the UO_2 density to Table 6-2b.*

b. *Add the dimensions and material specifications for the center poison rod and spacer wire to Table 6-2b.*

c. *Specify in Table 6-2b, or other table, the dimensions and material specifications used in the pathfinder criticality models.*

Response:

Table 6-2b has been revised to include these additional dimensions. Table 6-2b was revised to show KENO model values.

The material specifications used in the KENO models are clarified in Table 6-2b. Also, Table 2-7b shows the Incoloy 800 atom densities calculated for the KENO model. The only other materials used in the KENO models are fuel and water. The fuel specifications are identified in the text and Table 6-2b, and are shown in the KENO inputs listed in Appendix 6-1.

6-3 *Revise the diagram in Figure 6-1b to specify the dimensions used in the KENO criticality model.*

Response:

Figure 6-1b has been revised to show center-to-center pin pitch, fuel clad IR and OR, Sheath IR and OR, and Fuel pellet radius.

6-4 a. *Specify the type and quantity of "fill material" that may be loaded with the Pathfinder Canister, as shown in Drawing No. 5016270, Rev 0.*

b. *Discuss any impacts from the filler material on the reactivity of package configuration.*

Response:

The following statement has been added to Chapter 6 following Figure 6-8.

> "The preferred dunnage material for less than full loads is wood. Wood is a hydrogenous material with an overall lower density than water, and with a much lower hydrogen concentration. It is seen by the previously discussed analysis that the Pathfinder container is under-moderated, and that it achieves maximum reactivity at fully flooded conditions. The addition of wood would have the effect of decreasing the total hydrogen

concentration in the container, by displacing water in the fully flooded. It can be inferred that wood would have less of an impact on reactivity than the comparable fully flooded condition. Wood then is an acceptable material with respect to criticality concerns."

Section 6.3.2 – WE-1 Normal Array Evaluation

6-5 *Clarify the k_{eff} value stated for the Pathfinder normal condition analysis.*

This value appears to be inconsistent with the normal condition value reported in Table 6-16.

Response:

This value has been corrected. The correct value is that given in Table 16. The value should be 0.25620 ± 0.00050.

6-6 *Clarify the statement that nickel and chromium in Incoloy 800 contain the strongest neutron absorbers and were therefore minimized in the criticality analysis.*

It appears that titanium and manganese constituents of Incoloy 800 have the highest thermal neutron absorption cross sections.

Response:

This discussion will be clarified. The sentence will now read:

"The weight percentages of each element that give the low nickel and chromium concentration (which are stronger neutron absorber than the primary element, iron) were assumed for the KENO-V.a model."

Section 6.4 – Criticality Calculation

6-7 *a. Discuss the configuration of the Pathfinder fuel assemblies after the hypothetical accident test conditions.*

b. Clarify the type of damage to the fuel and any impacts on the accident criticality analyses.

c. Justify why the criticality analysis assumes normal assembly configuration of the fissile material within Pathfinder fuel pins, whereas Section 2.9 states that "no credit is taken for the fuel rod cladding providing containment of radioactive material under normal or hypothetical accident conditions."

Response:

The criticality analysis evaluates the most reactive accident scenario. This includes a variety of cladding and fuel configurations, and water intrusion. The following discussion was added to Chapter 6, Section 6.4, under Table 6-14.

> "The data shows that the fuel is more reactive when it is intact and optimally moderated, than when the assemblies do not remain intact and when the pellets are allowed to move freely in the container This is demonstrated by comparing the calculated k_{eff} for the homogeneous case, with no Incoloy removed (0.68008 $\pm$ 0.00073), from Table 6-14, to that for the comparable heterogeneous case (0.68898 $\pm$ 0.00078), from Table 6-10. Even when half of the Incoloy clad material is removed from the canister, k_{eff} is less than when the assemblies are allowed to spread apart into an optimally moderated configuration. As such, the worst case situation for criticality is when the fuel remains intact, and is allowed to spread apart rather than collapse together. This is clearly demonstrated by comparing the k_{eff} values presented in Table 6-10 with those presented in Table 6-14."

Section 6.5 – Criticality Benchmark Experiments

General:

Section 6.5 discussing criticality benchmarking has been completely revised. It now reflects the methodology of NUREG/CR-6361 for transportation rather than NUREG/CR-6698. Due to the similarity in both the methods, the expected agreement of final results, and the clearer statistical basis, the latter NUREG was initially proposed for the original submittal to provide a consistent benchmark methodology for the Framatome ANP fuel plant and transportation from the plant. The change in methodology to 6361 has been made to facilitate the review of the Pathfinder application.

6-8 *a. Specify how each value in the maximum k_{eff} equation for the "historical approach" in Section 6.2B.4 of Appendix 6-2 were derived from the benchmark experiments listed in Tables 7.1 and 8.1.*

Response:

The equation for the maximum k for the 'historical' approach is:

$$K_{Max} = k_{calc} + bias + (^{95/59}Factor)\sqrt{(\sigma_{calc})^2 + (\sigma_{bias})^2}$$

This equation is used to find the maximum k_{eff} for the system being analyzed. The results from the KENOVa calculation of the system are k_{calc} and σ_{calc}. The other terms are obtained from the statistical evaluation of the benchmark cases using the Single-Sided Tolerance Limit methodology NUREG/CR-6698 in which the Upper Safety Limit (USL) is defined as:

$$USL = K_L - \Delta_{sm} - \Delta_{AOA}$$

where,

Δ_{sm} = subcritical safety margin, generally ≤0.05,
Δ_{AOA} = an additional safety margin if system is outside the 'Area of Applicability of the benchmark cases,
K_L = the one-sided lower tolerance limit = $k_{avg} - US_p$,
k_{avg} = weighted average of calculated k_{eff} values,
U = one-side lower tolerance factor obtained from statistical tables dependent upon the number of experiments and the desired confidence level (95/95 generally), and
S_p = square root of the pooled variance with the pooled variance equal to the sum of the variance about the weighted mean and the average total uncertainty.

Note that in this methodology the average k_{eff} is obtained from calculated k_{eff} values normalized to the experimental k_{eff}, i.e., calculated divided by experimental, to compensate for experimental values that are not 1.0000. Similarly the total uncertainty of the benchmark calculation is the square root of the sum of the calculated uncertainty and the experimental uncertainty. This total uncertainty is the weighting factor used to obtain the weighted average k_{eff} term for K_L above.

The USL is applied as follows:

$$USL \leq k_{calc} + 2\sigma_{calc},$$

or $$K_L - \Delta_{sm} = k_{avg} - US_p - \Delta_{sm} \leq k_{calc} + 2\sigma_{calc},$$

where it is assumed the system is within the Area of Applicability of the benchmark data. Rearranging,

$$-(1 - k_{avg}) + (1 - \Delta_{sm}) \leq k_{calc} + 2\sigma_{calc} + US_p$$

but the bias is defined as $1 - k_{avg}$ and the sum of the two uncertainty terms can by approximated as the square root of the sum of the squares times U, so this becomes:

$$(1 - \Delta_{sm}) \leq k_{calc} + \text{bias} + U(\sigma_{calc}^2 + S_p^2)^{1/2} = K_{max}.$$

In the 'historical' approach Δ_{sm} is 0.05, so the left-hand side of the above equation becomes 0.95 and represents the 'limit' in the 'historical' approach. Thus, the USL method and the historical method are essentially the same given a safety margin of 0.05. The values used in the equation in Section 6.2.B.4 are the

bias = (1 - mean k_{eff}) = (1 – 0.99997) from the 48 benchmark cases of Table 8.2,
U = 2.0458 the one-sided upper tolerance factor for n=48 at a 95/95 confidence level, and
S_p = 0.0066 of Table 8.2 for 48 cases.

Based upon the values in Table 8.2, the single-sided tolerance limit for this case with a 0.05 safety margin is 0.9365 from the 48 experiment set. A single-sided tolerance limit of 0.9356 from the 45-experiment set represented the lowest value.

b. *Clarify or revise the benchmarking analysis in Section 6-2B to correlate the determination of biases and the maximum k_{eff} value to the approach in NUREG/CR-6361, "Criticality Benchmark Guide for Light-Water-Reactor Fuel in Transportation and Storage Packages."*

Response:

The benchmarking description has been completely revised to reflect the methodology of NUREG/CR-6361. However, as discussed in the response to 6.8c, the USL values from both methods are not significantly different, at least for the Pathfinder fuel evaluation.

c. *Specify how the "historical approach" and the NUREG/CR-6698 approach correspond to the upper safety limit (USL) methodologies in the NUREG/CR-6361 approach for transportation packages.*

NUREG/CR-6361 describes USL determination procedures for transportation packages, whereas NUREG/CR-6698 describes USL determination procedures for nuclear fuel cycle facility licensees.

Response:

NUREG/CR-6698 was published 4 years after NUREG/CR-6361, and, based upon the bibliography, relied on the information in the latter report. The methods in 6698 seem to be more statistically based but the sources of the methods are not sufficiently referenced to directly determine the source. However, the information provided in 6698 is sufficient to perform the calculations via a spreadsheet or to generate a computer program for solution. The information in 6361 does not provide the information needed to do the calculation with a spreadsheet without considerable effort to obtain the referenced papers (primarily for the D table). A program is provided in 6361, however, without the referenced papers, verification is not possible. Without verification, the usefulness of the ULSTATS program is reduced.

The historical approach and the single-sided tolerance band in NUREG/CR-6698 are different formulations of the same basic approach, as described in the response to 6.8a above. This approach is primarily to be used when there is no trend to the data. It is directly related to the weighted average k_{eff} of the benchmark cases included in the validation. This approach does not have a parallel in NUREG/CR-6361 but is most closely related to the Confidence Band with added margin, i.e., USL-1 in the latter report. If there is no trend in the data, then both approaches would provide about the same result.

More closely related are the Tolerance Band approach of 6698 and the Closed Interval approach (USL-2) of 6361. Both are statistical approaches that use very similar equations to arrive at the tolerance band. The primary difference between the formulations is that in 6361, the tolerance band is based only upon either the minimum or maximum value of the trending variable, while 6698 is based upon the range of data. This does allow a tolerance band defined by a simple linear equation for the 6361 method as opposed to tabular values for 6698. Another difference is that USL-2 is used primarily as a verification of the margin associated with USL-1 in 6361. In 6698, the tolerance band with an added margin is used as the USL for data showing a trend.

A key difference in the two methods is the assigned value of the added safety margin. In 6361 it can be no less that 0.05, while in 6698 the lower limit is 0.02. However, for 6698, justification must be provided for the added safety margin used, while for 6361 USL-2 provides some basis for accepting a 0.05 safety margin.

The following figure illustrates a comparison between the methods in the two reports. The benchmark k_{eff} values are represented by the plus signs at the top of the figure. The solid line through the points represents the unweighted least-squares fit while the dashed line is that for the weighted least-squares fit. The two fits are very close with the weighted fit having a slightly steeper slope. The plots between ~ 0.97 and 0.99 are for the tolerance band of 6698 and USL-2 of 6361 both of which represents a fitted curve above which the true population is expected to lie. The tolerance band method adds a negative tolerance value to the weighted-difference fit for the all the independent variables in the area of applicability. The USL-2 method performs a similar addition but the tolerance value is only based upon the first and last independent variables over the

closed interval. The USL-2 method[1] is seen to provide more conservative values over most of the range. However, the tolerance band for 6698 will have an administrative margin applied and be used as a USL rather than merely as a check on the administrative margin used for USL-1 in 6361. The curves between 0.93 and 0.94 are the single-side tolerance limit of 6698 and USL-1 of 6361. As noted above, the single-sided tolerance limit is dependent only upon the weighed average k_{eff} and thus, is a flat line as compared to the curve of USL-1. The vertical lines represent the ECF of the Pathfinder fuel assembly in the inner container. For the range of values for the Pathfinder fuel, the single-sided tolerance limit provides the conservative limit. However, it would be non-conservative for systems with higher ECF values.

The following table lists the independent variable and the USL-1 values for the three bounding conditions examined for the Pathfinder package. The lowest value is 0.9359, which is about the same as that for the Single-Sided Tolerance Limit value, i.e., 0.9356. Thus, for the range of applicability for the Pathfinder fuel, the two methods provide essentially the same limit.

	48 Flooded		48 Optimum		Homogeneous	
	Parameter	USL	Parameter	USL	Parameter	USL
Pitch, cm					-	-
Rod	0.7341	0.9359	0.7341	0.9359	-	-
Cell	2.5426	0.9383	3.8126	0.9383		
ECF, eV	0.306251	0.9368	0.105085	0.9378	0.104816	0.9378
Enrichment, wt%	7.51	0.9377	7.51	0.9377	7.51	0.9377
H20/fuel	2.268036	0.9365	4.951	0.9378	-	-
AFG, group	195.1	0.9364	208.6	0.9380	207.3	0.9380
H/U	160.8	0.9373	289.7	0.9383	189.2	0.9376
Temperature, °C	20	0.9369	20	0.9369	20	0.9369
Minimum		**0.9359**		**0.9359**		**0.9369**

[1] It is noted that there is a formulation error in this method. The formulation provided in 6361 is a for a two-sided uniform width approach rather than the one sided approach as advertised (see "Query: Tolerance Interval in Regression," Norman Johnson, Ed., Technometrics, Vol, 10, No. 1, February 1968, pages 207-209. The effect of this is to reduce the expected confidence from 95% to 92.5% when the two-sided approach is applied as single-sided which results in a slight non-conservative bias in the approach.

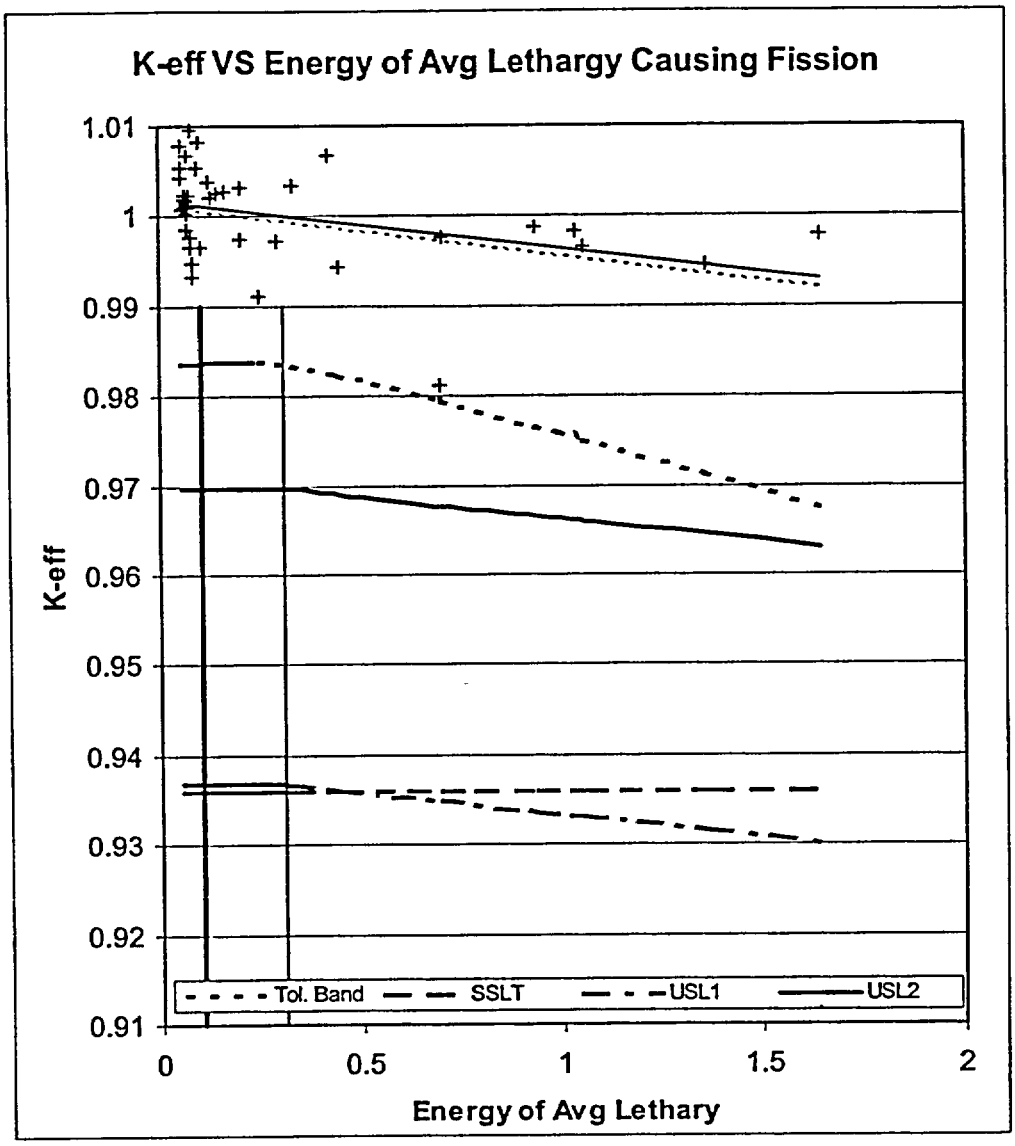

6-9 *a. Specify the range of H/U ratios for the benchmark experiments in Appendix 6-2 and specify the H/U ratio for the Pathfinder fuel accident configuration.*

Response:

The first table below lists the range of H/U or Water/Fuel ratios for the various configurations of the fuel in the cylindrical package for the flooded accident condition. The first set of data represents these ratios for only the hex array within the package. For the 2.54-cm pitch (the 'normal' arrangement), the water outside the hexagonal 'core' is ignored. For the optimum pitch of 3.81 cm, the 'core' radius exceeds the radius of the package cylinder but only considers water in the hexagonal core for the H/U calculation. The model assumes that water fills the central absorber tube, which is represent by the

'water in center tube' data. The ratios were also examined for the case when the center tube remains intact. The second set of data provides the ratios for 48 and 40 assemblies in the package with and without the center tubes breached. All the water within the cylindrical inner package is factored into H/U. The third set of data provides the H/U ratio for a homogeneous mixture of fuel and water, i.e., the clad was completely removed from the model in the inner package. From this table it is seen that the H/U ratio can range from about 82 to 290 depending upon the model assumed.

H/235U and Fuel/Water Values for Pathfinder Fuel Arrangements

48 Sheath Cells in Hex Array				
	Water in center tube		No water in center tube	
Cell Pitch, cm	2.54	3.81	2.54	3.81
Water/Fuel	2.43	7.80	2.22	7.59
$H/^{235}U$	90.37	289.65	82.48	281.77
Inner Package Array				
No. assemblies in inner package	48	40	48	40
Water/Fuel	3.30	4.33	3.08	4.12
$H/^{235}U$	122.45	160.79	114.56	152.91
Homogeneous Fuel/Water in Package				
$H/^{235}U$	189.19			

This second table lists the range of parameters for the benchmark experiments used in the validation process. The range for the H/U ratio is about 40 to 657 and thus, the benchmark cases bound the possible values for the Pathfinder fuel.

Range of Parameters for Benchmark Experiments

Parameter	Minimum Value	Maximum Value
Pitch	0.62	1.85
ECF	0.0539	1.64
Enrichment	4.9200	9.83
H20/fuel Vol ratio	0.8339	20.35
AFG	174.8810	216.0410
Temperature	16.0000	274.0000
$H/^{235}U$	39.7060	657.4696

b. Justify the reason for not including a trending analysis for the H/U ratio in the benchmarking analysis.

Response:

The energy of the lethargy causing fission (ECF), the average fission group (AFG), the $H/^{235}U$, and the water/fuel parameters are all correlated and provide information on the neutron energy in the system. From past experience and more specifically a review of the examples in NUREG/CR-6361, it was judged that the H/U ratio would not be the parameter that provides the bounding trend relationship for fuel rod arrays. This coupled with uncertainty in the definition the H/U ratio for the Pathfinder fuel in the cylindrical package led to deleting this trend from the evaluation.

6-10 *Clarify the method for determining the "fit line" for k_{eff} in Figures 8.1 through 8.9.*

It is not clear how the fit line for Figures 8.2 and 8.3 was determined because a significant portion of data points over the trending parameter appear to lie above the "fit line."

Response:

The 'fit' line for all trending analyses were obtained from a computer program using the weighed least squares method of described by Equations 10-13 of NUREG/CR-6698. The figures were illustrations of the fit equations. Unfortunately, the sign on the slope of the fit equation was incorrect in the Excel Spreadsheet generating Figures 8.2 and 8.3 resulting in a negative slope and a line that lies below the higher enrichment data points

6-11 *a. Specify the average energy causing fission for the Pathfinder accident configuration.*

Response:

The Pathfinder values for the trending parameters are listed in the following table.

Pathfinder Model Trending Parameter Values

Parameter	48 Flooded	48 Optimum	Homogeneous
Pitch, cm			
Rod	0.7341	0.7341	-
Cell	2.5426	3.8126	-
ECF, eV	**0.306251**	**0.105085**	**0.104816**
Enrichment, wt%	7.51	7.51	7.51
H20/fuel	2.268036	4.951	-
AFG, group number	195.1	208.6	207.3
$H/^{235}U$	160.8	289.7	189.2
Temperature, °C	20	20	20

The first column represents the values for the flooded configuration with 48 assemblies inside the cylindrical inner package. The second column provides the values for the optimum spacing of 48 assemblies (note this array can not fit in the inner package). The last represents values for a homogeneous fuel/water mixture inside the inner container with all cladding removed. A comparison of this table with the second table in Response 6.9a shows that values for all cases except the optimized cell pitch are within the area of applicability of the benchmark cases. For the optimized cell pitch, the trend has a positive slope with a constant value above a pitch of ~1.1 cm so that the curve can be extended to 3.81 with no loss in conservatism.

b. Specify how the uncertainty in the trending analysis for average energy of fission was treated with respect to the stated range of applicability to be 0.0539 eV to 3.508 eV.

It appears there is sparse benchmark data between 1.6422 eV and 3.508 eV.

Response:

The revised calculations remove the benchmarks for aluminum clad fuel which contained the 3.5 eV point. The upper limit of applicability is now 1.64 eV and the data has a relatively uniform spread over the range of applicability. The Pathfinder ECF resides in the lower area where the data points are relatively dense.

In general, there may be sets of data that are relatively sparse due to lack of critical experiments. The options are to accept the sparseness if additional applicable data in not

available, find and incorporate additional data, or neglect the point and extrapolate outside the range of applicability if necessary. Generally, it seems that accepting the sparse data if additional applicable data is not available would be chosen over extrapolation.

6-12 *a. Specify the cross-section libraries that were used for the benchmark experiment calculations.*

Response:

The benchmark calculations used the 238 group 'Law ' Library. This was also used for the Pathfinder container analysis.

b. Justify any differences in cross-section libraries between the bias determined for the benchmark calculations and the values determined in the Pathfinder criticality analysis.

Response:

The same library was used for both the benchmark and licensing cases.

6-13 *Clarify how the review of benchmark calculations obtained by Framatome, as discussed in Section 6.2B.7 of Appendix 6-2, considered differences in methodology and modeling techniques with respect to treatment of boundary conditions, dimensional tolerances, uncertainties in experimental data, and other important modeling parameters.*

Response:

The benchmark cases were either generated at Framatome or carefully examined to ensure their correctness. Those generated in-house used the methodology, modeling techniques, and boundary conditions generally used at Framatome for criticality analyses. During the examination of those obtained from external sources, e.g., ORNL, no significant differences between in-house techniques and those used in the benchmark cases were noted.

Relative to experimental uncertainties, the experimental critical value and its uncertainties were obtained from the International Handbook evaluation. These values may have been obtained using methodologies other than KENOVa, e.g., MCNP. However, the uncertainties represent differences in k_{eff} with and without experimental tolerances/uncertainties included in the model. Thus, uncertainties are considered to be independent if the methodology used in the evaluation and any effects that may result from different calculational techniques and/or cross section sets are judged to be

insignificant. Thus, complete recalculation of tolerance uncertainties with the SCALE system was not deemed necessary, and was not done.

The experimental uncertainties, both in critical k_{eff} and due to experimental tolerances, are directly factored into the statistical evaluation of the benchmark results. This is accomplished by normalizing the calculated k_{eff} to the experimental value, i.e., $k_{norm} = k_{calc}/k_{exp}$. The k_{norm} values are used in the statistical analysis of the data, e.g., least squares fit. The experimental uncertainties are similarly included in the calculation uncertainty by using a total uncertainty in the statistical evaluation. The total uncertainty is just the statistical combination of the calculational uncertainty and the experimental uncertainty, i.e., the square root of the sum of the squares. These are more appropriately added into the evaluation by using a weighted least-squares method of linear regression with the weighting factor chosen as the total uncertainty.

7.0 OPERATING PROCEDURES

7-1 *Revise the Operating Procedures for the Pathfinder Canister as follows:*

a. Number the paragraphs (bullets) to indicate sequencing of the procedures (note that alternative sequencing of steps may be indicated).

Response:

The SAR has been revised to include paragraph numbers instead of bullets in Section 7.2.16.

b. Include more description of visual inspections that are to be performed on the Pathfinder Canister.

This information is needed to assure compliance with 10 CFR 71.7.

Response:

The SAR has been revised to include a description of the Pathfinder Canister visual inspection in paragraph 3 of section 7.2.2.

7-2 *Revise the section that describes the pre-shipment leak test to include the following:*

a. A calculation that shows that the proposed leak test results in a sensitivity of at least 1 x 10^{-3} std cc/sec. Note that the information in ANSI N14.5 Section B.12 provides information concerning this topic.

Response:

A representative calculation of an option for the pre-shipment leak test is included in Section 4.5.

b. Include the inter-seal region volume and the total test volume (note that the test volume includes the volume of the inter-seal region and any instrument lines).

This information is needed to assure compliance with 10 CFR 71.51.

Response:

The seal region volume and a representative instrument line volume are included in the Section 4.5 representative calculation.

8.0 ACCEPTANCE TESTS AND MAINTENANCE PROGRAM

8-1 *Revise Section 8.13, Leak Tests, to address the following:*

Describe in detail all leak testing performed on the Pathfinder Canister. Include the test methods, the test setup, and acceptance standards for all tests. The tests should include tests of welds during fabrication and tests of the seal region. Note that this information should be consistent with that provided in Chapter 4.
This information is needed to show that the canister provides adequate containment as required in 10 CFR 71.51.

Response:

Leak tests of the Pathfinder Canister closure seals are performed to verify the O-rings will seal properly. The pressure drop test, to verify the O-ring sealing, will be performed per paragraph A.5.1 of ANSI N14.5-1997, "American National Standard for Radioactive Material – Leakage Tests on Package for Shipment." The acceptable leak rate is $1x10^{-3}$ atm cc/sec using a pressure drop test.

The revised Section 4.5 provides a representative calculation of a test method and setup. Weld joints are nondestructively examined by tests at fabrication and leak tested to verify

they are sound. The fabrication leak test, to verify welds, will be performed per test method #A.5.9 of Annex A of ANSI N14.5-1997. The acceptable leak rate is $1x10^{-7}$ atm cc/sec. This information is added to SAR Section 8.1.3.

8-2 *Revise Section 8.2.2 to address the following:*

Clarify that the leak test is performed on the Pathfinder Canister. Describe in detail the leak testing performed on the Pathfinder Canister annually. Also note that if maintenance or repair is performed that may affect other parts of the containment system besides the seal, that a leak test of the affected components should be specified. Include the test methods, the test setup, and acceptance standard for the tests.

This information is needed to assure compliance with 10 CFR 71.51.

Response:

No annual leak test will be required. A positive pressure leak test of the closure seal will be made before each fuel shipment. The pressure drop test, to verify the O-ring sealing, will be performed per paragraph A.5.1 of ANSI N14.5-1997, "American National Standard for Radioactive Material – Leakage Tests on Package for Shipment." The acceptable leak rate is $1x10^{-3}$ atm cc/sec using a pressure drop test.

Section 4.5 provides a representative example of a test method and setup. If maintenance or repair is performed that affect other parts of the containment besides the seal, the weld test of the affected component will be performed per test method #A.5.9 of Annex A of ANSI N14.5-1997. The acceptable leak rate is $1x10^{-7}$ atm cc/sec. This information is added to Section 8.2.2.

Enclosure (2)

Manufacture data sheets for Zircar Alumina-Silica Blanket type ASB-2300

Zircar® FIBROUS CERAMICS

ALUMINA-SILICA BLANKET TYPE ASB-2300 & ASB-2600

GENERAL INFORMATION

ZIRCAR Alumina-Silica Blanket Type ASB-2300 & ASB-2600 are comprised of refractory ceramic fiber tightly needled into a blanket form. These lightweight forms exhibit superior handling strength, extremely low shot content and low thermal conductivity and are ideal as furnace insulation in sintering, heat treating and chemical process applications. **Type ASB-2300** is for use up to 1260°C(2300°F) and **Type ASB-2600** up to 1426°C(2600°F). Both varieties are available in various thicknesses and densities.

ZIRCAR Alumina-Silica Blankets contains no organic binders and will produce no smoke or odors when heated.

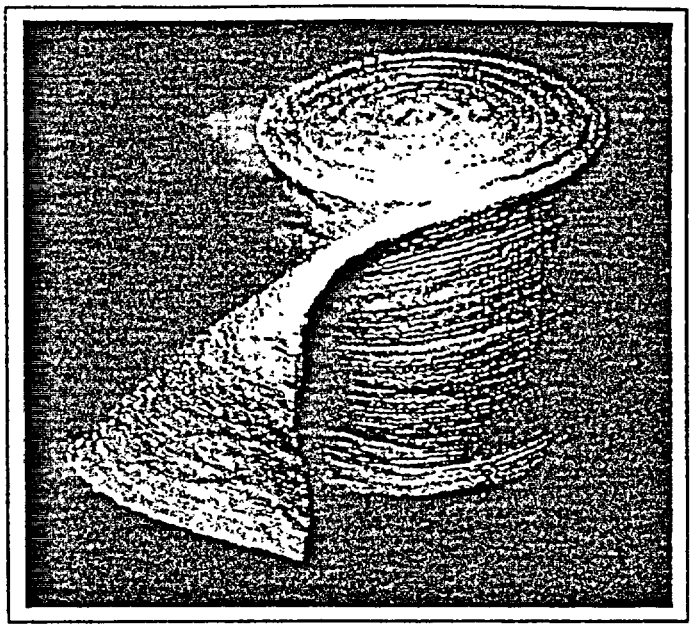

CHARACTERISTICS & PROPERTIES

Type,	ASB-2300	ASB-2600
Typical Composition, %		
Al_2O_3	47+	51+
SiO_2	49	47
Fe_2O_3	1	<.1
TiO_2	2	<.1
CaO	<.1	<.1
Na_2O	<.1	.1
MgO	<.1	<.1
Color,		
Maximum Use Temp*,C(F)	1260(2300)	1426(2600)
Fiber Length, in.	3 - 5	4 - 7

	ASB-2300	ASB-2600
Fiber Diameter, microns	8	6
Fiber Specific Gravity, g/cc	2.64	2.76
Specific Heat,		
BTU/lb °F at 1100°C(2012°F)	.28	.28
Linear Shrinkage‡, %		
8 pcf blanket after 25 hrs at:		
982°C(1800°F)	1.2	-
1093°C(2000°F)	1.9	-
1260°C(2300°F)	3.3	2.1
1315°C(2400°F)	-	2.6
1426°C(2600°F)	-	5.1

Bulk Density	4 pcf	6 pcf	8 pcf	10 pcf
Thermal Conductivity**, W/m °K(BTU/hr ft² °F/in)				
260°C(500°F)	.08(.56)	.06(.45)	.05(.39)	-
538°C(1000°F)	.15(1.13)	.13(.94)	.11(.78)	.10(.73)
816°C(1500°F)	.28(1.96)	.24(1.70)	.18(1.31)	.16(1.17)
1093°C(2000°F)	-	.40(2.80)	.29(2.02)	.24(1.72)

* Maximum use temperature is dependent on variables such as stresses, both thermal and mechanical, and the chemical environment that the material experiences.
** Properties expressed parallel to thickness
‡ Properties expressed perpendicular to thickness.

ZIRCAR Products, Inc.
PO BOX 458, FLORIDA, NY 10921-0458
Tele: (914)-651-4481, Fax: (914)-651-3192
e-mail: sales@zircar.com
Home page: http://www.zircar.com

Technical Data
Bulletin No. ZPI-407
April, 1998
img0240.doc

ALUMINA-SILICA BLANKET TYPE ASB-2300 & ASB-2600

SUGGESTED APPLICATIONS

- ZIRCAR Alumina-Silica Blankets are used for furnace and kiln insulation and door seals.
- ZIRCAR Alumina-Silica Blankets are used for heat shielding.
- ZIRCAR Alumina-Silica Blankets are used for trough and ladle cover insulation.
- ZIRCAR Alumina-Silica Blankets are used for duct insulation.

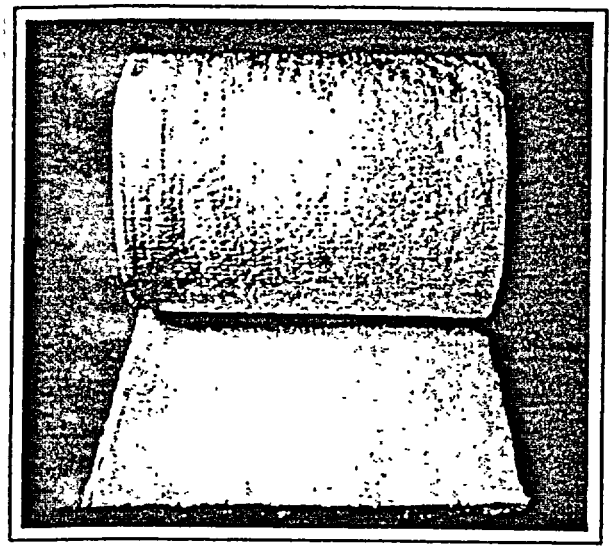

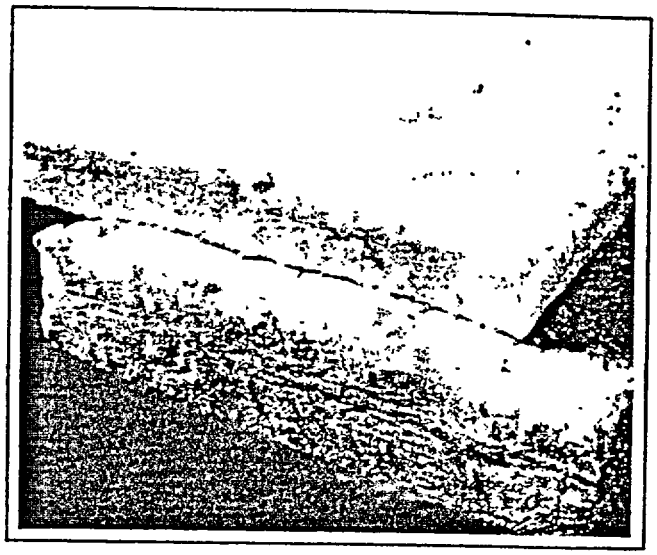

AVAILABILITY

STANDARD BLANKET:	ITEM #	DESCRIPTION
	D3110	ASB-2300 6 PCF 24" X 25' X 1"
	D3120	ASB-2300 6 PCF 24" X 12.5' X 2"*
	D3130	ASB-2300 8 PCF 24" X 25' X 1"
	D3140	ASB-2300 8 PCF 24" X 12.5' X 2"
	D3150	ASB-2600 8 PCF 24" X 25' X 1"
	D3160	ASB-2600 8 PCF 24" X 12.5' X 2"

- **Bold item listings** are normally stocked for immediate delivery.
- ZIRCAR Alumina-Silica Blankets are available in custom sizes. Type ASB-2300 can be produced in 4, 6, 8 and 10 pcf from 1/2" up to 2"* in up to a 48" roll width. Type ASB-2600 is available in 6, 8, and 10 pcf from 1" up to 2"* in up to a 48" roll width. Please contact ZIRCAR with your requirements.

  * ASB-2300 in 4 pcf is only available 1" & 2" thicknesses and 10 pcf in a 1" thickness. ASB-2600 10 pcf is only available in a 1" thickness.

TO ORDER:

STANDARD BLANKET:
SPECIFY: Quantity, Item # and Description. Example 25 each, Item # D3160, ASB-2600 8 PCF 24" X 12.5' X 2".

CUSTOM BLANKET:
SPECIFY: Quantity, and Description. Example 50 each, ASB-2600 10 PCF 24" X 12.5' X 1".

Zircar® FIBROUS CERAMICS

ZIRCAR Products, Inc.
PO BOX 458, FLORIDA, NY 10921-0458
Tele: (914)-651-4481, Fax: (914)-651-3192
e-mail: sales@zircar.com
Home page: http://www.zircar.com

Enclosure (3)

Measurements of Gas Velocities and Temperatures in a Large Open Pool Fire, Heat and Mass Transfer in Fire

MEASUREMENTS OF GAS VELOCITIES AND TEMPERATURES IN A LARGE OPEN POOL FIRE

M. E. Schneider and L. A. Kent
Thermal Test and Analysis Division
Sandia National Laboratories
Albuquerque, New Mexico

ABSTRACT

There is an interest in determining the response and survivability of a variety of items subject to engulfment in a large fire which may occur in a transportation accident. In order to estimate this response, knowledge of the thermal and flow conditions prevailing in these pool fires is required. Few experiments have been performed with large (>3 meter diameter) fires. In particular, velocity measurements in the continuous flame region of low Froude number fires are very scarce. Scaling up the results of small pool fires is problematic due to the large number of relevant dimensionless variables to be matched.

A total of ~ 48,500 liters of JP-4 fuel was burned in a 9x18 meter pool, producing peak temperatures in excess of 1230 °C (2250 °F), over much of the instrumented region of the flame. Temperatures were measured at 28 locations throughout the continuous flame region with 1.587 mm OD Inconel sheathed, ungrounded, type K thermocouples. Four 0.127 mm diameter bare wire thermocouples were used to make high frequency response temperature measurements. Velocities were measured at four vertical stations near the centerline of the pool, with glass coated, velocity probes. Heat fluxes were estimated from measurements on and near vertically suspended mild steel plates.

As is often the case in fires of this size, the effects of mild ambient winds on the measurements were pronounced. Attempts have been made to mitigate these effects by the application of conditional sampling. Temperatures are compared with measurements made in other large aviation fuel fires. The measured velocities are slightly less than would be predicted from an empirical model that was developed from experimental results for methane diffusion flames that are orders of magnitude smaller.

This test program was funded by the Department of Energy (DOE) and was directed by the Transportation Technology Center at Sandia National Laboratories. Sandia National Laboratories is operated by AT&T Technologies for the U.S. Department of Energy (DOE) under Contract DE-AC04-76DP00789

NOMENCLATURE

A	-	Pool surface area [m^2]
C	-	Calibration constant (near 1.00)
$C_{p,\infty}$	-	Specific heat of ambient air [J/kg °K]
D	-	Pool Diameter [m]
Fr_o	-	Froude number, W_o^2 / gD
g	-	Acceleration of gravity [m/s^2]
h	-	Convective heat transfer coefficient [W/m^2 °K]
$\dot{Q}$	-	Heat release rate [kW]
Q_c	-	Convective heat release rate [kW]
Q^*	-	Dimensionless heat release rate
Re_D	-	Reynolds number based on probe diameter
T_f	-	Flame temperature [°K]
T_s	-	Surface temperature [°K]
T_∞	-	Ambient temperature [°K]
W	-	Upward gas velocity [m/s]
W_o	-	Initial upward velocity [m/s]
z	-	Vertical distance [m]
z'	-	Scaled vertical distance
ΔP	-	Pressure difference [N/m^2]
ϵ	-	Emissivity
σ	-	Boltzmann constant [W/m^2 °K^4]
ρ	-	Gas density [kg/m^3]
ρ_∞	-	Ambient air density [kg/m^3]

INTRODUCTION & LITERATURE REVIEW

In order to estimate the response of items in fires resulting from transportation accidents, an understanding of the flow field and temperature distribution in such fires is crucial. Fires resulting from transportation accidents are most often due to the spillage and ignition of hydrocarbon fuels. There is interest in improving the understanding of large turbulent fires resulting from such spills.

It is quite difficult and expensive to perform experiments at full scale; the question of scaling must therefore be addressed. It would be desirable to perform tests with smaller fires, if the results can be scaled up to the sizes of typical accidental fires. Much work has been done investigating the problem of scaling fires. A number of considerations are pertinent when comparing fires:

- Is the fire's flowfield dominated by buoyancy or momentum forces ?
- Is the burning rate determined by radiation or convection of the flame's heat back to the pool surface ?
- What fraction of the radiation from the flame region escapes to the ambient ?
- Is the flow laminar or turbulent ?

The question of buoyancy vs. momentum domination will be addressed first. The available literature indicates that a number of different flow regimes are possible. If the velocity of fuel vapor is high at the pool surface, or if a jet of gaseous fuel is being burned, the initial jet momentum will control the fluid mechanics. As the jet velocity is lowered the transition between momentum dominated flow and buoyancy dominated flow starts above the flame tip and moves down toward the burning surface, or jet exit. At very low exit velocities, the flow is buoyancy dominated from the start. This buoyancy domination is commonly the case with pool fires, due to the low initial velocities near the pool surface. The entrainment rate of ambient air into the fire plume is quite different for buoyancy controlled flames than for momentum dominated flames. The exit velocity to buoyancy ratio is related to the heat release per unit area. Zukoski [1], defines a dimensionless heat release, Q^*, which can be used to determine the expected behavior of a buoyant fire. The definition is :

$$Q^* = \frac{\dot{Q}}{\rho_\infty C_{p\infty} T_\infty \sqrt{gD}\, D^2} \qquad (1)$$

Other studies have used the Froude number to perform similar analyses. The Froude number is based on the initial velocity, W_o, and is given by : $Fr = W_o^2/gD$. It should be noted that Q^* is proportional to the square root of the Froude number. The flow can be divided into three flame regimes. The flame may be totally dominated by momentum, it may switch from momentum domination to buoyancy domination at some height, or it may be totally buoyancy driven. Zukoski splits the buoyancy driven flames into two regimes, one where the flame height is a function of fire diameter, and one in which individual flamelets of fixed height determine the total flame height independent of pool size. The buoyancy starts to play some role near the upper portion of the flame for $Q^* \approx 10000$. When $Q^* \approx 100$ the buoyancy has influence even at the pool surface, (burner exit). A transition is observed at $Q^* \approx 0.3$ at which the flame breaks up into individual flamelets. It is expected that at this point it becomes very difficult for oxygen to be entrained to the pool center. Typical values of Q^* for large fuel spill fires range from 0.6 to 1.0. In scaling down the large open pool hydrocarbon fire, it is necessary to insure that Q^* is less than 1.

In buoyant diffusion flames with Q^* near 1, McCaffrey [2] has defined 3 fire zones based on the vertical distance scaled by the heat release rate. The scaling is meant to allow data at various heights from fires of different fuels to be compared. The scaled distance is given by : $z' = z/Q^{2/5}$. The region $z' < 0.08$ is referred to as the continuous flame region. The intermittent flame region is $0.08 < z' < 0.2$, with the upper portion, $z' > 0.2$, being the characteristic thermal plume region.

Another criterion for making comparisons between different fires is related to the heat transfer mechanism controlling the vaporization of fuel at the burning pool surface. Babrauskas [3], in a paper discussing the estimation of large pool fire burning rates, divides fires into 4 modes. The following table, which was excerpted from his paper, is based on the simplest assumptions. It relates the mechanism of heat transfer to the approximate size of the pool.

Diameter [m]	Burning Mode
< 0.05	laminar convection
0.05 - 0.2	turbulent convection
0.20 - 1.0	radiation, optically thin
> 1.0	radiation, optically thick

Thus when comparing features of fires which may be effected by the heat transfer mode, it is likely that the fires should be greater than one meter in diameter in order that this feature of large fires is duplicated.

The diffusion limited burning of hydrocarbon fuels results in the production of large amounts of soot. This soot strongly affects the radiative properties of the flame. Two effects are present:

- The soot causes the flame to be luminous, allowing radiation losses from the glowing soot to the ambient.
- In contrast to small luminous flames, optical paths are short compared to the flame thickness, thus energy from the center of the flame cannot easily escape.

Typical mean optical paths in these fires are near $1\ m^{-1}$ (Longenbaugh [4]). This implies that in a large fire, $D >> 1$ m, much of the energy in the flame zone cannot be radiated out to the ambient. This leads to a situation, listed in the table above as "radiation, optically thick", in which the fuel surface can no longer see the ambient conditions. It also is expected that this will lead to higher temperatures. Thus, higher buoyancy forces prevail in the flame zone in these large fires in contrast to smaller luminous flames. This effect is difficult, if not impossible, to reproduce in smaller combustion experiments.

It should be noted that the optical thickness of the fire should be considered when examining thermocouple measurements in flames. In a small fire, the hot thermocouple radiates to the cool ambient. With large sooty fires, the thermocouple may not give the exact local temperature, but the error mentioned above is smaller because the thermocouple may only interact radiatively with hot combustion gases and soot within a few optical paths of it's location.

With the above information, it is clear that great care must be taken in extrapolating results for small fires to larger scales. The measurements of velocity and temperature made in the current study have been compared with the results of other measurements. Table 1 lists references in which velocity measurements have been made in low Froude number fires, of medium to

large area. The table lists the fuel type, pool size, estimated convective heat flux, heat flux per unit area, and value of Q^*. The measurements made in the current study were all within the continuous flame region, $z/Q^{2/5} < 0.08$, therefore, the range of vertical station locations is also listed in both dimensional and scaled forms.

The measurements of Cox and Chitty [5,6], and McCaffrey [2], were made with methane burner flames which are not highly luminous, however, the gas flow was very slow, giving values of Q^* comparable to large fires. The Raj paper [7] refers to experiments performed by NASA/White Sands. This work is also referenced as Johnson et al [8], and as Harsha et al [9]. Raj reports the velocity only at a single station above a JP-4 fire which lasts less than 4 minutes. Heskestad [10], has reported velocity measurements above a 0.29 m methanol fire. The only velocity measurements other than Raj made near pool fires greater than 1 meter in diameter were those of Kung and Stavrianidis [11]. This data was for various liquid fuels burning in pools ranging from 1.2 to 2.4 meters in diameter. Unfortunately, very few velocity measurements were made in the continuous flame zone in this work; most of the measurements are made in the intermittent region. Comparisons of these studies with the present results will be made in the results section of this paper.

Table 2 lists studies in which temperatures have been measured in large aviation fuel fires. The list is in order by pool surface area. The largest fires were the three huge tests by Yamaguchi and Wakasa [12] in which pool diameters range from 30 to 80 meters. Unfortunately, the results of these tests have only been made available in very sketchy form. Some studies have been left out of the table due to the presence of thermally massive test units in the fire near the thermocouples, and the possibility of these units causing changes in the thermal and flow fields near the point of measurement. All the fuels have similar heat release rates; so the value of burning rate has replaced the heat release rate in the table.

EXPERIMENTAL APPARATUS

This paper describes a test which was performed to evaluate a hazardous material shipping container. The test, performed February 26, 1986, involved the burning of approximately 48,500 liters of JP-4 fuel in a 9x18 meter pool. The test unit was 3.97 meters long by 2.44 meters wide by 2.74 meters in height, and was supported such that its' lower surface was 1.8 meters above the floor of the pool. In addition to measurements made within the test unit, measurements were made to help characterize the open pool fire environment. The discussion in this paper centers on these measurements. Figure 1 is a top view of the instrumentation in the pool. The instrumentation of primary interest involves the east tower and the plate calorimeter. A list of the instrumentation locations to be discussed is shown in Table 3.

A diagram of the location of measurement stations on the east tower is included as Figure 2. There were eight standard, ungrounded, 1.587 mm OD Inconel sheathed thermocouples protruding about 0.1 meter from the insulated, water cooled instrumentation tower at the locations listed in the figure. In order to make measurements of temperature with higher frequency response, smaller thermocouples were also used. Four bare junction thermocouples were used in this test. The thermocouples were type K, chromel-alumel, with a diameter of 127 μm. 20 gauge chromel and alumel wires were routed from the water cooled support tower to the measurement point through a 6.35 mm diameter ceramic rod 0.45 meter in length. The fine thermocouple wires were welded to the 20 gauge supporting wires, and butt welded together to form the measurement junction. Previous experience with this type of thermocouple indicates that mechanical failure occurs within minutes unless some protective measures are taken. In this case, a thin sol-gel glass coating (Brinker & Reed [19]) was applied to the fine wires which allowed measurements to be acquired over the entire 45 minute test. These thermocouples were placed at 0.152 meter intervals as is also indicated in Figure 2 and Table 3.

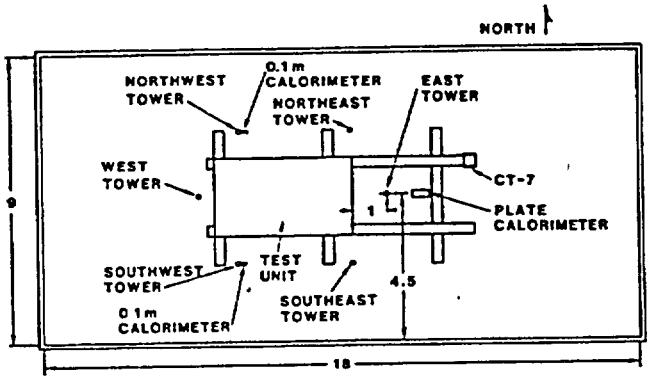

Figure 1 Open Pool Fire Test Facility
(Dimensions in meters)

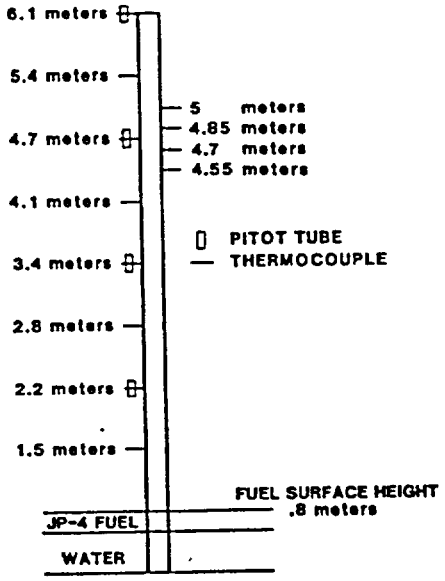

Figure 2. East Tower Instrumentation Scheme

The measurement of velocity above pool fires has been wrought with difficulties. Typical velocities are low, and the gas density is also low, thus the need for a very sensitive instrument exists. The fire environment is very harsh. The design of a sensitive probe which is durable has been problematic. A durable bidirectional, low-velocity probe, which is somewhat insensitive to changes in flow direction, was selected to measure the velocity in the fire plume. The design

is basically that of McCaffrey and Heskestad [20]. The only modifications were the addition of ruggedizing features, and a change in size. The probe is a device measuring, approximately, the difference between static and dynamic pressures, and using the Bernoulli relation to relate the measured pressure difference to fluid velocity.

$$W = \left[\frac{\Delta P}{\frac{1}{2} \rho C^2} \right]^{\frac{1}{2}} \qquad (2)$$

The four probes were manufactured from AISI 304 stainless steel. This material deteriorates under the conditions encountered in a large pool fire. In order to prevent deterioration, the probes were coated with sol-gel/glass powder film and the pressure sensing lines were water cooled and insulated. More specific details regarding the probe design and calibration can be found in Kent, et al. [21]. The probes were mounted on the 6 meter water cooled east tower as indicated in Figure 2. The sheathed thermocouples placed near each velocity probe measured the temperature of the gas near the probe. These temperatures were used in calculating the density of the fire products which in turn was used to calculate flame velocities. The pressure differences in inches of water were detected by electronic manometers (Airflow Developments Limited Model EDM 2500E).

Due east of the east tower on the long pool axis, a two sided mild steel panel calorimeter was mounted on an A-frame assembly. Each panel was 3.05 meters high by 0.61 meter wide. The bottom of the calorimeter was placed 2.13 meters above the pool floor. The south facing side was 6.35 mm thick, and the north side was 1.02 mm in thickness. The inside of this box was filled with insulation. The backface temperature measurements were made with intrinsic junction thermocouples at different heights along the centerlines of each of the two plates. Table 3 indicates the vertical placement of the measurement stations. An attempt to measure flame temperatures near the thicker south panel was also made. Sheathed thermocouples which protruded about 0.1 meter directly out from the centerline into the flames were installed at a number of vertical stations. Table 3, again, gives the exact placements.

The wind speed and direction were monitored with a propeller type anemometer located about 45 meters west of the pool at a height of about 3 m. A pressure transducer was used to record the fuel recession rate. This transducer was tapped into a 50 mm pipe that ran from the bottom of the west end of the pool to a sight glass located ≈45 meters away.

EXPERIMENTAL PROCEDURE

The ignition was performed at a single point in the northwest corner of the pool with an electric spark. Full engulfment of all instrumentation and the test unit occurred within 20 seconds. Data was gathered from the instrumentation using two systems. Temperatures from the thin plate calorimeter were measured with intrinsic thermocouples and logged on analog tape at a recording speed of 15 inches per second, with a Honeywell model 101 recorder. This data was digitized over 40 minutes of the fire at 40 samples per second and decimated down to 1000 data points. The same Honeywell tape recorder was used to record the signals from the bare wire thermocouples. In both cases it was necessary to amplify each thermocouple output with an Analog Devices thermocouple amplifier, AD595. The remaining data was acquired at six second intervals with an HP mini-computer and an HP 3497A data acquisition/control unit.

DATA REDUCTION AND UNCERTAINTIES

The signals from the thermocouples were converted to temperature using the standard type K curvefit equation. It should be noted that the flame temperatures reported here have not been corrected for radiation errors or compensated in any way. It is expected that when the thermocouple is surrounded by flames of depths greater than one meter, the errors due to radiation are small. There is concern when the thermocouple is not in a uniform temperature environment, but can see regions of widely varying temperatures. Thermocouples near the pool surface can see the pool, causing them to report temperatures lower than the actual local gas temperature.

Thermocouples near the test unit are affected by the presence of the test unit; errors of this type have been investigated by J. J. Gregory, et al. [22]. It should be noted that the test unit has a thin (~ 1 mm) stainless steel skin with insulation inside. Thus it is expected that the outer temperature responds fairly rapidly (within minutes) to the flame temperatures. Temperatures measured near the flame boundary, but in the ambient air, are expected to read high due to radiation coming from the flames. In this case, the errors are positive due to the low absorption of radiation by the ambient air. Typical time constants for the 1.58 mm diameter thermocouples used here range from 1 to 4 seconds depending on the local gas velocities and temperatures. Typical uncertainties in measured flame temperatures, considering only the thermocouples and measurement system, were ± 8°C.

The velocity probes were calibrated in a low speed wind tunnel for Reynolds numbers (based on probe diameter) from 300 to 3900, and tilt angles of 5 to 50 degrees. High uncertainties were present for Re_D less than 600. The probe Reynolds numbers, calculated from measured temperature and velocity histories, range from 700 to 2000. Thus all probes were operating in the range of low uncertainty. Typical uncertainty values for the calculated velocities, based on uncertainties in the pressure and temperature measurements, were estimated to be ± 0.7 meters/sec.

The density used in the calculation of velocity from the pressure difference is that of air at the measured temperature. This could lead to errors in the lower flame region where it is expected that significant fractions of unburned fuel vapor may be present. This factor was not included in the previous uncertainty estimate.

EXPERIMENTAL RESULTS AND DISCUSSION

Temperatures on Towers

The temperatures on the five towers were averaged over the test. This average was calculated from a start time, 20 seconds after ignition, to a final time near the end of the test, 2630 seconds after ignition. Figure 3 shows the average temperature versus distance from the pool floor for each of these towers. The standard deviations in temperature were also calculated and are plotted in Figure 4. At the higher stations, the wind more easily blows the flames away from the towers thus the variations in temperature become more pronounced.

Figure 5 shows a typical temperature history at a 6.1 meter station (east tower). The effects of wind on the temperature history are quite pronounced at this height. The low temperature dips were found to correspond to times when the tower tip was visible, uncovered by flame, and times which the wind measurements commonly indicated a strong component of wind blowing from the south. The probability density

function (pdf) of temperature measurements at the higher stations was examined, and found to be bimodal in shape. One mode at low temperatures corresponding with data taken when wind effects were strong, and the other mode at higher temperatures corresponding to the case when the instrumentation was fully covered with flame. The shape of the pdf's varied slightly from tower to tower, but all data including that taken from the small bare wire thermocouples showed a bimodal distribution of temperatures. A bimodal gaussian curve was fit to the sum of all pdf's from upper stations and the local minimum temperature was chosen as a setpoint temperature. In the current test this temperature was calculated to be 614 °C. Table 4 includes information about the bimodal curvefit coefficients calculated for thermocouple data mentioned above. A signal was generated from the temperature history at the 6.1 meter height for each tower, which was high when the temperature was above the setpoint, and low when the temperature was below the setpoint. This corresponds to a signal representing the "presence" or "absence" of flames at the 6.1 meter level. The correspondence is not exact; however, this is a simple starting place to help in examining the fire data with an attempt to account for the variability in wind effects.

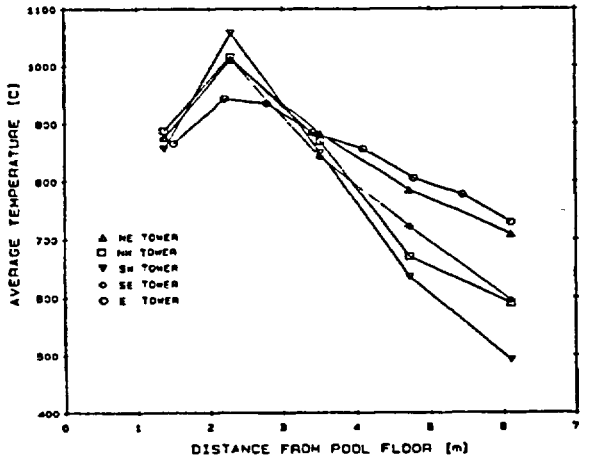

Figure 3 Average Flame Temperature (5 Towers)

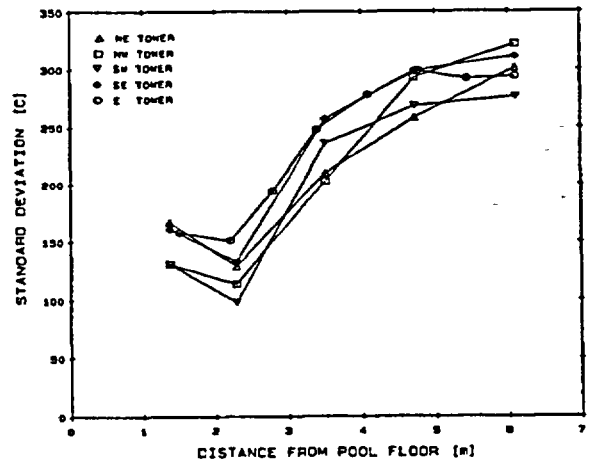

Figure 4 Standard Deviations in Temperature

Table 5 shows the correlation between thermocouples at various heights measured on the east, centrally located, tower. Temperatures along a tower were found to correlate quite strongly with each other near the top of the tower. The correlation degrades as the pool surface is approached. One interesting result is the reversal in correlation coefficient between the lowest and the upper stations. This implies that the wind which causes the temperatures at high stations to decline, is increasing temperatures near the pool surface. This negative correlation coefficient was found for data from all five tower locations.

Average temperatures were calculated for each thermocouple on the east tower based on data points taken when the "flame present at 6.1 meters" signal was high. Similar averages were calculated for the reverse condition. The averages for the other towers were calculated using the same procedures, the conditioning signal again generated for each tower from the temperature history at the top station. All of these averages are presented in Table 6. The averages during the times of low wind, which are the "flame present" averages, show a maximum temperature at approximately 4-5 meters above the pool floor, (3-4 meters above the fuel surface), and a significant decrease at the lowest stations. The maximum average temperature during flame present state is in a range from 950-1100 °C for all five towers. The flame absent averages look similar in shape to the averages with no conditioning, however the spread is smaller from tower to tower with the maximum difference being about 100°C at high stations.

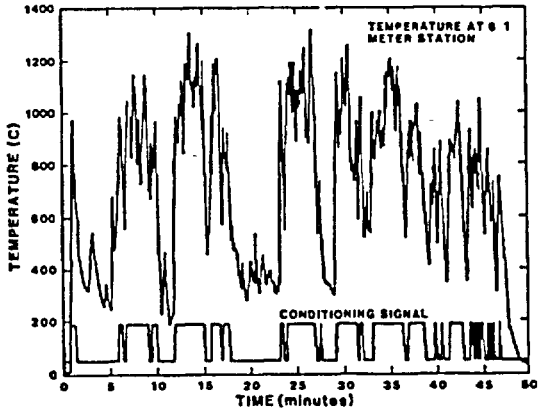

Figure 5. Temperature History at the 6.1 Meter Station and Conditioning Signal

Using the idea of conditioning allows the calculation of some other statistics which may reveal something about the nature of wind effects. The conditioning signal shown in Figure 5, can be described by two parameters: the fraction of time during the fire when the signal is high, and the typical frequency at which the signal flips back and forth. These two numbers were calculated for each of the five towers. The fraction of the time during which the flame is present will be defined as the flame intermittency. The intermittency gives some information as to the relative strength of wind effects on each tower. The typical durations of flame "presence/absence" lends some information about the time scales over which these wind effects act. This time scale data, it should be noted, may be strongly affected by the sampling rate and the time constant of the thermocouples used. The frequencies measured by looking at the intermittency signals here are likely to correspond to low frequency fluctuations in gross wind speed and direction. Table 7

lists the flame intermittency and typical flame duration times for each of the five towers. The strongest wind effects are present in the southwest corner of the pool, as was expected from the prevailing winds. The lowest wind effects, corresponding to the highest flame present fraction were found at the east tower. This condition is expected for a centrally situated tower that is less vulnerable to wind effects.

The bare wire thermocouple data was closely examined and two main conclusions were drawn. First, the temperatures reported by a bare wire thermocouple and a sheathed thermocouple near each other were very similar. This indicates that the local gas temperature must be fairly near the temperatures reported due to the difference in the radiative/convective partitioning between the two sizes of thermocouples. Secondly, it was observed that the flame present fluctuations were larger for the bare wire measurements than for standard sheathed thermocouples when both data sets were conditioned by the same signal (the conditioning signal derived from sheathed thermocouple data at the uppermost station). Table 8 shows the values of average and conditional average temperatures from the bare wire and sheathed thermocouple data. All the data presented in the table is for instrumentation located on the east tower.

Figure 6 compares the flame present data with results from the fires of Johnson, et al. [8], Bader [14], and Canfield and Russell [18]. In all of these investigations the averages are available over time periods when the wind effects are expected to be small, or the entire test took place in extremely mild wind conditions. In the case of Bader, it is expected that the use of thermally massive thermocouples also helped in reducing wind effects. Other studies listed in Table 2 which are not included in this comparison show clear effects of wind either in the test descriptions, or in the plots of flame temperature histories, and only report average values over the entire test. For examples, see Figure 3 in Gordon & McMillan [15], and Figure 3 in ...er, et al. [13]. Hagglund mentions the presence of 4 m/s winds and "large temperature variations within the flames". In contrast, Russell [17,18] states that "temporal mean quantities are applicable only to the quasi-steady burning interval of the test flames as they exist in a quiescent atmosphere".

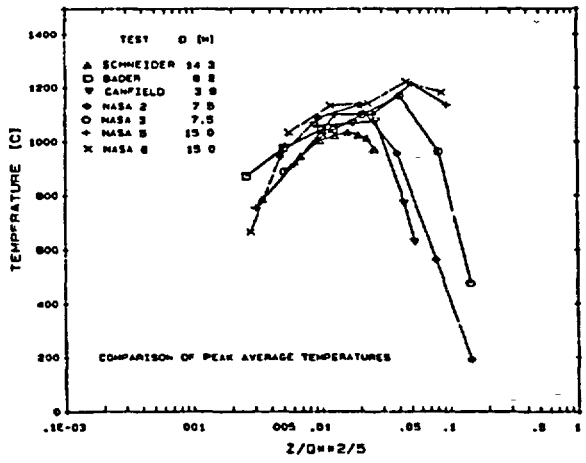

Figure 6. Temperature — Comparison with Literature

The data from Johnson is labeled "NASA #", where the # specifies his fire test number. An equivalent pool diameter is used in the figure for non-circular pools. That is the diameter of a round pool having the same surface area as the non-circular test pool. The actual pool shapes and sizes can be found in Table 2. The fires reported by Johnson showed strong decreases in temperature along the centerline compared with temperatures measured at slightly off center radial positions. These short tests were run under wind conditions of 0.08 m/s wind (tests 5 & 6), 0.22 m/s winds (test 3), and 0.44 m/s winds (test 2). The data plotted here is maximum average temperature reported at a given height. The low centerline temperatures were not observed in the present case and symmetry was not expected to be very good due to the presence of the test unit in the fire. It is expected that for these reasons the current data is more easily compared with maximum average temperatures. In general the curves agree in the lower continuous flame region and disagreement becomes quite pronounced as the intermittent flame region is approached. This is in part due to increasing sensitivity to differences in wind conditions in conjunction with averaging problems arising from the natural flame intermittency anticipated at these higher stations.

Gas Velocities on the East Tower

The velocity history for each probe station is shown in Figure 7. The large fluctuations in the velocities are primarily due to wind effects. Table 9 indicates the correlation between temperature and velocities measured at various vertical stations on the tower near the pool centerline. Note the strong correlation between velocity and temperature. It is not known how strong the correlation would be if only the flame present state was examined.

The velocity and temperature data was conditioned with the same signal. The average and conditioned average velocities are presented in Table 6. As previously mentioned the velocities during flame presence are significantly higher than those during flame absence.

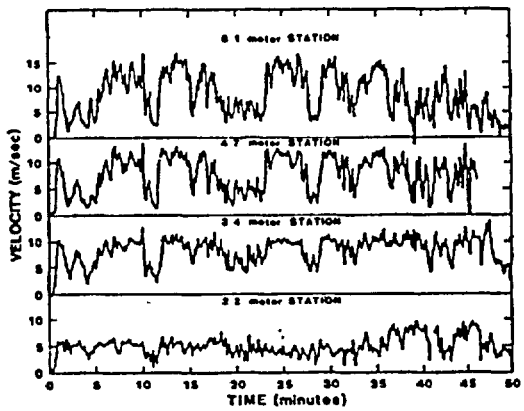

Figure 7. Velocity History at Each Station

Figure 8 compares the average measured velocities during the "flame present" state with the mean centerline velocity data for a number of much smaller fires. The vertical distance, z, has been scaled in a way which normalizes the flame height with the thermal

power of the fire. The data of McCaffrey [2] includes a large number of points with very little spread. In the figure, these points have been represented with a single line. The data of Cox and Chitty is in very good agreement with the data from McCaffrey. For this reason, only a single line is used. From a review of Table 1, it can be seen that the data of Kung and Stavrianidis is not in the same region of the flame as the current results; thus these data have not been included in Figure 8.

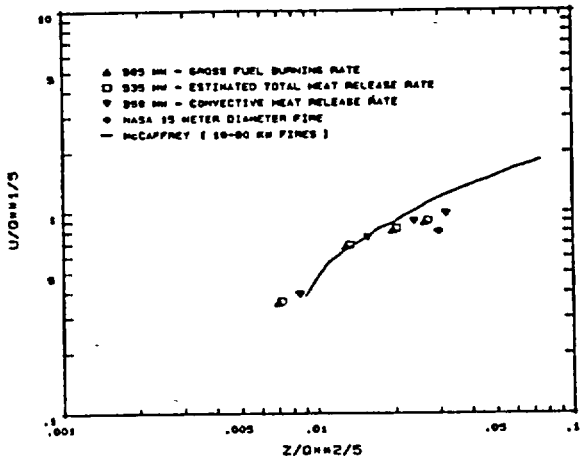

Figure 8. Velocity — Comparison with Literature

McCaffrey defines three zones in the fire: flame, intermittent flame and plume. The point $z/Q^{2/5} = 0.08$ is the end of the continuous flame region, $z/Q^{2/5} = 0.20$ is the end of the intermittent flame region. The vertical velocity was found to vary according to the relation of equation 3:

$$\frac{W}{Q^{1/5}} = 6.83 \left[\frac{z}{Q^{2/5}} \right]^{1/2} \qquad (3)$$

in the continuous flame region. The value of Q used in equation 3 by McCaffrey was the estimated total heat release. In McCaffrey's work, the flames studied were methane flames which were not highly luminous. In this case the theoretical maximum heat release (from gross fuel consumption), the estimated total heat release (considering combustion efficiency), and the convective heat release, were very near the same values for a given flame. In the case of a sooty pool fire these values will differ considerably from each other. It is likely that only the convective heat released contributes to the buoyancy, and thus to vertical velocities. Due to the lack of velocity data from sooty pool fires, velocities for all three heat release rates are plotted in Figure 8. The single data point from the NASA fire, which was reported in the paper by Raj, has also been included in Figure 8.

Exterior Temperatures on the Plate Calorimeter

Nine thermocouples were placed with a 0.305 meter vertical spacing on the south (6.35 mm thickness) side of the large plate calorimeter. The thermocouples protruded 0.1 meter from the plate into the flames. The average temperature over the time of the fire was calculated from the temperature histories for these thermocouples. Conditional sampling similar to that used with the tower thermocouples was used to calculate conditional averages. The conditional signal was generated from the uppermost temperature. When this temperature was above the setpoint value, the flame present condition was assumed. Averages for each of the nine thermocouples were calculated using this conditioning signal generated from the top station. These averages are listed along with the average temperatures over the entire test in Table 10.

The flame absent average temperatures, external to the plate, follow the flame absent average tower temperatures in Table 6 very closely. The flame present and entire test average temperature curves show the same general trends as have been described for the tower data, however the values are ≈40°C higher. This may be due to some attenuation of the wind effects by the presence of the nearby plate.

The average fire temperature during the flame present state was relatively constant with height, with a value of ~1065°C. The temperature histories of these thermocouples, though not included here, look very similar to the east tower temperature histories.

Results from the Thick Plate Calorimeter

The steel backface temperature data for the 2 stations on the 6.35 mm thick panel calorimeter are presented in Figure 9 along with 2 backface temperatures from the thin (1.02 mm thickness) walled calorimeter. The maximum thick wall backface temperature at any given time was at the lowest, 2.5 meter, station with the temperature decreasing with elevation. The maximum temperature difference between the 2.5 and 5 meter stations was 330°C.

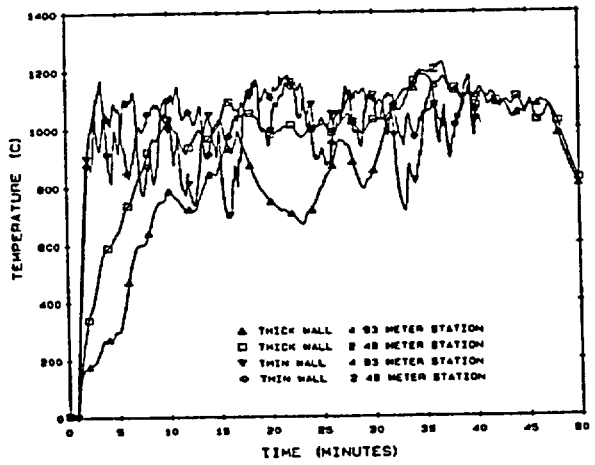

Figure 9. Calorimeter Backface Temperature Histories

Figure 10 shows a plot of typical results obtained from the thick walled calorimeter. The plot indicates the flame and plate temperatures which were measured at the uppermost, 4.93 meter, station. The Sandia One Dimensional Direct and Inverse Thermal Code, (SODDIT), was employed to estimate the plate surface temperatures and heat fluxes using only the plate backface temperature history, and the calorimeter material properties. The details of the code can be found in Blackwell, et al. [23], and more general theoretical considerations are referred to Beck, et al. [24]. The calculated surface temperature was near enough to the backface temperature at all times that plotting the two on the scale of Figure 10 would show no difference. Thus the plate temperature has been characterized in the figure as a single line labeled "plate temperature".

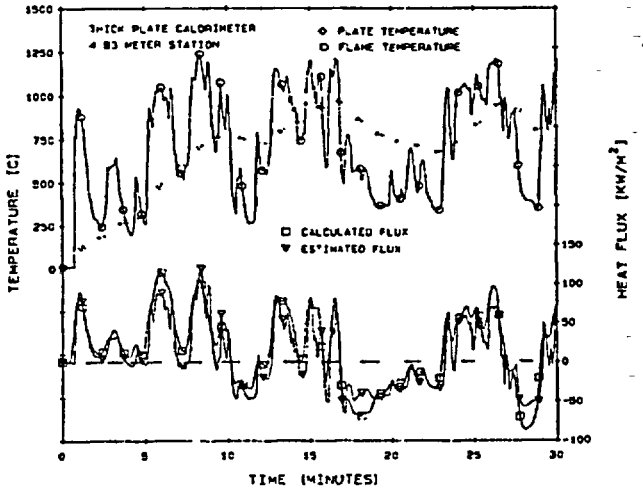

Figure 10 Heat Fluxes and Temperatures for Thick Plate Calorimeter

The calculated heat flux has also been plotted in the figure and is labeled as "Heat Flux Calculated". The assumption was made that the external thermocouple measurements were reasonably accurate representations of the flame temperatures and a simple model was used to estimate the expected flux given the surface and flame temperature histories. A simple equation for Q is:

$$Q_{est} = \sigma \epsilon (T_f^4 - T_s^4) + h (T_f - T_s) \qquad (4)$$

An estimate of h and ϵ were made utilizing a non-linear parameter estimation routine. The values of ϵ and h were assumed constant over the duration of the fire. For the case shown in the figure the values of h and ϵ found which minimize the least squares difference between the estimated Q and the calculated Q were:

$$\epsilon = .462 \qquad h = 39.11 \frac{W}{m^2 \cdot K}$$

The heat flux calculated using equation 4 and the above constants is shown in the Figure labeled "Estimated Flux". Note that the fit between the flux calculated by the inverse code and the flux estimated by equation 4 is fairly good. The partitioning of the heat flux between radiation and convection using the above assumptions will depend on the flame and surface temperatures; for a flame temperature of 1100°C and a surface temperature of 540°C this gives a radiant Q of 86 kW/m² and a convective Q of 22 kW/m². Thus, in this example the radiative fraction is about 80% of the total flux.

The heat flux histories for all the stations on the panel were calculated using the inverse code. From these histories and some simplistic assumptions about the mechanism of heat transfer, flame temperatures may be estimated. Peak fluxes to the calorimeter ranged from 80 - 120 kW/m². The effective flame temperatures for blackbody fluxes ranged from 815 - 930 °C. The theoretical convective/radiative partitioning for a flat plate was also estimated. The average convective contribution to the flux at a surface temperature of 150 °C would be ~5% for the entire length of the plate. For a given flame temperature, the convective flux would be higher at the lower stations and would decrease with height. Initially, the fluxes were highest at the lowest elevation and decreased with increasing elevation. This trend, however, reversed as the test continued.

The flame temperatures at the 2.5 meter station were, in general, higher and more uniform than the temperatures at the 5 meter station. The fluctuating nature of the fire that is seen for the flame temperature data is also exhibited in the heat flux to the plate. The large amplitude oscillations in flame temperature at the upper stations create oscillations in the heat flux that are larger in amplitude than those experienced at the lower stations.

Thin Plate Calorimeter

Temperatures were measured at 4 stations on the insulated backface of the thin walled (1.02 mm thickness) north side, of the large plate calorimeter. The stations are located at elevations which range from 2.5 meters to 5 meters above the pool floor.

The average values and standard deviations of the plate temperatures were calculated over the entire test ignoring the first 100 seconds of heat up data. These results are included in Table 10. The average temperature of the plate was higher than any flame temperature averages. It is expected that this is in part due to the fact that the plate faced north, and the prevailing winds were from the south or southwest. The standard deviation in the plate temperature was about half the standard deviation in flame temperatures at corresponding heights from the pool. This is due to the damping of thermal fluctuations by the plates' thermal mass.

Fuel Levels and Burn Rate

The fuel recession rate in this type of test is usually found in two ways. An average rate can be determined simply by dividing the total fuel consumed by the duration time of the test. Secondly, a pressure transducer can be used to determine the variation in recession rate during the test by recording the pressure in the pool. In this test a leak in the fuel delivery system caused some problems in the interpretation of the pressure transducer results, however the average burning rate could still be determined with good accuracy by the first method.

Initially, 0.61 meters of water was brought into the pool. In the 9.1 meter by 18.3 meter pool, a one millimeter height of liquid is 167 liters. 34,000 liters of fuel was then added to achieve a total burn time of approximately 30 minutes. This increased the total liquid level to 0.814 meters. This was verified by a tape measure located inside the pool. During the test, a leak in the fuel delivery system introduced additional fuel into the pool, thereby increasing the burn time to 46 minutes. A total of 48,460 ± 380 liters of fuel was brought into the pool. The average fuel recession rate was therefore calculated to be 6.29 ± 0.06 mm of fuel per minute. This is very consistent with previous burning rates in this pool.

Wind Speed Measurements

Figure 11 is a plot of the magnitude and components of the wind speed during the time of the test. On this plot ignition occurred at approximately 50 seconds, and the fire was out at a time of about 46 to 47 minutes. The mean wind speed over the time of the burn was 1.68 meters per second. The standard deviation from the mean value was 0.95 meters per second. The wind speed was seen to increase as the test progressed with the maximum value of 4.2 meters

per second occurring ~ 37 minutes into the test. The velocity components of the wind in the east/west, and the north/south directions were also computed and examined exhaustively for any connection with the intermittency. Though some correlation exists, it is expected that the fire influenced the flow field around it. The wind measurements needed to anticipate the flame's shape are much more extensive than those gathered in these tests.

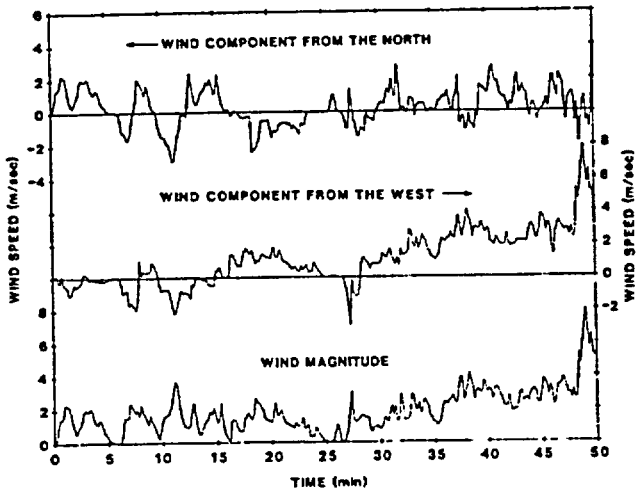

Figure 11 Wind Speed and Direction During Test

CONCLUSIONS

The measurements of gas velocity made in the lower continuous flame region in this study agree well with the data available from smaller fires. Velocity measurements at higher stations than those addressed here, (in the upper continuous flame and the intermittent flame region), in fires of this size have not been published to date. These measurements should be attempted to see if the agreement with small fires continues in this region.

Temperatures measured in this study have been compared with the results of others. Comparisons are difficult to make due to the lack of information in many cases about the existing winds, and the known strong wind effects. In spite of these difficulties, a scheme has been attempted which mitigates, to some degree, the effects of mild wind conditions. The average temperatures conditioned for times of low wind have been compared with results of other workers taken during times of "quasi-steady" burning and reasonable agreement was found at low stations ($z/Q^{2/5} < 0.02$).

The measurements of heat flux to a large vertical plate was reported. Some simple attempts at estimating the flux from measured surface and flame temperatures are also included.

ACKNOWLEDGEMENTS

The authors would like to acknowledge the effort and significant contributions of all those who participated in the planning and execution of this test. Our appreciation is extended to Ned Keltner, Julie Gregory, Bob Mata, Dan Luna, Bill Jacoby, and to any and all technical, millwright, and labor support whose work was instrumental in the performance of this test.

REFERENCES

1. Zukoski, E.E., "Fluid Dynamic Aspects of Room Fires", Proceedings of the First International Symposium on Fire Safety Science, pp. 1-30, 1986.
2. McCaffrey, B.J., "Purely Buoyant Diffusion Flames: Some Experimental Results," NBSIR 79-1910, National Bureau of Standards, 1979.
3. Babrauskas, V., "Estimating Large Pool Fire Burning Rates," *Fire Technology*, 19, No. 4, pp 251-261, 1983.
4. Longenbaugh, R.S., "Experimental and Theoretical Analysis of the Radiative Transfer Inside of a Sooty Pool Fire," M.S. Thesis, New Mexico State University, 1985.
5. Cox, G., and Chitty, R., "A Study of the Deterministic Properties of Unbounded Fire Plumes," *Combustion and Flame*, 39, pp. 191-209.
6. Cox, G., and Chitty, R., "Some Source Dependent Effects of Unbounded Fires," *Combustion and Flame*, Vol. 60, pp. 219-232.
7. Raj, P.K., "Analysis of JP-4 Fire Test Data and Development of a Simple Fire Model," ASME Paper Number 81-HT-17.
8. Johnson, H.T., Linley, L.J., and Mansfield, J.A., "Measurement of the Spacial Dependence of Temperature and Gas and Soot Concentrations Within Large Open Hydrocarbon Fuel Fires," NASA Technical Memorandum 58230, 1980.
9. Harsha, P.T., Bragg, W.N., and Edelman, R.B., "A Mathematical Model of a Large Open Fire," Science Applications Inc., NASA Contract Report # NAS2-10675. also NASA #SAI-81-026-CP
10. Heskestad, G., "Peak Gas Velocities and Flame Heights of Buoyancy-Controlled Turbulent Diffusion Flames," *Eighteenth Symposium (International) on Combustion*, pp. 951-959, The Combustion Institute.
11. Kung, H.C., and Stavrianidis, P., "Buoyant Plumes of Large-Scale Pool Fires," *Nineteenth Symposium (International) on Combustion*, pp 905-912, The Combustion Institute.
12. Yamaguchi, T., and Wakasa, K., "Oil Pool Fire Experiment," Proceedings of the First International Symposium on Fire Safety Science, pp. 911-918.
13. Alger, R.S., Corlett, R.C., Gordon, A.S., and Williams, F.A., "Some Aspects of Structures of Turbulent Pool Fires," *Fire Technology*, 15, pp. 142-156.
14. Bader, B.E., "Heat Transfer in Liquid Hydrocarbon Fuel Fires", *Chemical Engineering Progress Symposium Series*, Vol. 61, No. 56, pp. 78-90, 1965.
15. Gordon, W., and McMillan, R.D., "Temperature Distribution within Aircraft-Fuel Fires," *Fire Technology*, Feb. 1965, pp. 52-61.
16. Hagglund, B., "The heat radiation from Petroleum Fires," FoU-brand, pp. 18-24, 1977.
17. Russell, L.H., "Quantification of the Heat Transfer Parameters Relevant to a Cylinder Immersed in a Large Aviation Fuel Fire," M.S.M.E. Thesis, University of Pittsburgh, 1970.
18. Russell, L.H., and Canfield, J.A., "Experimental Measurement of Heat Transfer to a Cylinder Immersed in a Large Aviation-Fuel Fire", *J. Heat Transfer*, 95, p. 397, 1973.
19. Brinker, C.J., Reed, S.T., "Low Temperature Process for Obtaining Thin Glass Films", Sandia National Laboratories, Patent No. 4476156, October, 1984, Albuquerque, New Mexico.
20. McCaffrey, B.J., and Heskestad, G., "A Robust Bidirectional Low-Velocity Probe for Flame and Fire Application", *Combustion and Flame*, 26, pp. 125-127, 1974.

21. Kent, L.A., and Schneider, M.E., "The Design and Application of Bi-directional Velocity Probes for Measurements in Large Pool Fires," ISA Symposium, Las Vegas, NV, 1987.
22. Gregory, J.J., Mata, R. Jr., Keltner, N.R., "Thermal Measurements in a Series of Large Pool Fires", SAND 85-0196, Sandia National Laboratories, Albuquerque, New Mexico, 1987.
23. Blackwell, B.F., Douglas, R.W., "A Users Manual for the Sandia One-Dimensional Direct and Inverse Thermal Code", SAND85-2478, Sandia National Laboratories, Albuquerque, New Mexico, 1986.
24. Beck, J.V., Blackwell, B.F., St. Clair, C.R. Jr., Inverse Heat Conduction, John Wiley & Sons, 1985.
25. McCaffrey, B.J., "Momentum Implications for Buoyant Diffusion Flames," *Combustion and Flame*, 52, pp. 149-167.

Table 1 - Velocity Measurements in Low Froude Number Fires.

Author	Fuel	Pool Diameter [m]	Measurement Height [m]	Estimated Q_c [kW]	z/Q_c^{*4} [m/kW^{-4}]	Q_c/A [kW/m^2]	Q^*
Kung & Stavrianidis [11]	Heptane	1.219	1.26 - 8.88	2180	0.057 - 0.40	1870	1.2
	Heptane	1.737	1.26 - 8.88	4367	0.044 - 0.31	1840	1.0
	Methanol	2.438	1.26 - 8.88	1498	0.067 - 0.47	321	0.15
	Hydrocarbon #1	1.737	1.26 - 8.88	1546	0.067 - 0.47	652	0.35
Raj [7]	JP-4	15.24	5.73	348000	0.0348	1910	0.35
Cox & Chitty [5] & [6]	Methane	0.3 (square)	?	14 - 47	0.030 - 0.4	160 - 520	0.3 - 0.9
	Methane	0.45 (square)	?	45 - 120	?		
	Methane	0.60 (square)	?	45 - 120	?	127 - 327	0.13 - 0.28
McCaffrey [2]	Methane	0.30 (square)	.10 - 1.5	14.4 - 57.5	0.009 - 0.50	160 - 640	0.3
Heskestad [10]	Methanol	.29 (square)	?	30.77	?	366	0.45
Current	JP-4	9 x 18 (rect)	1.4 - 5.3	359000	0.0084 - 0.032	2216	0.42

$Q_c/Q_{theory} = 0.61$

Table 2 - Temperature Measurements in Aviation Fuel Fires.

Author	Fuel	Pool Diameter [m]	Measurement Height [m]	Burning Rate [mm/min]
Canfield & Russell [17]	JP-5	2.4 x 4.9 (rec)	.6,1.2,1.8,3.0,3.6	?
Alger [13] et. al.	JP-5	3.05	.01,.40,1.2	5.78±1.55
Johnson et. al [8]	JP-4	7.5	0.7,1.4,2.9,5.7,21.3	?
	JP-4	15.24	0.7,1.4,2.9,5.7,21.3	5.3
Bader [14]	JP-4	5.5 (square)	0.2,0.4,0.56,0.76,1.0,1.27	?
Gordon & McMillan [15]	JP-4 AvGas JP-5	3.6 x 7.3 (rec)	0.152 - 1.67	
Yamaguchi & Wakasa [12]	Kerosene	30,50,80	?	4.7
Hagglund[16]	JP-4	.5 - 10 (sq)	?	≈ 4.0
Current	JP-4	9 x 18 (rect)	1.4 - 5.3	6.29

Table 3 - Instrumentation Locations

Instrumentation	Vertical Distance from pool floor [m]
East tower - 1.59 mm CO Thermocouples	1.5, 2.21, 2.79, 3.4, 4.09, 4.78, 5.44, 6.1
East tower - 0.13 mm CO Thermocouples	4.55, 4.7, 4.85, 5.0
East tower - 25.4 mm CO Velocity probes	2.21, 3.4, 4.78, 6.1
TCs on insulated backface of Thick wall	On 0.30 centers from 2.44-4.84
TCs on insulated backface of Thin wall	On 0.81 centers from 2.44-4.88
TCs external to Thick Wall	On 0.30 centers from 2.44-4.84
Northeast tower thermocouples	1.37, 2.29, 3.51, 4.72, 6.1
Northwest tower thermocouples	1.37, 2.29, 3.51, 4.72, 6.1
Southeast tower thermocouples	1.37, 2.29, 3.51, 4.72, 6.1
Southwest tower thermocouples	1.37, 2.29, 3.51, 4.72, 6.1
Initial Fuel Level	0.81

Table 4 - Table of Bimodal Fit Coefficients

A probability density function of temperature was constructed from all temperatures measured at the 6.1 meter station from all 5 poles during the time of the fire. A curve was fit to the pdf of the form :

$$Y = a_1 e^{-\frac{1}{2}\left[\frac{T - T_{off1}}{\sigma_{t1}}\right]^2} + a_2 e^{-\frac{1}{2}\left[\frac{T - T_{off2}}{\sigma_{t2}}\right]^2}$$

Where Y is the number of temperatures measured within 7 °C of the temperature T. The values of the constants were found to be :

$a_1 = 29 \pm 1.62$ $\quad a_2 = 16 \pm 1.07$

$\sigma_{t1} = 112 \pm 8$ °C $\quad \sigma_{t2} = 252 \pm 28$ °C

$T_{off1} = 349 \pm 7.9$ °C $\quad T_{off2} = 911 \pm 22.5$ °C

Table 5 - Correlation between Temperatures on the East Tower

	Vertical Stations [meters]							
	6.10	5.44	4.78	4.09	3.40	2.79	2.21	1.50
6.10	1.00							
5.44	.98	1.00						
4.78	.91	.97	1.00					
4.09	.83	.90	.97	1.00				
3.40	.73	.80	.90	.95	1.00			
2.79	.52	.58	.69	.78	.92	1.00		
2.21	.15	.22	.34	.47	.67	.88	1.00	
1.50	-.53	-.54	-.49	-.39	-.19	.15	.52	1.00

Table 6 - Average Temperatures and Velocities

	Height [m]	Average	Std Dev	Flame Present	Flame Absent
Velocity [m/s]	6.10	9.5	4.1	12.6	6.0
	4.78	8.9	3.4	11.6	6.0
	3.40	8.2	2.2	9.6	6.6
	2.21	4.8	1.7	5.0	4.6
East Tower Temperatures [°C]	6.10	729	294	932	408
	5.44	777	292	979	457
	4.78	805	299	1000	496
	4.09	857	278	1020	598
	3.40	885	248	1012	684
	2.79	936	194	1004	828
	2.21	944	151	957	924
	1.50	866	158	798	975
SW Tower	6.10	492	276	959	369
	4.72	635	268	1034	530
	3.51	850	236	1131	776
	2.29	1057	98	1059	1057
	1.37	857	131	751	885
NW Tower	6.10	590	322	918	349
	4.72	670	293	969	450
	3.51	870	203	1046	740
	2.29	1016	114	1026	1008
	1.37	888	131	793	958
NE Tower	6.10	709	301	935	407
	4.72	785	258	954	558
	3.51	883	210	975	760
	2.29	1010	129	979	1051
	1.37	876	167	788	993
SE Tower	6.10	595	311	933	365
	4.72	722	299	1024	517
	3.51	842	257	1050	700
	2.29	1012	133	978	1035
	1.37	875	161	752	959

Table 7 - Flame Intermittency and Wind Frequencies

Tower	Flame Intermittency	Typical Time of Flame Presence [s]
SW	20.8 %	598
SE	40.5 %	414
E	61.3 %	270
NE	57.2 %	358
NW	42.4 %	538

Table 8 - Bare Wire Thermocouple Comparison

	Bare Wire (127 μm)	Sheathed TC
Height from pool floor	4.70 m	4.78 m
Average temperature	721.7 °C	786.7 °C
Standard Deviation	323.9 °C	310.5 °C
Flame present average	887.1 °C	1005.0 °C
F.P. Std. Deviation	256.9 °C	163.3 °C

Intermittency = 0.613; Averaged from 50-2750 Seconds;
Both signals subject to conditioning signal generated from 6.1 meter station sheathed thermocouple data.

Table 9 - Correlations with Velocities

	Velocity probe locations [meters]			
	6.10	4.78	3.40	2.21
Tower Temps [meters]				
6.10	.86	.89	.77	.13
5.44	.81	.89	.83	.24
4.78	.70	.82	.85	.33
4.09	.61	.75	.84	.37
3.40	.53	.66	.79	.33
2.79	.38	.47	.62	.24
2.21	.07	.14	.35	.21
1.50	-.38	-.48	-.43	-.24
Velocities [meters]				
6.10	1.00			
4.78	.93	1.00		
3.40	.68	.85	1.00	
2.21	-.05	.18	.53	1.00

Table 10 - Average Temperatures from plate calorimeter

Measurement	Height From Floor [Meters]	Average [°C]	Std. Dev. [°C]	Flame Present [°C]	Flame Absent [°C]
Temperatures External to Plate	4.93	846	303.1	1006	675
	4.62	855	294.3	1009	689
	4.31	886	275.3	1030	731
	4.01	902	262.1	1039	756
	3.71	920	242.9	1044	786
	3.40	942	221.8	1052	825
	3.10	964	198.1	1057	865
	2.79	984	174.4	1058	906
	2.49	1003	149.3	1050	953
Thin Plate Backface Temperatures	4.93	985	116.7		
	4.11	1015	109.1		
	3.30	1102	98.3		
	2.49	1044	74.9		

reprinted from

Heat and Mass Transfer in Fire — HTD-Vol. 73
Editors: A.K. Kulkarni, and Y. Jaluria
(Book No. H00392)

published by

THE AMERICAN SOCIETY OF MECHANICAL ENGINEERS
345 East 47th Street, New York, N.Y. 10017
Printed in U.S.A.

Enclosure (4)

Thermal Measurements in Large Pool Fires, Heat and Mass Transfer in Fire

THERMAL MEASUREMENTS IN LARGE POOL FIRES

J. J. Gregory, N. R. Keltner, and R. Mata, Jr.
Thermal Test and Analysis Division
Sandia National Laboratories
Albuquerque, New Mexico

ABSTRACT

During the summer of 1983, a series of pool fire tests was conducted in which the test item was a 1.4 m diameter, 6.4 m long, mild steel calorimeter with a mass of approximately 10,000 kg. The purpose of these tests was to study the thermal response of a large test item in a specified fire configuration, to define thermal boundary conditions, and to assess the repeatability of the fire environment. The calorimeter was used to simulate a nuclear waste transportation cask.

INTRODUCTION

There is an interest in determining the response and survivability of a variety of items when subjected to large fire which might occur in a transportation or petrochemical industry accident. Specifications for conducting simulated transportation accident tests are given by the U.S. Department of Transportation (DOT) [1] and the International Atomic Energy Agency (IAEA) [2].

The thermal environment in an actual large open pool fire is not well-defined. The highly turbulent nature of a large open pool fire and its susceptibility to winds produces flow and temperature fields that are very non-uniform in both space and time. Complete and representative theoretical models that describe the environment are not available.

The tests described in this paper involved a large cylindrical test item in a hydrocarbon pool fire configured along the guidelines of [1,2]. To address the question of the repeatability of the pool fire environment and provide empirical information that could aid in modelling it, three tests were performed using identical instrumentation. A large calorimeter was used to represent a physically large, thermally massive shipping cask. Complete details of this test program are given in [3].

TEST DESCRIPTION

The series of three half-hour tests was conducted in a 9.1 m by 18.3 m by 0.9 m deep concrete pool. The test item was a large calorimeter supported by a steel stand such that the bottom was 0.9 m above the initial level of the fuel in accordance with [1], and centered within the pool boundaries, its central axis aligned with the long side of the pool.

Each calorimeter was a 6.4 m long, 1.4 m O.D., A517 steel pipe with 3.2 cm thick walls. The calorimeters were fabricated from surplus pipe which already had 5 cm thick by 15 cm wide reinforcing ribs fillet welded to the outside of the pipe on 61 cm centers. At the ends of the pipe, 1.3 cm thick steel plates, referred to as the end caps, were bolted on to seal the interior of the pipe. Three layers of 2.5 cm thick Cerablanket insulation were installed against the inner wall of the pipe and against the inside of the end caps.

The east end of the calorimeter was 5.9 m from the east edge of the pool. Instrumentation was located at three axial stations in the calorimeter. Starting from the east end of the calorimeter, Station 1 was 0.46 m away, Station 2 was 2.82 m away, and Station 3 was 5.94 m away. Each station was centered between a pair of exterior ribs. At each axial station, there were four sensing locations on the interior of the pipe. Angular location 000 was on the underside of the calorimeter, then viewing from the east and moving clockwise, angular location 090 faced south, angular location 180 was at the top, and angular location 270 faced north. There was an instrumentation station located at the center of each end cap.

At each station, a type K thermocouple was spot-welded to the inner surface of the pipe, forming an intrinsic junction. A welded bead thermocouple was placed between the first and second layers of insulation. At some stations, multiple thermocouples were used in case of failure. The use of multiple temperature measurements also increases stability and reliability for the inverse heat conduction procedure, used to estimate the heat flux, by minimizing the random error from the temperature readings.

To measure flame temperatures, 1.6 mm stainless steel sheathed, ungrounded junction, type K

thermocouples were placed at various heights on water cooled towers arranged about the large calorimeter and 5 cm from the exterior surface at each measurement station on the calorimeter. Three of the towers, named A, B, and C, were 6.1 m high and had thermocouples at 142 cm and 262 cm above the initial fuel level. Five other towers, named 2, 3, 4, 6, and 7 were 12.2 m high and had thermocouples at 142 cm, 262 cm, 549 cm, and 1118 cm above the initial fuel surface. Figure 1 shows the placement of the calorimeter and the towers within the pool.

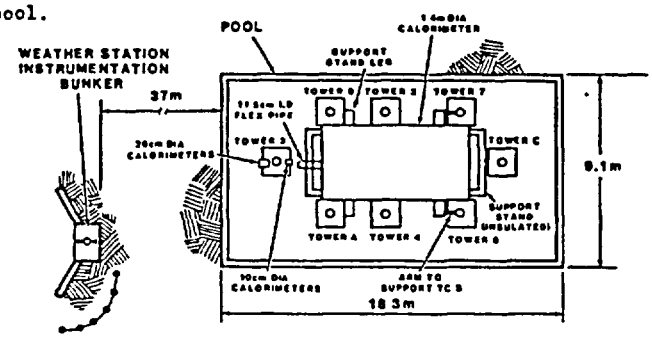

Figure 1
Plan View of the Test Facility

Four small calorimeters, constructed of 1018 mild steel, were installed on tower 3 which was located to the west of the large calorimeter. Two of these calorimeters were 10.2 cm diameter cylinders and the other two were 20.3 cm diameter cylinders (from this point on referred to as the 10 cm or 20 cm calorimeters). These calorimeters had 3.2 cm thick walls, were 20.3 cm long, and cut into four quadrants. The wall thickness of these calorimeters was the same as that of the large calorimeter. The mild steel was also chosen such that the thermal properties would be similar to those of the larger calorimeter. To minimize circumferential heat conduction between the calorimeter quadrants, a felt insulating strip was placed between them. The interior of each calorimeter was filled with Cerablanket insulation. The whole assembly was held together by 2.5 cm thick steel caps bolted on both ends of a calorimeter.

Thermocouples were located at the center of each quadrant; these correspond to the angular stations on the large calorimeter. Type K thermocouples were spot-welded (intrinsic junctions) to the inside surface of the cylinder at each station. A welded bead thermocouple was placed within the insulating material in the center of the calorimeter, in order to give an internal boundary condition.

The four smaller calorimeters were installed on tower 3 such that their axes were aligned in the same vertical plane as the axis of the large calorimeter. These calorimeters were placed on the tower such that the upper stations of a 10 cm and 20 cm calorimeter lined up with the upper station of the large calorimeter and the lower stations of the other two calorimeters lined up with the lower station of the large calorimeter, as shown in Figure 2.

Because the wind can drastically change the flow patterns of the fire, an average wind speed of 2 m/s is the upper limit prescribed in the IAEA test specifications [2]. An anemometer, which was located atop the bunker that housed the data logger, served as the instrument for monitoring wind speed and direction.

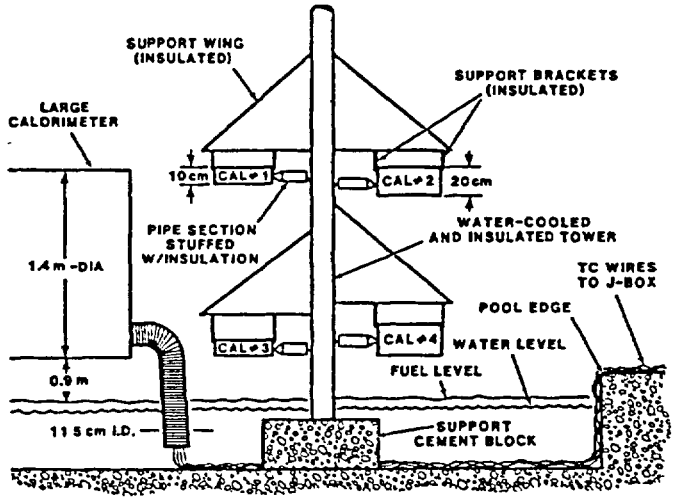

Figure 2
Placement of Small Calorimeters in Relation to the Large Calorimeter

TEST DURATION AND FUEL CONSUMPTION

For the tests, JP-4 aviation fuel was added to 66 cm of water in the pool, where one centimeter depth corresponds to 1670 liters. The depth of fuel added for the first and second tests, tests A and B was 22 cm, and for the final test, test C, was 19 cm. Tests A and B were 35 minutes long, while test C was 29 minutes long. The average fuel recession rate for tests A and B was 6.3 mm/min (17.5 liters per second) while that for test C was 6.6 mm/min (18.2 liters per second). These values are in agreement with a nominal fuel recession rate of 6.3 mm/min observed in a number of large pool fires using JP-4 fuel that have been conducted at Sandia.

In comparison, Babrauskas [4] reports burn rates for gasoline and liquid natural gas pool fires; the values extracted from his plots are 4.3 mm/min for gasoline and 5.8 mm/min for LNG for pools of equivalent diameter, i.e., 14.6 m. Blinov and Khudyakov [5], give experimental burning rates for gasoline and tractor kerosene; for pool diameters of 9 m and 23 m, the value as reported by Hottel [6] for both fuels and pool sizes is about 3.8 mm/min.

After the test item and instrumentation were installed and the pool filled, the fuel was ignited by a hand-held torch. The time for the flame front to travel across the surface of the pool along the long axis and fully engulf the large calorimeter was ~ 8 seconds.

WIND EFFECTS

Large scale turbulence results in the large temporal and spatial fluctuations that characterize the test medium of a large open pool fire. The variable most affecting the conditions in an open pool fire is the ambient wind. The average values and standard deviations of wind speed for each test in this series were 2.0±.9 m/s, 1.2±.8 m/s, and 1.5±.8 m/s for tests A, B and C respectively. The prevailing wind direction for test A was from the east by southeast. For test B, the wind prevailed from the southeast. While for test C, the prevailing wind direction was from the southwest. The wind history for Test C is given in Figure 3.

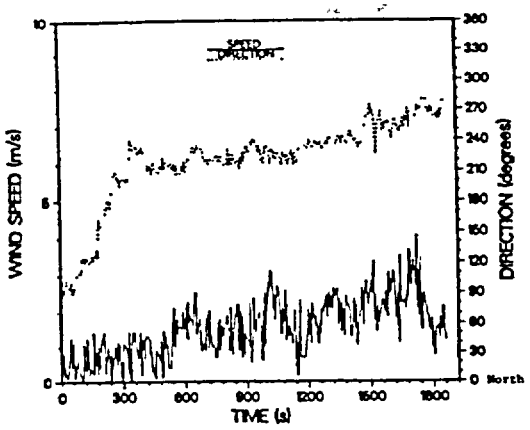

Figure 3
Wind History for Test C

Wind influences the entrainment patterns in an open pool fire, enhancing air entrainment in some areas. As a result, the temperatures are elevated or depressed depending on local air to fuel ratios and efficiency of mixing. Instabilities are enhanced and turbulent flow patterns of the flame are affected. Wake regions are formed downstream of the plume and at times, spiralling vortex flows are seen in the plume at the leeward edges of the pool. Another wind effect is the tilting of the plume such that there were times when the calorimeter, towers and other instrumentation were not fully engulfed by the flames. These wind effects are erratic in nature and result in the large spatial and temporal variations that were noted within and between tests.

FLAME (GAS) TEMPERATURE DATA

A typical flame temperature history from a tower is shown in Figure 4 (tower 2, test C). The data from a single elevation possesses large fluctuations, demonstrating the effects of both the characteristic turbulence of a large open pool fire and the wind. The erratic nature of the fire plume is evident from temperature histories. There are variations from tower to tower within a test and variations from test to test.

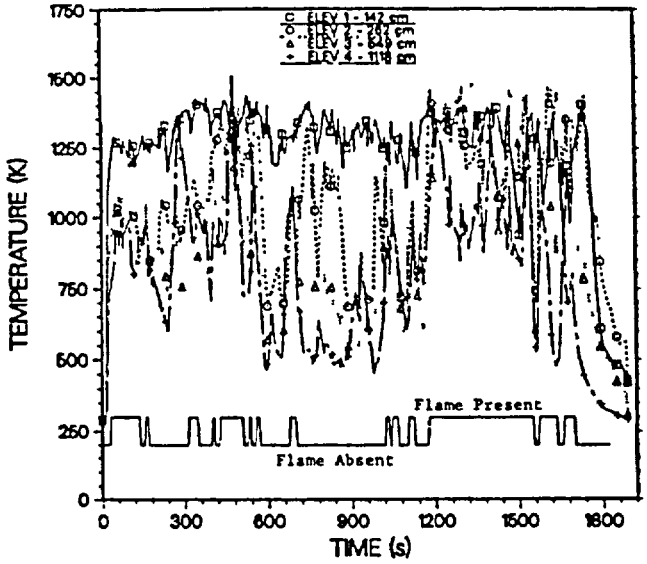

Figure 4
Flame Temperature History
Tower 2, Test C

The mean temperatures were computed for all four measurement locations on each of the five 12.2 m high towers in each test. Table 1 presents these mean temperatures. The average values for elevation 1 range from 1065 to 1320 K, from 810 to 1270 K for elevation 2, from 610 to 1050 K for elevation 3, and from 470 to 905 K at elevation 4. The trend is for the mean temperature to be highest at the lowest elevation and to decrease as the elevation increases. Emphasizing the fact that the dominant wind direction was from the south for all the tests, the towers on the south side of the pool experienced lower mean temperatures. The north towers indicate higher mean values since they may be more centrally located in the plume as a result of the wind induced tilt.

Table 1
Tower Temperature Averages
Over Entire Test and Over "Presence" and "Absence" of Flame

Tower Temperature Averages
e1 - elevation 142 cm e2 - elevation 362 cm, e3 - elevation 849 cm, e4 - elevation 1118 cm

	Test A				Test B				Test C			
	Test Avg (K)	Test St Dev (K)	Low Avg (K)	High Avg (K)	Test Avg (K)	Test St Dev (K)	Low Avg (K)	High Avg (K)	Test Avg (K)	Test St Dev (K)	Low Avg (K)	High Avg (K)
Twr 2												
e1	1232	107	1212	1254	1264	93	1248	1276	1292	90	1299	1286
e2	1119	121	1061	1163	1089	162	873	1263	1076	213	946	1206
e3	857	215	724	1048	979	265	644	1131	960	245	655	1187
e4	628	232	532	735	811	304	552	995	834	234	694	973
Twr 3												
e1	1065	220	968	1222	****	****	****	****	1206	147	1186	1242
e2	907	353	674	1220	1080	278	909	1391	1020	270	974	1255
e3	836	413	531	1291	812	366	548	1252	611	236	548	1256
e4	904	352	635	1160	893	283	537	974	672	155	624	828
Twr 4												
e1	1188	220	1151	1298	1145	190	1083	1297	1093	168	1078	1159
e2	1066	215	992	1253	997	205	905	1238	****	****	****	****
e3	816	260	721	1247	839	223	713	1147	777	175	764	1054
e4	584	248	478	917	623	244	508	982	549	167	515	804
Twr 6												
e1	1205	167	1194	1257	1102	181	1062	1263	1078	116	1056	1197
e2	1063	196	1002	1256	923	201	832	1258	835	212	738	1193
e3	697	225	606	1162	765	243	641	1165	710	240	628	1310
e4	550	297	439	1120	571	244	473	968	615	235	544	979
Twr 7												
e1	1278	101	1277	1284	1220	106	1217	1223	1252	123	1208	1275
e2	1062	227	1015	1284	1271	193	1140	1443	1169	154	1169	1320
e3	728	248	632	1171	948	268	647	1184	1050	225	794	1181
e4	****	****	****	****	****	****	****	****	****	****	****	****

Notes
**** No Data Available
Low Average Flame "Absent"
High Average Flame "Present"

The standard deviations from the means are also given in Table 1. The trend is for the standard deviations to be smaller at the lowest elevation and to increase as the elevation increases. This is demonstrated by the fact that standard deviations at elevation 1 average 12% of the mean temperature readings, 23% at elevation 2, 31% at elevation 3, and 38% at elevation 4. The larger spread in temperatures at the upper elevations is expected because at these heights, the wind effects are greater. The average of the mean temperature values obtained at a single elevation from all of the towers in a test agree with the average values from the other two tests to within 8%. This agreement is very good considering the differing ambient wind conditions for each test.

In an attempt to account for wind effects, conditional sampling was used to examine the temperature data. All the data from elevation 4 on the five 12.2 m high towers for all the tests was gathered. The probability density function of these temperature measurements was found to be bimodal in shape. One mode, at low temperatures, roughly corresponds to data taken when the wind effects were strong. The other mode, at higher temperatures, corresponds to times when the flames engulfed the towers. A setpoint temperature which corresponded to the local minimum between the peaks of the probability density function was chosen.

This temperature was 935 K. A signal was generated which was high when the temperature was above the setpoint and low when the temperature was below the setpoint. This corresponds to a signal representing the "presence" or "absence" of flames about the towers, as shown in the conditioning signal in Figure 4. This correspondence is not exact; however, this is a simple starting place to help in examining the fire data.

Statistics were obtained from the conditioned temperature data. The tower temperatures at each elevation were averaged during the flame present and absent periods based on the conditioning signal described above; the results are shown in Table 1. The general trends for these conditional averages are the same as the trends in the total test averages, with the mean temperatures decreasing with elevation. As can be expected, the mean flame present temperature at each elevation is higher than the mean temperature over the entire test at the corresponding elevation. The mean temperatures for the flame present condition are very consistent at the two lower elevations for all of the towers in all of the tests.

The readings obtained for the flame temperature thermocouples are lower than the true flame temperatures. The main source of error in the readings is believed to be due to radiative heat loss from the thermo- couples. The error is probably the greatest for the flame thermocouples that are near the large calorimeter. This occurs because the extinction coefficient in the flames is on the order of 1/m [7] and these thermocouples are only 5 cm from a large, relatively cool surface. For the thermocouples mounted on the towers, the errors are believed to be small during the flame present condition and will increase during the flame absent condition. Other sources of error include transient effects, soot buildup on the thermocouples, thermocouple calibration, and data system inaccuracies; these errors were not considered in this analysis.

For the thermocouples near the calorimeter, this error is a maximum at the early times in the test and decreases as the calorimeter heats up. The error was estimated from a simplified one parameter radiative model. The radiative view factors between the thermocouple and both the flames and the large calorimeter were found using the cross-string method with the thermocouple at the cross point. Other assumptions are a non- participating gas medium and blackbody radiative exchange between the thermocouple, calorimeter, and fire. Then, by performing a heat balance on a thermocouple assumed to be in radiative equilibrium with the fire at 1255 K and the calorimeter surface, this error is estimated to be approximately 12% of the assumed fire temperature when the calorimeter surface is cold (365 K) and 4% when the surface is hot (1090 K). This error estimate does not encompass all factors affecting the thermocouple readings.

METHOD OF OBTAINING HEAT FLUX DATA

For these tests, the calorimeter backface temperatures were measured; however, the net heat flux at the outer surface is desired. To determine the net heat flux, the temperature data becomes the "boundary condition" in the inverse problem of heat conduction. This problem was solved by a numerical technique presented by Beck, Blackwell, and St. Clair [8]. The numerical technique was utilized by Blackwell and Douglass [9] to develop a computer code, known as the Sandia One Dimensional Direct and Inverse Thermal (SODDIT) Code, to generate net heat flux and surface temperature information given interior temperature data.

The calorimeter design was checked in several ways. The use of backface measurements was evaluated in a series of experiments in which a wall section, with multiple frontface and backface thermocouples, was exposed to known radiative heat fluxes. A thermal model was used to show that the local heat conduction was effectively one-dimensional.

Because noisy data can promote instabilities in any inverse calculation, a series of simple numerical studies were used to evaluate potential errors. As a result, two approaches were used to reduce the effects of noise in the data analysis procedure. A light smoothing of the actual temperature data was introduced by fitting the data with a smoothing spline with an allowed standard deviation of 0.5 K (a fairly tight fit). An additional smoothing feature in SODDIT is the use of what is termed "future temperature" information, a concept developed by Beck [8]. The future temperature approach allows the use of smaller computational time steps and increases stability. After an extensive review of the data from test A, four future times were chosen to provide calculational stability over the temperature ranges expected in the test series without eliminating the ability to resolve specific thermal events in the tests.

A study of the sensitivity of this inverse procedure to noise in the data was made by analyzing "exact" data to which varying amounts of random noise had been added. The exact temperature data was generated for a triangular heat flux pulse into a planar section of the calorimeter material that had an insulated backface. Random noise with a standard deviation of 0.05 K to 1.1 K was added to this data. To evaluate any differences in stability as a function of the temperature, the thermophysical properties of the material were evaluated at 530 K or 895 K.

The heat flux profiles calculated from the noisy data sets were compared to the heat flux profile used to generate the exact temperature data. The maximum errors at the lower temperature ranged from 7% for the highest noise level to a minimum of 2% and then up to 4% at the lower noise level. At higher temperature, the values were 17%, 4%, and 5% respectively. For reference, the random noise in the temperature data taken during the lead-in periods before the tests had a standard deviation of less than 0.03 K.

In spite of the smoothing effects, the heat flux calculations still exhibited oscillations at later times in the tests. This occurs because mild steel experiences a Curie point transition centered at ~ 1035 K. From measurements made on samples taken from the calorimeter wall, this transition is characterized by a sharp spike in specific heat capacity between 975 and 1090 K. Such an abrupt change in thermal properties causes instabilities in the inverse code; the natural fluctuations in the fire temperatures compound the instability problem. As a result, the heat flux calculations at temperatures above the transition temperature are not as reliable. Therefore, when heat flux is presented as a function of surface temperature, data is reported for values less than 1035 K.

LARGE CALORIMETER HEAT FLUX DATA

Temperature histories for all twelve stations are presented in Figures 5, 6 and 7 for the three tests. These "temperature envelopes" can be used to examine the

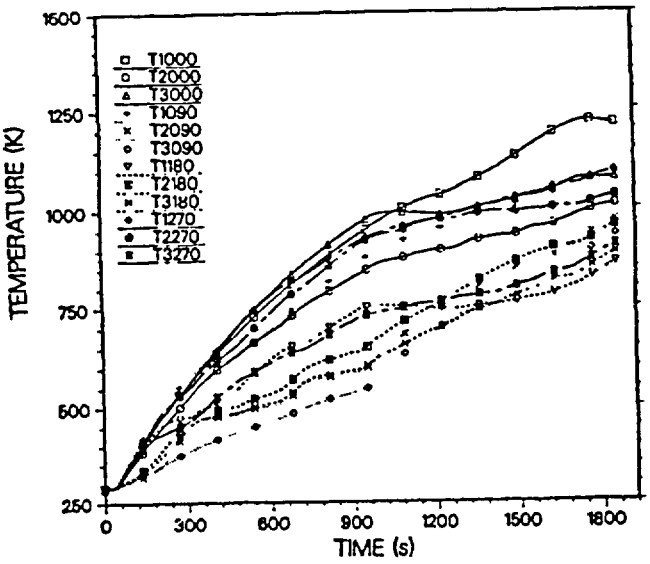

Figure 5 Steel Backface Temperature History - Test A

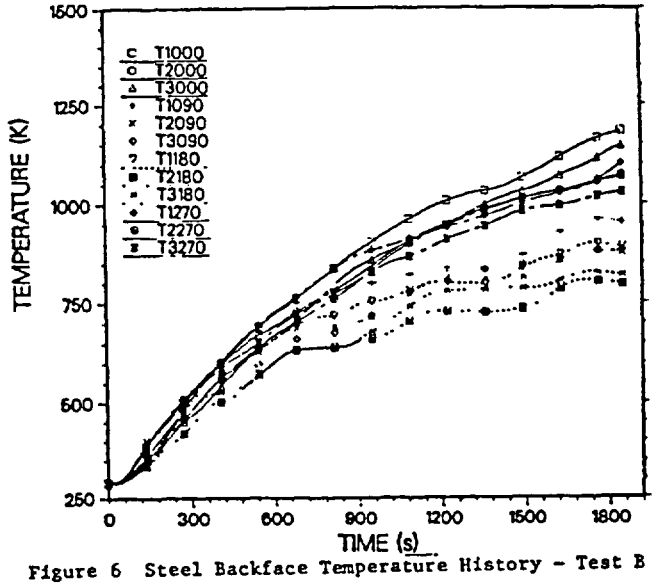

Figure 6 Steel Backface Temperature History - Test B

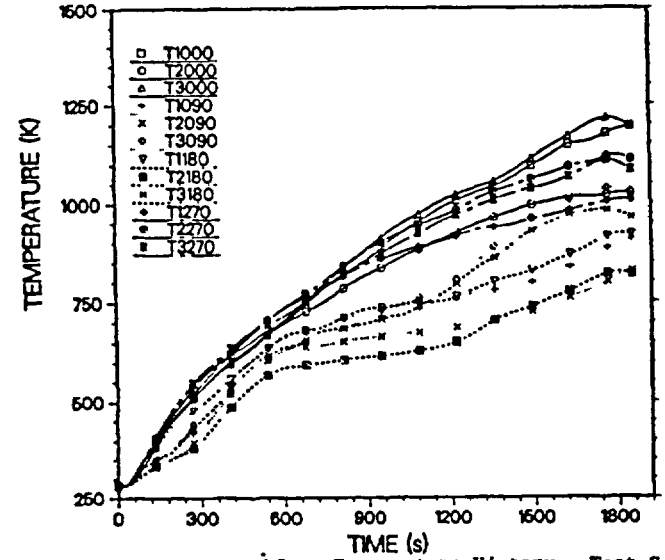

Figure 7 Steel Backface Temperature History - Test C

uniformity in a fire, the integrated heat flux which is directly related to the total temperature rise, and the repeatability from fire to fire by overlaying the envelopes. A narrower envelope indicates a more uniform thermal exposure over the surface of the calorimeter. This method of comparison is limited to test items with the same thermal properties, wall thickness, and geometry.

For the four stations in the axial center of the large calorimeter, the net heat flux, the steel backface temperature, and the external flame temperature histories from Test C are given in Figures 8 through 11. Typically, the net heat flux to the calorimeter peaked at test startup, to values between 100-160 kW/sq.m, and diminished as the calorimeter surface heated up. The heat flux values naturally tracked the external flame temperature values, but there was a significant amount of filtering. Some of this filtering was due to the natural damping effects of the calorimeter; note the smooth rise of the steel backface temperature curve (thermal response time is on the order of 9 seconds). There was additional filtering due to the slight smoothing introduced in pre-processing the data and to the use of future temperature information in the actual data analysis.

The trends in the flame temperatures adjacent to the calorimeter are similar to the trends for the tower flame temperature data. For the southern or 090 station, there were periods of lower values due to wind effects. This also applies to the upper, or 180 station. Videotapes of the test show times when the southern and upper parts of the calorimeter were not fully engulfed in flame and these times correlate with times of low heat flux on the plots. Even though the winds are within the prescribed limits, changes in the winds produce fluctuating, nonuniform temperature fields in the regions around the top and windward side of the large calorimeter.

Temporal data is important in the presentation of the heat flux information, because events in the fire, such as fluctuating flame temperatures, can be correlated with heat transfer events. From the heat flux histories, total thermal input can be studied and trends within a test defined. Another useful means of data presentation is to plot heat flux as a function of surface temperature. This is the format by which test specifications are made [1,2]; thus, presenting the data in this manner facilitates a direct comparison. In this form, thermal transport mechanisms in the fire can also be studied. SODDIT provides surface temperature estimates as well as heat fluxes. These estimates are used when presenting the surface temperature data.

The heat fluxes with respect to angular station, i.e., all the heat flux values from 3 stations in each of the 3 tests, were averaged together at specific surface temperature values (note that the time at which a specific temperature is reached is different for each station in a test and from test to test). The mean values are plotted against surface temperature in Figure 12. The average of the peak fluxes for the lower stations (TX000) and the north stations (TX270) were about 130 kW/sq.m. For the southern stations (TX090), the average of the peak fluxes was 110 kW/sq.m. For the upper stations (TX180), it was 100 kW/sq.m. In general, TX000 exhibited the highest, most uniform peak heat fluxes and TX180, the lowest. Stations TX270, which were on the leeward side of the calorimeter, showed much higher peak heat fluxes than TX090 which were windward during the tests.

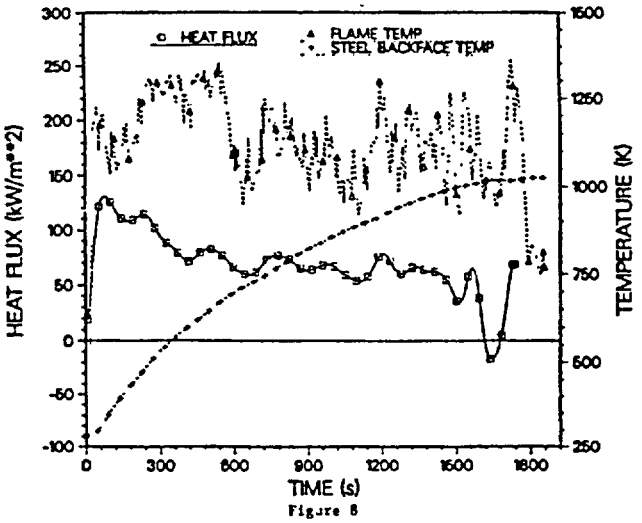

Figure 8
Net Heat Flux, Steel Backface Temperature and External Flame Temperature Histories - Bottom Station

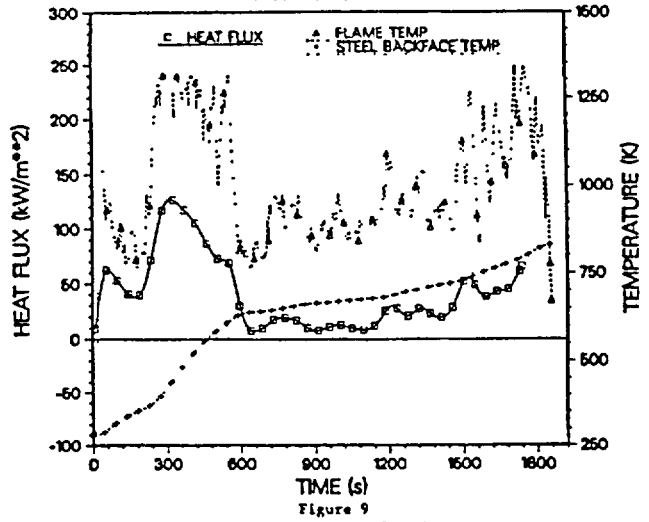

Figure 9
Net Heat Flux, Steel Backface Temperature and External Flame Temperature Histories - South Station

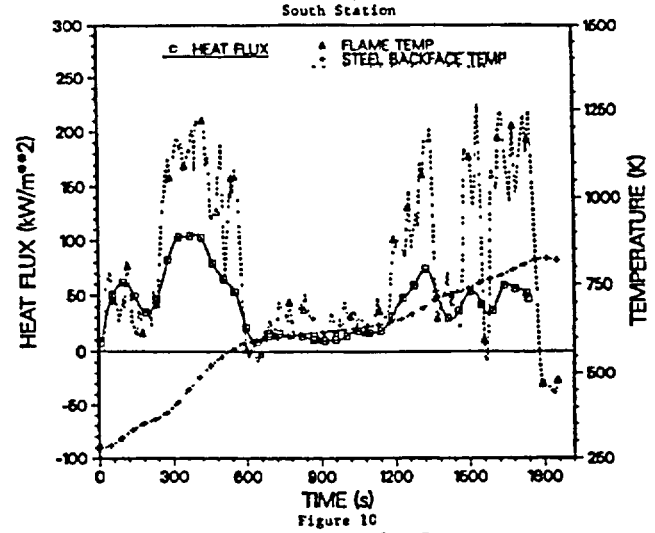

Figure 10
Net Heat Flux, Steel Backface Temperature and External Flame Temperature Histories - Top Station

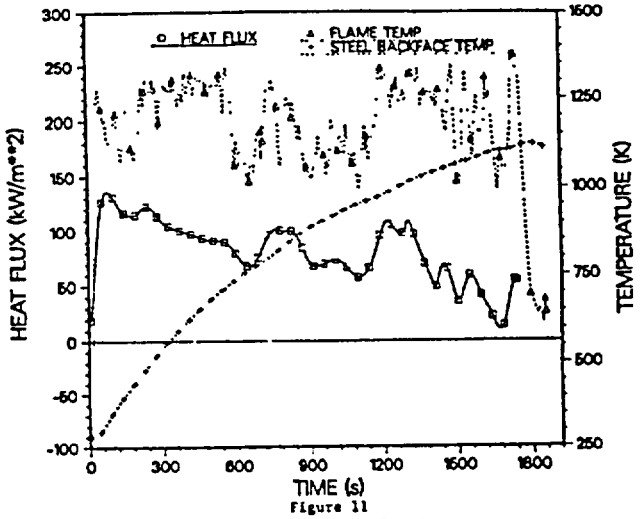

Figure 11
Net Heat Flux, Steel Backface Temperature and External Flame Temperature Histories - North Station

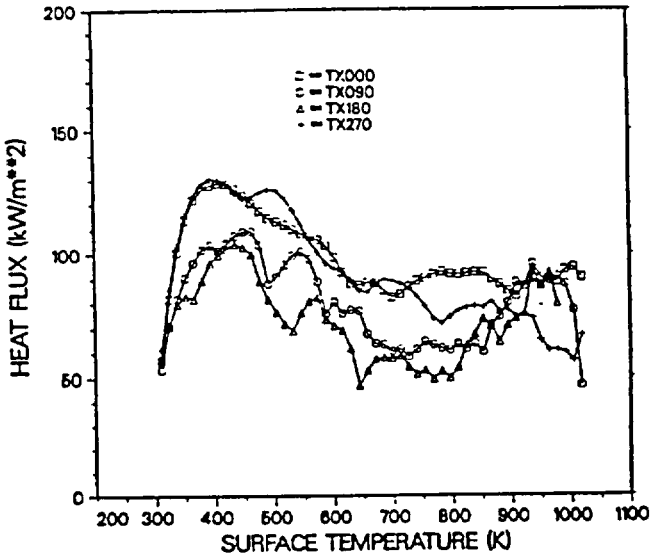

Figure 12
Average Heat Fluxes for the Test Series

Standard deviations from the mean values were computed; they are relatively large for all stations, demonstrating the random nature of the fire. Stations TX000 exhibited the smallest values, on the order of 15% of the mean. For stations TX270, the standard deviations are on the order of 25%, for stations TX090 and TX180, on the order of 35%. The stations that had greater exposure to the wind (stations TX090 and TX180) experienced larger fluctuations than the stations that were sheltered from wind effects (stations TX000 and TX270). From the visual data, the south side of the calorimeter could actually be seen at times during all three tests. Even when the plume engulfed the test item, the flame thickness was not as great on the

windward and upper stations of the calorimeter; this lowers the radiative transport to these portions of the calorimeter.

Integrated heat flux values at 30 minutes are presented for the test series in Table 2. Statistics for these values are presented in Table 3. High, low, and mean values, as well as standard deviations from the mean, are provided for various groups of data. The data is grouped as follows: all cylindrical surface data with respect to test, all data for the series with respect to axial station, all data for the series with respect to angular station, and all end cap data for the test series. Note that there is approximately a two to one ratio between the high and low values for the first and second groupings and the standard deviations are about 25%. When grouped with respect to angular station, however, the spread and the standard deviations are smaller.

Table 2. Integrated Heat Flux at 30 Min* (kW-hr/sq m)

Test	Angle Degrees	Station 1 (East)	Station 2 (Middle)	Station 3 (West)
A	0	43 8	32 0	37 5
	90	38.2	28 8	26 4
	180	22.5	28.1	24 0
	270	36 5	34.5	25 0
	End Cap	18 3	*****	19 6
B	0	42 3	37 3	41 0
	90	28 2	23 6	23 6
	180	24 3	19.8	20 7
	270	38.5	37.3	33 9
	End Cap	19 6	*****	20 6
C	0	42.8	33 3	43 4
	90	25.7	21 4	33 5
	180	26 1	20 8	29 6
	270	33.7	39 1	38 3
	End Cap	21 6	*****	18 8

*Test C was only 29 min, so values were extrapolated to 30 min

Table 3. Statistics for the Integrated Heat Flux at 30 Min* (kw-hr/sq m)

Cylindrical Surface	Low	Mean	High	Standard Deviation (%)
Test A-All	22.5	31.6	43.8	6.8 (21.5)
Test B-All	19.8	30.8	42.3	8.3 (26 9)
Test C-All	20 8	32 3	43.4	7.7 (23 8)
Station 1-All	22.5	33.7	43.8	7.9 (23 4)
Station 2-All	19 8	30.0	39.1	6.8 (23 0)
Station 3-All	20 7	31 4	43.4	7.6 (24 2)
0 degrees-All	32 0	39 3	43.8	4.4 (11.2)
90 degrees-All	21 4	27.7	38 2	5.3 (19 1)
180 degrees-All	19 8	24 0	29 6	3 4 (14 2)
270 degrees-All	25 0	35 4	39.1	4.5 (12 7)
End Caps-All	18.3	19 8	21.6	1 2 (6 1)

*Test C was only 29 min, so values were extrapolated to 30 min.

SMALL CALORIMETER HEAT FLUX DATA

Heat flux histories for the 10 cm and 20 cm calorimeters from Test C are presented in Figures 13 through 16 along with the closest flame temperatures located above each calorimeter. For the lower calorimeters, these flame temperatures were measured ~ 50 cm above the upper stations and for the upper calorimeters, ~ 25 cm above the upper stations. The fluctuations in heat flux for the smaller calorimeters were generally greater than for the large calorimeter. This phenomena is believed to be due to the fact that the large calorimeter damps out the local temperature variations in the flame to a greater degree. Peak fluxes for the smaller calorimeters were generally between 160-200 kW/sq.m, with the exception of the upper calorimeters in test A. These calorimeters experienced relatively low fluxes for the first half of the test.

Typically, the trends in the heat flux histories from all angular stations for a single calorimeter track each other. For the upper calorimeters, however, the heat flux values differ by as much as a factor of two from one station to the next on a single calorimeter.

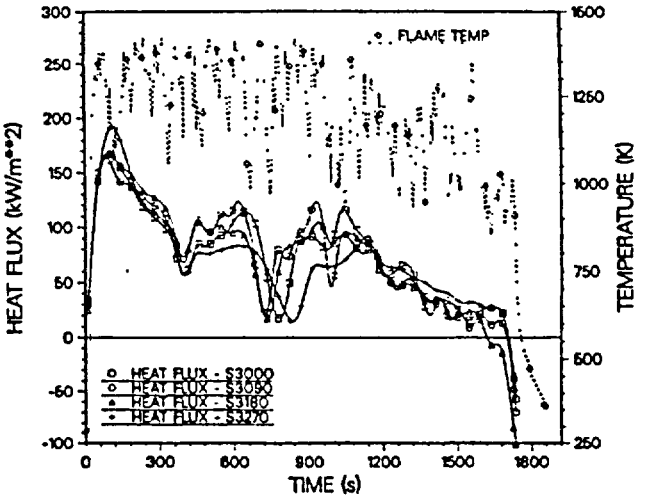

Figure 13
Heat Flux and Flame Temperature Histories
Lower 10 cm Calorimeter

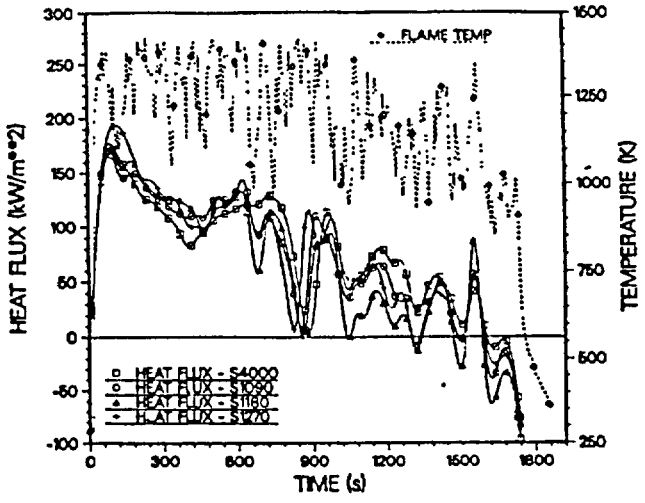

Figure 14
Heat Flux and Flame Temperature Histories
Lower 20 cm Calorimeter

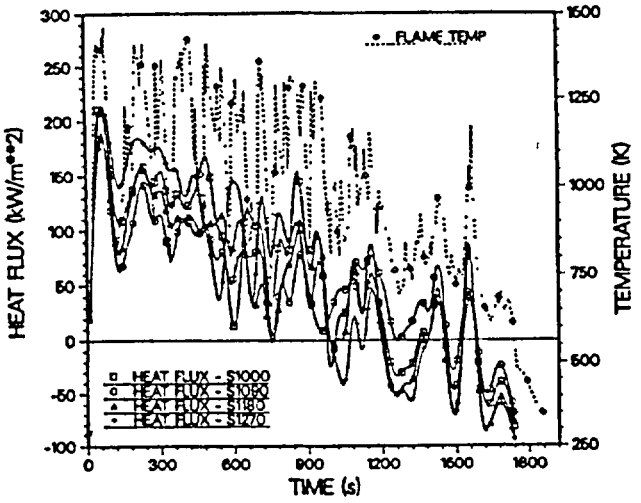

Figure 15
Heat Flux and Flame Temperature Histories
Upper 10 cm Calorimeter

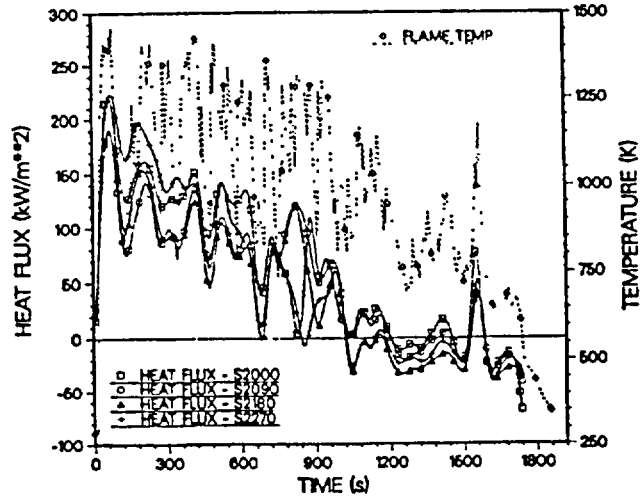

Figure 16
Heat Flux and Flame Temperature Histories
Upper 20 cm Calorimeter

There are general trends for the angular variation in heat fluxes; station 270, on the leeward side, demonstrates the highest heat fluxes. The bottom station 000, follows closely, and as on the larger calorimeter, the upper and windward stations (180 and 090) demonstrate lower fluxes. The heat flux values for the small calorimeters in test A, are in general, lower than those in the other tests; a result of the generally lower local flame temperatures at the west end of the pool.

DISCUSSION OF RESULTS

HEAT FLUX DATA

There is evidence of dome-like fuel rich vapor regions above the fuel surface in small pool fires. It has been assumed that such a region would be found in larger pool fires [10]. If the vapor dome was present in the fires in this test series, then the heat flux levels would be lowest at the 000 stations on the underside of the large calorimeters, due to a decrease in the radiant field intensity. The fact that the heat flux values are highest at the 000 stations is contrary to what would be expected. These findings indicate that no vapor dome is present; this fact is in agreement with Corlett's designation of pool fires of more than 1 m diameter as having "unstructured" flames.

There have been studies which predict the radiant heat transfer to a horizontal cylinder engulfed in luminous flames [12,13]. In both analyses, the flame is considered as a uniform temperature, participating medium, where scattering is negligible. Formulations were done for cases in which the bottom of the cylinder was 0.3 m and 1 m above the pool and the width of the pool perpendicular to the cylinder axis was between 2.4 m and 7.6 m. The positioning of the cylinder in the fire will strongly affect the predicted heat flux distribution. The analyses predict the highest heat fluxes will be at the top and the values will decrease along the periphery to the underside of the cylinder. Again, these predictions are contrary to the findings in this test series in which the top portions of the calorimeter (stations 180) receive the lowest net fluxes and the portions on the underside of the calorimeter (stations 000) receive the highest fluxes.

On the large calorimeter, the circumferential variations in the heat flux and the integrated heat flux are probably the result of several phenomena. Fluctuating, nonuniform temperature fields have been previously noted in the vicinity of the top and windward stations due to the wind effects. Variations in the convective heat transfer are significant. For a cylinder in cross flow, the local heat transfer coefficients are highest at the lower stagnation point, decrease appreciably at the sides, and then increase up to the top of the cylinder. Because the calorimeter is a massive heat sink (the maximum absorption rate was approximately 5 MW), a cooler, soot-laden boundary layer probably exists around the calorimeter; this boundary layer is believed to act as a radiation shield. Because the boundary layer is thinner on the underside of the calorimeter, shielding would be lower than at the top, where the boundary layer in the wake region is much thicker.

An attempt was made to estimate the radiative/convective partitioning of heat transfer to the calorimeters. Using McCaffrey's velocity correlation [14] for a 544 MW fire, the velocity was estimated to be 6.8 m/s at an elevation of 1 m above the initial fuel surface. This was the location of the bottom stations on the large calorimeter and the lower 10 cm and 20 cm calorimeters. Using this velocity, the convective heat transfer coefficients at the stagnation point were calculated for the three cylinders in cross flow. The coefficients were computed for surface temperatures of 423 K and a flame temperature of 1283 K. The convective fluxes for the 1.4 m, 20 cm, and 10 cm calorimeters respectively, were 11, 36, 42 kW/sq.m. For the test series, the average total heat fluxes estimated by SODDIT at these stations for surface temperatures of 423 K, were 130, 170, and 170 kW/sq.m. Thus, the convective flux was estimated to be 8%, 21%, and 25% of the total cold wall flux for the calorimeters.

It should be noted that the flame velocity field is directly related to the temperature field. Because the flow is buoyancy driven, when the temperature drops then the velocity will drop. However, changes in the gas properties roughly offset the effects of the lower gas velocity. As a result, the heat transfer coefficient remains approximately constant. Based on the temperature and flame velocity measurements in [15], the

calculated heat transfer coefficient varied by less than 15% over a temperature range of 775 to 1275 K using the assumption of turbulent flow over a cylindrical body.

The convective heat transfer to a flat plate in parallel flow was also calculated. The analysis included the same surface and flame temperatures as above, but the velocity was estimated to be 9 m/s, using McCaffrey's correlation for an elevation of 1.6 m. This was the elevation of the instrumentation stations on the end plates of the large calorimeter. Hence, the convective flux estimate was 7 kW/sq.m. The average total heat flux estimated by SODDIT on the end plates for a surface temperature of 423 K was 108 kW/sq.m; thus, of the total cold wall heat flux to the end plates, ~ 6% is convective, and the balance radiative.

LARGE VS. SMALL CALORIMETERS

The small calorimeters were placed with either top or bottom stations at the same vertical heights as the large calorimeter, in an attempt to compare the heat transfer to objects of differing geometry and total thermal capacity. The stations of interest on the large calorimeter are the bottom west station, T3000, and also the top west station, T3180. The stations from the 10 cm and 20 cm calorimeters are the bottom stations of the lower calorimeters, stations S3000 and S4000, and the top stations of the upper calorimeters, S1180 and S2180. The heat flux was averaged for each station for all three tests with the results plotted for the lower stations in Figure 17 and for the upper stations in Figure 18.

The average heat flux curves for the lower stations in Figure 17 are relatively smooth. The cold wall flux of 130 kW/sq.m to the 1.4 m calorimeter is about 80% that of the cold wall fluxes of 165 kW/sq.m to the 10 cm and 20 cm calorimeters. The magnitudes of the fluxes to the 10 cm and 20 cm calorimeters are roughly equivalent throughout the temperature range, and above approximately 705 K, all three curves converge to the same values.

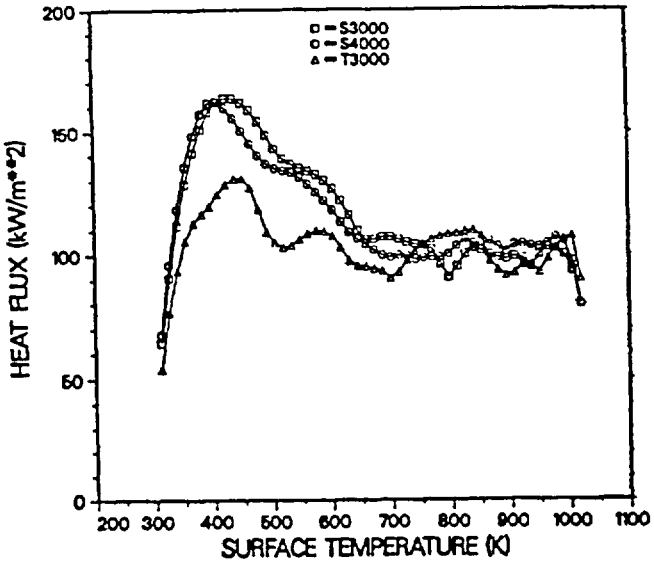

Figure 17
Average Heat Flux versus Surface Temperature
Lower Stations, Large and Small Calorimeters

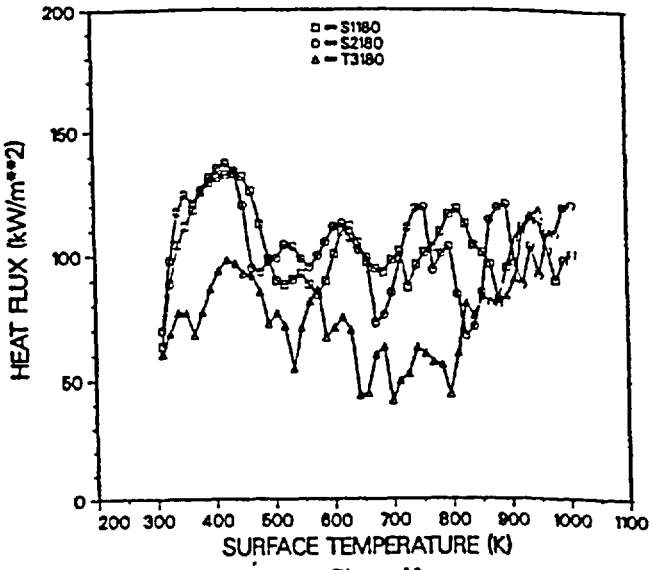

Figure 18
Average Heat Flux versus Surface Temperature
Upper Stations, Large and Small Calorimeters

The average heat flux curves for the upper stations in Figure 18 fluctuate a great deal more than for the lower stations, and the magnitudes of the fluxes are noticeably smaller. The lower heat fluxes and larger fluctuations may be due to the amount of time these calorimeters were engulfed by flames. The cold wall flux of 90 kW/sq m to the large calorimeter is two-thirds that of the cold wall fluxes of 135 kW/sq.m to the smaller calorimeters. The fluxes to the 10 cm and 20 cm calorimeters are almost equal in magnitude but lower than the fluxes for the lower lower calorimeters reported above. The curve for the large calorimeter never approaches the curves for the smaller calorimeters.

The phenomena noted here support the postulation of an interaction between an object and the fire that surrounds it. The large calorimeter appears to alter its local environment because it is physically large and thermally massive. This indicates that the heat transfer to a test item in an engulfing fire can be highly dependent on the properties of the test item.

SUMMARY

The DOT fire test series was conducted to supply information about the thermal exposure of a large object immersed in a fire and the repeatability of the thermal environment. Thermal measurements have been presented from three large open pool fire tests run with duplicate instrumentation. Heat flux and temperature data within the lower part of the fire have been studied in a variety of ways and the strong influence of the wind has been noted. Statistics have been developed to evaluate the test to test repeatability of the fire environment. The largest factor affecting the reproducibility of the environment in a large open pool fire is the wind.

Average flame temperatures at 8 locations around the test item ranged from 1065-1320 K at a height of 104 cm and from 810-1270 K at a height of 262 cm above the initial pool surface. The spread in these values is quite large. When the temperatures are averaged for all 8 locations in each test (a larger sample size), however, the spread in values decreases. For elevation 104 cm, averages for tests A, B, and C, respectively

were 1195, 1210, and 1185 K; these values are within 2% of each other. For elevation 262 cm, the average values were 1040, 1070, and 1050 K; these values are within 3% of each other.

The cold wall or peak heat fluxes to the large test item for various locations on the item ranged from 100-160 kW/sq.m. The fluxes to the underside of the calorimeter were highest, and those to the top the lowest; this distribution is counter to the heat flux distributions predicted with simplified radiation modelling. When averaged for all locations, the cold wall flux for each test was between 115-120 kW/sq.m.

The partitioning of the cold wall heat flux to the bottom location of the cylinders in cross flow was estimated to be from 8% to 25% convective and the balance radiative. The larger the radius of the cylinder, the lower the convective contribution to the total flux. For flat plates in parallel flow, the partitioning of the heat transport was estimated to be 6% convective and the balance radiative.

The total heat input or the time-integrated heat flux values for the test item were determined. The values for a single test varied with respect to location by as much as a factor of two; again, the highest values were on the bottom and lowest on the top. When all stations were averaged for a single test, the values of 31.6, 30.9 and 32.3 kW-hr/sq.m for tests A, B and C, respectively, were within 5% of each other.

The physical size and thermal capacitance of a test item has also been shown to affect the thermal environment. The effects are demonstrated when heat fluxes to the large test item are compared to the heat fluxes to smaller items in the fire. The average cold wall peak fluxes to the large calorimeter are about 75% of those to the smaller calorimeters.

REFERENCES

1. Title 10, Code of Federal Regulations, Part 71, "Packaging of Radioactive Materials for Transport and Transportation of Radioactive Material Under Certain Conditions", 1983.
2. "Regulations for the Safe Transport of Radioactive Materials", Safety Series No. 6 of the International Atomic Energy Agency Safety Standards, Paragraph A628.11 "Fire Conditions", Advisory Material on Paragraph 628 - "The Thermal Test", 1985 Revised Edition, IAEA, Vienna, STI/PUB/323.
3. "Thermal Measurements in a Series of Large Pool Fires", J. J. Gregory, R. Mata Jr., N. R. Keltner, SAND 85-0196, Sandia National Laboratories, Albuquerque, New Mexico, 1987.
4. "Estimating Large Pool Fire Burning Rates," V. Babrauskas, Fire Technology, Vol. 19, No. 4, pp. 251-261, 1983.
5. "Certain Laws Governing Diffusion Burning of Liquids," V. I. Blinov and G. N. Khudyakov, Doklady Akademi Nauk SSSR 113, pp. 1094-1098, 1957.
6. "Review of Certain Laws Governing Diffusive Burning of Liquids by V. I. Blinov and G. N. Khudyakov," Fire Research Abstracts and Reviews 1, pp. 41-43, 1959.
7. "Experimental and Theoretical Analysis of the Radiative Transfer Inside of a Sooty Pool Fire," R. S. Longenbaugh, Master's Thesis, New Mexico State University, 1985.
8. Inverse Heat Conduction, Ill-posed Problems, J. V. Beck, B. Blackwell, and R. St. Clair, Jr., John Wiley and Sons, New York, 1985.
9. "A User's Manual for the Sandia One-Dimensional Direct and Inverse Thermal (SODDIT) Code," B. F. Blackwell and R. W. Douglas, SAND 85-2478, Sandia National Laboratories, Albuquerque, NM, 1985.
10. "Mathematical Model of a Large Open Fire," P. T. Harsha, W. N. Bragg, R. B. Edelman, NASA, Ames Research Center, Moffett Field, CA, SAI-81-026-CP, 1981.
11. "Velocity Distributions in Fires," R. C. Corlett, in Heat Transfer in Fires, pp. 239-255, John Wiley and Sons, New York, 1974.
12. "Model for the Prediction of Radiant Heat Transfer to a Horizontal Cylinder Engulfed in Flames," A. M. Birk and P. H. Oosthuizen, ASME Paper 82-WA/HT-52, 1982.
13. "Three-Dimensional Formulation of the Radiant Heat Flux Variation on a Cylinder Engulfed in Flames," M. M. Tunc and A. Karakas, Journal of Heat Transfer, Vol. 107, pp. 949-952, 1985.
14. "Purely Bouyant Diffusion Flames: Some Experimental Results", B. J. McCaffrey, National Bureau of Standards, NBSIR 79-1910, 1979.
15. "Measurements of Gas Velocities and Temperatures in a Large Open Pool Fire", M. E. Schneider and L. A. Kent, SAND 87-0095C Sandia National Laboratories, Albuquerque, New Mexico, 1987.

The test program was funded by the Federal Rail Administration of the U.S. Department of Transportation (DOT). This project was directed by the Transportation Technology Center at Sandia National Laboratories. Sandia National Laboratories is operated by AT&T Technologies for the U.S. Department of Energy (DOE) under Contract DE-AC04-76DP00789.

reprinted from

Heat and Mass Transfer in Fire — HTD-Vol. 73
Editors: A.K. Kulkarni, and Y. Jaluria
(Book No. H00392)

published by

THE AMERICAN SOCIETY OF MECHANICAL ENGINEERS
345 East 47th Street, New York, N.Y. 10017
Printed in U.S.A.

Enclosure (5)

Supplement to the amendment application for approval of packaging of fissile radioactive material (WE-1 Container),

Package Identification Number USA/9289/B(U) –85.
(Six copies)

Enclosure (6)
Change Summary

Chapter	Page Number	Description of Change
Cover Sheet	1	Corrected spelling errors
Table of Contents	All	Addition of Sections/Appendices added in response to RAIs Page number changes related to additional information added to the chapters in response to RAIs
1	All	Footer Changed due to total number of pages
1	1	paragraph 1.1, changed "leak-tight canister" to "Pathfinder Canister"
1	2	added "Transport Index - 100" (Section 1.2.3.1)
1	Table 1-3	modified table to include center-to-center pin pitch, nominal UO2 density, and nominal values with tolerances for pellet diameter and clad outer and inner diameter. Also, corrected assembly k_{eff} value in response to RAI 1-7.
1	5	Added discussion of Quality Assurance Program (Section 1.3)
2	All	Footer Changed due to total number of pages
2	1	Removed reference to Appendix 2-2 (now Section 2.10).
2	3	Added 2nd paragraph to explain the history of the WE-1, and the changes make for this submittal. Changed reference from the 1992 ASME Standard to the 1995 ASME standard, through the 1996 addenda, in bottom paragraph.
2	4	Changed reference from the 1992 ASME Standard to the 1995 ASME standard, through the 1996 addenda, in 2nd paragraph. Added last sentence to last paragraph
2	7	Added 3rd sentence to 1st paragraph. Corrected Aluminum specification (from T6 to T651) Added Rubber Pad specification.
2	8	Corrected 1st value in the "300" column (from 23.5 to 23.4) Corrected Aluminum specification (from T6 to T651) Changed page number in references for "Wood Impact Absorbers" Adjusted crush values in response to RAIs.
2	10	Added discussion of the Rubber to the last paragraph of section 2.4.4.
2	15	Added discussion of the Rubber to the last paragraph of section 2.6.2.
2	16	Removed reference to Appendix 2-2 (now Section 2.10).
2	17	Changed acceleration from 135 g's to 142 g's, and adjusted calculation accordingly.

Enclosure (6)
Change Summary

Chapter	Page Number	Description of Change
2	19	Changed wording in 1st paragraph of Section 2.7.1.2 to clarify impact stiffness discussion.
2	20	Changed wording in 1st paragraph (formerly the last paragraph of p. 19) to clarify discussion. Revised Table 2.7-1.
2	23	Added discussion of WE-1 with Pathfinder Canister to 1st paragraph of section 2.7.1.5. Revised Table 2.7.1.5-1. Revised calculation for "Buckling of Cylinder"
2	25	Removed reference to Appendix 2-2 (now Section 2.10). Added "," to numbers in equations.
2	26	Added "," to numbers in equations. Corrected 10CFR reference in 1st paragraph of section 2.7.6 Removed reference to Appendix 2-2 (now Section 2.10).
2	27	Added "," to numbers in loads listing.
2	28	Reworded paragraph
2	Section 2.10	Moved from Appendix 2-2 to Chapter 2. Revisions from the May 15, 2002 submittal are noted by Revision Bars in the right-hand margin.
3	2	Added discussion of thermal properties between -20 °F and -40 °F in response to RAI 3-4.
3	3	Added data, down to -40 °F, and Alloy 600 to Table 3.2-1 in response to RAI 3-4. Added clarification to note #2.
3	4	Corrected references in Note #1 in response to RAI 3-1.
3	5	Corrected references in Note #2 in response to RAI 3-1. Added clarification to note #2 regarding absoptivity and emissivity in response to RAI 3-2.. Added reference in Table 3.2-4 to Note #1 in response to RAI 3-5.
3	6	Added discussion of ductile-to-brittle transition to Section 3.2 in response to RAI 3-3 and 3-7.
3	7	Corrected units for Stefan-Boltzman constant in response to RAI 3-6.
3	9	Corrected references in Section 3.5.2 in response to RAI 3-1. Corrected units for the convection coefficient in Section 3.5.2 in response to RAI 3-9.
3	10	Added reference to the Section 2.10.1.1 internal pressure calculation in Section 3.5.4 in response to RAI 3-10.

Enclosure (6)
Change Summary

Chapter	Page Number	Description of Change
4	All	Footer Changed due to total number of pages
4	4	Corrected viscosity of air to 0.0185 from 0.00185.
4	8-13	Added "Calculation for Pre-shipment Test of Seals" (Section 4.5) in response to RAIs 7-2, 8-1, and 8-2.
4	13	Changed "Section 4.5 References" to "Section 4.6 References" to facilitate addition of "Calculation for Pre-shipment Test of Seals" (Section 4.5).
6	2	Table 6-1b, Row 4, Column 2; changed "spaced" to "arranged"
6	4 & 4a	Table 6-2b; expanded to include tolerances, additional parameters, and KENO modeled values in Response to RAIs 6-1 and 6-2.
6	4b	Added to maintain page number consistent with current submittal.
6	8	Added dimensions to Figure 6-1b in response to RAI 6-3.
6	17	Corrected k_{eff} value in 2nd paragraph in response to RAI 6-5.
6	18	Clarified wording in bottom paragraph in response to RAI 6-6.
6	21	Section "Pathfinder Fuel Assemblies", paragraph following the number list; added parenthetical statement explaining the 0.001 in. assembly spacing
6	21a	Table 6-10, row 2, column 1; changed 0 to 0.001 to be consistent with previous paragraph
6	24	Added explanation of row and location numbering to the 2nd paragraph.
6	24a	Added discussion of dunnage material and affects on reactivity in response to RAI 6-4.
6	26	Added discussion of accident configurations below Table 6-14 in response to RAIs 2-14 and 6-7.
6	30-31	Section 6.5(b) was rewritten in response to RAIs 6-8 through 6-13.
7	1-3	Changed bullets to paragraph numbering in Section 7.2 in response to RAI 7-1.
7	2	Added description of "visual inspection" to paragraph 3 of Section 7.2.2 in response to RAI 7-1.
7	2	Added reference to the Section 4.5 inner seal region volume and sample calculation in paragraph 7 of Section 7.2.2 in response to RAI 7-2
7	4	Added "end cover plate, and thrust plate" to paragraph 6 of Section 7.6.4.
8	1	Added reference to ANSI N14.5-1997 and details regarding pressure drop test and fabrication leak test to Section 8.1.3 in response to RAI 8-1.

Enclosure (6)
Change Summary

Chapter	Page Number	Description of Change
8	2	Added requirement in Section 8.2.1 to "Inspect closure bolts and replace if damaged."
8	2	Added reference to ANSI N14.5-1997 and details regarding pressure drop test and fabrication leak test to Section 8.2.2 in response to RAI 8-2.
App. 1-1	1 & Drwg.	Revised Drawing No. 5016270 in response to RAI 1-1. Added Drawing No. 5021426 in response to RAI 1-1.
App. 1-2	All	Added appendix to provide additional information regarding the Pathfinder Fuel Assemblies in response to RAI 1-2.
App. 2-1	All	Added figure labels in response to RAI 2-8.
App. 3-1	1	Corrected Reference at the end of the 1st paragraph in response to RAI 3-11. Attached copy of Ref. 1 and 2 to the cover letter in response to RAI 3-12.
App. 3-2	All	Added appendix in response to RAI 3-8.
App. 6-2	All	Footer Changed due to total number of pages
App. 6-2	22-89	Rewrote the appendix to better explain the benchmarking process and methods in response to RAIs 6-8 through 6-13. Discussion has been completely revised. It now reflects the methodology of NUREG/CR-6361 for transportation rather than NUREG/CR-6698.

Enclosure (5)

Supplement to the amendment application for approval of packaging of fissile radioactive material (WE-1 Container),

Package Identification Number USA/9289/B(U) –85.
(Six copies)

FRAMATOME ANP

FRAMATOME ANP, INC.
MOUNT ATHOS ROAD FACILITY

APPLICATION FOR APPROVAL OF PACKAGING OF FISSILE RADIOACTIVE MATERIAL (WE-1 SHIPPING CONTAINER)

PACKAGE IDENTIFICATION NUMBER USA/9289/B(U)-85

MAY 2002

U.S. NUCLEAR REGULATORY COMMISSION

DOCKET
71-9289

TABLE OF CONTENTS

NUMBER AND TITLE

CHAPTER 1: GENERAL INFORMATION

1.1 INTRODUCTION

The WE-1 package is to be used for transporting one low-enriched uranium fuel assembly for light water power reactor core, or up to 48 Pathfinder fuel assemblies in the Pathfinder Canister. The nominal number of packages per shipment is to be one.

1.2 PACKAGE DESCRIPTION

1.2.1 PACKAGING

1.2.1.1 WE-1

Designation – WE-1 Shipping Container
Gross Weight – (Test Weight) 9090 lbs.
Fabrication – The design & fabrication details for WE-1 series shipping containers are detailed in drawings included in Appendix 1-1.
Coolants – Not applicable.

1.2.2 OPERATIONAL FEATURES

Not applicable.

1.2.3 CONTENTS OF PACKAGING

1.2.3.1 WE-1 CONTAINER – CONTENTS DESCRIPTION (REF. TABLE 1-1AND TABLE 1-3)

Identification and Enrichment of Special Nuclear Material (SNM) – The SNM will be low enriched uranium derived from surplus off-specification (reprocessed) highly enriched uranium enriched up to 4.6 weight percent in the isotope U-235, or legacy Pathfinder assemblies enriched up to 7.5 weight percent in the isotope U-235.

Form of SNM – The SNM will be in the form of a clad fuel assembly. In the clad form, the assembly will not disruptively react or decompose at the Accident Thermal Condition. No chips, powders, or solutions will be offered for transport in the packaging.

Maximum Weight of Fissile Contents – 22.14 Kg 235U

Maximum Fuel Assembly Weight – 1610 lbs.

Maximum Decay Heat – Negligible

Transport Index - 100

1.2.3.2 BW 17x17 FUEL ASSEMBLY PARAMETERS

The attached tables are the fuel assembly parameters for the BW17x17 design to be transported in the WE-1 fuel shipping container. The parameters indicated are used in the Criticality Analysis section to support un-contained and contained fuel assembly calculations.

TABLE 1-1

FUEL ASSEMBLY DESCRIPTION	17 X 17
FUEL ASSEMBLY TYPE	BW
NOMINAL PELLET DIAMETER	0.3195
NOMINAL CLAD THICKNESS	.022
CLAD MATERIAL	ZIRC
NOMINAL CLAD OUTER DIAMETER	0.3740
MAXIMUM STACK LENGTH	144 +/-0.225
NOMINAL ASSEMBLY ENVELOPE	8.565
Kg's 235U ASSEMBLY	24
NOMINAL LATTICE PITCH	0.496
ASSEMBLY KEFF	0.93144

Note: Geometric dimensions are in inches.

MAXIMUM URANIUM ISOTOPIC, FISSION PRODUCT, AND TRANSURANIC LIMITS FOR CONTENTS OF WE-1 SHIPPING CONTAINER
TABLE 1-2

ISOTOPE	COMPOSITION
U-232	0.010 µgm/gmU
U-234	0.10 w/o
U-235 (BW17x17)	4.60 w/o
U-235 (Pathfinder)	7.51 w/o
U-236	1.30 w/o
TC-99	5 µgm/gmU
FISSION PRODUCTS	4.4×10^5 MevBq/KgU
NP+PU	35 Bq/gmU

1.2.3.3 PATHFINDER FUEL ASSEMBLY PARAMETERS

The tables in this section detail the fuel assembly parameters for the Pathfinder design to be transported in the WE-1 fuel shipping container. The parameters indicated are used in the Criticality Analysis section to support un-contained and contained fuel assembly calculations. The fuel assemblies include a stainless steel or inconnel sleeve that protects and supports the assembly.

TABLE 1-3

FUEL ASSEMBLY DESCRIPTION	6 fuel rod triangular array
FUEL ASSEMBLY TYPE	Pathfinder
# of FUEL ASSEMBLIES PER SHIPMENT	≤ 48
NOMINAL PELLET DIAMETER	0.207 ± 0.0005 in.
NOMINAL UO_2 DENSITY	10.61 g/cm^3
CENTER-TO-CENTER PIN PITCH	0.289 in.
CLAD MATERIAL	Incoloy 800
NOMINAL CLAD OUTER DIAMETER	0.247 ± 0.001 in.
NOMINAL CLAD INNER DIAMETER	0.211 ± 0.001 in.
MAXIMUM STACK LENGTH	72 in.
NOMINAL ASSEMBLY ENVELOPE	1 (with Sleeve)
Kg's ^{235}U ASSEMBLY	2.206
NOMINAL SLEEVE INNER DIAMETER	0.945 in.
NOMINAL SLEEVE OUTER DIAMETER	1.00 in.
ASSEMBLY KEFF (MAXIMUM OF 48 ASSEMBLIES)	0.82126

For the Pathfinder fuel, the Assembly k_{eff} is based on the optimal spacing calculations for up to 48 assemblies. The value reported is $k_{calc} + 2\sigma$. This calculation is reported in Chapter 6.

1.3 Quality Assurance Program

All of the Pathfinder activities were performed per Framatome ANP Quality Assurance Program, document #NFQM, titled "Nuclear Fuel Business Group Quality Management Manual," (US Version) Rev 0 dated June 2002. The NRC has reviewed the program under 10 CFR 71.12(b). The NRC approval is documented in docket #71-0003, Revision 21, dated June 14, 2002.

Previous work on the WE-1 was also performed per and NRC approved Quality Assurance Program that was active at the time of those activities.

CHAPTER 2: STRUCTURAL EVALUATION

2.1 STRUCTURAL DESIGN

This chapter presents the structural evaluations that demonstrate that the design of the WE-1 Package meets all applicable structural criteria to ensure safe, reliable shipment of its unirradiated fresh fuel contents. Normal conditions of transport and hypothetical accident conditions are addressed by analytical and experimental evaluations performed in accordance with the requirements of 10 CFR 71.45, 71.71, and 71.73. Results from full-scale testing of a WE-1 Type B shipping container loaded with a standard MK-BW fuel assembly (except that the rods were loaded with tungsten carbide pellets in place of UO_2) were used to determine hypothetical accident (drop from 30 feet and pin puncture) loads.

A summary of the structural design of the WE-1 Package is presented including the design criteria used to evaluate the packaging performance. Section 2.2 is a listing of the weights of the packaging and contents. Materials of construction are presented in Section 2.3. Results from the evaluations that demonstrate compliance with the design criteria for general standards for all packages, normal conditions of transport, and hypothetical accident conditions are presented in Sections 2.6, 2.7 and 2.10.

2.1.1 Discussion

The WE-1 package consists of a cylindrical outer container that is designed to open into two, semi-cylindrical halves. The outer container's inner structure is a U-shaped channel supported on multiple elastomeric shock mounts. The outer container and associated structural components are fabricated primarily of mild carbon steel. Positive closure of the outer container is provided by 58 T-bolts.

Interfacing to the outer container's U-shaped channel via ten, 1 inch diameter stainless steel bolts, is a boxy inner container. Wood dunnage surrounds the periphery between the inner container and the U-shaped channel. To supplement the ten stainless steel bolts, 8 external clamp arms secure each side of the inner container to the U-shaped channel (16 total).

The inner container is comprised entirely of one inch thick, HY-80 carbon steel armor plate on all sides. The long edges are adjoined with 28, 1/2 inch diameter, Series 300 stainless steel bolts. The end plates are secured with 12, 1/2 inch diameter, Series 300 stainless steel bolts. Nine integral clamp frames, fabricated of one inch thick, HY-80 carbon steel armor plate, are used for supporting and securing a single fuel assembly within the inner container.

Refer to the Package General Arrangement Drawings for details of this design, which are included in Appendix 1-1 of this application.

The WE-1 package design has been subjected to the hypothetical accident condition (HAC), free drop and puncture conditions of 10 CFR §71.73[1]. These tests demonstrate the package's ability to adequately protect the fuel assembly payload, and establish initial conditions for the HAC fire event discussed in Chapter 3, *Thermal Evaluation.*

The WE-1 Package has been modified for shipment of non-irradiated Pathfinder fuel assemblies. A newly designed Pathfinder Canister will be used for the shipment of up to 48 Pathfinder fuel assemblies.

For Pathfinder fuel shipments, the shipping package consists of three layers of protective structures, a cylindrical outer container (or shell), a rectangular inner container (or box) and cylindrical inner sealed canister (Pathfinder Canister). All three layers provide protection against mechanical and thermal loads under normal and accident conditions of transport.

The outer container is constructed of 11-gauge carbon steel and opens into two semi-cylindrical halves. The inner rectangular container is comprised of 1-inch thick, high strength carbon steel plates that are bolted together. This inner rectangular container is bolted to a strongback. The inner most stainless steel structure is a sealed cylindrical canister (Pathfinder Canister). The fuel assemblies will be housed in this inner canister.

The Pathfinder Canister is surrounded by thermal insulation and is secured inside the rectangular container with five integral clamp frames. The clamp frames, which consist of bolted clamp arms, are bolted to the inner rectangular container. Wood blocks surround both ends of the Pathfinder Canister.

The inner rectangular container with strongback is supported to the outer cylindrical container by 14 shock mounts. Wooden blocks surround the inner rectangular container. These blocks limit the impact resulting from accident conditions.

The Pathfinder Canister serves as the primary containment for the contents. The Pathfinder Canister is made of austenitic stainless steel and has a welded body and bolted closure lid. The Pathfinder Canister is a 8 inch schedule 40 S stainless steel pipe with welded bottom plate and welded top 8"-150# weldneck flange. The closure lid is machined from an 8"-150# austenitic stainless steel blind flange. The lid has two machined grooves that contain metallic O-rings that complete the closure. The primary and secondary closure seals are 0.125 inch cross section Alloy 600 O-rings. A gasket wall thickness of 0.010 inch permits

[1] Title 10, Code of Federal Regulations, Part 71 (10 CFR 71), *Packaging and Transportation of Radioactive Materials*, United States Nuclear Regulatory Commission (USNRC), 1998.

sufficient compression (nominal 21%) of the O-ring to produce a forgiving seal design that is not impaired by minor surface imperfections. A test port on top of the lid allows a vacuum or pressure test of the annulus between the O-rings. The closure is held in place by eight 3/4-10UNRC-2A by 2.5 inch long ASTM-A-193-B8M Class 2 bolts. The bolts are located on an 11.75 inch diameter bolt circle. The bolts have a flat washer bent into place to prevent inadvertent loosening. The Pathfinder Canister has a cavity nominally eight inches in diameter and 88 inches long. The payload is cushioned within the cavity by placing filler material in any void above the stack fuel. The cavity contains air at ambient conditions.

The WE-1 shipping container is a descendent of containers 51032-1 (Docket 71-6581)[2.35] and 51032-2 (Docket 71-9252)[2.36]. The major components such as the outer container, skid, stacking brackets, shock mount, and strongback are the same among these shipping packages. For WE-1 with Pathfinder Canister, the outer container including skid and stacking brackets, shock mount, strongback, and HY-80 inner container are not altered from the previously licensed package. The only change made to accommodate the Pathfinder Canister is removal of the end clamp. The effect of the end clamp removal is discussed in Section 2.10.2.8.

2.1.2 Design Criteria

The design of the WE-1 package complies with the normal conditions of transport (NCT) structural requirements of 10 CFR §71.71. Compliance is demonstrated through the application of design criteria that requires no yielding of the container shell under a static loading of five times the weight of the loaded package.

The design of the WE-1 package also complies with the hypothetical accident condition (HAC) structural requirements of 10 CFR §71.73. A WE-1 package, loaded to the maximum gross weight, was subjected to the HAC free drop and puncture test conditions. These drop tests resulted in minor damage to the inner container assembly and fuel assembly. As such, analytic assessments of the WE-1 package for the HAC tests are not performed.

The Pathfinder Canister is designed to meet the standards and criteria for radioactive shipping containers as set forth in the Code of Federal Regulations 10CFR71, "Packaging and Transportation of Radioactive Material." U.S. Nuclear Regulatory Commission (NRC) Regulatory Guide 7.6, "Design Criteria for the Structural Analysis of Shipping Cask Containment Vessels" Revision 1, dated March 1978, and Regulatory Guide 7.8, "Load Combination for the Structural Analysis of Shipping Casks for Radioactive Material," Revision 1, dated March 1989 are used in the structural evaluation.

The Pathfinder Canister materials, design, fabrication, examination and testing meet the requirements of ASME Boiler and Pressure Vessel Code, Section III, 1995 edition and addenda through 1996 addenda (herein after is referred to as a Code). Additional fabrication and welding requirements of NUREG/CR-3854,

"Fabrication Criteria for Shipping Containers" and NUREG/CR-3019, "Recommended Welding Criteria for Use in the Fabrication of Shipping Containers for Radioactive Materials," are also considered. Vessel buckling is evaluated per ASME Code.

Level A (normal) and Level D (accidental) service limit stress allowable for primary membrane, primary bending, secondary, bearing, shear and buckling stresses for containment structures and fasteners are taken from Section III of the American Society of Mechanical Engineers Boiler & Pressure Vessel (ASME B&PV) Code. Table 2.1-1 provides the stress allowable used for the Pathfinder Canister. Material data used in the evaluation correspond to the design stress value Sm, yield strength Sy, and ultimate strength Su, at specified temperature given in the ASME B&PV Code, Section III, Class 1.

For conditions addressed by analysis, the margin of safety is calculated. The margin of safety (M.S.) is defined as

$$\text{Margin of Safety} = \frac{\textit{Allowable Stress}}{\textit{Actual Stress}} - 1$$

If the margin of safety is 10 or higher, it is defined as 'Large.'

For the Pathfinder Canister, the matrix of load combinations given in Regulatory Guide 7.8 is evaluated to determine the worst case combinations. Acceptance criteria are those presented in the applicable portions of the ASME B&PV code as outlined in Regulatory Guide 7.6.

The evaluation of the Pathfinder Canister includes results from full-scale testing of a WE-1 Type B shipping container loaded with a standard MK-BW fuel assembly (except that the rods were loaded with tungsten carbide pellets in place of UO_2) for accident conditions as specified in 10CFR7l. The drop test results are modified to account for the Pathfinder Canister stiffness and weight.

Table 2.1-1 Pathfinder Canister Allowable Stresses

Stress Category	**Normal Condition**	**Accident Condition**
Primary membrane stress intensity [A]	S_m	Lesser of 2.4 S_m and 0.7 S_u
Primary membrane + bending stress intensity[B]	1.5 S_m	Lesser of 3.6 S_m and S_u
Range of primary + secondary stress intensity[C]	3.0 S_m	Not applicable
Extreme stress range of total stress intensity[D]	2 S_a	2 S_a @ 10 cycles
Bearing stress	S_y[E]	S_y for seal surface S_u elsewhere
Pure primary shear stress[F]	0.6 S_m[F]	0.42 S_u
Buckling	Margin 2	Margin 1.34
Bolts		
Membrane Stress[G]	Lesser of 2.0 S_m and S_y[I]	Lesser of 0.7 S_u and S_y[J]
Membrane + Bending Stress[G]	Lesser of 3.0 S_m and S_y[I]	S_y[H]
Shear Stress	Not Applicable	Lesser of 0.42 S_u and 0.6S_y[J]
COMBINED STRESS	Not Applicable	$(f_t/F_{tb})2 + (f_v/F_{vb})^2 \leq 1$[J]

Applicable to Pathfinder Canister, closure lid and closure bolts.

(A) Per NRC Regulatory Guide 7.6, Paragraphs C.2 and C.6, and ASME Code NB-3221.1 and Appendix F-1331.1.
(B) Per NRC Regulatory Guide 7.6, Paragraphs C.2 and C.6, and ASME Code NB-3221.3.
(C) Per NRC Regulatory Guide 7.6, Paragraph C.4, and ASME Code NB-3222.2.
(D) Per NRC Regulatory Guide 7.6, Paragraph C.7.
(E) Per ASME Code NB-3227.1.
(F) Per ASME Code NB-3227.2 and Appendix F-1331.1(a).
(G) Not considering stress concentrations.
(H) A conservative value used for accident conditions.
(I) Per ASME Code NB-3232
(J) Per ASME Code F-1335

The design requirements for the Pathfinder Canister are summarized below:

1. No significant deterioration of the effectiveness of the canister from ambient conditions of -40° F to 100°F.
2. No susceptibility of brittle fracture at cold -40°F condition.
3. Canister to maintain pressure tight seal for external pressure from 3.5 psia to 20.3 psia, and for all drop-puncture-thermal accident cases. The leakage rate of the canister less than 10^{-3} atm cc/sec air.
4. Insensitive to vibration environment.
5. Positive closure device for canister.
6. Maintain geometric form of canister as a containment barrier. No loss of contents or effectiveness of gasket.

2.2 WEIGHTS AND CENTERS OF GRAVITY

The maximum gross weight of the WE-1 package is 9,090 pounds. Of that weight, the fuel assembly is 1,610 pounds, the inner container is 3,390 pounds, and the outer container is 4,090 pounds. The center of gravity is situated near the geometric center of the package.

The maximum gross weight of the WE-1 Package containing the Pathfinder Canister and fuel is 8,500 lbs. Of that weight, the Pathfinder fuel is 480 lbs. For a fully loaded Pathfinder Canister, the center of gravity is 2.4 inches from the geometric center of the inner rectangular container, towards the Pathfinder Canister bolted closure end.

2.3 MECHANICAL PROPERTIES OF MATERIALS

The major structural components of the WE-1 package's outer container are fabricated of mild carbon steel, and the closure T-bolts are fabricated of SAE J429, Grade 5, carbon steel bolting material. The following conservative stress values are utilized for NCT analytical evaluations of the outer container: tensile yield, σ_y = 36,000 psi; shear yield, $\tau_y = 0.6 \times \sigma_y$ = 21,600 psi, tensile ultimate, σ_u = 58,000 psi; shear ultimate, $\tau_u = 0.6 \times \sigma_u$ = 34,800 psi.

The major structural components of the inner container are fabricated of HY-80 carbon steel armor plate (conforming to MIL-S-16216/SH/REV K, June 19, 1987, Type II). The inner container closure bolts are fabricated of Series 300 stainless steel bolting material. No analytic evaluations are performed on the inner container.

The non-metallic structural materials include the rubber shock mounts for the load suspension system, wood shoring used as dunnage for the inner container, rubber gaskets, and ceramic fiber insulation surrounding the fuel assembly.

Pathfinder Canister: Standard commercial material, 300 series stainless steel, is used in the construction of the Pathfinder Canister. Aluminum 6061 is used for the support spacers. Commercial Nitrile Duro 60 rubber pad is used between the support spacer and canister to prevent metal to metal contacts. The pine and oak wood spacers are used for energy absorbers. A listing of the materials and specifications is presented below.

Materials of Construction

Component	Material	Specification
Pathfinder Canister		
Cylinder	304L or 316L Pipe	ASTM-A312-Tp 304L or Tp 316L 8" Sch 40S Pipe
Bottom Plate	304L or 316L Plate	ASTM-A240 Type 304L or 316L ASTM-A479 Type 304L or 316L
Weld Neck Flange	F304L or F316L	ASTM-A182-F304L or F316L 8"-150# Welding Neck Flange
Closure Lid	F304, F304L, F316 F316L	ASTM-A182-F304L, F304, F316L or F316L, 8"-150# Blind Flange, raised
Closure Bolts	Stainless Steel	ASTM-A193 B8M Class 2
O-ring	Metallic Seal	Alloy 600
Spacer Tube		
Cylinder	304L or 316L Pipe	ASTM-A312-Tp 304L or Tp 316L 8" Sch 40S Pipe
End Plate	304L or 316L Plate	ASTM-A240 Type 304L or 316L ASTM-A479 Type 304L or 316L
Support Spacer	Aluminum Rubber Pad	ASTM B-209 6061 T651 Commercial Nitrile Duro 60
Impact absorber	Wood	pine and oak (flame retardant treated per MIL-L-19140)

Materials used in the fabrication of the Pathfinder Canister are in accordance with ASTM standards, which are equivalent to materials listed in the ASME B&PV Code Section III. Options are given to use either 304L or 316L stainless steel for the welded components (i.e. the pipe and its mating weldneck flange, and the bottom plate). 304 and 316 stainless steel are additional options for the closure. The properties given in ASME Section III for 304L stainless steel are the lowest of these options and are used as the acceptance criteria for the analysis.

Material properties used in the structural analysis are tabulated on the following pages. The ASME B&PV Code[2.2] is the source for the mechanical properties. For

the closure bolting material, the conservative properties of the Class 1 material are used instead of ASTM-A193 B8M Class 2 material.

Table 2.3-1 Pathfinder Canister/Spacer Tube Material Properties
ASTM-A182-F304L; ASTM-A312-TP304L; ASTM-A240-TYPE 304L (Plate)

Material Temperature [°F]	**-40°F(7)**	**100**	**200**	**300**	**800**
$S_y \times 10^{-3}$ [LBS/IN^2] (1)	>25	25	21.3	19.1	14.4
$S_u \times 10^{-3}$ [LBS/IN^2] (2)	>70	70	66.2	60.9	55.5
$S_m \times 10^{-3}$ [LBS/IN^2] (3)	16.7	16.7	16.7	16.7	13.0
$\alpha_m \times 10^{-6}$ [IN/IN-°F] (4)	8.21	8.55	8.79	9.00	9.82
TC [BTU/HR-FT-°F] (5)	<8.7	8.7	9.3	9.8	12.2
TD [FT^2/HR] (5)	<.152	.152	.156	.160	.184
$E \times 10^{-6}$ [LBS/IN^2] (6)	29.3	28.3	27.6	27.0	24.1

Notes:
(1) Yield Strength, ASME Section III[2.2], Table Y-1
(2) Tensile Strength, ASME Section III[2.2], Table U
(3) Design Stress Intensity, ASME Section III[2.2], Table 2A
(4) Coefficient of Thermal Expansion, Table TE-1[2.2] (18CR-8Ni)
(5) Thermal Conductivity and Diffusivity, Table TCD[2.2] (18CR-8Ni)
(6) Moduli of Elasticity, Table TM-1[2.2] (Austenitic Steels)
(7) -40° F properties are extrapolated values from ASME Section III

Table 2.3-2 Bolts – (Closure Lid) Material Properties
ASTM-A193-B8M Class 1

Material Temperature [°F]		-40°F[7]	100	200	300	800
$S_y \times 10^{-3}$ [LBS/IN^2]	(1)	>30	30	25.8	23.4	17.4
$S_u \times 10^{-3}$ [LBS/IN^2]	(2)	>75	75	64.5	58.7	43.5
$S_m \times 10^{-3}$ [LBS/IN^2]	(3)	>10	10.0	8.6	7.8	5.8
$\alpha_m \times 10^{-6}$ [IN/IN-°F]	(4)	8.26	8.54	8.76	8.97	9.90
TC [BTU/HR-FT-°F]	(5)	<7.9	7.9	8.4	9.0	11.5
TD [FT^2/HR]	(5)	<.136	.136	.141	.145	.173
$E \times 10^{-6}$ [LBS/IN^2]	(6)	29.3	28.3	27.6	27.0	24.1

Conservative value of Class 1 material properties are used for the Class 2 bolts.

Notes: Conservative values of S_y and S_u are taken at 800 F.
(1) Yield Strength values given change with temperature as "S_m" given in, Table 4[2.2]
(2) Tensile Strength Values given change with temperature as "S_m" given in, Table 4[2.2]
(3) Design stress Intensity, Table 4[2.2]
(4) Coefficient of Thermal Expansion, Table TE-1[2.2] (16CR-12Ni-2Mo)
(5) Thermal Conductivity and Diffusivity, Table TCD[2.2] (16CR-12Ni-2Mo)
(6) Moduli of Elasticity, Table TM-1[2.2] (Austenitic Steels)
(7) -40° F properties are extrapolated values from ASME Section III

Support Spacers at Clamp Locations
ASTM B-209 6061 T651 aluminum

S_y = 35 ksi — ASME Section III, Table Y-1,
ρ = 0.098 lbs/in^3 — ASM Metals handbook[2.34]

Wood Impact Absorbers
Pine (Eastern White, Ref. [2.7], pgs. 6-113 and 6-115)
σ_{crush} = 4,800 psi ±18%, parallel to grain
ρ = 24 lbs/ft^3 ± 15%

Oak (White, Ref. [2.7], pgs. 6-113 and 6-115)
σ_{crush} = 1,070 psi ±15%, perpendicular to grain (conservative tolerance)
ρ = 48 lbs/ft^3 ± 15%

2.4 GENERAL STANDARDS FOR ALL PACKAGES

2.4.1 Minimum Package Size

The minimum transverse dimension (i.e., the diameter) of the WE-1 package is approximately 43 inches, and the minimum longitudinal dimension (i.e., the length) is approximately 216 inches. Thus, the requirement of 10 CFR §71.43(a) is satisfied.

2.4.2 Tamper-indicating Feature

A tamper-indicating seal is installed between the outer container cover and base, as delineated on the drawings in Appendix 1-1. Failure of the tamper-indicating device provides evidence of possible unauthorized access. Thus, the requirement of 10 CFR §71.43(b) is satisfied.

2.4.3 Positive Closure

The WE-1 package is positively closed by means of fasteners that require use of tools and deliberate action to facilitate their removal. A total of 58, 1/2-13UNC, SAE J429, Grade 5, T-bolts are used to close the outer container. A total of 136, 1/2-13UNC, Series 300 stainless steel bolts are used to assemble and close the inner container. Additional detail of the packaging closure system is provided on the Package General Arrangement Drawings in Appendix 1-1 of this application. Thus, the requirement of 10 CFR §71.43(c) is satisfied.

2.4.4 Chemical and Galvanic Reactions

The WE-1 package is primarily fabricated from carbon steel, and the fuel assemblies are fabricated from stainless steel, Inconel, and Zircaloy. The inner container's thermal insulation is comprised of non-reactive ceramic fiber. Thus, no potential exists for chemical or galvanic reactions to occur. Thus, the requirement of 10 CFR §71.43(d) is satisfied.

The Pathfinder Canister is fabricated from austenitic stainless steel. Welded materials in the Pathfinder Canister are specified to be low carbon alloys to provide maximum resistance to intergranular corrosion. Non-metallic insulating materials separate the canister and the strongback box/clamps, therefore galvanic reactions are not expected. Commercial Nitrile Duro 60 rubber will separate the aluminum support spacers and the stainless steel canister. No chemical or galvanic reactions are possible between all these materials and the intended contents of the Pathfinder Canister.

2.4.5 Valves

No valves are utilized in the design of the WE-1 package. Thus, the requirements of 10 CFR §71.43(e) are not applicable.

2.4.6 Package Design

As shown in Chapter 2.0, *Structural Evaluation*, Chapter 3.0, *Thermal Evaluation*, Chapter 5.0, *Shielding Evaluation*, and Chapter 6.0, *Criticality Evaluation*, the structural, thermal, shielding, and criticality requirements, respectively, of 10 CFR §71.43(f) are satisfied for the WE-1 package.

2.4.7 External Temperatures

The WE-1 package is designed for exclusive use shipment. As shown in Chapter 3, *Thermal Evaluation*, the maximum accessible surface temperature with the fuel assembly's negligible decay heat load and no insolation is 100 °F. Since the maximum external temperature does not exceed 122 °F, the requirements of 10 CFR §71.43(g) are satisfied.

2.4.8 Venting

The WE-1 package does not provide a containment boundary as no pressure-tight seals are included in the design. The fuel rod cladding is the containment boundary, and does not include any features intended to allow continuous venting during transport. The Pathfinder Canister does not include any features intended to allow continuous venting during transport. Thus, the requirements of 10 CFR §71.43(h) are satisfied.

2.5 LIFTING AND TIE-DOWN STANDARDS FOR ALL PACKAGES

2.5.1 Lifting Devices

2.5.1.1 Lifting Lug Load Calculation

Four lifting attachments that are a structural part of the WE-1 package are designed with a minimum safety factor of three against yielding to lift the loaded package in the intended manner. The lifting lugs are loaded at an angle 45° from horizontal. The lifting lugs are located symmetrically about the package's center of gravity, with the four cables/chains/straps meeting at a point directly above the package's center of gravity. The cable/chain/strap tension, T, given the vertical load is one-fourth of the 9,090 pound WE-1 package gross weight, is:

$$T = \frac{9{,}090}{4(\sin 45°)} = 3{,}214 \text{ lbs}$$

A conservative value of 3,300 pounds shall be used in the subsequent analyses.

The Pathfinder Canister will not be handled when loaded with fuel (i.e. the canister is secured in the inner rectangular container before the fuel is placed into the canister). During assembly, the Pathfinder Canister without the lid and bolts weighs approximately 260 lbs and is handled by commonly available slings and/or

hoist equipment. The canister does not have any lifting devices, which are part of the canister.

2.5.1.2 Lifting Lug Tear-out Analysis

Each lifting lug is fabricated of 3/8 inch thick mild steel with a 2.0 inch hole. The hole centerline is 2.0 inches from the lug outside edge and 1.5 inches above the horizontal edge of the lug's base.

For a square-edged lug, the shear stress due to tear-out may be determined from Equation D26 and Figure D10 of Faupel and Fischer[2]. For a lifting lug thickness of t = 0.375 inches, a distance from the hole centerline to the outside lug edge of d = 2.0 inches, and a hole diameter of D = 2.0 inches, the shear stress is:

$$\tau = \frac{T}{2t[d-(0.383)D]} = \frac{3{,}300}{2(0.375)[2.0-(0.383)(2.0)]} = 3{,}566 \text{ psi}$$

From Section 2.3, *Mechanical Properties of Materials*, the shear yield allowable is 21,600 psi. Thus, for a factor of safety of three, the resulting Margin of Safety is:

$$\text{M.S.} = \frac{21{,}600}{3(3{,}566)} - 1 = +1.02$$

2.5.1.3 Lifting Lug Attachment Weld Analysis

For simplicity, the 1/4 inch fillet welds (see Figure 2.5-1) that attach the bracket to the rolled angle are conservatively assumed to carry the entire load. The weld throat length is 1/4 × sin(45°) = 0.177 inches.

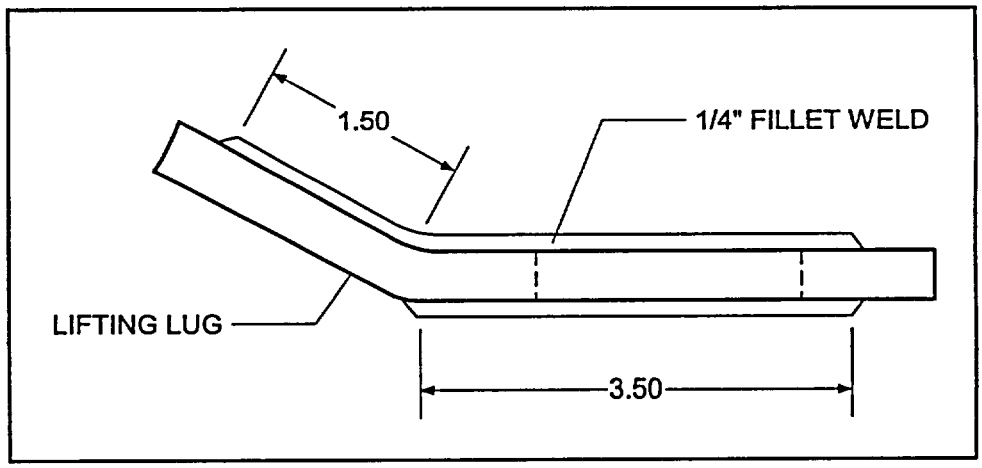

Figure 2.5-1 Lifting Lug Weld Configuration

[2] J. H. Faupel, F. E. Fisher, *Engineering Design – A Synthesis of Stress Analysis and Materials Engineering*, Second Edition, John Wiley & Sons, Inc., 1981, p1023.

The weld shear stress due to direct shear load on the weld is:

$$\tau_s = \frac{T}{t_w L_w} = \frac{3{,}300}{(0.177)(3.50+5.00)} = 2{,}193 \text{ psi}$$

The weld bending stress due to the 1.5 inch vertical offset is:

$$\tau_b = \frac{Mc}{I}$$

where the bending moment is 3,300 pounds × 1.5 inches = 4,950 inch-lbs. For simplicity, the 5.0 inch long top weld is treated as being parallel to the 3.5 inch long bottom weld. The distance from the right end of the two welds, shown in Figure 2.5-1, to the weld group neutral axis is:

$$\bar{x} = \frac{5.0^2 + 3.5^2}{2(5.0+3.5)} = 2.19 \text{ inch}$$

The moment of inertia of the weld group is:

$$I = \left(\frac{0.177}{12}\right)\left[5.0^3 + 3.5^3\right] + (0.177)\left[(5.0)\left(\frac{5.0}{2} - 2.19\right)^2 + (3.5)\left(2.19 - \frac{3.5}{2}\right)^2\right] = 2.68 \text{ in}^4$$

The maximum weld stress due to bending is:

$$\tau_b = \frac{(4{,}950)(5.0 - 2.19)}{2.68} = 5{,}190 \text{ psi}$$

The combined shear and bending stress is:

$$\tau = \sqrt{\tau_s^2 + \tau_b^2} = \sqrt{2{,}193^2 + 5{,}190^2} = 5{,}634 \ psi$$

From Section 2.3, *Mechanical Properties of Materials*, the shear yield allowable is 21,600 psi. Thus, for a factor of safety of three, the resulting Margin of Safety is:

$$M.S. = \frac{21{,}600}{3(5{,}634)} - 1 = +0.28$$

The above results demonstrate that the lifting lug and its attachment welds are adequate to withstand the required lifting loads. In addition, the relatively low Margin of Safety of the attachment welds ensure that failure of the welds occur before failure of the heavier underlying structure should inadvertent lifting lug overloading occur.

2.5.2 Tie-down Devices

There is no identified tie-down system on the WE-1 package. A combination of shoring, positioning studs and/or axial and transverse chokers (chains or straps) shall be used to secure the WE-1 package to the transport vehicle. Chokers will be passed over the package top to enable package restraint.

2.6 NORMAL CONDITIONS OF TRANSPORT

The performance requirements specified in Subpart F of 10 CFR 71 for normal conditions of transport (NCT) are met by the WE-1 package. Regulatory compliance is demonstrated in the following subsections where each normal condition is shown to meet the applicable regulatory criteria.

2.6.1 Heat

In Chapter 3.0, *Thermal Evaluation*, of this application concludes that the normal heat conditions specified in 10 CFR §71.71(c)(1) will have a negligible effect on the WE-1 package. The maximum package temperature for NCT is 122 °F.

2.6.1.1 Summary of Pressures and Temperatures

The WE-1 package is designed to provide confinement rather than containment; thus only a dust/debris seal is utilized at the outer container closure interface. Therefore, no internal pressure exists within the WE-1 package. The fuel rods comprise the containment boundary, and are pressurized with helium to 315 psig.

The fuel assembly exhibits negligible decay heat. The WE-1 package and all internal components, when loaded with the required 10 CFR §71.71(c)(1) insolation conditions, develop a maximum temperature of 122 °F.

Pathfinder Canister: The payload in the Pathfinder Canister generates no internal heat. Conservatively, the fuel is considered to be pressurized and to have leaked the gas into the canister.

Pressure	1 Atmosphere to 25.0 psia
Package Temperature	150°F maximum

2.6.1.2 Differential Thermal Expansion

Due to the relatively low temperature differentials and lack of internal restraint within the WE-1 package, differential thermal expansion is negligible.

The Pathfinder Canister is a cylinder with a bolted blind flange closure. The canister is insulated by Zircar insulation. The contents are unirradiated and have no decay heat. The canister materials are all austenitic stainless steel and have the same coefficient of thermal expansion. The closure bolts have a slightly

different coefficient of thermal expansion. The components of the bolted closure have similar mass and external surfaces, therefore any thermal transient will cause negligible differential expansion. The Alloy 600 O-rings with a temperature rating of 1000°F is used for the canister gaskets.

2.6.2 Cold

As with the heat condition, the cold conditions specified in 10 CFR §71.71(c)(2) will not adversely affect the performance of the package. Brittle fracture is not a concern due to the materials of construction and the dimensions of the material's cross-section, as demonstrated in the following discussion.

The inner container is fabricated of one inch thick, high alloy, quenched and tempered, HY-80 carbon steel armor plate. Per Figure 3 of NUREG/CR-1815[3], for one inch thick, Category I fracture critical components with the component stress equal to the dynamic yield strength (i.e., $\sigma/\sigma_{yd} = 1$), the "A" temperature is 45 °F. For a NCT lowest service temperature (LST) of -20 °F per 10 CFR §71.71(b), the nil ductility transition temperature, T_{NDT} = LST - A = -20 °F - 45 °F = -65 °F. Per Table 3 of NUREG/CR-1815, -160 °F $\leq T_{NDT} \leq$ -80 °F for HY-80 plate material between 5/8 and 4 inches thick. Thus, HY-80 plate will not exhibit a ductile-to-brittle transition in the temperature range of interest.

The outer container is fabricated of relatively thin sections of mild carbon steel. Per Table 5 of NUREG/CR-1815, for Category II fracture critical components with thicknesses of 0.19 inch or less, brittle fracture is not of concern. Similarly, per Table 6 of NUREG/CR-1815, for Category III fracture critical components with thicknesses of 0.4 inch or less, brittle fracture is not of concern.

The Pathfinder Canister and closure bolts are fabricated from austenitic stainless steel. This material is not subject to a ductile-to-brittle transition above -40°F, therefore it is safe from brittle fracture. Contents of the Pathfinder Canister will not contain sufficient liquids to cause the canister to expand due to freezing. The Alloy 600 O-rings are rated for cryogenic applications. No deterioration of the O-rings are expected during normal transport. Commercial Nitrile Duro 60 rubber pad is used between the support spacer and canister. This rubber has excellent weather resistance between –67 °F to +275 °F. No deterioration of the rubber is expected in the NCT.

2.6.3 Reduced External Pressure

The WE-1 package contains no pressure-tight seal and, therefore, cannot develop differential pressure. Therefore, the reduced external pressure requirement of 3.5 psia delineated in 10 CFR §71.71(c)(3) will have no effect on the package.

---

[3] W. R. Holman, R. T. Langland, *Recommendations for Protecting Against Failure by Brittle Fracture in Ferritic Steel Shipping Containers Up to Four Inches Thick*, NUREG/CR-1815, UCRL-53013, August 1981.

Compared with the 315 psig internal pressure in the fuel rods, a reduced external pressure of 3.5 psia will have a negligible effect on the fuel rods.

The 3.5 psia external pressure translates into a bursting pressure of 11.2 psig. Stress analysis of the Pathfinder Canister is documented in Section 2.10.2. Table 2.6.3-1 summarizes the stress analysis results.

Table 2.6.3-1 Reduced External Pressure – Pathfinder Canister Stress Summary

Component	Primary Membranne Stress Intensity – psi (or Rated Pressure – psig)			Primary Membrance Plus Bending Stress Intensity – psi (or Rated Pressure – psig)		
	Actual	Allowable	Margin of Safety	Actual	Allowable	Margin of Safety
Cylinder	378	16,700	Large	1004	25,050	Large
Bottom Plate	38	16,700	Large	408	25,050	Large
Weld Neck Flange	ΔP = 21.5 psig	Rated at 212 psig	8.86	ΔP = 21.5 psig	Rated at 212 psig	8.86
Blind Flange	ΔP = 21.5 psig	Rated at 212 psig	8.86	ΔP = 21.5 psig	Rated at 212 psig	8.86
Closure Bolt	17353	18,600	0.07	Fatigue Life > 4000 shipments		

2.6.4 Increased External Pressure

The WE-1 package contains no pressure-tight seal and, therefore, cannot develop differential pressure. Therefore, the increased external pressure requirement of 20 psia delineated in 10 CFR §71.71(c)(4) will have no effect on the package.

Pathfinder Canister: Calculations based on ASME criteria indicate that an 8 inch schedule 40 S pipe made from 304L stainless steel is capable of withstanding an external pressure differential of at least 431 psig. The 20.3 psia external pressure specified in 10CFR7l.71(c)(4) is equivalent to less than a 5.6 psi increase in differential pressure, and is well within the allowable external pressure for the Pathfinder Canister. The pressure stresses in the canister will be lower than the reduced external pressure loading condition (Section 2.6.3). Stress analysis of the Pathfinder Canister is documented in Section 2.10.2.

2.6.5 Vibration

The WE-1 package contains an internal shock mount system and, therefore, cannot develop significant vibratory stresses for the package's internal structures. Therefore, vibration normally incident to transportation, as delineated in 10 CFR §71.71(c)(5), will have a negligible effect on the package.

2.6.6 Water Spray

The materials of construction utilized for the WE-1 package are such that the water spray identified in 10 CFR §71.71(c)(6) will have a negligible effect on the package.

2.6.7 Free Drop

The WE-1 package weighs less than 11,000 pounds (5,000 kg), requiring a NCT free drop test of 4 feet as delineated in 10 CFR §71.71(c)(7). The hypothetical accident condition (HAC), 30 foot free drop test required in 10 CFR §71.73(c)(1) is substantially more damaging than the 4 foot NCT free drop test. Section 2.7.1, *Free Drop*, demonstrates the WE-1 package's survivability and bounds the free drop requirements of 10 CFR §71.71(c)(7). Due to the relatively fragile nature of the fuel assembly payload in maintaining its configuration for operational use, any event that would come close to approximating the NCT free drop would cause the package to be removed from service and re-examined prior to continued use.

Pathfinder Canister: This four foot drop test is much less severe than the 30-foot free drop specified under hypothetical accident conditions of 10CFR71.73(c)(1). Previous 4 foot drop tests of similar type packages have experienced acceleration levels of approximately 10 g's for this Normal condition. The acceleration values used in the Pathfinder Fuel Canister Faulted condition analysis are 142 g's and higher. Since the Faulted condition stresses are acceptable, the Normal condition stresses are also acceptable if

$(G_{Normal} / G_{Faulted}) <$ (Normal stress allowable / Faulted stress allowable)

Primary membrane stress is most limiting and from Table 2.1-1

$(10 / 142) < (S_m / 2.4\ S_m)$
$0.07 < 0.42$

Therefore, the stress margins from the Faulted condition drops will bound those drops under Normal conditions.

2.6.8 Corner Drop

The WE-1 package is fabricated primarily of carbon steel and exceeds 110 pounds (50 kg) gross weight. Therefore, the corner drop test requirement of 10 CFR §71.71(c)(8) is not applicable to the WE-1 package.

2.6.9 Compression

The compressive load requirement of 10 CFR §71.71(c)(9) is easily satisfied by the WE-1 package. This conclusion can be easily demonstrated by conservatively treating the package's outer container as a simply supported beam loaded by a

uniformly distributed load of five times the gross package weight. For a simply supported beam with a length L = 216.25 inches and a uniformly distributed load of W = 5 × 9,090 / 216.25 = 210 lbs/inch, the resultant maximum bending moment, M_B, in the outer container shell is:

$$M_B = \frac{WL^2}{8} = \frac{(210)(216.25)^2}{8} = 1{,}227{,}557 \text{ inch - lbs}$$

Conservatively neglecting any of the reinforcement due to the 2½ inch angle stiffeners on the outer container exterior, the moment of inertia of the 11-gauge (0.12 inch thick), 43.00 inch outside diameter outer container shell is:

$$I = \frac{\pi}{64}\left[D_o^4 - D_i^4\right] = \frac{\pi}{64}\left[(43.00)^4 - (42.76)^4\right] = 3{,}715 \text{ in}^4$$

The maximum bending stress, σ_B, is then:

$$\sigma_B = \frac{M_B c}{I} = \frac{(1{,}227{,}557)(43.00/2)}{3{,}715} = 7{,}104 \text{ psi}$$

From Section 2.3, *Mechanical Properties of Materials*, the tensile yield allowable is 36,000 psi. Thus, the resulting Margin of Safety is:

$$M.S. = \frac{36{,}000}{7{,}104} - 1 = +4.07$$

Therefore, the WE-1 package satisfies the requirements of 10 CFR §71.71(c)(9).

2.6.10 Penetration

The WE-1 package has relatively thick shells on both the outer and inner container. Further, the package is designed without external protuberances that, if damaged, could reduce the effectiveness of the packaging. Therefore, the penetration test of dropping a 13 pound (6 kg) steel rod 40 inches (1 m) onto the package, as defined in 10 CFR §71.71(c)(10), is of negligible consequence.

2.7 HYPOTHETICAL ACCIDENT CONDITIONS

The performance criteria specified in Subpart E of 10 CFR 71 are satisfied when the WE-1 package is subjected to the hypothetical accident conditions (HAC) of transport specified in 10 CFR §71.73. The package's ability to meet the design criteria, as discussed in Section 2.1, *Structural Design*, for the various accident conditions is presented below.

Following HAC free drop and puncture testing, the fuel assembly must remain within the inner container as protection from the HAC fire event. Further, the fuel rod cladding must not leak in excess of A_2 per week per 10 CFR §71.51(a)(2) following the HAC tests delineated in 10 CFR §71.73(c). Subsequent to HAC free

drop and puncture testing of a prototypic WE-1 package, leak testing of the fuel rods showed that the leak rate limit of A_2 per week was not exceeded.

The standards for the hypothetical accident conditions stipulate that a package used for shipment of radioactive material shall be designed and constructed such that if it is subjected to the specified drop, puncture, thermal, and water immersion conditions, a) the reduction in containment would not be sufficient to increase the external radiation dose rate to more than regulatory limit; b) no radiation material would be released from the package except for gases containing a total radioactivity not to exceed regulatory limit; c) the contents would remain subcritical.

Evaluation of the Pathfinder Canister for the hypothetical accident conditions described in the regulations is addressed by a combination of drop tests and analytical evaluation.

2.7.1 Free Drop

2.7.1.1 Introduction

Subpart F of 10 CFR 71 requires that a package withstand a free drop from a height of 30 feet (9 meters) onto a flat, essentially unyielding, horizontal surface in accordance with 10 CFR §71.73(c)(1). The package is to strike the surface in a position for which maximum damage is expected.

To comply with this free drop requirement, it is necessary to determine the orientation that would produce the maximum damage to and/or failure of the package. For the WE-1 package, failure is defined as leakage of the containment boundary (i.e., the fuel rod cladding) in excess of A_2 per week per 10 CFR §71.51(a)(2). Two scenarios may initiate failure: 1) causing the inner container to open sufficiently to produce fuel rod overheating and rupture during the subsequent HAC fire event, or 2) direct mechanical damage to the fuel rods resulting in excessive leakage.

2.7.1.2 Determination of the Primary Impact Angle for the Slapdown Drop

To determine the worst-case impact angle for free drop testing, a simplistic model of the WE-1 inner container/fuel assembly was modeled using the Shipping Cask Analysis System (SCANS) program[4]. The SCANS model consisted only of the inner container/fuel assembly, since the outer container can be effectively decoupled from the inner container because of the relatively soft elastomeric shock mounts. The SCANS model was then analyzed at primary impact angles of 15°, 30°, and 45° using an impact stiffness simulating the inner container's behavior after impact with the surface.

[4] M. A. Gerhard, D. J. Trummer, G. L. Johnson, G. C. Mok, *SCANS (Shipping Cask ANalysis System) – A Microcomputer Based Analysis System for Shipping Cask Design Review*, Version 2a, NUREG/CR-4554.

The results of the various computer runs of the SCANS model are provided in Table 2.7-1. The data indicates, for both the WE-1 with BW17x17 fuel or with the Pathfinder Canister, that a primary impact angle of 15° always bounds the maximum impact acceleration. Thus, a primary impact angle of 15° was utilized for certification free drop testing to maximize the slapdown acceleration.

Table 2.7-1 Comparison of Impact Accelerations for Various Primary Impact Angles

	Drop Angle degree	Primary Impact Acceleration in g's	Secondary Impact Acceleration in g's
WE-1 BW17x17 Fuel	15	83.9	126.5
	30	97.4	123.7
	45	116.	99.9
WE-1 Pathfinder Fuel	15	87.6	131.2
	30	101.5	127.8
	45	121.1	100.4

2.7.1.3 Description of the WE-1 Prototype Package used for Certification Testing

The WE-1 prototype package was fabricated identically to the configuration depicted in the Packaging General Arrangement Drawing found in Appendix 1-1. The fuel assembly was a standard BW 17×17, with tungsten carbide slugs in place of the uranium dioxide fuel pellets. The fuel rods were pressurized with helium gas to the normal fuel rod pressure of 315 psig. In addition, the 24 guide tubes were filled with solid stainless steel or brass rods to maximize fuel assembly gross weight. The as-tested weight of the fuel assembly was 1,610 pounds. No other modifications/variations of the packaging or payload design were introduced.

2.7.1.4 Results of WE-1 Prototype Package Free Drop Certification Testing

The WE-1 prototype package was tested at the drop test facility at Oak Ridge National Laboratory during December 1998. As illustrated in, the WE-1 prototype package was suspended 30 feet above the impact surface. As discussed in Section 2.7.1.2, *Determination of the Primary Impact Angle for the Slapdown Drop*, the package was oriented at an angle of 15° from horizontal to maximize the slapdown force. In addition, the package was oriented at an angle 135° circumferentially clockwise from the normally transported position (aligned with a set of stacking brackets located on the outer container exterior). This circumferential orientation was chosen to maximize damage to both the inner container and internal clamp frames by striking both components on their top corner.

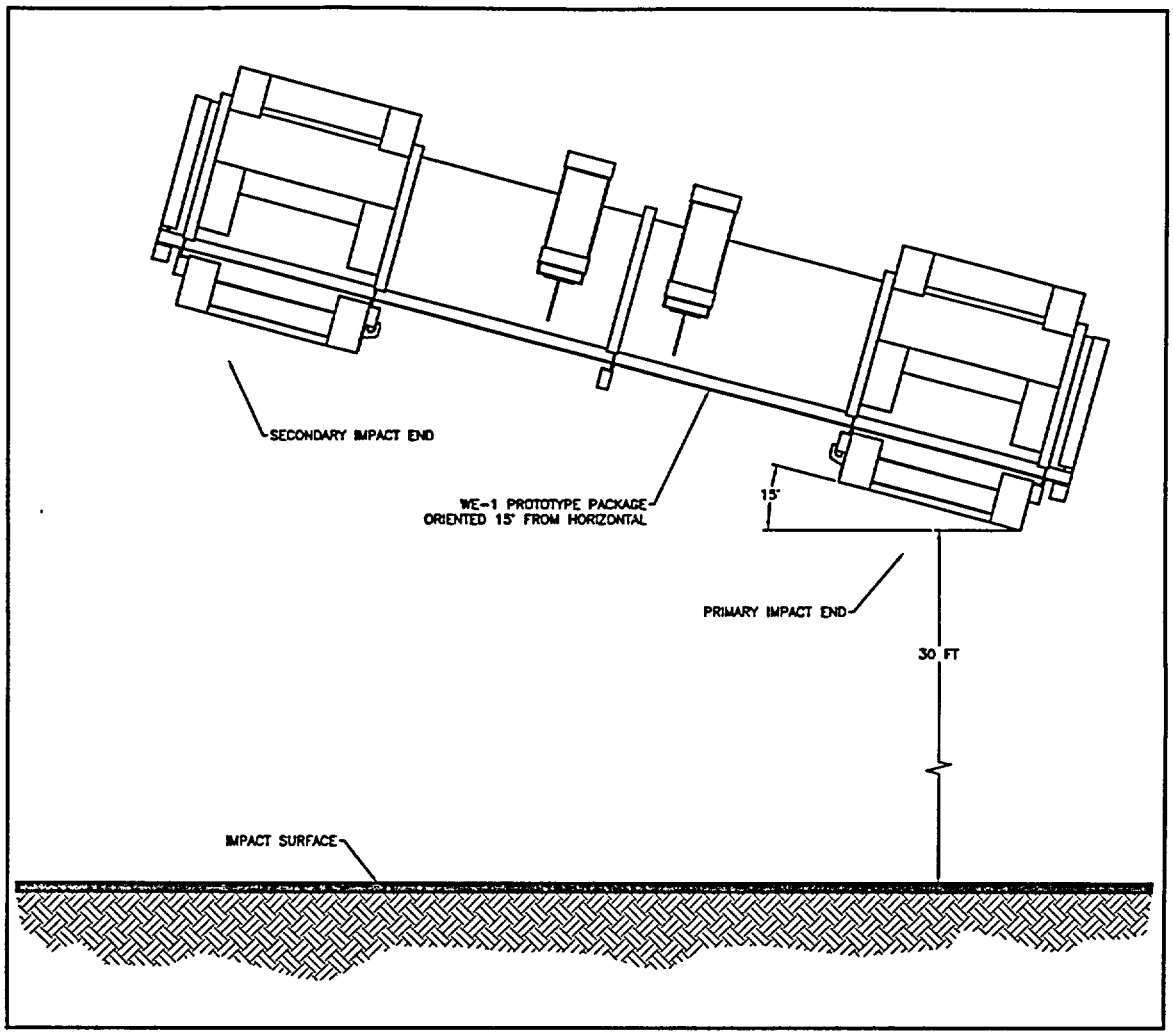

Figure 2.7-1 WE-1 Prototype Package 30 Foot Free Drop Orientation

Appendix 2-1, *WE-1 Prototype Package Certification Testing Photographs*, photo-documents the certification testing process and subsequent package disassembly.

Components located in the impact zone such as the outer container's stacking brackets and exterior, 2½ inch stiffening angles were crushed nearly flat during the 30 foot slapdown drop test. The outer container exhibited permanent radial deformations of approximately 3/4 inch at the primary impact end, and 2 inches at the secondary (slapdown) impact end. None of the 58 T-bolts securing the outer container cover to its base failed. The outer container shell was penetrated in the impact zone by each of the eight external clamp arms that were used to secure the inner container to the U-shaped channel inside the outer container.

After the 30 ft. drop and puncture tests, the sixteen external clamp arms were found intact, with none of the fasteners broken at either the inner container or U-shaped channel. Of the 56, 1/2-13UNC stainless steel bolts used to secure the top plate on the inner container, 16 were broken on the impacted corner, at the farthest (slapdown) end. Failure of these fasteners allowed the top plate to

separate approximately 3/16 inch at the farthest end. Further, all of the end plate bolts (also 1/2-13UNC stainless steel bolts) on the farthest (slapdown) end of the inner container were broken. Failure of these 12 fasteners allowed the end plate to separate approximately 1/2 inch from the inner container end. The end plate was restrained from further motion due to the end bracing and surrounding wood dunnage securing the inner container. Because of the presence of the 3 inch thick ceramic fiber insulation inside the inner container, these relatively small gaps have negligible effect on the subsequent HAC fire event presented in Chapter 3, *Thermal Evaluation.*

Four, 1/2-13UNC stainless steel bolts secure each internal clamp frame to the bottom and side of the inner container. Seven of the nine fasteners failed for the clamp frames; however, the clamping force exerted by the clamp frames on the fuel assembly ensured stability for both components.

Upon opening the inner container, the ceramic fiber insulation was found intact, with little permanent deformation (i.e., <1/2 inch at one localized region at the slapdown end of the inner container). For purposes of conservatism, however, the HAC thermal analysis in Chapter 3, *Thermal Evaluation*, assumes that all the insulation is permanently crushed to 2/3 its original thickness resulting in a 150% increase in thermal conductivity. The internal clamp frame at the slap down end exhibited a small permanent diagonal displacement aligned with the axis of the drop. None of clamp frame fasteners failed.

The fuel assembly exhibited modest permanent lateral deformation of the fuel rods at the slapdown end of the inner container (2¼ inch, maximum). Permanent bending of the fuel rods in the last grid span, but not in any other span, was probably caused by three factors: 1) the largest angular acceleration and, hence, translational impact force occurred at the slapdown end, 2) the grids provide intermittent supports for the fuel rods; at each fuel assembly end the fuel rods are essentially free to move longitudinally (i.e., not axially restrained), and 3) the largest span between grids occurs at the slapdown end. These three factors combined to cause the bending stress in the fuel rods to exceed their elastic limit. Those fuel rods adjacent to the ceramic fiber insulation exhibited the least amount of permanent deformation due to the lateral support provided by the insulation. All grids "racked" in the axis of the drop; however, grid effectiveness was not diminished and structural integrity was maintained with the fuel assembly remaining intact. Less permanent deformation was noted for the end grids constructed of Inconel rather than Zircaloy for intermittent grids.

Subsequent helium leak testing was performed for the individual fuel rods once removed from the fuel assembly. With the exception of a single fuel rod, all fuel rods demonstrated "leaktight" containment integrity to a leak rate of 1×10^{-7} cc/sec, air. The exception was a single fuel rod that exhibited a leak rate of 1.0×10^{-6} cm^3/sec, helium.

10 CFR 71.51(a)(2) states that after hypothetical accident testing, no escape of radioactive material exceeding a total amount A2 in 1 week; a typical A2 quantity for this material is 5.4 kg UO_2.

In summary, certification testing of the WE-1 prototype package demonstrated its ability to satisfactorily meet the requirements of 10 CFR §71.73(c)(1) and 10 CFR §71.51(a)(2).

2.7.1.5 Free Drop – WE-1 with Pathfinder Canister

The acceleration levels for 30-foot drop were determined by analysis using the deformed condition of the MK-BW Fuel Assembly which occurred during the drop test of the WE-1 Type B container qualification (Section 2.10.3). The drop acceleration for the WE-1 package with Pathfinder was increased by a factor of 1.05 from the drop test acceleration to account for the canister stiffness and weight. The Pathfinder Canister stresses are within the ASME stress limits for an accident condition. Stress analysis of the Pathfinder Canister is documented in Section 2.10.2. The results of the stress analysis are summarized below.

Table 2.7.1.5-1 30 Foot Drop – Pathfinder Canister Stress Summary

Component	Stress Intensity - psi		
	Actual	Allowable	Margin of Safety
Cylinder			
Slapdown	36,451	40,080	0.10
End Drop	26,298	40,080	0.52
Bottom Plate			
End Drop	6,944	40,080	4.77
Bling Flange			
End Drop	<6,944	40,080	>4.77
Closure Bolt			
Tension	17,874	27,900	0.56
Shear	2,656	16,740	5.30
Tension + Shear	Ratio sum = 0.44	Ration sum = 1.0	1.27
Thread Engegment	L = 0.551 in	L = 0.948 in	0.72

Buckling of Cylinder:

$S \leq 0.4\ s'$

26,298 psi $\leq$ 524,800 psi, $\therefore$ Design Margin = large

This buckling margin of safety is larger than the 1.34 permitted by the ASME Code.

2.7.2 Crush

Subpart F of 10 CFR 71 requires performing a dynamic crush test in accordance with the requirements of 10 CFR §71.73(c)(2). Since the WE-1 package weight exceeds 1100 pounds (500 kg), the dynamic crush test is not required.

2.7.3 Puncture

2.7.3.1 Introduction

Subpart F of 10 CFR 71 requires performing a puncture test through a distance of 40 inches (1 m) onto the upper end of a solid cylindrical, mild steel bar mounted vertically on an essentially unyielding horizontal surface in accordance with 10 CFR §71.73(c)(3). The package is to strike the puncture bar in a position for which maximum damage is expected. The puncture bar shall be 6.0 inches (15 cm) in diameter, with the top horizontal and its edge rounded to a radius of not more than 0.25 inches (6 mm), and of sufficient length to cause maximum damage to the package, but not less than 8 inches (20 cm) long. The long axis of the bar shall be vertical.

A description of the WE-1 prototype package is provided in Section 2.7.1.3, *Description of the WE-1 Prototype Package used for Certification Testing.*

2.7.3.2 Results of WE-1 Prototype Package Puncture Certification Testing

The WE-1 prototype package was tested at the drop test facility at Oak Ridge National Laboratory during December 1998. As illustrated in Figure 2.7-2, the WE-1 prototype package was suspended 1 meter above a 60 inch high puncture bar. The puncture bar was mounted to a 1 inch thick, 4 foot square steel plate that was secured to the drop pad with a plurality of intermittent welds.

The WE-1 package was oriented horizontally with respect to the longitudinal axis. As before for the free drop test, the package was oriented at an angle 135° circumferentially clockwise from the normally transported position (i.e., identical to the free drop circumferential orientation to maximize cumulative damage to the top corner of the inner container). A portion of the outer container outer shell was removed to facilitate aligning the corner of the inner container directly over the puncture bar.

Little damage to the inner container was noted; a slight denting occurred at the impacted corner. The mild steel puncture bar, however, exhibited a deep gouge caused by impact of the relatively high strength armor plate. Further discussion of package disassembly and observations is provided in Section 2.7.1.4, *Results of WE-1 Prototype Package Free Drop Certification Testing.*

In summary, certification testing of the WE-1 prototype package demonstrated its ability to satisfactorily meet the requirements of 10 CFR §71.73(c)(3).

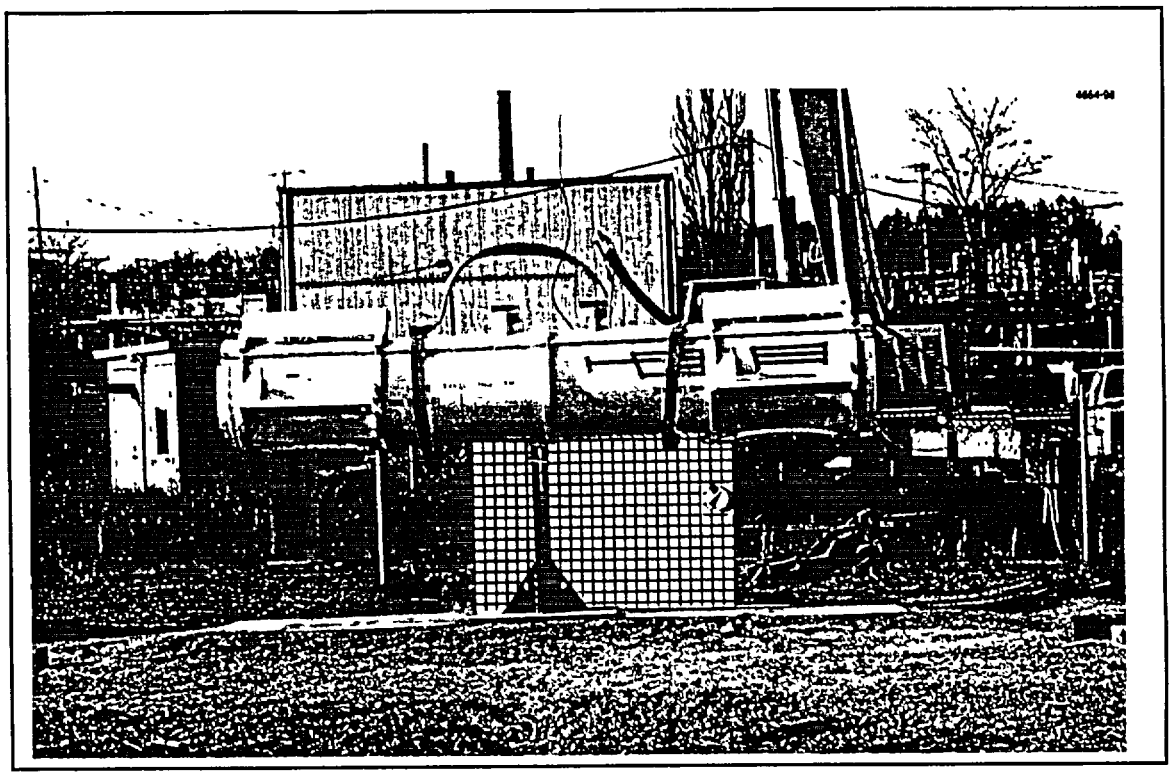

Figure 2.7-2 WE-1 Prototype Package 40 Inch Puncture Orientation

2.7.4 Thermal

The thermal evaluation of the WE-1 package for the HAC heat condition is presented in Chapter 3.0, *Thermal Evaluation*. Because the WE-1 package does not contain a pressure-tight seal, the HAC pressure is zero. The fuel assembly exhibits negligible decay heat. The maximum predicted HAC temperature for the fuel assembly is 792 °F during the fire event. The fuel rods are designed to withstand a temperature of 1,200 °F without bursting.

The thermal and thermal stress analysis of the Pathfinder Canister is documented in Section 2.10.2. Results of the analysis are summarized below.

The maximum temperature of the Pathfinder Canister is less than 792 °F and occurs near the support saddles. The maximum circumferential temperature gradient is 5.2 F° / inch and occurs near the support saddles. The maximum axial temperature gradient is 168 F° / inch and occurs between the bolted closure and the first support saddle. The combined thermal and internal pressure stress in the canister is

S = 81,054 psi
S < 2 Sa at 10 cycles
81,054 psi < 1,416,000 psi
Design Margin = large

Closure Bolts:
$S < S_y$ at 800 °F
15,458 psi < 17,400 psi

2.7.5 Immersion - Fissile Material

Subpart F of 10 CFR 71 requires performing an immersion test for fissile material packages in accordance with the requirements of 10 CFR §71.73(c)(5). The criticality evaluation presented in Chapter 6.0, *Criticality Evaluation*, assumes optimum hydrogenous moderation of the contents, thereby conservatively addressing the consequences and effects of water in-leakage.

Pathfinder Canister: For fissile material, in those cases where water leakage has not been assumed for criticality analysis, the regulation requires an immersion test under a head of three feet for period of not less than eight hours in an attitude for which maximum leakage is expected. The fully flooded condition is addressed in the Pathfinder Canister criticality analysis. Therefore, the three feet immersion test is not required.

2.7.6 Immersion - All Packages

Since the WE-1 package is not sealed against pressure, there will not be any differential pressure with the water immersion loads defined in 10 CFR §71.73(6). The water immersion will have negligible effect on the WE-1 container or the BW 17x17 fuel assembly payload.

Pathfinder Canister: The regulations require a separate undamaged canister which must be subject to water pressure equivalent to immersion under a head of water at least 50 feet for period of not less than eight hours. The Pathfinder Canister, functioning as the sealed containment boundary, is the only structural component affected by a pressure differential. Stress analysis of the Pathfinder Canister, based on ASME criteria, is documented in Section 2.10.2. The results of the stress analysis are summarized below.

Table 2.7.6-1 50 Feet Immersion – Pathfinder Canister Stress Summary

Component	Primary Membranne Stress Intensity – psi (or Rated Pressure – psig)			Primary Membrance Plus Bending Stress Intensity – psi (or Rated Pressure – psig)		
	Actual	Allowable	Margin of Safety	Actual	Allowable	Margin of Safety
Cylinder	382	16,700	Large	1014	25,050	Large
Bottom Plate	38	16,700	Large	412	25,050	Large
Weld Neck Flange	ΔP = 21.7 psig	Rated at 212 psig	8.77	ΔP = 21.7 psig	Rated at 212 psig	8.77
Blind Flange	ΔP = 21.7 psig	Rated at 212 psig	8.77	ΔP = 21.7 psig	Rated at 212 psig	8.77
Closure Bolt	17,257	18,600	0.08	Fatigue Life > 4000 shipments		

Stability Summary 50 Feet Immersion

Component	Actual Load	Critical Load	Margin of Safety
Vessel Cylinder	21.7 psid	431 psid	Large
Vessel Bottom Plate	24 lb/in	29,910 lb/in	Large

Both of these margins of safety are larger than the 1.34 permitted by the ASME Code.

2.7.7 Summary of Damage

The most significant damage to the WE-1 prototype package occurred to the fuel assembly. The conservative nature of the drop testing ensures containment integrity of the fuel rods is maintained per the requirements 10 CFR §71.51(a)(2). The thermal analysis demonstrated acceptable fuel assembly temperatures during the HAC fire event for a fully exposed inner container. Drop testing demonstrated that the outer container remains intact and closed. The corresponding result would be a significant reduction in fuel assembly temperatures during the HAC fire event resulting in an even larger margin for fuel rod burst.

2.8 SPECIAL FORM

This section does not apply to the WE-1 package since special form is not claimed.

2.9 FUEL RODS

BW 17x17 fuel rod cladding is considered to provide containment of radioactive material under both normal and accident test conditions. Discussion of this cladding, and its ability to maintain sufficient mechanical integrity to provide such containment, is described in Section 1.2.3, *Contents*, and Chapter 4, *Containment*.

Pathfinder Canister: The Pathfinder Canister is considered to provide containment of radioactive material under both normal and accident test conditions by the leak tightness of the bolted closure. No credit is taken for the fuel rod cladding providing containment of radioactive material under normal or hypothetical accident conditions. The structural analysis, for maximum pressure calculation, assumes no cladding integrity. The canister will be filled with filler material during transport. Due to space limitations, the fuel will remain within the Pathfinder Canister space.

2.10 Stress analysis

2.10.1 Stress Analysis Pathfinder Canister

Stress analysis of the Pathfinder Canister is performed per ASME B&PV Code[2.2] Section III, Subsection NB. The loading conditions considered in the analysis are:

- Lifting (10CFR71.45)
  Shop handling only, the canister will not be lifted after the fuel is loaded.

- Normal Condition of Transportation (10CFR71.71)
  a) Reduced external pressure to 3.5 psia (ambient air -40 °F to 100 °F)
  b) Increased external pressure to 20.3 psia (ambient air -40 °F to 100 °F)
  c) Vibration - normal incident to transportation.
  d) Water spray - rain at 2 in/hr for at least one hour.
  e) Free drop - 4 feet on an unyielding flat surface.
  f) Penetration - 13 pound object dropped from 40 inches.

- Hypothetical Accident Conditions (10CFR71.73)
  a) Impact from 30-foot drop on unyielding horizontal surface.
  b) Immersion - water head of 50 feet.
  c) Thermal - Fire 1475 °F for 30 minutes

For all other loading conditions of 10CFR71[2.1], the stresses for the canister are negligible.

The Pathfinder Canister, support spacer, energy absorber design parameters (See Figure 2.10-1:

Cylinder	8"-schedule 40S pipe (300 series sst) OD = 8.625", ID = 7.981", wall thickness = 0.322", weighs 28.55 lb/ft
Weld Neck Flange:	8" - 150 lb. (300 series sst), ANSI B16.5[2.14] Flange diameter 13.5", flange thickness 1 1/8", hub length 4", approximate weight 42 lbs.
Blind Flange:	8" - 150 lb. (300 series sst), raised face, ANSI B16.5[2.14] Flange diameter 13.5", flange thickness 1 1/8", 8 bolt holes at 11.75" diameter bolt circle, approximate weight 47 lbs.
End Plate:	8.625" diameter, 1" thick (300 series sst)

Canister Cavity	88" long, 7.9" diameter minimum envelope
Spacer Tube	8"-schedule 40S pipe, Length 61" (approximately) OD = 8.625", ID = 7.981", wall thickness = 0.322", weighs 28.55 lb/ft
Spacer Tube Plate:	14.5" x 14.5" x 0.5" thick (300 series sst)
Wood Spacers	14.5" x 14.5" x 8" thick, white oak wood, density 48 lbs/ft^3 ± 15% 14.5" x 14.5" x 2" thick, eastern white pine wood, density 24 lbs/ft^3 ± 15%
Bolts:	Eight 3/4-10UNRC-2A by 2 1/2 long (ASTM-A193-B8M class 2)
Bolt Torque:	40 ft-lbs minimum, 50 ft-lbs maximum
Lubrication:	Neolube
Inner Seal:	Garlock Helicoflex metallic o'ring (U5410-09250 NPA) 9.25" OD, 0.125" tube diameter, 0.010" thick, Alloy 600
Outer Seal:	Garlock Helicoflex metallic o'ring (U5410-10250 NPA) 10.25" OD, 0.125" tube diameter, 0.010" thick, Alloy 600
Support Spacers	2" thick plate, material ASTM B-209 Alloy 6061, Temper T651
Rubber Pad:	Commercial Nitrile Duro 60, minimum 1/8 thickness at clamp location.

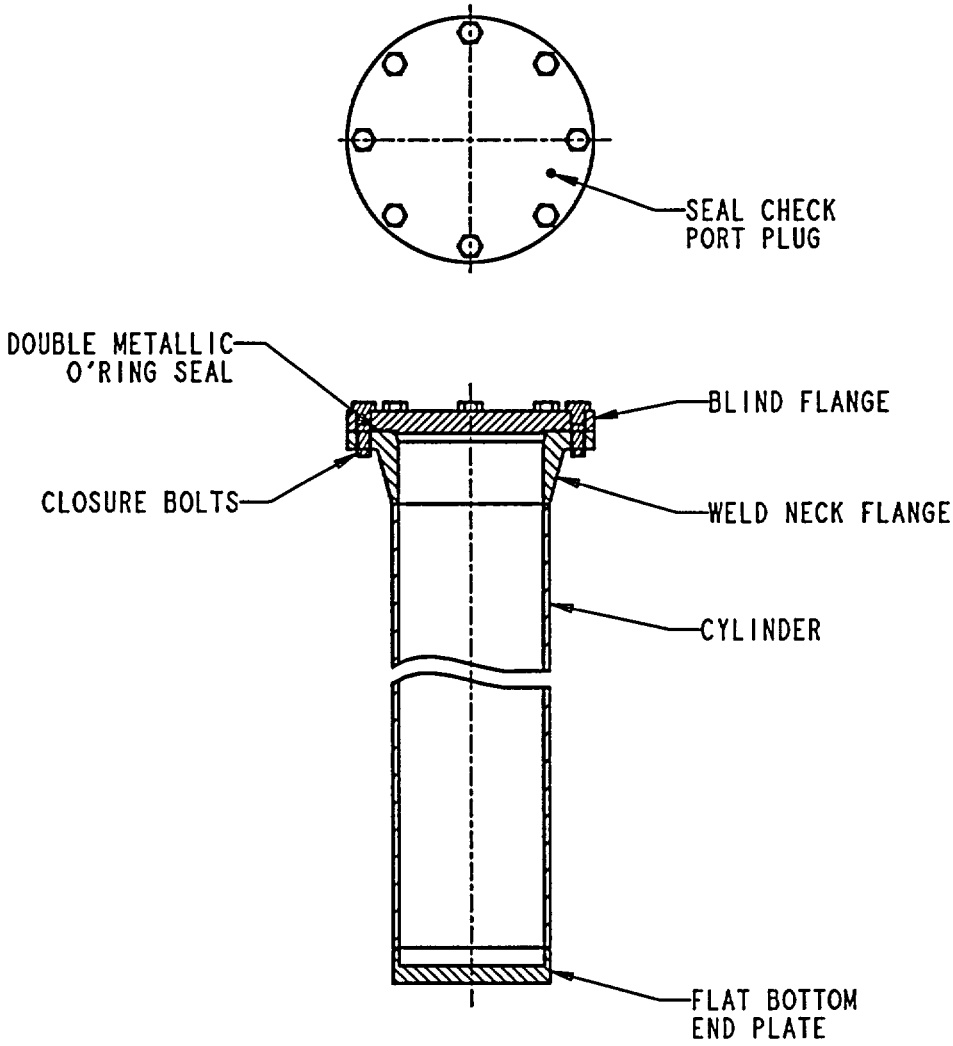

Figure 2.10-1 Pathfinder Canister Arrangement

2.10.1.1 Pressure and Temperature

For all normal and accident conditions, the temperature of the Pathfinder Canister never exceeds 800°F (Section 2.7.4). Zircar insulation is used to insulate the Pathfinder Canister. For various loading conditions, the pressure of the canister is calculated using the gas law:

$$\frac{P_1V_1}{T_1} = \frac{P_2V_2}{T_2}$$

It is unlikely that the pathfinder fuel assemblies were pressurized during manufacturing. However, it will conservatively be assumed that the fuel was pressurized to 315 psig, typical Mark BW fuel pressure. If the fuel were to leak during shipping this gas would create an internal pressure for the canister some amount Δp above atmospheric. The pressurized volume in the fuel assembly consists of the void above the fuel pellet and the annular gap between the fuel pellet and the cladding ID.
Where:

Plenum Length = 3″

Fuel Stack Length = 72″

Fuel Clad ID = 0.211″

Fuel Pellet Diameter = 0.207″

No. Of Fuel Pins = 6 per fuel assembly

$V_{f1} = 6\ ((\pi/4)\ (0.211)^2)\ 3 = 0.6294$ in.^{3} neglecting plenum springs

$V_{f2} = 6\ ((\pi/4)\ ((0.211)^2 - (0.207)^2)\ 72 = 0.5672$ in.^{3}

For 48 fuel assemblies: $V_f = 48\ (0.6294 + 0.5672) = 57$ in.^{3} gas volume in the pin per fuel assembly

The maximum void in the canister consists of the volume of the canister minus that occupied by the fuel assemblies and sheaths. The total weight of a fuel assembly and sheath is 10 lbs. The density of Inconel is 0.297 lbs/in.^{3} For conservative volume calculations the density of the heavier fuel pellet is used to be the same as Inconel.

$V_{cyl} = (\pi/4)8.625 - 2(0.322))^2)88 = 4402$ in.^{3} empty canister cavity volume

$V_{fuel} = W/\rho = 48(10) / 0.297 = 1616$ in.^{3}

$V_{void} = 4402 - 1616 = 2786$ in.^{3} fully loaded Pathfinder Canister

$\Delta p = 315(57 / 2876) = 6.24$ psig use 7 psig

If all 48 fuel assemblies break open, the pressure inside the canister will increase by 7 psig. This pressure will be lower for a less than full payload, or less than 48 assemblies.

At room temperature the pressure in the canister will be one atmosphere + 7 psi. Using the gas law listed above and considering constant volume, the pressures for various temperatures are calculated.

$$P @ 150°F = \frac{150° F + 460}{70° F + 460}(14.7) = 17 \text{ psia}$$

$$P @ 800°F = \frac{800° F + 460}{70° F + 460}(14.7) = 35 \text{ psia}$$

With all fuel rod rupture:

$$P @ 70°F = 14.7 + 7 = 21.7 \text{ psia}$$

$$P @ 150°F = \frac{150° F + 460}{70° F + 460}(14.7+7) = 25.0 \text{ psia}$$

$$P @ 800°F = \frac{800° F + 460}{70° F + 460}(14.7+7) = 51.6 \text{ psia}$$

The external pressure during the 50-foot immersion loading is:

$$P = (62.4 \text{ lb/Ft}^3)(50 \text{ ft})/(144 \text{ in}^2/\text{Ft}^2) + 14.7 = 36.4 \text{ psia}$$

Summary of Pressure and Temperature

Loading condition	Max Temp °F	Internal Pressure Psia	External Pressure psia	Max Δ Pressure psid
Reduced External Press 3.5 psia	150	14.7 to 25.0	3.5	21.5
Increased External Press 20.3 psia	150	14.7 to 25.0	20.3	-5.6
Thermal fire accident	800	14.7 to 51.6	14.7	36.9
Immersion 50 feet of Water	150	14.7 to 25.0	36.4	-21.7

The detail stress analysis of the canister at 21.5 psid is performed. For the linear elastic structure, stresses are directly proportional to the product of the ratio of load times the inverse ratio of elastic modulus. Using this, stresses at other loading conditions are obtained by:

$$\sigma_2 = \sigma_1 (P_2/P_1) * (E_1/E_2)$$

Stress Ratio for Loading Conditions:

Reduced External Pressure: 1.0

Increased External Pressure: (5.6/21.5) * (27.95/27.95)= 0.26

Thermal fire accident: (36.9/21.5) * (27.95/24.1) = 1.99

Immersion 50 feet of water: (21.7/21.5) * (27.95/27.95)= 1.01

2.10.2 Component Stress Analysis

The Pathfinder Canister stress analysis is performed on a component basis. For the stress analysis, the Pathfinder Canister is subdivided into:

1) A cylindrical vessel
2) A bottom plate
3) A weldneck flange and a [blind] closure flange
4) Closure bolts

The stress analysis addresses each in the order delineated. ASME B&PV Code standard nomenclature is used in the equations.

2.10.2.1 Cylindrical Vessel

The cylindrical vessel is an 8" SCH 40S Pipe made of ASTM-A312-TP 304L. Its evaluation is based on the requirements of ASME B&PV Code[2.2]. The minimum wall thickness of a pipe per Code[2.2] Para. NB-3641 is:

$$t_m = \frac{PDo}{2(Sm+Py)} + A \text{ or } t_m = \frac{Pd + 2A(Sm+Py)}{2(Sm+Py-P)}$$

Where: P = 25.0-3.5 = 21.5 psid
D_o = 8.625 + .062 = 8.687 in [Table 2.3-1, and ASTM Spec[2.12]]
S_m = 16,700 psi @ 150°F
y = 0.4
A = 0.0

t_m = 21.5(8.687)/(2(16700+21.5(0.4))) = 0.0056 <<(.322-12.5%), Section 2.10.1

The tentative thickness for vessel per Code[2.2] Para. NB-3324.1 is:

$t_m = (P R_o) / (S_m + 0.5P)$
t_m = 21.5(8.687)/(2(16700+21.5(0.5))) = 0.0056 <<(.322-12.5%), Section 2.10.1

Allowable external pressure per Code[2.2] Para. NB-3641.2 and NB-3133.3

T = 0.322- 12.5% => 0.281 in
Do = 8.625 + .062 = 8.687 in

L = 20.6 in (distance between supports)

∴ L/Do = 20.6/8.687 = 2.371 A=.0029 [Ref 2.2, Fig G]
Do/T = 8.687/0.281 = 30.9 A=.0029 [Ref 2.2, Fig G]

ASME Code[2.2], Figure HA-2

B = 10000 @ 150°F
Pa = 4B / (3Do/T)
P_a = 4(10000)/(3(30.9)) = 431 psi >> 21.7 psi (50-foot immersion condition)

2.10.2.1.1 Normal Condition Stresses per ASME Code[2.2] Paragraph NB-3200:

a) Midsection Internal Pressure

Axial Stress = $PR_i/2t$ = (25-3.5)(8.687/2-0.322)/(2(0.322) = 134 psi
Hoop Stress = PR_i/t = 2(134) = 268 psi
Principal Stress: S1 = 134; S2 = 268; S3=-25
Stress Intensities: S12 = 134; S23 = 293; S31 = 159
Max. Stress Intensity: S23 = 293 « 16,700 S_m @ 150°F

b) Cylinder Bottom Plate Juncture

For internal Pressure 1 atmosphere or Greater
The following analysis is consistent with ASME Code[2.2], Articles A-2000, A-3000, A-5000, and A-6000

$$\lambda \text{ for cylinder} = \sqrt[4]{\frac{3(1-\mu^2)}{(Rt)^2}},\ \mu = 0.3$$ *Table XIII* of Roark[2.24]

$$\lambda = \sqrt[4]{\frac{3(1-.3^2)}{[(8.687/2-.322/2)(.322)]^2}} = 1.108$$

L = 18$^+$ > 6/λ = 6/1.108 = 5.415 (∴ Long Cylinder)

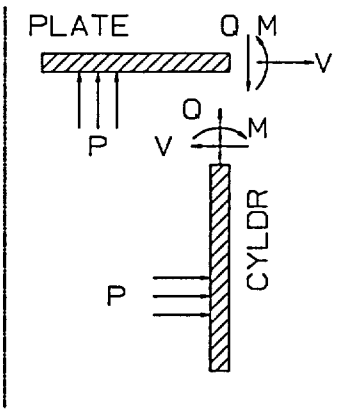

$$Q = \pi(R-\frac{1}{2}t_c)^2 P/2\pi R = \left[\frac{(R-\frac{1}{2}t_c)^2}{2R}\right]P$$

$$Q = [((4.183-0.5(0.322))^2/(2(4.183))]\ [21.5] = 41.57 \text{ lbs/in}$$

Per Roark[2.24], Table XIII, Cases 1, 14 and 15:

$$\delta_{CLY} = -\frac{V}{2D\lambda^3} + \frac{M}{2D\lambda^2} + \frac{PR^2}{Et_c}\left(1-\frac{1}{2}\mu\right)$$

$$\theta_{CLY} = -\frac{V}{2D\lambda^2} + \frac{M}{D\lambda}$$

$$\delta_{PLT} = \frac{R}{Et_p}(1-\mu)V$$

$$\theta_{PLT} = \frac{3P\pi R^3[\frac{1}{\mu}-1]}{2\pi E[\frac{1}{\mu}]t_p^3} + \frac{12[\frac{1}{\mu}-1]MR}{E[\frac{1}{\mu}]t_p^3}$$

Parameter Values (Internal Pressure, 25 psia @ 150°F)

$P = 25 - 3.5 = 21.5$ psid
$\lambda = 1.108$
$R = 8.687/2 - 0.322/2 = 4.183$ in mean radius
$E = 27.95 \times 10^6$ psi @ 150°F
$\mu = 0.3$
$t_c = 0.322$ in minimum cylinder wall thickness
$t_p = 1. - 0.003 = 0.997$ in minimum plate thickness
$D = Et_c^3/12(1-\mu^2) = 27.95x10^6(0.322^3)/12(1-0.3^2) = 85{,}453$ lb/in

Substituting:

$\delta_{CLY} = -4.30153 \times 10^{-6}V + 4.76610 \times 10^{-6}M + 35.53001 \times 10^{-6}$
$\theta_{CLY} = -4.76610 \times 10^{-6}V + 10.56168 \times 10^{-6}M$
$\theta_{PLT} = 1.26853 \times 10^{-6}M - 59.6519 \times 10^{-6}$
$\delta_{PLT} = 0.10508 \times 10^{-6}V$

Boundary Conditions

$\theta_{CYL} = -\theta_{PLT}$; $\delta_{CLY} = \delta_{PLT}$

Solving

$-4.30153x10^{-6}V+4.76610x10^{-6}M+35.53001x10^{-6} = 0.10508x10^{-6}V$
$-4.76610x10^{-6}V+10.56168x10^{-6}M = -1.26853x10^{-6}M+59.6519x10^{-6}$
$-4.40661x10^{-6}V +4.76610x10^{-6}M = -35.53001x10^{-6}$
$-4.76610x10^{-6}V +11.83021x10^{-6}M = 59.6519x10^{-6}$

V = +23.95 lb/in Q = 41.57 lb/in
M = +14.69 in-lb/in

b.1) Membrane Stresses

Average Stress Components
$\sigma_R = -\frac{1}{2}(P_i + P_o) = -\frac{1}{2}(25.0 + 3.5) = -14$ psi

$$\sigma_H = -\frac{2V}{t_c}\lambda R + \frac{2M}{t_c}\lambda^2 R$$

Table XIII, Cases 14, 15 of Roark[2.24]

$\sigma_H = -[2(23.95)(1.108)(4.183)/0.322] + [2(14.69)(1.108)^2(4.183)/0.322]$

$\sigma_H = -221$ psi
$\sigma_Z = Q/t_c = 41.57/0.322 = 129$ psi
$\tau = V/t_c = 23.95/0.322 = 74$ psi

Principal Stresses

$S1,2 = (-221+129)/2 \pm 0.5((-221-129)^2 + 4(74)^2)^{0.5}$
S1 = 143 psi
S2 = -235
S3 = -14

Stress Intensities
S12 = | 143 + 235 | = 378 psi
S23 = | -235 + 14 | = 221 psi
S31 = | -14 -143 | = 157 psi

Maximum Stress Intensity is S12
S12 = 378 < 16,700 psi S_m @ 150°F ∴ O.K.

b.2) Membrane + Bending at Surface

Since there is no shear on the surface, the stress components are the principal stresses.

b.2.1) Inside Surface

Principal Stresses

$$S1 = \frac{6\mu M}{t_c^2} - \frac{2V}{t_c}\lambda R + \frac{2M}{t_c}\lambda^2 R \qquad \text{Roark}^{2.24}$$

$S1 = [6(0.3)(14.69)/(0.322)^2] - [2(23.95)(1.108)(4.183)/0.322]$
$+ [2(14.69)(1.108)^2(4.183))/0.322]$

S1 = 34 psi

$$S2 = \frac{6M}{t_c^2} + \frac{Q}{t_c} \qquad \text{Roark}^{2.24}$$

$S2 = [6(14.69)/(0.322)^2] + [41.57/0.322] = 979$ psi
S3 = Pressure = -25 psi

Stress Intensities

S12 = | 34 - 979 | = 945 psi
S23 = | 979 + 25 | = 1004 psi
S31 = | -25 - 34 | = 59 psi

The maximum stress intensity is S23
S23 = 1004 < 25,050 psi $1.5S_m$ @ 150°F

b.2.2) Outside Surface

$$S1 = -\frac{6\mu M}{t_c^2} - \frac{2V}{t_c}\lambda R + \frac{2M}{t_c}\lambda^2 R = -476 \quad psi$$

$$S2 = \frac{-6M}{t_c^2} + \frac{Q}{t_c}$$

S2 = [-6(14.69)/(0.322)^2] + [41.57/0.322] = -721 psi

S3 = -3.5 psi

S12 = | -476 + 721 | = 245 psi
S23 = | -721 + 3.5 | = 718 psi
S31 = | -3.5 + 476 | = 473 psi

Maximum Stress Intensity is S23
S23 = 718 < 25,050 psi $1.5S_m$ @ 150°F ∴ O.K.

2.10.2.1.2 Accident Condition Stresses per ASME Code[2.2] Paragraph F-1331

In this section the local stresses in the container at a support location are determined considering all loads during an accident condition.

2.10.2.1.2.1 Canister Dead Weight Loads and Reactions

The reaction forces and bending moments on the canister are determine for a dead weight load (i.e., 1g). The canister acts as a four-span continuous beam with an overhang at the bolted joint end.

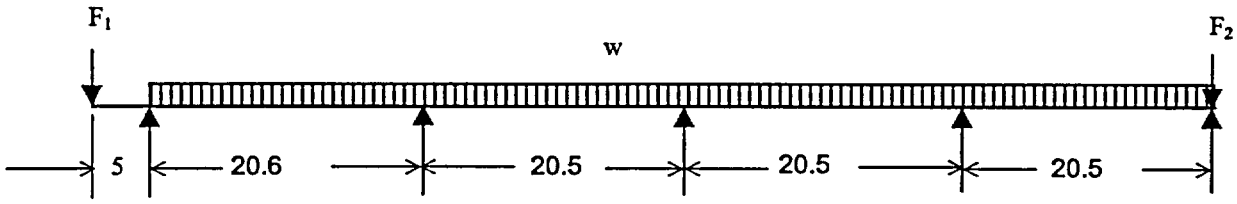

The force F_1 is the sum of the weights of the blind flange, welded neck flange and the bolts.

Blind Flange = 47 lbs	(for 8"-150 lb blind flange)
Welded Neck Flange = 42 lbs	(for 8"-150 lb weld neck flange)
Bolts = 3 lbs	estimated for 3/4" bolts (8 total)

$F_1 = 47 + 42 + 3 = 92$ lbs

The force F_2 is the weight of the welded end cap plate.

$F_2 = \rho V$

$\rho = 0.290$ lbs/in^3 ASTM Spec[2.29]

$V = [\pi/4]\,[(8.625)^2]\,[1] = 58.426$ in.^{3} Section 2.10.1

$F_2 = 0.290\,(58.426) = 16.9$ lbs use 17 lbs

The uniformly distributed weight (w) is the sum of the weights for the fuel assemblies, sheaths for the fuel assemblies, and the canister.

Fuel Assemblies + Sheath = N x weight / length

Where: N = 48 fuel assemblies per canister
weight = 10 lbs weight per Pathfinder fuel assembly
length = 82.55 in. length of Pathfinder fuel

Fuel Assemblies + Sheaths = 48 (10) / 82.55 = 5.815 lbs/in

Canister = 28.55 lbs/ft = 2.379 lbs/in (for 8" schedule 40S pipe)

$w = 5.815 + 2.379 = 8.194$ lbs/in

This continuous beam problem was solved using ANSYS[2.28]. The ANSYS beam element BEAM3 was used to model the canister. The required real constants for the beam elements are:

$A = [\pi/4]\,[(8.625)^2 - (7.981)^2] = 8.399$ in.^{2} for 8" schedule 40S

$I = [\pi/64]\,[(8.625)^4 - (7.981)^4] = 72.489$ in.^{4}

$H = 8.625$ in.

The material properties used are:

$E = 28.3 \times 10^6$ psi	Table 2.3-1
$\mu = 0.3$	Poisson's ratio for steel

The input listing is given on next page. Figure 2.10-2 shows the deflected shape of the beam. The maximum reaction force occurs at the fourth support from the bolted joint and is 189.61 lbs. The maximum moment along the canister is 460.0 in-lbs and occurs at the left support (nearest the bolted joint).

The ANSYS results are summarized below for the reaction forces and the moments over the supports, from left to right for 1g dead weight loading.

Force (lbs)	Moment (in-lbs)
186.70	460.00
156.61	247.88
165.43	278.25
189.61	360.88
83.39	0.00

Total = 781.73

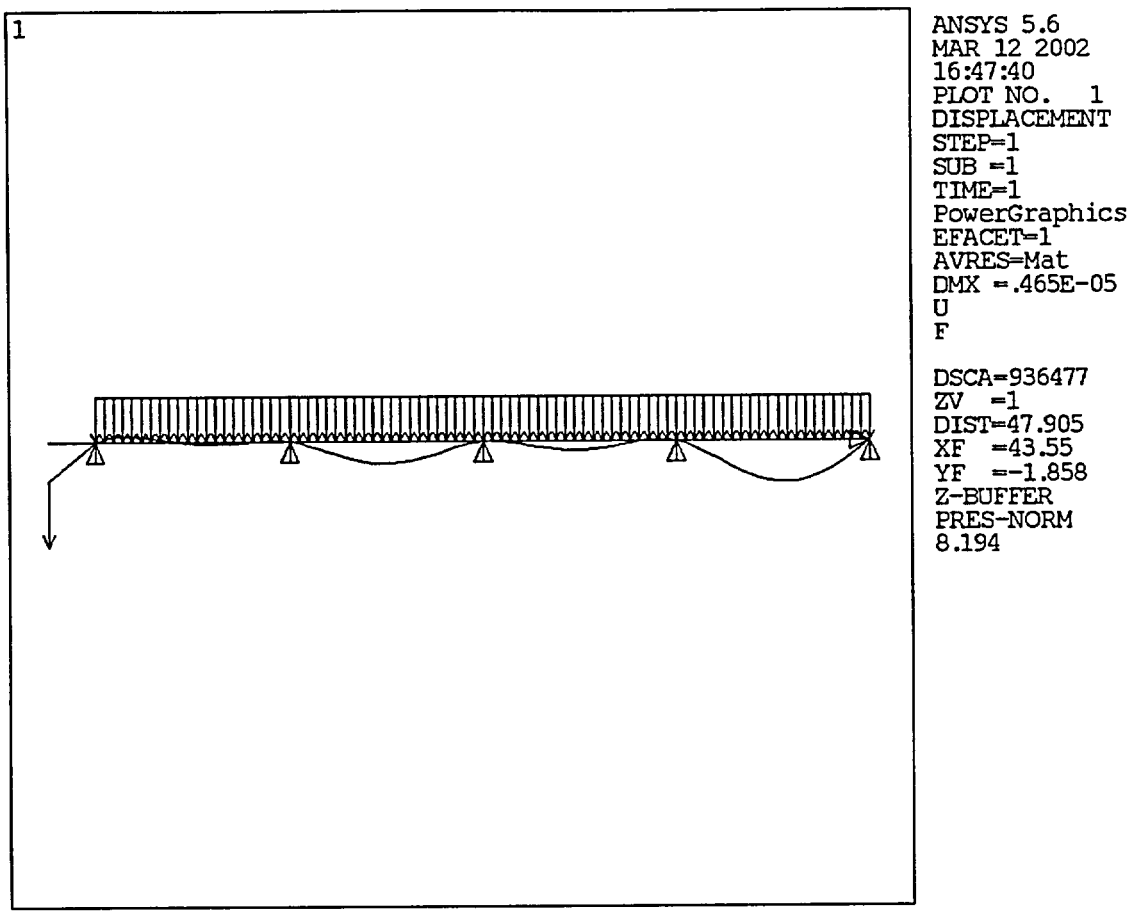

Figure 2.10-2 Pathfinder Canister Loading and Displaced Shape – 1g Side Loading

ANSYS Command Listing for Canister 1 g Side Loading Reaction Loads

```
/PREP7
/TITLE, PATHFINDER CONTAINER DEAD WEIGHT (1G) LOADS
ET,1,BEAM3,,,,,,1
MP,EX,1,28.3E6
MP,NUXY,1,0.3
R,1,8.399,72.489,8.625
N,1,0
N,2,5.
N,23,25.6
FILL
N,44,46.1
FILL
N,65,66.6
FILL
N,86,87.1
FILL
E,1,2
EGEN,85,1,-1
NLIST
FINISH
/SOLU
ANTYPE,STATIC,NEW
TIME,1
OUTRES,ALL,LAST
OUTPR,ALL,LAST
KBC,1
D,2,UY,0.0,,86,21
D,86,UX,0.0
F,1,FY,-92
F,86,FY,-17
ESEL,S,ELEM,,2,85,1
SFBEAM,ALL,1,PRES,8.194,8.194
ESEL,ALL
SFELIST
LSWRITE
SAVE
LSSOLVE,1,1,1
FINISH
```

2.10.2.1.2.2 Container Stresses at a Support

The canister stresses at a saddle support are primarily due to the reaction load of the support but also consist of beam bending, internal pressure and an effective internal pressure of the fuel rods pressing against the inner surface of the canister.

The canister stresses due to the reaction load are determined by finite element analysis using the ANSYS[2.28] code. A quarter symmetry model of the canister is modeled using the eight node SHELL93 element type. The geometry and material inputs for the model are:

$t = 0.322$ in.	cylinder wall thickness
$R_m = (8.625 - 0.322)/2 = 4.1515$ in.	mean radius of cylinder
$L = 8$ in.	(end boundary condition is sufficiently remote from high stress region)
$w = 1$ in.	conservative, actual saddle is 2" wide
$E = 28.3 \times 10^6$ psi	Table 2.3-1
$\mu = 0.3$	Poisson's ratio for steel

Symmetry boundary conditions are used on all edges except the end remote from the pressure loading where the nodes are restrained in the circumferential direction to simulate a beam shear load.

The saddle reaction load is idealized to act as a pressure over a one-inch width of the saddle and to vary in the circumferential direction by a typical cosine distribution. Pressure loadings at supports for tanks or pipes with large radius to thickness ratio are typically assumed to extend 90 or 120 degrees along the saddle. However, since the canister's radius to thickness ratio is relatively small, the contact area is conservatively assumed to extend only 60 degrees. Also, since a complete saddle consist of four individual pieces separated by a 0.5 inch gap, the contact area in the saddle's worse orientation, would extend from approximately 3 to 30 degrees (θ_1 to θ_2) on each side of the gap. The pressure distribution for a unit reaction load of 10,000 lbs is calculated as follows:

$$\text{Reaction Force} = 4\int_{\theta_1}^{\theta_2} (P_{max} \cos(\theta))(\cos(\theta))\ ((w/2)R_m\, d\theta)$$

$$\text{Reaction Force} = 4\,(P_{max})(w/2)R_m\,[0.5(\sin\theta_2 \cos\theta_2 - \sin\theta_1 \cos\theta_1) + 0.5\,(\theta_2 - \theta_1)]$$

substituting for known values:

$P_{max} = 2{,}827$ psi for a 10,000 lbs reaction force

The ANSYS input command listing is given on following pages. The maximum stress and displacement values for a unit 10,000 lbs load are given below (X-radial, Y-hoop, Z-axial):

Maximum radial displacement occurs at node 1: UX = -0.01255 in.
Maximum stress intensity for the middle surface occurs at node 6, the stresses at this node are:

Top Surface	Middle Surface	Bottom Surface
SI = 31742 psi	SI = 13538 psi	SI = 12074 psi
SX = 0 psi	SX = 0 psi	SX = 0 psi
SY = -27856 psi	SY = -13426 psi	SY = 1004 psi
SZ = -31717 psi	SZ = -10087 psi	SZ = 11543 psi
SXY = -835 psi	SXY = -869 psi	SXY = -903 psi
SYZ = 0 psi	SYZ = 0 psi	SYZ = -2 psi
SXZ = 8 psi	SXZ = 8 psi	SXZ = 8 psi

Figure 2.10-3 shows the finite element model with the cosine pressure loading at the saddle support. Figure 2.10-4 shows the stress intensity (membrane) plot for the middle surface.

ANSYS Command Listing for Canister Local Stresses- Slapdown Drop

```
/PREP7
/TITLE, PATHFINDER CONTAINER STRESSES AT A SUPPORT CLAMP LOCATION
C***ASSUME REACTION LOAD IS TRANSMITTED INTO THE SHELL AS A COSINE FUNCTION
ET,1,SHELL93
MP,EX,1,28.3E6
MP,NUXY,1,0.3
T=0.322                          ! container wall thickness
RM=(8.625-T)/2                   ! container midplane radius
L=8                              ! length of model
W=1                              ! contact width on saddle
RF=10000                         ! reaction force at saddle
PHIMIN=3                         ! minimum contact angle on saddle (deg)
PHIMAX=30                        ! maximum contact angle on saddle (deg)
PHIMINR=(PHIMIN/180)*3.14159     ! phimin in radians
PHIMAXR=(PHIMAX/180)*3.14159     ! phimax in radians
R,1,T,T,T,T                      ! real constants for container elements
C***GENERATE CONTAINER SHELL ELEMENTS
CSYS,1
*AFUN,DEG
K,1,0,0,0
K,2,RM,0,0
K,3,RM,90,0
K,4,RM,180,0
LARC,2,3,1,RM
LARC,3,4,1,RM
```

```
LGEN,2,1,2,1,,,W/2
LGEN,2,3,4,1,,,L-W/2
L,2,5
*REPEAT,3,1,1
L,5,8
*REPEAT,3,1,1
AL,1,8,3,7
AL,2,9,4,8
AL,3,11,5,10
AL,4,12,6,11
LESIZE,1,,1
LESIZE,2,,2
LESIZE,7,W/4
LESIZE,10,W/4
MSHKEY,1
TYPE,1
MAT,1
REAL,1
AMESH,1,4,1
NROTATE,ALL
FINISH
/SOLU
ANTYPE,STATIC,NEW
TIME,1
OUTRES,ALL,LAST
KBC,1
CSYS,1
NSEL,S,LOC,Z,0
DSYM,SYMM,Z,0
NSEL,ALL
NSEL,S,LOC,Y,0
NSEL,A,LOC,Y,180
DSYM,SYMM,Y,0
NSEL,ALL
NSEL,S,LOC,Z,L
D,ALL,UY,0.0
NSEL,ALL
D,NODE(RM,180,L),UX,0.0
PMAX=RF/(W*RM*(SIN(PHIMAX)*COS(PHIMAX)-SIN(PHIMIN)*COS(PHIMIN)+(PHIMAXR-PHIMINR)))
*DO,I,PHIMIN,PHIMAX-1,1
        NSEL,S,LOC,Z,0,W/2
        NSEL,R,LOC,Y,I-0.1,I+1+0.1
        ESLN,R,1,ALL
        SFE,ALL,2,PRES,,PMAX*COS((2*I+1)/2)
        ALLSEL
*ENDDO
*STATUS
SFLIST
LSWRITE
SAVE
LSSOLVE,1,1,1
FINISH
/POST1
```

```
RSYS,1
DSYS,1
NSEL,S,LOC,Z,0,W
NSEL,R,LOC,Y,0,PHIMAX+5
NLIST,ALL
PRNSOL,U,COMP
SHELL,TOP
PRNSOL,S,COMP
PRNSOL,S,PRIN
SHELL,MID
PRNSOL,S,COMP
PRNSOL,S,PRIN
SHELL,BOT
PRNSOL,S,COMP
PRNSOL,S,PRIN
NSEL,ALL
NSEL,S,LOC,Z,L
NLIST,ALL
PRRSOL
RSYS,0
DSYS,0
PRRSOL
NSEL,ALL
FINISH
```

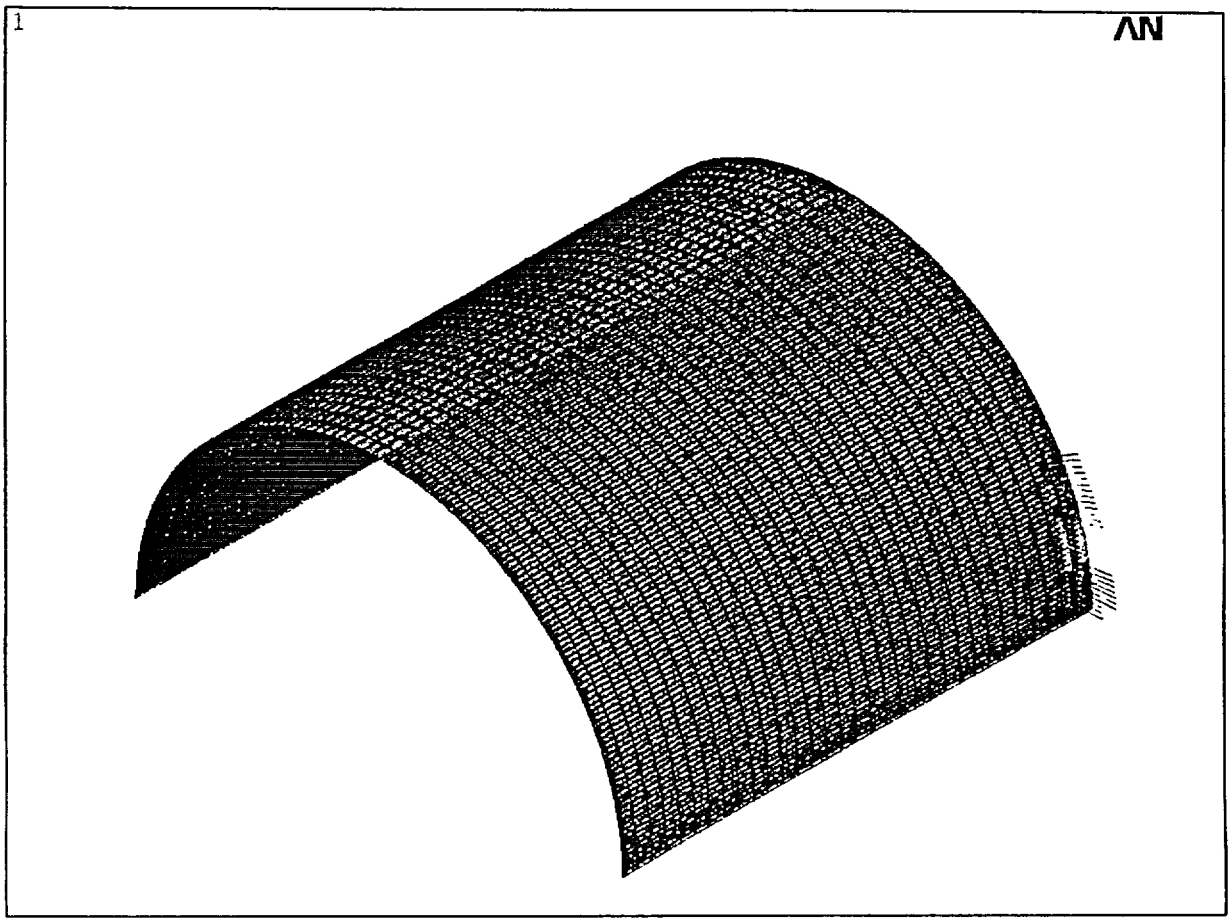

Figure 2.10-3 Pathfinder Canister Loading at a Saddle Support – Drop Analysis

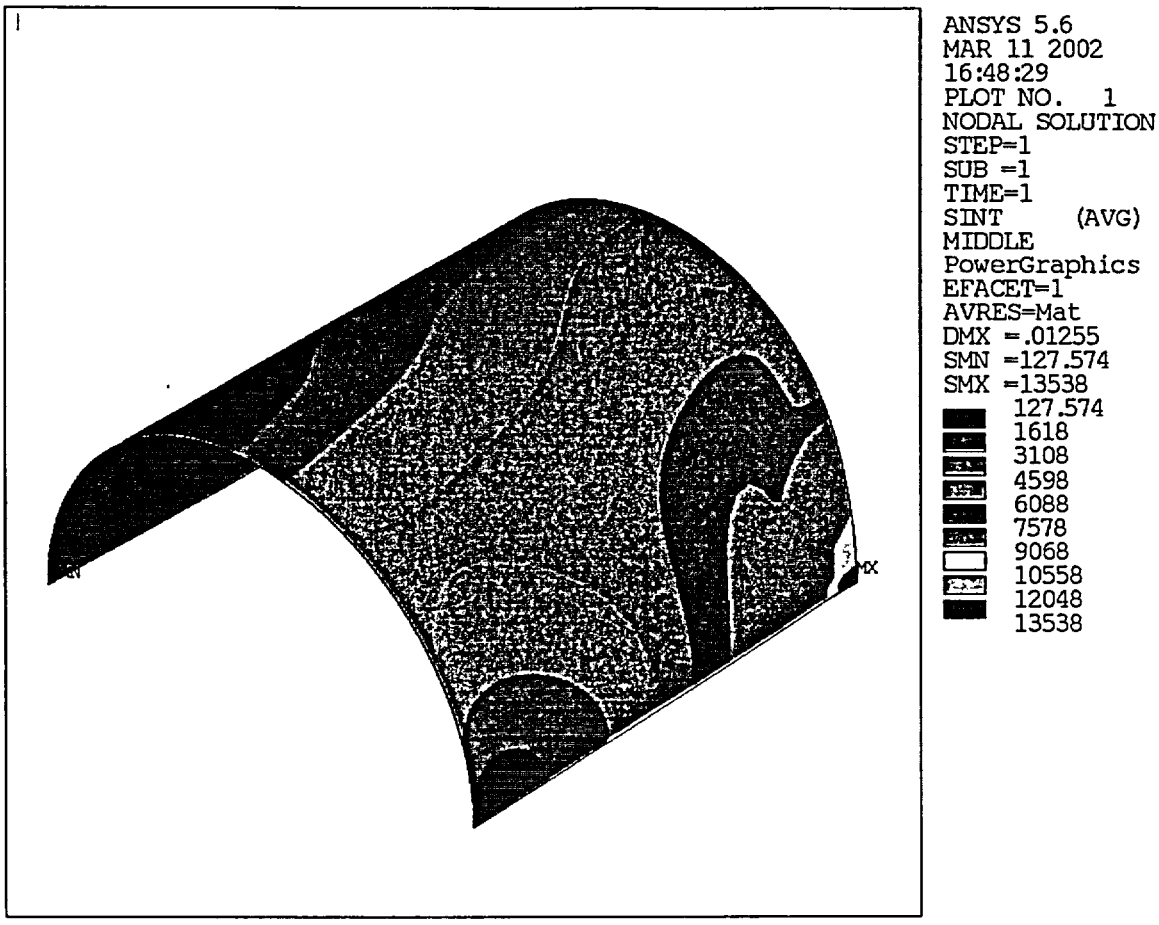

Figure 2.10-4 Pathfinder Canister Membrane Stress Intensity at a Saddle Support Due to a 10,000 lb Load

From Section 2.10.2.1.2.1, the maximum moment and reaction force acting on the canister for a 1g load is 460 in-lbs and 189.61 lbs, respectively. During the accident condition the lateral acceleration is 142 g (see Section 2.10.3). Thus, the maximum 30-foot drop accident loads are:

$M = 142\ (460) = 65{,}320$ in-lbs
$F = 142(189.61) = 26{,}925$ lbs

These maximum loads are conservatively taken occur at the same support location (maximum moment actually occurs at 1st support and maximum force at 4th support).

Membrane Stress

Stresses due to overall bending is classified as a membrane stress per ASME Code[2.2], Table NB-3217-1 and is:

$$SZ_{beam} = MR_m/I = 65320\ (4.1515) / 72.489 = \pm 3{,}741 \text{ psi}$$

For the saddle pressure loads, the membrane stresses are:

SI = (26925 / 10000) (13538) = 36,451 psi
SY = (26925 / 10000) (-13426) = -36,150 psi
SZ = (26925 / 10000) (-10087) = -27159 psi
SXY = (26925 / 10000) (-869) = -2,340 psi

Since SZ_{beam} is compressive on the bottom half of the canister, it is clear that this stress would have an negligible effect on the total SI since the SY stress component is larger and still controls. From Section 2.10.1.1, the external pressure (-5.6 psig) which would produce a compressive stress to combine with the above support induced stress is small and may be neglected. Also, the fuel rods pressing against the canister during the high g load produces a load similar to an internal pressure. However, this causes a hoop tension stress, which would decrease the total SY stress component and therefore it is conservative to neglect it. Thus, for the 30-foot drop slapdown accident condition, the maximum membrane stress intensity for the canister is 36,451 psi.

From the Figure 2.10-4, the maximum membrane stress is localized near the saddle contact area, but significant stress levels exist outside this area. Per ASME Code[2.2], Table NB-3217-1, shell membrane stresses near a nozzle or opening due to an external load is classified as a local membrane stress. However, NB-3213.10 places restrictions on the distance the stress can exceed 1.1 S_m. Due to this restriction, the membrane stresses are classified as primary.

$P_m \leq$ (lesser of 2.4 S_m or 0.7 S_u) — ASME Code[2.2], F1331.1(a)
2.4 S_m = 2.4 (16700) = 40,080 psi — Table 2.3-1

0.7 Su = 0.7 (70000) = 49,000 psi Table 2.3-1

36,451 psi ≤ 40,080 psi

Bending Stress

Per ASME Code[2.2], Table NB-3217-1, shell bending stresses near a nozzle or opening due to an external load is classified as a secondary stress. Therefore, the bending stresses near the saddle are considered secondary and the applicable stress limit for a Faulted condition is:

S_n < 2 Sa at 10 cycles (Table 2.1-1)

σ = (26925 / 10000)(31742) = 85,465 psi

K_t = stress concentration factor = maximum of 4 NRC R.G. 7.6[2.3], Section C 7.

$S_n = (E_{cold} / E_{hot}) K_t \sigma = (28.3 \times 10^6 / 27.95 \times 10^6)(4)(85465) = 346{,}141$ psi

Sa at 10 cycles = 708,000 psi ASME Code[2.2], Table I-9.1, Fig. I-9.2.1

346,141 psi < 2(708,000)

346,141 psi < 1,416,000 psi Therefore, OK

2.10.2.1.2.3 Gap Between Canister and Saddle

The purpose of this section is to demonstrate that adequate contact between the saddle and the canister occurs to justify the pressure distribution used in 2.10.2.1.2.2. The nominal gap between the canister and saddle is conservatively calculated using infinitely stiff parts.

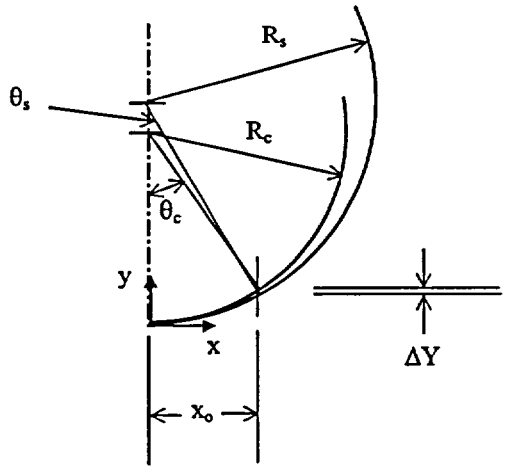

The vertical line at $x = x_o$ intersects the canister of radius R_c at y_c and the saddle of radius R_s at y_s.

$\theta_c = 30$ deg	used in stress analysis
$R_c = 8.625 / 2 = 4.3125$ in.	cylinder outer radius
$R_s = R_c + 0.1 = 4.3125 + 0.1 = 4.4125$ in.	design of saddle support

$x_o = R_c \sin(\theta_c) = 4.3125 \sin(30) = 2.15625$ in.
$y_c = R_c (1 - \cos(\theta_c)) = 4.3.125 (1 - \cos(30)) = 0.57777$ in.
$x_o = R_s \sin(\theta_s)$
$\theta_s = \sin^{-1}(x_o / R_s) = \sin^{-1}(2.15625 / 4.4125) = 29.25311$ deg.
$y_s = R_s (1 - \cos(\theta_s)) = 4.4125 (1 - \cos(29.25311)) = 0.56273$ in.
$\Delta y = y_c - y_s = 0.57777 - 0.56273 = 0.01504$ in.

The component of Δy that is perpendicular to the tangent of the R_c circle at (x_o, y_c) and to the tangent of the R_s circle at (x_o, y_s) is δ_c and δ_s, respectively.

$\delta_c = \Delta y \cos(\theta_c) = 0.01504 \cos(30) = 0.01303$ in.
$\delta_s = \Delta y \cos(\theta_s) = 0.01504 \cos(29.25311) = 0.01312$ in.

From ANSYS results, the radial deflection under the load is -0.01255 (node 1) for the 10,000 lb unit load. Thus, for the full load of 26,925 lbs:

$\delta_r = (26925 / 10000)(-0.01255) = -0.03379$ in.

Since $\delta_r > \delta_s$, the gap between the canister and saddle at the 30 degree location is most likely closed. In addition, local yielding ($S_y = 25000$ psi) and the rubber liner between the two components will help distribute the load to at least the 30 degree mark. Thus, the assumption of a cosine load distribution over a 60 degree (30 degrees on each side of the load center) contact area between the canister and saddle is a valid.

In the above calculation the saddle radius was 0.1 inch larger than the pipe OD. If the as built dimensions are less than this, the contact area will be larger and thus the canister stresses would be less than calculated in Section 2.10.2.1.2.2.

2.10.2.1.2.4 Canister Column Buckling

Since the canister is supported at the clamped positions the unsupported length is 20.5 in. The maximum axial compressive load on the canister occurs for an end drop when the acceleration is 1,037 g's (Section 2.10.3, Case 2). The axial load on the canister near the bolted connection is

$W_{max} = G_A W$

$W = 782 - 47 - 42 - 480 = 213$ lbs

$W_{max} = 1037\ (213) = 220{,}181$ lbs

$A = (\pi/4)((8.625)^2 - (7.981)^2) = 8.399$ in.^{2}

$\sigma = W_{max} / A = 220181 / 8.399 = -26{,}298$ psi axial stress in canister

The yield strength for the canister is 23,150 psi at 150 °F (Table 2.3-1).

radius of gyration = $r = [0.25((8.625)^2 + (7.981)^2)]^{0.5} = 5.88$ in.

$L/r = 20.5 / 5.88 = 3.49$

This is indicative of a very short column that does not fail in buckling and tensile limits are applicable.

$P_m \leq$ (lesser of $2.4\ S_m$ or $0.7\ S_u$) Per ASME Code[2.2], F1331.1(a)

$2.4\ S_m = 2.4\ (16700) = 40{,}080$ psi Table 2.3-1

or

$0.7\ Su = 0.7\ (70000) = 49{,}000$ psi Table 2.3-1

$26{,}298$ psi $\leq$ $40{,}080$ psi

As an additional check, buckling formula for a thin walled cylindrical tube is used. Per Roark[2.24], page 274, tests indicate that the critical buckling stress is usually only 40 to 60% of the theoretical value given by:

$s' = (E / (3(1 - \nu^2))^{0.5})\ (t / R)$

$s' = (27.95 \times 10^6 / (3(1 - (0.3)^2))^{0.5})\ )(0.322 / 4.1515) = 1.312 \times 10^6$ psi

$0.4\ s' = 0.4\ (1.312 \times 10^6\ ) = 524{,}800$ psi >> 26,298 psi therefore no buckling

2.10.2.2 Bottom Plate

The bottom plate stresses at the cylindrical vessel juncture are bounded by those calculated in Section 2.10.2.1.1.b. This is due to fact that bottom plate thickness is greater than the minimum wall thickness of the cylindrical vessel. The stresses for center of the plate are calculated below.

2.10.2.2.1 Normal Condition Stresses

At Bottom Plate Center

a) Membrane + Bending

Internal Pressure (21.5 psid @ 150^{0}F)

a.1) Outside Surface

Roark[2.24], Table X, cases 1 and 12

$$S1 = \frac{3\pi R^2 P}{8\pi\left(\frac{1}{\mu}\right)t_p^2}\left(\frac{3}{\mu}+1\right) - \frac{6M}{t_p^2} + \frac{V}{t_p}$$

$S1 = \{[3(4.183)^2(21.5)(3/.3 + 1)/(8(1/0.3)(0.997)^2$
$- [6(14.69)/(0.997)^2] + [23.95/0.997]$

S1 = 404 psi
S2 = S1 = 404 psi
S3 = -3.5 psi

S12 = 0
S23 = 408 psi
S31 = 408 psi

Max Stress Intensity is S23 or S31
S23 = 408 < 25,050 psi $1.5S_m$ @ 150°F ∴ O.K.

a.2) Inside Surface

$$S1 = -\frac{3\pi R^2 P}{8\pi\left(\frac{1}{\mu}\right)t_p^2}\left(\frac{3}{\mu}+1\right) + \frac{6M}{t_p^2} + \frac{V}{t_p}$$

S1 = -356 psi
S2 = -356 psi
S3 = -25 psi

S12 = 0
S23 = 331 psi
S31 = 331 psi

Max Stress Intensity is S23 or S31
S23 = 331 < 25,050 psi $1.5S_m$ @ 150°F ∴ O.K.

b) Membrane

$$S1 = \frac{V}{t} = \frac{23.95}{.997} = 24\ psi$$

S2 = S1 = 24 psi
S3 = -½ (P_i + P_o) = -½ (25 + 3.5) = -14 psi

Stress Intensities

S12 = | 24 - 24 | = 0
S23 = | 24 + 14 | = 38 psi
S31 = |-14 - 24 | = 38 psi

Maximum Stress Intensity

S23 = 38 < 16,700 psi 1.0S_m @ 150°F ∴ O.K.

c) Buckling

Buckling is addressed for external pressure load case. For the analysis, the 50-foot immersion condition is the worst external pressure load case.

Per Roark[2.24], Table XVI, Case H (This is also valid for a circular plate loaded laterally with a uniform load.)

$$S' = 0.35\frac{E}{1-\mu^2}\left(\frac{t_p}{R}\right)^2$$

$$= 0.35\frac{28.3x10^6}{1-.3^2}\left(\frac{.997}{4.18}\right)^2$$

= 618,340 psi

Above the proportional limit, E decreases. Since the proportional limit is < Sy = 30,000 @ -40°F, and since S' is twenty times Sy, the critical stress is assumed Sy. [Elastic-Perfect Plastic Material]

$V_{CRITICAL}$ = 30,000(t_p) = 30,000(.997) = 29,910 lb/in

$$V_{CAL'D} = V_{21.5psid}\ \frac{\Delta P\ 50\ Feet\ Immersion\ Case}{\Delta P\ Reduced\ External\ Press.\ Case}$$

$V_{CAL'D}$ = 23.95 (21.7/21.5) = 24.2 lb/in

$V_{CAL'D} = 24.2 << 29{,}910$ lb/in $= V_{CRITICAL}$

2.10.2.2.2 30-foot Drop Accident Condition Stresses

For impact, Section 2.10.3, Case 2 acceleration will produce the largest load on the end cap plate. The end cap plate is conservatively assumed to act as a simply supported circular plate (Roark[2.24], page 216, case 1). The edge support is assumed to be at the midwall of the canister (a = (8.625 - 0.322)/2 = 4.1515"). At the center of the plate the bending stress is:

$\sigma_r = \sigma_t = 3\,W\,(3\,m + 1) / (8\,\pi\,m\,t^2)$

$W = W_{flg}\,(G_A)$

$W_{flg} = 17$ lbs — Section 2.10.2.1.2.1

$G_A = 1037$ g — Section 2.10.3, Case 2

$t = 1$ in. — Section 2.10.1

$m = 1/0.3$

$\sigma_r = \sigma_t = 3\,(1037)(17)\,(3(1/.3) + 1) / (8\,\pi\,(1/.3)\,(1^2) = 6{,}944$ psi

conservatively use membrane stress allowable

$P_m \leq$ (lesser of $2.4\,S_m$ or $0.7\,S_u$) — ASME Code[2.2], F1331.1(a)

$2.4\,S_m = 2.4\,(16700) = 40{,}080$ psi — Table 2.3-1

or

$0.7\,Su = 0.7\,(70000) = 49{,}000$ psi — Table 2.3-1

$6{,}944$ psi $\leq$ 40,080 psi

2.10.2.3 Weldneck Flange and (Blind) Closure Flange

Weld Neck Flange and Cylinder (Pipe) Junction

Working Internal Pressure of 8" Schedule 40 [ASME Code[2.2], Para. NB-3641]

$Pa = 2\,S_m\,t / (D_o - 2\,y\,t)$

Where S_m, maximum allowable stress intensity at design temperature (the accident condition temperature of 800°F is used to envelop all conditions).

$Pa = [2(13000)(0.322)/(8.687 - 2(0.4)(0.322)) = 993$ psid @ 800 °F

Working Internal Pressure of 8"-150 lb Weld Neck Flange and Blind Closure Flange:

Pa = 80 psid @ 800°F [ANSI B16.5[2.14], Table 2-150]

The maximum differential pressure caused by internal pressure is 36.9 psid at 800°F. This is less than the allowable working pressure. Notwithstanding this, for completeness the juncture is analyzed. For conservatism and simplicity of analysis, the flange is considered rigid.

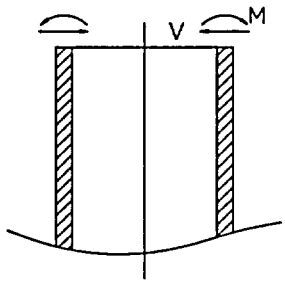

$$\delta_R = 0 = \frac{-1}{2D\lambda^3}V + \frac{1}{2D\lambda^2}M + \frac{PR^2}{Et_c}\left(1 - \frac{1}{2}\mu\right)$$

$$\theta = 0 = -\frac{1}{2D\lambda^2}V + \frac{1}{D\lambda}M$$

Or as shown before in Section 2.10.2.1

$0 = -4.30153\text{x}10^{-6}V + 4.76610\text{x}10^{-6}M + 35.53001\text{x}10^{-6}$
$0 = -4.76610\text{x}10^{-6}V + 10.5617\text{x}10^{-6}M$

Solving:
V = 16.52 lb/in
M = 7.45 in-lb/in

Since these loads are lower than the cylinder-bottom plate juncture loads for the accident condition, the cylinder-bottom plate juncture stresses govern. No additional stress calculations are needed. The cylinder-weld neck flange juncture is OK!

Weld Neck and Blind Flange Stresses

The weld neck flange and blind flange are manufactured from a standard (ANSI B16.5)[2.14] 8"-150lb, Class RF, weld neck flange and blind flange (F304L or similar material). Using a standard assembly with low strength bolts, these components are rated at 212 psig at 150 °F and 80 psig at 800 °F (ANSI B16.5[2.14], Table 2-150). From Section 2.10.1.1, the maximum differential pressure at 150 °F and 800 °F is 21.5 psig and 36.9 psig, respectively. Therefore, the components are qualified for the non-impact loading conditions.

For 30-foot end drop impact, Section 2.10.3, Case 3 acceleration will produce the largest load on the blind flange since Case 2 impact is balanced by the crushing of the wood. The blind flange is conservatively assumed to act as a simply supported circular plate (Roark[2.24], page 216, case 1). The edge support is assumed to be at the outer radius of the raised face (a = 10.625/2 = 5.3125"). At the center of the plate the bending stress is:

$\sigma_r = \sigma_t = 3\,W\,(3\,m + 1) / (8\,\pi\,m\,t^2)$

$W = W_{flg}\,(G_A)$

$W_{flg} = 47$ lbs — for 8"-150 lb flange

$G_A = 92$ g — Section 2.10.3, Case 3

$t = 1.125$ in. — for 8"-150 lb flange

$m = 1/0.3$

$\sigma_r = \sigma_t = 3\,(92)(47)\,(3(1/.3) + 1) / (8\,\pi\,(1/.3)\,(1.125)^2) = 1346$ psi

conservatively use membrane stress allowable

$P_m \leq$ (lesser of $2.4\,S_m$ or $0.7\,S_u$) — ASME Code[2.2], F1331.1(a)

$2.4\,S_m = 2.4\,(16700) = 40{,}080$ psi — Table 2.3-1

or

$0.7\,Su = 0.7\,(70000) = 49{,}000$ psi — Table 2.3-1

$1{,}346$ psi $\leq$ $40{,}080$ psi

2.10.2.4 Closure Bolts

The blind flange (closure lid) bolts to the canister body by eight 3/4-10UNRC-2A by 2.0 inch long bolts. Bolt stresses and fatigue usage factor are calculated. Part (f.) below uses the method outlined in NUREG/CR-6007[2.30] to determine the bolt loads for the impact loading condition. The following summarizes the major structural parameters used in the non-impact bolt stress analysis.

Eight 3/4-10UNRC-2A bolts

Tensile bolt area = 0.334 in^2

Thread engagement length = 0.9475" minimum (1 1/16 - chamfers)

Bolt circle diameter d_{bc} = 11.75"
Material ASTM-A193-B8M Class 2 (Class 1 properties used)
Circle diameter of O-ring seal = 9.25" for inner seal
Circle diameter of O-ring seal = 10.25" for outer seal
Lubrication - Neolube, nut friction factor 0.14 to 0.20
Bolt torque: 40 ft-lb minimum, 50 ft-lb maximum

a) Bolt Preload Stress

Bolt torque T_{min} = 40 ft-lb, T_{max} = 50 ft-lb
Nut friction factor K_{min} = .14, K_{max} = 0.20 (EPRI-NP-5067[2.8], Table G)
Nominal bolt diameter D = 0.75 in
T = KDF/12 or F = 12T/KD
F_{min} = 12 (40) / 0.20 (0.75) = 3,200 lbs. (total bolt load=25600 lbs)
F_{max} = 12 (50) / 0.14 (0.75) = 5,714 lbs. (total bolt load=45712 lbs)

Preload stress

Stress area for 3/4-10UNRC=0.3340 in.^{2} Machinery's Handbook[2.15], pg. 1266

$S_{1,min}$ = 3200 / 0.3340 = 9,581 psi
$S_{1,max}$ = 5714 / 0.3340 = 17,108 psi < 18,600 $2S_m$ @ 150°F
[ASME Code[2.2] NB 3232.1]

b) O-ring Seal Compression Load

The required bolt preload to compress both inner and outer O-ring seal is calculated. The seals are Alloy 600, 1/8" diameter, 0.010" wall metallic O-rings.

O-ring compression force =(1.1)(0.9)(343)= 340 lb/in, Ref.[2.32],page 6,alloy 600
O-ring circle diameters 9.25" and 10.25"

Total load require to compress both seals:
= π (9.25) (340) + π (10.25) (340)
= 20,829 lb for eight bolts

Load per bolt to compress seals:
= 20829 / 8
= 2,604 lb < 3,200 lb minimum bolt preload ∴ OK

c) Thermal Effect on Bolt Preload

As a result of different coefficients of expansion, at non-standard temperature (70°F), bolt load will change.

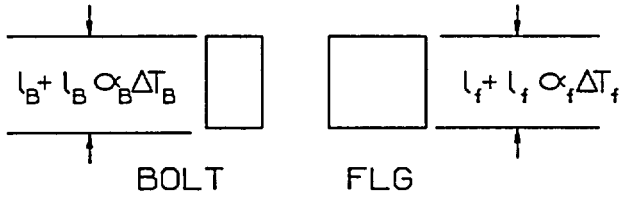

Elastic Strain

$$\delta_B = P / K_B \quad \& \quad \delta_F = P / k_f$$

Continuity requires bolt and flange be of the same length

$$l_B + l_B \alpha_B \Delta T_B + P / K_B = l_f + l_f \alpha_f \Delta T_f - P / K_f$$

$$(l_B - l_f) + l_B \alpha_B \Delta T_B - l_f \alpha_f \Delta T_f = -[(K_B + K_f) / K_B K_f)] P$$

For isothermal conditions $\Delta T_B = \Delta T_f = \Delta T$

$$(l_B - l_f) + l_B \alpha_B \Delta T - l_f \alpha_f \Delta T = -[(K_B + K_f) / K_B K_f)] P$$

Let $\delta \equiv l_B - l_f \Rightarrow l_f = l_B - \delta$

$$\delta + l_B (\alpha_B - \alpha_f) \Delta T + \delta \alpha_f \Delta T = -[(K_B + K_f) / K_B K_f] P$$

$$\delta (1 + \alpha_f \Delta T) + l_B (\alpha_B - \alpha_f) \Delta T = -[(K_B + K_f) / K_B K_f] P$$

$$\delta + l_B \alpha_B \Delta T - (l_B - \delta) \alpha_f \Delta T = -[(K_B + K_f) / K_B K_f] P$$

Now $\delta << l_B$, therefore $l_B - \delta \cong l_B$

$$\delta + l_B (\alpha_B - \alpha_f) \Delta T = -(K_B + K_f) / K_B K_f) P$$

If $\Delta T = 0$, then P equals the initial preload P_p

$$P_p = -[K_B K_f / (K_B + K_f)] \delta \qquad \text{and}$$

$$P = -[K_B K_f / (K_B + K_f)]\ \delta - [K_B K_f / (K_B + K_f)]\ l_B\ (\alpha_B - \alpha_f)\ \Delta T$$

Hence, the change in preload, ΔP, due to isothermal change in material temperature,

$$\Delta P = P - P_P = -[K_B\ K_f / (K_B + K_f)]\ l_B\ (\alpha_B - \alpha_f)\ \Delta T$$

Now, since $E_B = E_f = E$

$$K_B K_f / (K_B + K_f) = (E_B\ A_B\ A_f / A_B l_f + A_f l_B)$$

But, $l_f \cong l_B = l$

$$K_B K_f / (K_B + K_f) = [A_B\ A_f / (A_B + A_f)]\ (E/l)$$

$$\boxed{\Delta P = E\ [A_B\ A_f / (A_B + A_f)]\ [\alpha_f - \alpha_B]\ \Delta T}$$

$$A_B = n\ \pi / 4\ d_B^2 = 8\ (\pi / 4)\ (0.75)^2 = 3.534\ in^2$$

The effective area of the flange is assumed to be 50% of the actual area.
$A_f \cong 0.5(\pi / 4)\ (OD^2 - ID^2) = (\pi / 8)\ ((13.5)^2 - (7.98)^2) = 46.56\ in^2$

$$\Delta P = 3.285\ E\ (\alpha_f - \alpha_B)\ \Delta T$$

At the isothermal temperature of 150°F ($\Delta T = 80°F$)

$\alpha_B = 8.65 \times 10^{-6}$ in/in/°F
$\alpha_f = 8.67 \times 10^{-6}$ in/in/°F
$E = 27.95 \times 10^6$ lb/in^2
$\Delta P = 3.285\ (27.95 \times 10^6)\ (8.67 \times 10^{-6} - 8.65 \times 10^{-6})\ (80) = 147$ lb
Therefore, ΔP/ bolt = 18 lb per bolt

At the isothermal temperature of -40°F ($\Delta T = -110°F$)

$\alpha_B = 8.26 \times 10^{-6}$ in/in/°F
$\alpha_f = 8.21 \times 10^{-6}$ in/in/°F
$E = 29.3 \times 10^6$ lb/in^2
$\Delta P = 3.285\ (29.3 \times 10^6)\ (8.21 \times 10^{-6} - 8.26 \times 10^{-6})\ (-110) = 529$ lb
Therefore, ΔP/ bolt = 66 lb per bolt

At the isothermal temperature of 800°F ($\Delta T = 730°F$)

$\alpha_B = 9.90 \times 10^{-6}$ in/in/°F

$\alpha_f = 9.82 \times 10^{-6}$ in/in/°F
$E = 24.1 \times 10^6$ lb/in^2
$\Delta P = 3.285\ (24.1 \times 10^6)\ (9.82 \times 10^{-6} - 9.90 \times 10^{-6})\ (730) = -4{,}623$ lb
Therefore, ΔP / bolt = -578 lb per bolt

d) Change in Load Due to Mechanical Loading of Joint

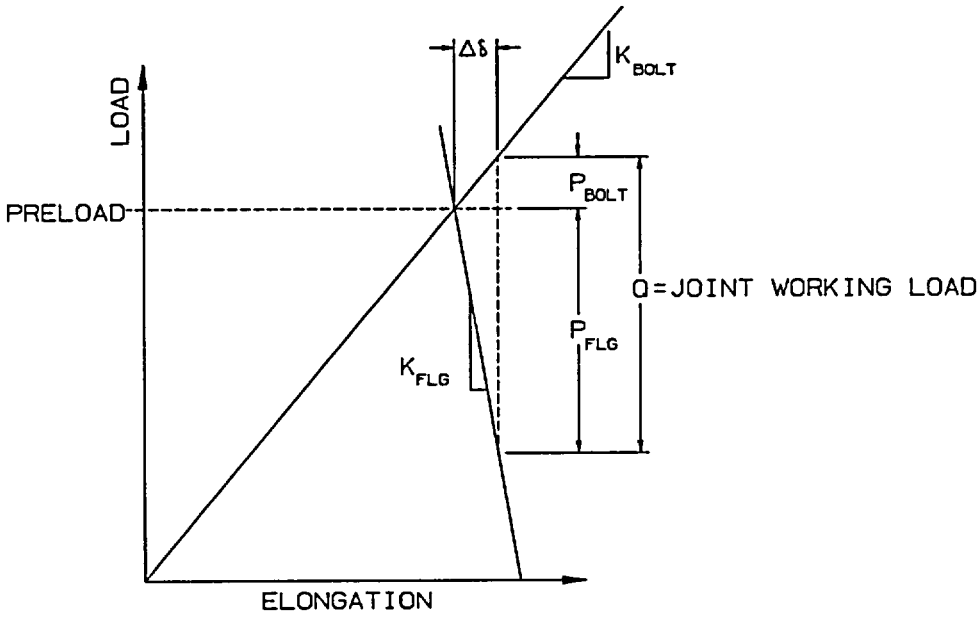

$\Delta\delta = (1 / K_{flg})\ \Delta P_{flg}$

$\Rightarrow (1 / K_{flg})\ \Delta P_{flg} = (1 / K_{bolt})\ \Delta P_{bolt}$

$\Delta\delta = (1 / K_{bolt})\ \Delta P_{bolt}$

$\Delta P_{bolt} + \Delta P_{flg} = Q \Rightarrow \Delta P_{flg} = Q - \Delta P_{bolt} \Rightarrow (Q - \Delta P_{bolt}) / K_{flg} = (1/K_{bolt})\ \Delta P_{bolt}$

or $Q = [(K_{flg} / K_{bolt}) + 1]\ \Delta P_{bolt}$

$$\boxed{\Delta P_{bolt} = [K_{bolt} / (K_{flg} + K_{bolt})]\ Q}$$

The elasticity modulus, E, is the same for both the flange and bolt. Also the length of the bolt and flange can be assumed equal for this calculation. Therefore,

$$\frac{K_{bolt}}{K_{flg}+K_{bolt}} = \frac{A_{bolt}}{A_{flg}+A_{bolt}} = \frac{3.534}{46.56 + 3.534} = 0.071$$

The working mechanical loads are due to internal pressurization, external pressurization, and impact acceleration.

Reduce External Pressure:

$Q = (\pi / 4) (10.25^2) (21.5) = 1,774$ lbs

$\Delta P_{BOLT} = 0.071 (1774) / 8 = 16$ lb per bolt

50-Foot Immersion:

$Q = (\pi / 4) (10.25^2) (-21.7) = -1791$ lbs

$\Delta P_{BOLT} = 0.071 (-1791) / 8 = -16$ lb per bolt

Fire:

$Q = (\pi / 4) (10.25^2) (36.9) = 3045$ lbs

$\Delta P_{BOLT} = 0.071(3045) / 8 = 27$ lb per bolt

e) Load Combination and Fatigue Life

Using worst load combinations per Regulatory Guide 7.8[2.4]:

Bolt load - Normal Condition of Transport:

Preload + Reduced External Pressure + Thermal Effects at –40 °F

5714 + 16 + 66 = 5,796 lb

Bolt load - Hypothetical Accident Conditions:

50 ft Immersion

Preload + 50 ft. Immersion + Thermal Effects at –40 °F

5714 – 16 + 66 = 5,764 lb

Fire

Preload + Fire Effects at 800 °F

5714 +27 – 578 = 5,163 lb

The bolting-and-unbolting load is the largest portion of the load and the number of bolt stress cycles is, when applying stress concentration factor (SCF) of 4.0,

$\sigma = 5796 / 0.334 = 17,353$ psi

$S_{range} = 4 \sigma = 4 (17353) = 69,412$ psi

The alternating stress is:

$S_{alt} = S_{range} / 2 = 69412 / 2 = 34{,}706$ psi

S_{ALT} corrected for elastic modulus = 34706 (30 / 27.95) = 37,252 psi. Allowable cycle per ASME Code[2.2], conservatively use fatigue curve for high strength bolting, Figure I-9.4 (and Table I-9.1) is 8,000 cycles. The bolts will be torqued twice per shipment. One for the loading and shipment and one time for return journey. Therefore, the number of shipments allowed is 4,000.

f) Impact from 30-Foot Drop

The maximum acceleration for this condition is 147 g's from Section 2.10.3, Case 1, 30-foot slapdown drop. Note, Case 2 does not control since this force is balanced by the crushing force of the wood and Case 3 would tend to unload the bolts since the flange joint would be in compression. The maximum bolt load is determined using the procedure from NUREG/CR-6007[2.30], page 17, Table 4.6. Using the nomenclature from Reference [2.30]. The tensile bolt force per bolt (Fa) and the shear bolt force per bolt (Fs) are given as

$Fa = 1.34 \sin(xi)\ (DLF)\ (ai)\ (W_L + W_C) / Nb$

$Fs = \cos(xi)\ ai\ W_{CK} / Nb$

where: xi = 15 degrees

ai = 147 g	Section 2.10.3, Case 1
DLF = 1	since it is based on test results
$W_L = 47 + 3 = 50$ lbs	8"-150 lb flange + 3 lbs for bolts
$W_C = 48(10) = 480$ lbs	Pathfinder fuel weight 10 lb/ assy
$W_{CK} = W_L = 50$ lbs	For bolt shear loading, the only unsupported weight is the blind flange and bolts since the fuel canister is supported at the clamp locations.

Nb = 8 bolts

$Fa = 1.34 \sin(15)\ (1)\ (147)\ (50 + 480) / 8 = 3{,}378$ lbs/bolt

Fa' = Fa + Fp

Fp = 1774/8 = 222 lbs/bolt from pressure, part d of this section

Fa' = 3378 + 222 = 3,600 lbs/bolt Load combination: 30 ft. drop + pressure load

$Fs = \cos(15)\ (147)\ (50) / 8 = 887$ lbs/bolt

The above tensile bolt load calculation neglects preload. As an additional conservative check for bolt tensile loads, the maximum bolt preload and joint stiffness is also used below with the above calculated Fa and Fp.

$F = \max F_{preload} + 0.071\ (Fa + Fp\ )$
$F = 5714 + 0.071\ (3378 + 222)$
$F = 5{,}970$ lbs/bolt

Since F is greater than Fa', F is used in the stress calculation below.

$\sigma = F / A_b = 5970 / 0.334 = 17{,}874$ psi
$\tau = Fs / A_b = 887 / 0.334 = 2{,}656$ psi

The Faulted Condition stress limits of ASME Code[2.2], F-1335 are used below.

Tensile

σ_{allow} = lesser of $0.7\ S_u$ or S_y at 150 °F (impact loads will be gone before fire starts)
$0.7\ S_u = 0.7\ (69750) = 48{,}825$ psi
$S_y = 27{,}900$ psi
$\sigma \le S_y$
17,874 psi ≤ 27,900 psi Therefore, OK

Shear

τ_{allow} = lesser of $0.42\ S_u$ or $0.6\ S_y$ at 150 °F
$0.42\ S_u = 0.42\ (69750) = 29{,}295$ psi
$0.6\ S_y = 0.6\ (27900) = 16{,}740$ psi
$\tau \le 0.6\ S_y$
2,656 psi ≤ 16,740 psi Therefore, OK

Combined Tensile and Shear

$(f_t / F_{tb})^2 + (f_v / F_{vb})^2 \le 1$
$(17874 / 27900)^2 + (2656 / 16740)^2 \le 1$
$0.44 \le 1$

g) Thread Engagement

The bolt is screwed into the weld neck flange. The flange is made of a material of lesser strength. The flange material dictates the required engagement. The flange thread is 3/4 - 10UNC - 2B. From Machinery's Handbook[2.15], pages 1068 & 1069:

$$L_e = \frac{2 A_t J}{\pi K_{n,max} [\frac{1}{2} + .57735N(E_{s,min} - K_{n,max})]}$$

$A_S = \pi N\ K_{n,max}\ [1/2N+0.57735\ (E_{s,min}-K_{n,max})]\ L_e$ Shear area of external thread

$A_n = \pi N\ D_{s,min}\ [1/2N+0.57735\ (D_{s,min}-E_{n,max}]\ L_e$ Shear area of internal thread

$A_t = 0.334\ in^2$ Tensile area of bolt

$N = 10$ Number of threads per inch

$K_{n,max} = 0.663$ in Maximum minor diameter of internal thread

$E_{n,max} = 0.6927$ in Minimum pitch diameter of internal thread

$D_{n,max} = 0.7353$ in Minimum major diameter of external thread

$E_{s,min} = 0.6773$ in Minimum pitch diameter of external thread

$S_{bolt} = 75{,}000$ psi @ 70°F Bolt tensile strength

$S_{flg} = 70{,}000$ psi @ 70°F Flange tensile strength

$A_s = \pi(10)(.663)[1/20+.57735(.6773-.663)]\ L_e = 1.2134\ L_e$

$A_n = \pi(10)(.7353)[1/20+.57735(.7353-.6927)]\ L_e = 1.7232\ L_e$

$$J = \frac{A_s S_{bolt}}{A_n S_{flg}} = \left(\frac{1.2134}{1.7232}\right)\left(\frac{75000}{70000}\right) = 0.7545$$

Therefore, J is set equal to 1.0

$$L_e = \frac{2(.334)(1.0)}{1.2134} = 0.5505$$

The thread length available is

$L_{avail} = 1.0625 - 0.1 - .015 = 0.9475 > 0.5505$ ∴ OK

2.10.2.5 Saddle Supports – Pathfinder Canister

The saddle supports the dead weight of the fuel canister and the only significant loads occur during an accident condition. From Section 2.10.2.1.2.2, the maximum load on a support is 26,925 lbs. From the same section, the maximum distributed (cosine) pressure load is p_{max} = 2,827 psi for a 10,000 lb load. Thus, the bearing stress acting on the aluminum saddle is:

$\sigma_{brg} = 2{,}827\ (26{,}925 / 10{,}000) = 7{,}612$ psi

Per ASME Code[2.2], F-1331.3, except for pinned and bolted joints, bearing stresses need not be evaluated. However, a Normal condition limit as given in ASME Code[2.2], NB-3227.1 is S_y. For ASTM B-209 6061 T651 plate aluminum, the room temperature yield is 35000 psi (ASME Code[2.2], Table Y-1). Thus,

$\sigma_{brg} < S_y$

7,612 psi < 35,000 psi OK, very conservative.

2.10.2.6 Spacer Pipe and End Plate

The spacer pipe is 8"-schedule 40S pipe and is the same size and schedule as the Pathfinder Canister. Since the loads on the spacer pipe are less than or equal to the fuel canister, it is adequate by inspection. The stress on the end plate for the spacer pipe is calculated below.

The load on the end plate is equal to the wood crush load from Section 2.10.3, Case 3, F_{max} = 71,898 lbs. Conservatively this load is uniformly distributed over the end plate.

$$w = 71{,}898 / (14.5)^2 = 342 \text{ psi}$$

The critical location for plate bending is across a corner (A-A) as shown below.

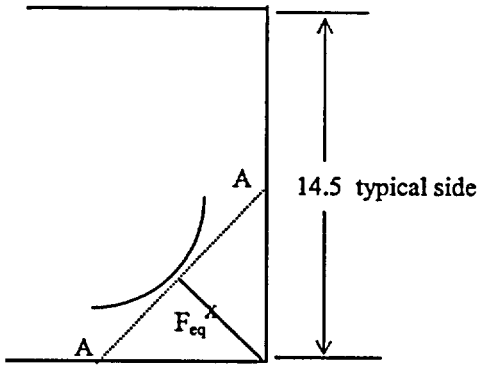

The area on this corner of the plate is:

$$A1 = (((2)^{0.5}(14.5) - 8.625) / 2)^2 = 35.29 \text{ in.}^2$$

The equivalent force (F_{eq}) is located at the centroid of this area:

$$F_{eq} = 342(35.29) = 12{,}069 \text{ lbs}$$

The moment arm from F_{eq} to line A-A is:

$$L1 = 0.333(((2)^{0.5}(14.5) - 8.625)/2) = 1.98 \text{ in.}$$

$$M = 1.98\ (12069) = 23{,}897 \text{ in-lbs} \quad \text{bending moment}$$

$$\sigma_b = 6\ (M / b) / t^2 \quad \text{bending stress}$$

Where b is the base of the triangle (i.e. 11.88 in.) and t is the thickness of the plate (0.5 in.)

$$\sigma_b = 6\ (23{,}897 / 11.88) / (0.5)^{0.5} = 48{,}277 \text{ psi}$$

This exceeds the yield strength of the material (25 ksi) but well below the ultimate strength of 75 ksi. This is considered satisfactory since the primary function of the end plate is to hold the wood is place. Note, the majority of the load will transmit through the wood within the area of the outer diameter of the spacer and canister.

2.10.2.7 Hypothetical Fire Accident Condition Container Stresses

From Figure 3.5-3 (Chapter 3), the maximum temperature for the fire accident condition on the inner surface of the clamps is 792 °F. The Pathfinder Canister temperature at a saddle support will be below this 792 °F since the resistance of the saddle support and two interfaces are between the clamp and the canister wall. The bolted closure is insulated from the end plate of the inner box by pine wood. The pine wood is treated with a fire retardant and with the restricted air flow through the bolted joints, will not burn. Thus, the primary heat source for this region is heat conducted from the nearest saddle support, which is 4 inches from the joint. This additional resistance in the heat flow path will reduce the temperature at the bolted closure below the 792 °F maximum clamp temperature.

From Figure 3.5-3 (Chapter 3), the maximum temperature gradient between points 90 degrees apart on the inner surface of the clamp is approximately 35 F°. The linear circumferential temperature gradient of the fuel canister is less then 35 / ((π/4) (8.625)) = 5.2 F° / inch since the saddle supports will help distribute the temperature. The thermal stresses due to this gradient are considered negligible. The axial temperature gradients may be significant. The space between the fuel canister and inner box (except at clamp locations) is filled with Zircar insulation and the temperature transient for the maximum clamp temperature point is approximately 1100 F°/hr (Figure 3.5-2). Thus, as a worse case, a linear temperature gradient from the bolted joint to the nearest clamp is (792 - 122)/4 = 168 F° / inch.

Note the maximum circumferential and maximum axial gradients can not occur at the same location and the axial gradient stresses will obviously bound those due to the circumferential gradient. The thermal stresses due to an axial gradient in a cylinder can be approximated by using Hartog[2.33]. For a finite tube of length L, hot in the center and cold at the ends with a half sine-wave of temperature (Hartog[2.33], Fig. 13b), the solution is given in Fig. 14 of Hartog[2.33]. Note this solution should approximate or be conservative for a linear temperature gradient since a portion of the sine-wave will have a slope greater than a straight linear representation.

L = 2 times distance from clamp center to bottom flange surface of weld neck flange

L = 2(4) = 8"

t = 0.322"

R = (8.625 - 0.322) / 2 = 4.1515"

$L/(R\,t)^{0.5} = 8/(4.1515(0.322))^{0.5} = 6.92$

$\tau_{max}/E\alpha T_o = 0.06$ Hartog[2.33]. Fig. 14

$\sigma_{thm} = 2\,\tau_{max} = 2(0.06)E\alpha T_o = 0.12\,E\alpha T_o$

$E = 27.0 \times 10^6$ psi Table 2.3-1, at 300 °F, max Eα

$\alpha = 9.00 \times 10^{-6}$ in/in/F° Table 2.3-1, at 300 °F, max Eα

$T_o = 792 - 122 = 670$ F° Figure 3.5-2

$\sigma_{thm} = 0.12(27.0 \times 10^6)(9.00 \times 10^{-6})(670) = 19{,}537$ psi

The hoop pressure stress due to the 36.9 psig internal pressure is:

$\sigma_{press} = 36.9(4.1515)/0.322 = 476$ psi

$\sigma = \sigma_{thm} + \sigma_{press} = 19537 + 476 = 20{,}013$ psi

$S_n = (E_{cold} / E_{hot})\,K_t\,\sigma = (28.3 \times 10^6 / 27.95 \times 10^6)(4)(20013) = 81{,}054$ psi

Since this thermal stress is due to an accident condition, the allowable stress is 2 Sa at 10 cycles (Ref. Table 2.1-1):

$S_n < 2$ Sa at 10 cycles

Sa at 10 cycles = 708,000 psi ASME Code[2.2], Table I-9.1, Fig. I-9.2.1

81,054 psi < 2(708,000)

81,054 psi < 1,416,000 psi Therefore, OK

2.10.2.8 Removal of WE-1 Clamp

Due to space required for the bolted closure and wood impact absorber, the first clamp from the one end plate (slap down end) will be removed. The effect on the stiffness of the WE-1 inner container and ultimately the g-load on the Pathfinder Canister is considered to be small due to this modification to the original test configuration. This region of the container still has one clamp, the inner container spacer, and the end plate to provide additional stiffness to that of the bolted container itself.

A conservative finite element stiffness analysis was performed for the HY-80 armor plate inner container with and without the end clamp. Computer program ANSYS was used for the stiffness calculations. The box stiffness in the diagonal direction was calculated. Due to structural symmetry, half of the box is analyzed. ANSYS 20-noded SOLID95 element type was used. Figure 2.10-5 shows the finite element model for original configuration i.e., with end clamp. Figure 2.10-6 shows the finite element model with end clamp removed. A listing of the ANSYS commands for the modified configuration with one clamp removed is provided. The ANSYS commands for the original configuration model can be obtained by removing three lines of commands starting with the comment 'remove 1st clamp from model.' The results of the analysis are:

Armor box local stiffness (half of the symmetrical box)

With all clamps	5,348,200 lb/inch
With last clamp removed	5,084,300 lb/inch

The localized stiffness after removing the end clamp is reduced by 4.9%, which is within the accuracy of the impact analysis. The end spacer, end plate and two end clamps are all so close together, that removal of one end clamp does not significantly alter the stiffness of the HY-80 armor plate inner container. This has been verified by the finite element analysis. There is no change in the beam bending stiffness with and without end clamp. Also, when one considers, all other structural members, the change in the overall stiffness or the dynamic response even diminishes.

ANSYS Command Listing for Localized Stiffness for HY-80 Armor Plate Inner Container

```
/PREP7
/TITLE, WE-1 ARMOR BOX L0CAL STIFFNESS WITH 1ST CLAMP REMOVED
ET,1,SOLID95        ! SIDE PLATES
ET,2,SOLID95        ! PORTION OF END PLATE IN CONTACT WITH SIDE PLATES
ET,3,SOLID95        ! PORTION OF END PLATE NOT IN CONTACT WITH SIDE PLATES
ET,4,SOLID95        ! INNER SPACER (CROSS) PLATE
ET,5,SOLID95        ! 1ST CLAMP
ET,6,SOLID95        ! 2ND CLAMP
ET,7,SOLID95        ! 3RD CLAMP
MPTEMP,1,70
MPDATA,EX,1,1,27.8E6
MPDATA,NUXY,1,1,0.3
/COM,  GEOMETRY FOR ARMOR BOX SIDE PLATES
CSYS,0
K,1,0,0,0
K,2,1,1,0
K,3,1.75,0,0
K,4,1.75,1,0
K,5,3.22,0,0
K,6,3.22,1,0
K,7,5.522,0,0
K,8,5.522,1,0
K,9,6.522,0,0
K,10,6.522,1,0
K,11,9.730,0,0
K,12,9.730,1,0
K,13,10.730,0,0
K,14,10.730,1
K,15,13.28,0,0
K,16,13.28,1,0
K,17,14.75,0,0
K,18,14.75,1,0
K,19,15.5,0,0
K,20,15.5,1,0
K,21,16.5,0,0
K,22,16.5,1,0
K,23,16.5,1.75,0
K,24,15.5,1.75,0
K,25,16.5,3.22,0
K,26,15.5,3.22,0
```

```
K,27,16.5,5.53,0
K,28,15.5,5.53,0
K,29,16.5,6.53,0
K,30,15.5,6.53,0
K,31,16.5,9.73,0
K,32,15.5,9.73,0
K,33,16.5,10.73,0
K,34,15.5,10.73,0
K,35,16.5,13.28,0
K,36,15.5,13.28,0
K,37,16.5,14.75,0
K,38,15.5,14.75,0
K,39,16.5,16.5,0
K,40,15.5,15.5,0
KGEN,2,1,40,1,,,-1.00,40
KGEN,2,41,80,1,,,-4.04,40
KGEN,2,81,120,1,,,-1.00,40
KGEN,2,121,160,1,,,-3.36,40
KGEN,2,161,200,1,,,-1.00,40
KGEN,2,201,240,1,,,-19.60,40
KGEN,2,241,280,1,,,-1.00,40
TYPE,1
MAT,1
*DO,I,1,7,1
  V,1+I*40,3+I*40,4+I*40,2+I*40,1+(I-1)*40,3+(I-1)*40,4+(I-1)*40,2+(I-1)*40
  *REPEAT,10,2,2,2,2,2,2,2,2
  V,22+I*40,23+I*40,24+I*40,20+I*40,22+(I-1)*40,23+(I-1)*40,24+(I-1)*40,20+(I-1)*40
  V,23+I*40,25+I*40,26+I*40,24+I*40,23+(I-1)*40,25+(I-1)*40,26+(I-1)*40,24+(I-1)*40
  *REPEAT,8,2,2,2,2,2,2,2,2
*ENDDO
ESIZE,1.01
VMESH,ALL
/COM,   GEOMETRY FOR ARMOR BOX END PLATE
KGEN,2,1,40,1,,,0,320
KGEN,2,321,360,1,,,1.00,40
TYPE,2
*DO,I,9,9,1
  V,1+I*40,3+I*40,4+I*40,2+I*40,1+(I-1)*40,3+(I-1)*40,4+(I-1)*40,2+(I-1)*40
  *REPEAT,10,2,2,2,2,2,2,2,2
  V,22+I*40,23+I*40,24+I*40,20+I*40,22+(I-1)*40,23+(I-1)*40,24+(I-1)*40,20+(I-1)*40
  V,23+I*40,25+I*40,26+I*40,24+I*40,23+(I-1)*40,25+(I-1)*40,26+(I-1)*40,24+(I-1)*40
  *REPEAT,8,2,2,2,2,2,2,2,2
*ENDDO
V,321,341,359,359,361,381,399,399
VSEL,S,VOLU,,134,153
VOVLAP,ALL        !deletes volume 153 and makes new volume 154
NUMCMP,LINE
NUMCMP,AREA
NUMCMP,VOLU
TYPE,2
VMESH,134,152,1
MSHKEY,0
MSHAPE,1,3D
MOPT,PYRA,ON
TYPE,3
VMESH,153
ALLSEL
ESEL,S,TYPE,,1,2
NSLE,R,ALL
NSEL,R,LOC,Z,-0.001,0.001
NUMMRG,NODE,0.02  !MERGE NODES ON CONTACT AREA BETWEEN SIDE PLATES AND END PLATE
ALLSEL
```

```
/COM,  GEOMETRY FOR INNER SPACER (CROSS) PLATE
K,401,1.375,1.375,0
K,402,1.75,1,0
K,403,3.22,1,0
K,404,6.97,4.75,0
K,405,8.25,4.75,0
K,406,9.53,4.75,0
K,407,13.28,1,0
K,408,14.75,1,0
K,409,15.50,1.75,0
K,410,15.50,3.22,0
K,411,11.75,6.97,0
K,412,11.75,8.25,0
K,413,11.75,9.53,0
K,414,15.50,13.28,0
K,415,15.50,14.75,0
K,416,15.125,15.125,0
LOCAL,11,1,8.25,8.25,0,45
K,417,3,0,0
KGEN,9,417,417,1,,-22.5,,1
CSYS,0
KGEN,2,401,425,1,,,-1,25
L,401,402
*REPEAT,16,1,1
CSYS,11
K,451,0,0,0
K,452,0,0,-1
LARC,417,418,451,3
*REPEAT,8,1,1,0,0
CSYS,0
L,425,401
L,426,427
*REPEAT,16,1,1
CSYS,11
LARC,442,443,452,3
*REPEAT,8,1,1,0,0
CSYS,0
L,450,426
L,426,401
*REPEAT,25,1,1
AL,953,903,954,928
*REPEAT,24,1,1,1,1
AL,977,927,953,952
LSEL,S,LINE,,903,927,1
AL,ALL
LSEL,S,LINE,,928,952,1
AL,ALL
ALLSEL
ASEL,S,AREA,,658,684,1
TYPE,4
VA,ALL
VMESH,154
ASEL,S,AREA,,10
ASEL,A,AREA,,40
ASEL,A,AREA,,60
ASEL,A,AREA,,90
ASEL,A,AREA,,659
ASEL,A,AREA,,664
ASEL,A,AREA,,666
ASEL,A,AREA,,671
NSLA,R,1
NUMMRG,NODE,0.02 !MERGE NODES ON CONTACT AREAS BETWEEN CROSS AND SIDE PLATES
```

```
ALLSEL
/COM,  GEOMETRY FOR CLAMPS, MESH FOR 1ST CLAMP
CSYS,0
K,461,5.522,1,-5.04
K,462,6.522,1,-5.04
K,463,9.730,1,-5.04
K,464,10.73,1,-5.04
K,465,15.50,5.53,-5.04
K,466,15.50,6.53,-5.04
K,467,15.50,9.73,-5.04
K,468,15.50,10.73,-5.04
K,469,2.570,1.863,-5.04
K,470,3.630,2.923,-5.04
K,471,4.510,2.130,-5.04
K,472,5.522,2.130,-5.04
K,473,6.522,2.130,-5.04
K,474,9.730,2.130,-5.04
K,475,10.73,2.130,-5.04
K,476,12.48,2.130,-5.04
K,477,13.98,2.130,-5.04
K,478,13.98,3.630,-5.04
K,479,13.98,5.530,-5.04
K,480,13.98,6.530,-5.04
K,481,13.98,9.730,-5.04
K,482,13.98,10.73,-5.04
K,483,13.98,12.48,-5.04
K,484,13.98,13.98,-5.04
K,485,2.216,2.216,-5.04
K,486,3.630,3.630,-5.04
K,487,4.510,3.630,-5.04
K,488,5.522,3.630,-5.04
K,489,6.522,3.630,-5.04
K,490,9.730,3.630,-5.04
K,491,10.73,3.630,-5.04
K,492,12.48,3.630,-5.04
K,493,12.48,5.530,-5.04
K,494,12.48,6.530,-5.04
K,495,12.48,9.730,-5.04
K,496,12.48,10.73,-5.04
K,497,12.48,12.48,-5.04
KGEN,2,461,497,1,,,-1,40
TYPE,5
V,501,502,513,512,461,462,473,472
V,503,504,515,514,463,464,475,474
V,505,506,520,519,465,466,480,479
V,507,508,522,521,467,468,482,481
V,509,510,526,525,469,470,486,485
*REPEAT,7,1,1,1,1,1,1,1,1
V,516,517,518,532,476,477,478,492
V,532,518,519,533,492,478,479,493
*REPEAT,5,1,1,1,1,1,1,1,1
V,537,523,524,524,497,483,484,484
VGEN,2,155,172,1,,,-4.36,80,1,0
VGEN,2,155,172,1,,,-24.96,160,1,0
VSEL,S,VOLU,,155,158,1
VSEL,A,VOLU,,160,171,1
MSHKEY,1
MSHAPE,0,3D
MOPT,PYRA,OFF
VMESH,ALL
VSEL,ALL
VMESH,159
```

```
MSHKEY,0
MSHAPE,1,3D
MOPT,PYRA,ON
VMESH,172
ASEL,S,AREA,,190
ASEL,A,AREA,,198
ASEL,A,AREA,,230
ASEL,A,AREA,,238
ASEL,A,AREA,,686
ASEL,A,AREA,,692
ASEL,A,AREA,,698
ASEL,A,AREA,,704
NSLA,R,1
NUMMRG,NODE,0.02 !MERGE NODES ON CONTACT AREAS BETWEEN 1ST CLAMP AND SIDE PLATES
ALLSEL
/COM,  MESH FOR 2ND CLAMP
TYPE,6
VSEL,S,VOLU,,173,176,1
VSEL,A,VOLU,,178,189,1
MSHKEY,1
MSHAPE,0,3D
MOPT,PYRA,OFF
VMESH,ALL
VSEL,ALL
VMESH,177
MSHKEY,0
MSHAPE,1,3D
MOPT,PYRA,ON
VMESH,190
ASEL,S,AREA,,344
ASEL,A,AREA,,352
ASEL,A,AREA,,384
ASEL,A,AREA,,392
ASEL,A,AREA,,776
ASEL,A,AREA,,782
ASEL,A,AREA,,788
ASEL,A,AREA,,794
NSLA,R,1
NUMMRG,NODE,0.01 !MERGE NODES ON CONTACT AREAS BETWEEN 2ND CLAMP AND SIDE PLATES
ALLSEL
/COM,  MESH FOR 3RD CLAMP
TYPE,7
VSEL,S,VOLU,,191,194,1
VSEL,A,VOLU,,196,207,1
MSHKEY,1
MSHAPE,0,3D
MOPT,PYRA,OFF
VMESH,ALL
VSEL,ALL
VMESH,195
MSHKEY,0
MSHAPE,1,3D
MOPT,PYRA,ON
VMESH,208
ASEL,S,AREA,,498
ASEL,A,AREA,,500
ASEL,A,AREA,,538
ASEL,A,AREA,,546
ASEL,A,AREA,,866
ASEL,A,AREA,,872
ASEL,A,AREA,,878
ASEL,A,AREA,,884
```

```
NSLA,R,1
NUMMRG,NODE,0.02 !MERGE NODES ON CONTACT AREAS BETWEEN 3RD CLAMP AND SIDE PLATES
ALLSEL
LOCAL,12,0,,,,45
NSEL,S,LOC,Y,-0.001,0.001
NROTAT,ALL      !ROTATE NOTES ON SYMMETRY PLANE FOR BC CONSTRAINTS LATER
ALLSEL
VSEL,S,TYPE,,5  !REMOVE 1ST CLAMP FROM MODEL
VCLEAR,ALL
ALLSEL
FINISH
/SOLU
CSYS,12
NSEL,S,LOC,Y,-0.001,0.001
D,ALL,UY,0.0
NSEL,S,LOC,X,-0.001,0.001
D,ALL,UX,0.0
D,14662,UZ,0.0
CSYS,0
NSEL,S,LOC,X,16.499,16.501
NSEL,R,LOC,Y,16.499,16.501
D,ALL,UX,-0.01
ALLSEL
LSWRITE
SAVE
LSSOLVE,1,1,1
FINISH
/POST1
CSYS,0
NSEL,S,LOC,X,16.499,16.501
NSEL,R,LOC,Y,16.499,16.501
RSYS,12
PRRSOL
FINISH
/EXIT,NOSAVE
```

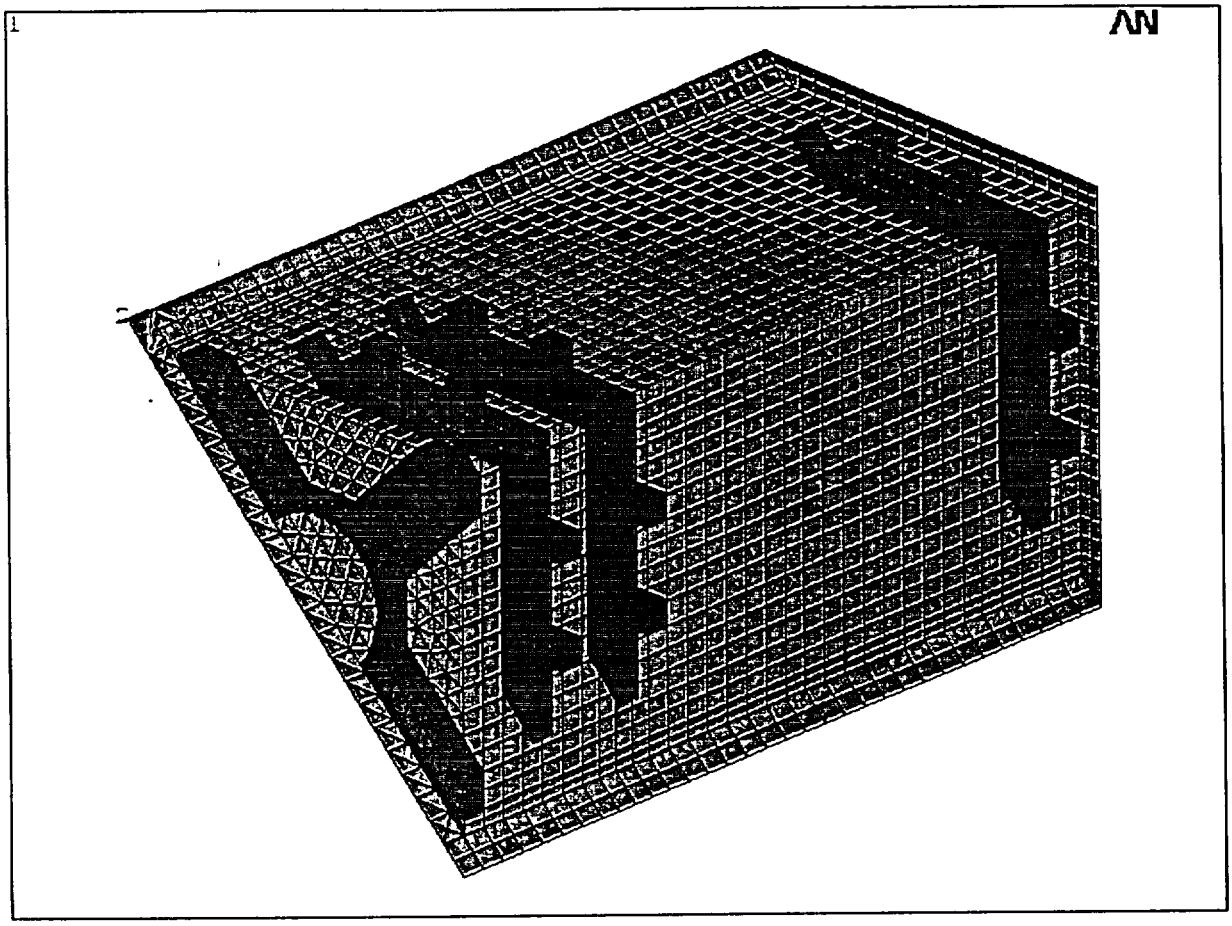

Figure 2.10-5 Finite Element Model for Armor Plate Inner Container
Original Configuration With All Three Clamps

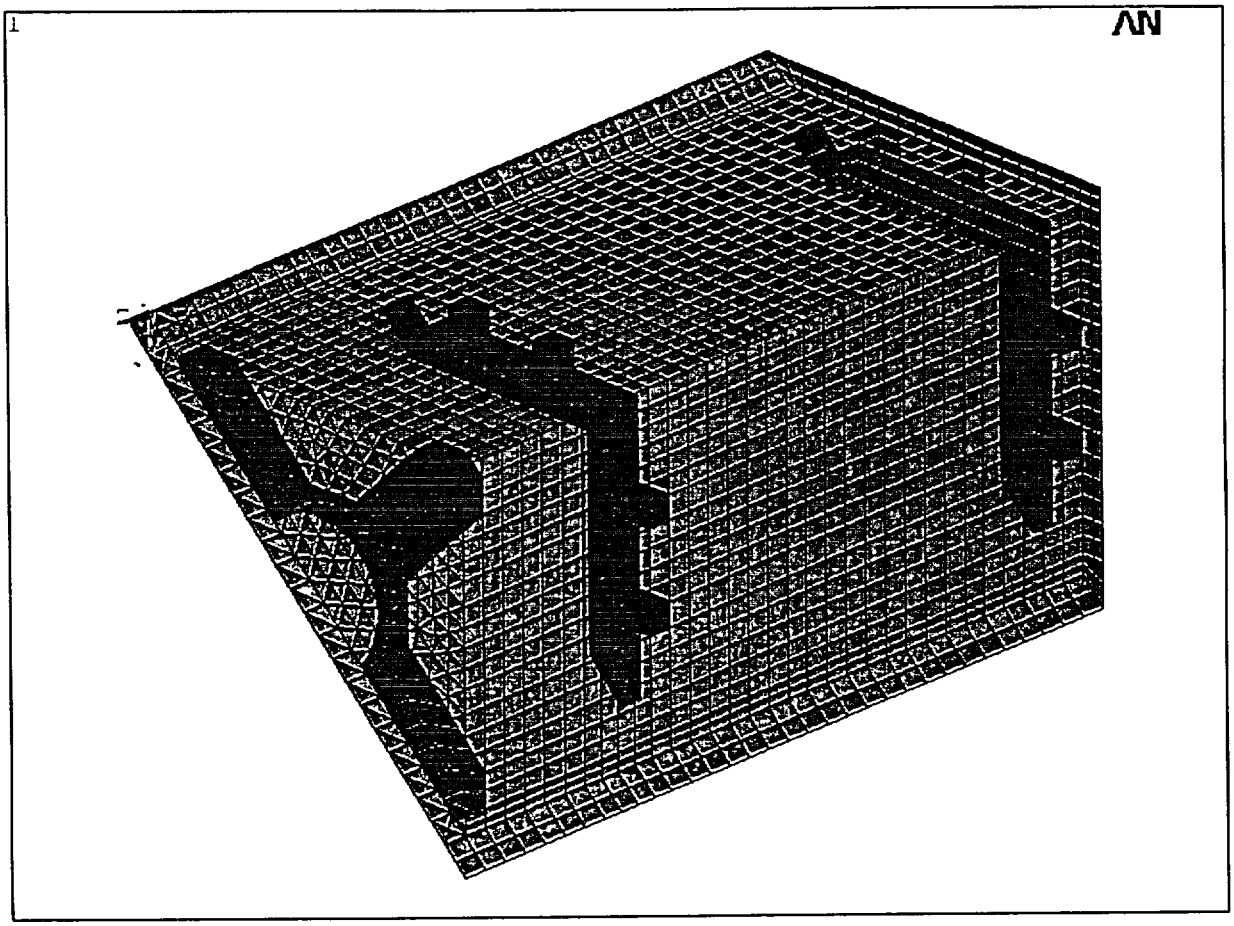

Figure 2.10-6 Finite Element Model for Armor Plate Inner Container With First Clamp Removed

2.10.2.9 Weight and Center of Gravity WE-1 With Pathfinder Canister

The component weight for the Pathfinder Canister and its support are summarized here:

Pathfinder Canister	
Blind Flange	47 lb
Weldneck Flange	42
Cylinder	200
Bottom Plate	17
Bolt / Washer	3
Sub total	309 lb
Pathfinder Fuel	480 lb, approximate weight for 48 fuel assemblies
Spacer Tube Assy	
Tube	145 lb
End Plate	30
Wood Spacer (Oak wood)	47 lb
Inner Rectangular box, strong Back, outer shell, insulation, etc	7,480 lb
WE-1 Package with Pathfinder Canister	8,500 lb

The C.G. shift from the WE-1 with BW 17x17 Fuel Assembly to the WE-1 with Pathfinder Canister and fuel is 2.4 inches.

The total weight of the WE-1 package with BW 17x17 fuel is 9,090 lbs. Of that weight, the BW 17x17 fuel assembly is 1,610 lbs. The center of gravity is situated near the geometric center of the package.

The WE-1 package with Pathfinder Canister is approximately 590 lb lighter and center of gravity is 2.4 inches from geometric center toward Pathfinder Canister closure end. These changes are incorporated for normal and accident condition evaluation of WE-1 package with the Pathfinder Canister.

2.10.2.10 WE-1 Normal Condition 4-foot Drops

Regulation 10CFR71.71(c)(7) requires a package of less than 11,000 pounds to withstand a free drop of four foot onto a flat, unyielding horizontal surface. Previous 4-foot drop tests of similar type packages have experienced acceleration levels of approximately 10 g's for this Normal condition. The acceleration values used in the Pathfinder Canister 30-foot drop accident condition analysis are 142 g's and higher. Since the Faulted condition stresses are acceptable, the Normal condition stresses are also acceptable if

$(G_{Normal} / G_{Faulted}) < (\text{Normal stress allowable} / \text{Faulted stress allowable})$

Primary membrane stress is most limiting and from Table 2.1-1

$(10/142) < (S_m / 2.4\ S_m)$

$0.07 < 0.42$

Therefore, the stress margins from the Faulted condition drops will bound those drops under Normal conditions.

2.10.2.11.1 Penetration

Regulation 10CFR71.71(c)(10) requires that a package withstand the impact of the hemispherical end of a vertical steel cylinder of 1¼ in diameter and weighing 13 pound dropped from a height of 40 inches onto the exposed surface of the package, which is expected to be most vulnerable to puncture.

The contents (Pathfinder Canister) of the WE-1 inner box obviously have no effect on this test. Thus, the conclusion of Section 2.6.10 remains unchanged (i.e. the penetration test has negligible consequence for the WE-1 package).

2.10.2.12 Vibration

By inspection, the Pathfinder Canister is securely clamped at five locations and any large void above the stack of fuel rods in the fuel canister is packed with filler material to prevent fuel rod movement. Thus, the conclusion of Section 2.6.5 remains unchanged (i.e. vibration normally incident to transportation, as delineated in 10CFR71.71(c)(5), will have a negligible effect on the package).

2.10.2.13 Water Spray

Regulation 10CFR71.71(c)(6) requires a package to withstand water spray that simulates exposure to rainfall of approximately 2 inches per hour for at least one hour. The contents (Pathfinder Canister) of the WE-1 inner container obviously have no effect on this test since the canister is constructed of metal and is sealed with metal gaskets. Thus, the conclusion of Section 2.6.6 remains unchanged (i.e. the water spray will have negligible effect on the package).

2.10.3 30-Foot Drop Accident - Pathfinder Canister Accelerations

The purpose of this section is to determine the design g-loadings for the Pathfinder Canister.

2.10.3.1 Lateral Acceleration

The WE-1 Shipping Container containing a MK-BW Prototype Fuel Assembly was drop tested from the 30 foot height. The results are documented in Section 2.7.1.4 and indicate that some of the fuel rods in the bottom span of the fuel assembly experienced a permanent set of approximately 2.25 inches. Since the test was not instrumented, the purpose of this section is to determine the decelaration (g-level) necessary to produce the 2.25-inch deflection. A factor is calculated to account for a dynamic response of the Pathfinder Canister stiffness and weight on a WE-1 package for a 30 foot drop acceleration. This factored acceleration will be used to establish the design lateral loads for the Pathfinder Canister when installed in the WE-1 Shipping Container.

Both the bottom Inconel spacer grid and the intermediate Zircaloy spacer grid of the MK-BW Fuel Assembly are designed to support the fuel rod with five tabs, one middle tab and a pair of tabs at each of the outermost support locations. The WE-1 fuel assembly clamps are at the spacer grid locations except the bottom clamp, which supports both the bottom spacer and the bottom nozzle at a middle location (about 1.86 inches beyond the center of the bottom spacer grid). Rubber shims between the clamp and a thin piece of aluminum sheet metal that contacts the spacer grid provide a secure fit during normal transportation. A special design for the bottom clamp uses a stainless steel sheet metal to bridge the span between the bottom spacer and bottom nozzle.

For a lateral load during an accident condition, the spacer grid design should provide significant moment restraint of the fuel rods. However, the photos from the drop test (Appendix 2-1) indicate that the bottom span of the test fuel rod experienced significant moment restraint only at the intermediate grid spacer. This is due, in part, to the stiffness of the adjacent span whereas the end of the fuel rod is slightly beyond the bottom spacer grid and just rotates with that spacer grid. Therefore, the following plastic limit analysis will assume that the bottom span of the fuel rod acts as a fixed-pinned beam as shown in configuration 1 (below). In addition, any secondary effects such as the spring load on dummy fuel pellets, internal pressure, slip force between spacer grid tabs and fuel rod, shear stress, fuel rod stiffening effect of the dummy fuel pellets, and high strain rate tensile properties of the fuel rod are conservatively omitted herein.

The limit analysis assumes that, at small strain levels, the fuel rod behaves as an elastic-perfectly plastic material. The plastic hinge location does not rotate until the

plastic moment is reached at which time unlimited rotation occurs when any small additional load is applied (i.e. a hinge is formed). The analysis proceeds as follows: First the w_1 uniform load for configuration 1 is determined which will produce a plastic hinge at the maximum moment location (fixed end). The fixed end with the plastic hinge now can only support additional shear load as shown in configuration 2 (below). The additional uniform load w_2 is determined which will produce a plastic hinge at the maximum moment location in configuration 2.

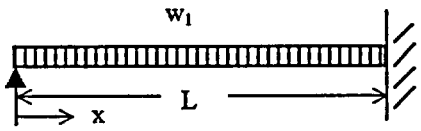

Configuration 1

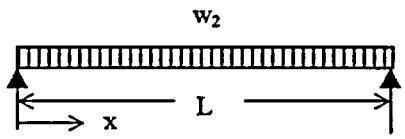

Configuration 2

L = Length of bottom span (distance between mid height of spacer grids).
L = 24.1395 in.
$M_p = K M_y$
$K = (16 r_o / 3 \pi)((r_o^3 - r_i^3)/(r_o^4 - r_i^4))$ Timoshenko[2.25], page 353, Fig. 222 (b)
$r_o = 0.187$ in.
$r_i = 0.163$ in.
K = 1.3563
$M_y = I S_y / r_o$
$I = (\pi / 4)(r_o^4 - r_i^4) = 0.000406$ in.^{4}
The fuel rod clad material is cold worked and stress relieved Zircaloy-4. The material tensile properties for the fuel clad material are given below.
S_y = 83,330 psi
Su = 109,370 psi
$M_y = 0.000406 (83330) / 0.187 = 180.920$ in-lbs
$M_p = 1.3563 (180.920) = 245.382$ in-lbs

For Configuration 1 , Roark[2.24], page 109, case 23.
$M_{max} = M_p = 0.125 w_1 L^2$
$w_1 = 8 M_p / L^2 = 8 (245.382) / (24.1395)^2 = 3.3688$ lbs/in
$M_{x1} = w_1 L (0.375 x - 0.5 x^2 / L)$
$M_{x1} = - 1.6844 x^2 + 30.4954 x$

For Configuration 2 , Roark[2.24], page 106, case 13.
$M_{x2} = 0.5 w_2 L (x - x^2 / L)$
$M_{x2} = - 0.5 w_2 x^2 + 12.0698 w_2 x$

The location of the final plastic hinge is near midspan but must be determined by setting the slope of the total moment equation to zero.

$M_x = M_{x1} + M_{x2}$

$M_x = = - 1.6844\ x^2 - 0.5\ w_2\ x^2 + 30.4954\ x + 12.0698\ w_2\ x$

$dMx/dx = - 3.3688\ x - w_2\ x + 30.4954 + 12.0698\ w_2$

$0 = (-3.3688 - w_2)x + (30.4954 + 12.0698\ w_2)$

$x = (30.4954 + 12.0698\ w_2) / (3.3688 + w_2)$

Since $M_x = M_p$ at the location of the plastic hinge, the value of x in terms of w_2 can be substituted into the equation for M_x and solved by iteration for w_2. Thus,
w_2 = 1.5399 lbs/in at x = 9.999 in. from the left support

Thus, the total uniform load when the fuel rod in the bottom span becomes a mechanism with two plastic hinges and a pinned support is:

w = w1 + w2 = 3.3688 + 1.5399 = 4.9087 lbs/in

The g-level is determined by dividing w by the dead weight (lbs/in) of the fuel rod.

$G's = w / w_{dw}$

$w_{dw} = \rho_p A_p + \rho_c A_c$

ρ_p = 10.4 g/cc = 0.3757 lbs/in.^{3} (dummy fuel pellet density)

ρ_c = 0.237 lbs/in^3 (for Zircaloy-4)

$A_p = \pi\ (0.15975)^2 = 0.08017$ in.^{2} (pellet cross section area)

$A_c = \pi\ ((0.187)^2 - (0.163)^2) = 0.02639$ in.^{2}

$w_{dw} = 0.3757(0.08017) + 0.237(0.02639) = 0.03637$ lbs/in

G's = 4.9087 / 0.03637 = 134.95 g

As a means to verify the acceleration load, the lower bound deflection is determined and compared to the drop test results. The maximum deflection can be approximated by setting the slope of the deflection equation to zero (Roark$^{2.24}$, Table III, cases 23 and 13).

$\delta_x = \delta_{x1} + \delta_{x2}$

$\delta_x = (w_1 / 48\ E\ I)(3\ L\ x^3 - 2\ x^4 - L^3\ x) - (w_2\ x / 24\ E\ I)(L^3 - 2\ L\ x^2 + x^3)$

$d\delta_x/dx = (w_1 / 48\ E\ I)(9\ L\ x^2 - 8\ x^3 - L^3) - (w_2 / 24\ E\ I)(L^3 - 2\ L\ x^2 + x^3)$

$- (w_2\ x / 24\ E\ I)(- 4\ L\ x + 3\ x^2) = 0$

Multiply by 48 EI gives

$d\delta_x/dx = w_1\ (9\ L\ x^2 - 8\ x^3 - L^3) - 2\ w_2\ (L^3 - 2\ L\ x^2 + x^3) - (2\ w_2\ x)(- 4\ L\ x + 3\ x^2) = 0$

by iteration, the solution is x = 11.038 in. from the left support.

Rearranging the equation for δ_x gives

$\delta_x = (1 / 48\ E\ I)\ [\ w_1\ (3\ L\ x^3 - 2\ x^4 - L^3\ x) - (2\ w_2\ x\ )(L^3 - 2\ L\ x^2 + x^3)]$

$E = 12.40 \times 10^6$ psi (for Zircaloy-4)

Substituting known values for the remaining variables, I, L, w_1, w_2, and x into the above equation gives:

$\delta_x = -1.22 - 1.34 = -2.56$ in.

However, the above displacement occurs when the maximum load is applied. When the load is removed a significant elastic springback will occur. The final or permanent set deflection can be conservatively (lower bound) estimated as:

$\delta_{x,set} = \delta_x - \delta_x / K = (-2.56) - (-2.56 / 1.3563) = -0.67$ in.

The drop test results indicated a maximum 2.25 in. permanent set (Section 2.7.1.4) occurred for some of the fuel rods in the bottom span. This indicates that some relatively small load, in addition to that calculated above, occurred to produce a larger permanent set as the plastic hinges rotated as a mechanism. The % elongation of the Zr-4 fuel rod tubing at ultimate strength is 19.49%. Since the difference between S_u = 109 ksi and S_y = 83 ksi is a relatively small fraction of the S_y value, it is reasonable to believe, significant strain hardening will not occur at the small strain levels necessary to produce this additional displacement. Therefore, the lateral G-level determined using an elastic-perfectly plastic material is appropriate and the design lateral G-level is

G_L = 135 g for WE-1 with BW17x17 fuel during slapdown drop

The Pathfinder Canister is stiffer than the BW17x17 fuel assembly, and the package weighs 8500 lb versus 9,090 lb with BW17x17 fuel. Dynamic effect of this stiffness and weight are evaluated using SCANS computer program to obtain acceleration values for the Pathfinder Canister design.

SCANS Studies

Parametric studies were performed using the Shipping Cask ANalysis System (SCANS)[2.37] computer program to investigate the performance of the WE-1 package with Pathfinder Canister during a 30-foot drop hypothetical accident event. The purpose of these studies was to:

- Evaluate the Pathfinder Canister stiffness and weight on dynamic performance of the package to obtain the change in acceleration from the WE-1 drop test package.
- Derive the worst case drop angle for the 30 foot slapdown drops.
- Obtain and compare the loading on internal hardware, such as strongback, HY-80 inner container and the attachment bolts.
- Benchmark of analysis against test data.

After the WE-1 drop tests, the package permanent deformations were measured. Based on the test results, the impact stiffnesses were developed. These impact stiffnesses were used in the SCANS analysis. Results of these analyses are summarized in following tables.

Summary of SCANS 30-foot Drop Analysis

	Drop Angle	Primary Impact Acceleration in g's	Secondary Impact Acceleration in g's
WE-1 BW17x17 Fuel	15	83.9	126.5
	30	97.4	123.7
	45	116	99.9
WE-1 Pathfinder Fuel	15	87.6	131.2
	30	101.5	127.8
	45	121.1	100.4

The result indicate that the primary impact angle of 15° is worst drop angle for both the WE-1 with BW17x17 or with Pathfinder Canister. The peak acceleration for the WE-1 with BW17x17 fuel is 126.5 g's. The calculation based on the WE-1 drop test in conjunction with fuel rod deformation calculated an acceleration of 135 g's. This indicates conservatism in the calculated acceleration. The peak acceleration for the WE-1 with Pathfinder Canister is 131.2 g's compared against 126.5 g's for the WE-1 with BW17x17 fuel. The acceleration went up by 3.7% due to stiffer Pathfinder Canister and lighter weight. A conservative 5% increase in acceleration will be used for the Pathfinder Canister analysis.

$G_L = 135 \times 1.05 = 142$ g's for WE-1 with pathfinder, slapdown drop

Strongback and HY-80 Inner Container Load Summary
15 Degree, 30 foot Drop - Loads due to Secondary Impact

Node No. (Location)	Axial Position - inch	WE-1 with BW17x17 Fuel			WE-1 with Pathfinder Canister		
		Maximum Axial Force (kips)	Maximum Shear Force (kips)	Maximum Moment (In-Kips)	Maximum Axial Force (kips)	Maximum Shear Force (kips)	Maximum Moment (In-Kips)
Primary	End	.0	.0	.0	.0	.0	.0
1	.0	-43.7	334.5	1249.4	-38.8	317.8	1176.3
2	18.9	-52.4	366.0	7657.4	-46.0	345.7	7228.8
3	37.8	-69.2	395.2	15455.3	-60.4	370.2	14575.1
4	56.7	-85.2	359.5	23182.6	-74.6	330.5	21764.2
5	75.6	-99.8	257.9	29508.3	-87.8	236.2	27565.4
6	94.5	-111.9	120.5	33252.8	-98.8	102.4	31066.5
7	113.4	-120.2	-97.6	33636.0	-106.5	-91.2	31488.1
8	132.3	-124.2	-280.0	30268.7	-110.2	-262.1	28297.8
9	151.2	-124.5	-466.6	23075.2	-110.3	-436.2	21587.4
10	170.1	-122.4	-629.8	12430.9	-111.6	-593.7	11672.1
11	189.0	-120.9	-706.8	-2362.3	-113.3	-670.0	-2374.8
Secondary	End	-125.1	-1152.4	-1923.1	-125.2	-1116.7	-1910.8

The strongback and HY-80 inner container loading were compared between two configurations. The peak axial force is approximately the same between the two configurations. The maximum shear force went down from 1152.4 kips to 1116.7 kips. The maximum bending moment was reduced from 33,636 in-kips to 31,488.1 in-kips for the WE-1 with Pathfinder Canister configuration. Even though the acceleration was increased by 3.7%, the loads were reduced due to lighter weight of WE-1 with Pathfinder. This comparison shows that the strongback, HY-80 inner container, and bolt connection qualification performed for the WE-1 with BW17x17 is also applicable for the WE-1 with Pathfinder. The WE-1 with stiffer Pathfinder canister does not impose any additional loading to the internal hardware. Only the changed hardware needs to be analyzed with the new acceleration loading.

Benchmarking Analysis against Drop Test: The WE-1 package 30-foot drop test was not instrumented. No measured drop accelerations are available for the WE-1. The shipping package 51032-1 (docket 71-6581)[2.35] was drop tested from a height of 30 ft. This package was instrumented during the drop tests. The outer container, shock mount and the strongback are the same for the 51032-1 and WE-1 packages. Due to the similarities between the two packages, and available drop acceleration data, a SCANS benchmark was performed for the 51032-1 package. For this benchmark, the impact stiffness of the outer container for the WE-1 and 51032-1 were kept the same. The drop test weight of the 51032-1 package with two fuel assembly was 7,486 lb. This weight was used in the SCANS analysis. The SCANS analysis result is summarized in the following table.

SCANS 30-foot Drop Analysis for 51032-1 Package

	Drop Angle	Primary Impact Acceleration in g's	Secondary Impact Acceleration in g's
51032-1 Container	0	146.7	146.7

For the 51032-1 package drop test, the accelerometer was mounted on the strongback. The measured peak acceleration for the 30 foot drop test was 125 g's (Appendix IV of docket 71-6581)[2.35]. The peak acceleration calculated by SCANS is 146.7 g's. The SCANS calculated number is conservative as compared to the test measured acceleration. One of the reasons SCANS acceleration is higher is due to the fact that, in an actual drop test, several pieces of the inside hardware deformed, the outer container buckled. The SCANS analysis does not account for the energy absorbed in internal hardware deformation, nor energy absorbed in buckling of the outer container. For this reason, the SCANS calculated number is conservative. This is an adequate benchmark of test versus analysis.

2.10.3.2 30-Foot Drop Accident - Axial Acceleration

The purpose of this section is to determine the design axial accelerations for the Pathfinder Canister. Three axial accelerations will be calculated, one which is acting with the worse case lateral acceleration and the other two for a 30-foot end-drop (container is oriented with the axial length in the vertical direction).

For the WE-1 package no measured end drop accelerations are available. The 30 foot end drop test was performed on 51032-1 package. The drop test was instrumented. For the 30 foot end drop, the peak acceleration of the strongback was 110 g's (Appendix IV, Docket 71-6581)[2.35]. The outer container and the strongback for the 51032-1 package are the same as that for WE-1 package. For the WE-1 package, as a conservative design, no benefit will be taken for the energy absorbed in outer container nor in the strongback deformation for the 30 foot end drops. Wood spacers are provided to absorb the Pathfinder Canister drop energy.

Wood is an excellent energy absorber. Wood crush strength is function of type of wood, wood density, wood moisture content and the grain orientation. Eastern white pine and white oak wood is selected for the Pathfinder Canister end spacers. This selection is based on easily or commercially available lumber. The grain is oriented in the design to get maximum benefit of the wood properties to absorb energy. The moisture content is selected as S-dry, which is <12% moisture content. This S-dry wood is widely available for construction industry. The thickness of the pine spacer was based on the available space inside the inner container. There was plenty of space, so that the thickness of oak spacer is kept generously large.

Per Mark's Handbook[2.7], tenth edition, page 6-113, the wood crush strength tolerance is of ±18% parallel to grain and ±14% perpendicular to grain. The analysis uses ±18% tolerance for the wood crush strength parallel to grain. As a conservative design, the tolerance of ±15% is kept for crush perpendicular to grain, since it envelop the ±14% specified in the Mark's Handbook. The wood properties used, in addition to Marks Handbook, 10th Edition, are also from Wood Handbook, Forest Products Laboratory, 1999 – Wood as an Engineering Material, General Technical Report, FPL-GTR-113, Madison, WI; U.S. Department of Agriculture, Forest Service, Forest Products Laboratory. These properties have been used as engineering material for decades.

Wood is used as a second level of energy absorber and the analysis does not benefit of the energy absorbed in the outer container and the strongback, this will provide adequate conservatism in the acceleration values used for the structural qualification.

Case 1

The 142 g lateral acceleration calculated in Section 2.10.3.1 occurred during the second hit or slapdown. The angle of the container at the time of the slapdown is conservatively taken as the same as the initial drop angle (i.e., 15 degrees, Section 2.7.1.4) for the initial hit. The axial acceleration (G_A) can be approximated from the sketch below as:

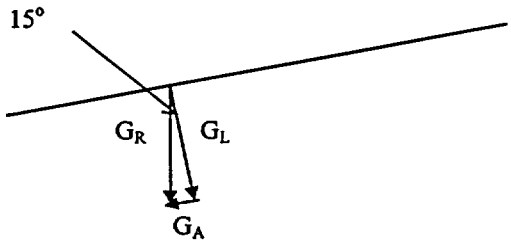

$G_A = G_L \tan(15) = 142 \tan(15) = 38$ g's

$G_R = G_L / \cos(15) = 142 / \cos(15) = 147$ g's use 147 g's for design

Case 2

For an end drop impacting on the bolted connection end of the canister, a worse case is assumed whereby all the potential energy (P.E.) of the fuel and fuel canister is absorbed by the crushing of a 2" thick pine wood. Pine wood grains oriented parallel to the axis of the impacting container.

P.E. = W h

W = 782 lbs Pathfinder canister with fuel

h = 30 ft. = 360 in.

P.E. = 782 (360) = 281,520 in-lbs

P.E. = Work = $F_{max}\ \delta$

$F_{max} = \sigma_{crush}\ A$

σ_{crush} = 4,800 psi ± 18% Mark's Handbook[2.7], pgs. 6-113 and 6-115, for Eastern White Pine. The ± 18% is a range for wood crush strength parallel to grain.

$A = (\pi/4)\ (13.5)^2 = 143.14$ in.^{2} blind flange surface area

$F_{max} = 1.18(4,800)(143.14) = 810,745$ lbs

$F_{min} = 0.82\ (4,800)\ (143.14) = 563,400$

δ = P.E. / F_{min} = 281,520 / 563,400 = 0.5 in.

$F_{max} = m\ G_A$

$G_A = F_{max} / m = 810,745 / (782 / 386.4) = 400,063$ in/in/sec = 1,037 g's

Case 3

For an end drop impacting on the welded end cap of the canister, a worse case is assumed whereby all the potential energy (P.E.) of the fuel and fuel canister must be absorbed by the crushing of a 8" thick oak wood with grains oriented perpendicular to the axis of the impacting container. P.E. = Work = $F_{max}\ \delta$

$F_{max} = \sigma_{crush}\ A$

σ_{crush} = 1,070 psi ± 15% Mark's Handbook[2.7], pgs. 6-113 and 6-115, for White Oak. The ± 14% is a range for wood crush strength perpendicular to grain, ± 15% is conservatively used.

$A = (\pi/4)\ (8.625)^2 = 58.43$ in.^{2} bottom plate surface area

$F_{max} = 1.15(1,070)\ (58.43) = 71,898$ lbs

$F_{max} = 0.85(1,070)\ (58.43) = 53,142$ lbs

δ = P.E. / F_{min} = 281,520 / 53,142 = 5.3 in.

$F_{max} = m\ G_A$

$G_A = F_{max} / m = 71,898 / (782 / 386.4) = 35,526$ in/in/sec = 92 g's

Note, the worse case assumption used above assumes the 4 bolts attaching the clamp (nearest the bolted closure) to the WE-1 inner container are sheared off. The load required to do this is calculated as follow:

$\tau_u = 0.75\ S_u = 0.75\ (75,000) = 56,250$ psi approximate for steel

$\tau_u = 0.75\ (75,000) = 56,250$ psi Section 2.3

$A_s = A_t = 0.1419$ in.^{2} Machinery's Handbook[2.15], pg. 1,266 for 1/2"-13 UNC

$F_{shear} = 4(0.1419)(56,250) = 31,928$ lbs

From Section 2.10.2.1.2.1, the total weight of the canister and fuel is approximately 782 lbs. Thus, the acceleration required to produce the F_{shear} load is:

$a = 31,928/782 = 40.8$ g's

30-Foot Drop Accident Accelerations Summary:

30-Foot Drop		Impact Acceleration g's	Direction	
			Lateral – g's	Axial g's
Slapdown Drop	Case 1	147	142	38
CG Over Corner Drop		Enveloped by other drops		
End Drop – Closure End	Case 2	1,037	0	1,037
End Drop – Bottom Plate End	Case 3	92	0	92

2.10.4 Stress Summary

Results show that the Pathfinder Fuel shipping canister stresses are below ASME Code and Regulatory Guide 7.6 allowables. The canister also has adequate margin to preclude buckling during normal and hypothetical accident conditions. As demonstrated by analysis performed herein, the Pathfinder Fuel shipping canister meets the structural design criteria of 10CFR71.

Reduced External Pressure Load Condition (21.5 psid) – Stress Summary

Component	Location	Stress Intensity - psi			
		Membrane	Membrane Allowable	Membrane + Bending	Membrane + Bending Allowable
Cylinder	Mid Section	293	16,700	293	25,050
	Flat Head Juncture	378	16,700	1,004	25,050
	Weld Neck Flange Juncture	Bounded by flat head juncture stresses			
Flat Head	Cylinder Vessel Juncture	Bounded by cylinder vessel-flat head juncture streses			
	Center	38	16,700	408	25,050

The weld neck flange and blind flange are both standard class 150 lb components with pressure-temperature ratings of 212 psid at 150 °F which is greater than the Normal conditions of 21.5 psid at 150 °F.

50-Foot Immersion Condition (-21.7 psid)

Stresses are multiplied by following ratio to the reduced external pressure load case:

Cylinder and bottom flat plate: 1.01
Weld neck and blind flange: <1.00

The biggest contribution to the flange stress is due to compression of seals. For internal pressure case, the compression of seal and pressure load add to produce total stress. For 50-foot immersion condition, stress due to seal compression and pressure load are opposite. For this reason, the flange stresses due to 50-foot immersion will be lower than the reduced external pressure case.

50-foot Immersion Load Case Buckling Stability Summary

COMPONENT	CRITICAL LOAD	ACTUAL LOAD
Vessel Cylinder	431 psig	21.7 psig
Vessel Flat Head	29,910 lb/in	24 lb/in
Blind Flange	Adequate by comparison to flat head	

Hypothetical Accident Condition Stress summary

Component	Stress Intensity - psi		
	Actual	Allowable	Margin of Safety
30-Foot Slapdown Drop			
Cylinder – Primary*	36,451	40,080	0.10
Cylinder – Secondary*	346,141	1,416,000	3.09
Saddle Support	7,612	35,000	3.60
30-Foot end Drop			
End Plate	6,944	40,080	4.77
Cylinder	26,298	40,080	0.52
Fire			
Cylinder - Secondary	81,054	1,416,000	Large

Note: * Cylinder stress bounds end plate, weld neck flange

Closure Bolts

Preload 45 ± 5 ft-lbs less thermal expansion effects
Minimum preload of 3,200 lbs at 70°F
Minimum preload of 3,182 lb at 150°F
Minimum preload 3,182 lbs > 2,604 lb to compress seals

Working load (preload + working-mechanical + thermal load)
Normal Condition of Transport 5,796 lbs
Hypothetical Accident Condition 5,970 lbs, 5,764 lbs

Pathfinder Canister Closure Bolt Stress Summary

Component	Stress - psi		
	Actual	Allowable	Margin of Safety
Normal condition of Transport	17,353	18,600	0.007
Hypothetical Accident			
30-foot slapdown drop			
Tensile Stress	17,874	27,900	0.56
Shear Stress	2,656	16,740	5.30
Combined	0.44	1.	1.27
50-foot Immersion	17,257	18,600	0.08
Fire	15,458	17,400	0.13
Fatigue life of the bolt	> 4,000 shipment		
Minimum thread engagement	$L_{e,\ available}$ = 0.948 > 0.551		0.72

2.10.5 References

2.1 Code of Federal Regulation 10CFR71 "Packaging and Transportation of Radioactive Material," 1996.

2.2 American Society of Mechanical Engineers Boiler and Pressure Vessel code Sections II and III, 1995 Edition and through 1996 Addenda.

2.3 U.S. Nuclear Regulatory Guide 7.6, "Design Criteria for the Structural Analysis of Shipping Cask Containment Vessel," Revision 1, March 1978.

2.4 U.S. Nuclear Regulatory Guide 7.8, "Load Combination for the Structural Analysis of Shipping Casks for Radioactive Material," Revision 1, March 1989

2.5 NUREG/CR-3854, "Fabrication Criteria for Shipping Containers," March 1985.

2.6 NUREG/CR-3019, "Recommended Welding Criteria for Use in the Fabrication of Shipping Containers for Radioactive Materials," March 1985.

2.7 Aavallone, A., et al, "Marks' Standard Handbook for Mechanical Engineers," Tenth Edition, McGraw-Hill Book Company, 1996.

2.8 Bickford, J. H. and Looran M. E., "Good Bolting Practices," EPRI Report EPRI-NP-5067, Volume 1, 1987.

2.9 to 2.11 Not used

2.12 ASTM Specification A 312/A 312M-91b, "Standard Specification for Seamless and Welded Austenitic Stainless Steel Pipes," 1991 and ASTM Specification A 530/A530M-91a, "Standard Specification for General Requirements for Specialized Carbon and Alloy Steel Pipe," 1991.

2.13 Roark and Young, "Formulas for Stress and Strain," 5th Edition, McGraw-Hill Book Company, 1975.

2.14 American National Standard ANSI B16.5 -1981, "Pipe Flanges and Flanged Fittings."

2.15 Oberg, E. et al, "Machinery's Handbook," 22nd Edition, Industrial Press Inc., 1985.

2.16 to 2.23 Not Used

2.24 Roark, Raymond J., Formulas for Stress and Strain, Fourth Edition, McGraw-Hill Book Company, New York, 1965.

2.25 Timoshenko, S., Strength of Materials, Part II, Advanced Theory and Problems, Third Edition, D. Van Nostrand Company, New York, 1958.

2.26 and 2.27 Not Used

2.28 ANSYS Finite Element Computer Code, Version 5.6, ANSYS Inc., 2000.

2.29 ASM Metals Handbook, Volume 1, Tenth Edition, Properties and Selection: Irons, Steel, and High-Performance Alloys, ASM International, 1990.

2.30. NUREG/CR-6007, Stress Analysis of Closure Bolts for Shipping Casks, 1993.

2.31 Not Used

2.32 Garlock Helicoflex Metallic O-Ring Technical Bulletin.

2.33 Den Hartog, J.P., "Temperature Stresses In Flat Rectangular Plates and In Thin Cylindrical Tubes", Journal of the Franklin Institute, Volume 222, 1936.

2.34 ASM Metals Handbook, Vol. 2, Ninth Edition.

2.35 Safety Analysis Report for Packaging , "Consolidated License Application for Siemens Power Corporation Model 51032-1 Shipping Container," Docket 71-6581, Rev 6B, July 2000.

2.36 Safety Analysis Report, "Application for use of 51032-2 Shipping Container for Transport of Radioactive Materials," Docket 71-9252, July 1993.

2.37 NUREG/CR-4554, "SCANS (Shipping Cask ANalysis System) A Microcomputer Based Analysis System for Shipping Cask Design Review," Gerhard, M., Trummer, D., Johnson, G., Mok, G. Version 2a.

The Pathfinder Canister is surrounded by Zircar thermal insulation and is secured inside the rectangular inner container with five integral clamp frames. Wood blocks surround the both ends of the Pathfinder Canister. The wood used is flame retardant. The wood is an extremely effective thermal insulator.

3.2 MATERIAL PROPERTIES

The WE-1 inner container is constructed primarily of HY-80 armor plate, Series 300 stainless steel bolts, and Zircar ASB-2300 ceramic fiber insulation. The void spaces within the inner container are filled with air at atmospheric pressure. The thermal properties of the principal materials used in the thermal evaluations are presented in Table 3.2-1, , Table 3.2-3, Table 3.2-4, Table 2.3-1 and Table 2.3-2. Where necessary, the properties are presented as functions of temperature. Note that only properties for materials that constitute a significant heat transfer path are defined. The thermal properties at –20 °F and –40 °F are extrapolated values from ASME Code for HY-80, 304 SS and Alloy 600. Review of Metals Handbook indicate that the thermal properties follow smooth curve in the temperature range of –40 °F to 1500 °F and extrapolation at –20 °F and –40 °F is justified.

Table 3.2-1 Material Properties for Principal Structural/Thermal Components

Material	Temperature, °F	Thermal Conductivity, Btu/hr-in-°F	Specific Heat, Btu/lbm-°F	Density, lbm/in^3	Notes
HY-80 Armor Plating	-40	1.73	0.10	0.283	①
	70	1.83	0.11		
	250	1.94	0.12		
	450	1.93	0.13		
	650	1.84	0.14		
	850	1.74	0.15		
	1,050	1.62	0.17		
	1,250	1.45	0.22		
	1,350	1.31	0.23		
	1,500	1.27	0.15		
Type 304 Stainless Steel	-40	0.66	0.109	0.289	②
	-20	0.692	0.11		
	0	0.70	0.111		
	70	0.717	0.114		
	100	0.725	0.115		
	200	0.775	0.124		
	400	0.867	0.130		
	600	0.942	0.134		
	800	1.017	0.140		
	1,500	1.275	0.158		
Zircar ASB-2300 8 pcf Ceramic Fiber Insulation	0	0.0024	0.28	0.0046	③
	500	0.0024			
	1,000	0.0053			
	1,500	0.0087			
	2,000	0.0140			
Alloy 600	-40	0.68	0.107	0.289	②
	70	0.717	0.112		
	400	0.842	0.123		
	800	1.008	0.133		
	1500	1.333	0.154		

Notes:

① Thermal Conductivity and Specific Heat are taken from Section II, Part D, Table TCD, of the ASME Code. Density is taken from Section II, Part D, Table NF-2, of the ASME Code. Material properties for 3½Ni-1¾Cr-½Mo-V are used.

② Thermal Conductivity and Specific Heat are taken from Section II, Part D, Table TCD, of the ASME Code. Density is taken from Section II, Part D, Table NF-2, of the ASME Code. Material properties for 18Cr-8Ni are used for 304 stainless steel and for 72Ni-15Cr-8Fe are used for Alloy 600. The -20°F and –40°F value is an extrapolation of ASME Code Data.

③ Zircar Products, Inc. Product Data Sheet, *Alumina-Silica Blanket Type ASM-2300 and ASB-2600,* Florida, NY. Thermal conductivity values reflect the ceramic fiber insulation in an uncompressed condition for NCT. HAC thermal analyses assume the ceramic fiber material is conservatively compressed to 2/3 of its original thickness resulting in thermal conductivities that are 150% of NCT values.

Table 3.2-2 Material Properties for Air

Temperature, °F	Thermal Conductivity, Btu/hr-in-°F	Specific Heat, Btu/lbm-°F	Density, g/cc	Viscosity, in^2/sec	Prandtl Number	Notes
-40	0.0011	0.242	Use ideal gas law	- - -	- - -	
-20	0.0011			- - -	- - -	
70	0.0013			0.0261	0.708	
100	0.0013			- - -	- - -	
200	0.0015			0.0348	0.704	
300	0.0017			0.0446	0.700	①②
400	0.0018			0.0588	0.680	③④
500	0.0020			- - -	- - -	
600	0.0021			0.0796	0.680	
700	0.0023			- - -	- - -	
800	0.0024			0.1027	0.684	
900	0.0026			- - -	- - -	

Notes:

① Y.S. Touloukian, *Specific Heat – Nonmetallic Liquids and Gases*, Thermophysical Properties Research Center Data Series, Volume 6, Purdue University, 1970.

② Y.S. Touloukian, *Thermal Conductivity – Nonmetallic Liquids and Gases*, Thermophysical Properties Research Center Data Series, Volume 3, Purdue University, 1970.

③ E.R.G. Eckert, R. M. Drake, *Analysis of Heat Mass Transfer*, McGraw-Hill, New York, 1972.

④ Rohsenow, Hartnett, and Ganic, *Handbook of Heat Transfer Fundamentals*, 2nd Edition, McGraw-Hill Publishers, 1973.

Table 3.2-3 Radiative Heat Transfer Material Properties, Surface Emittance

Component	Material	Surface Emittance, ε	Solar Absorptivity, α	Notes
Outer Container Exterior Surface	Paint	0.80	0.25	①
Inner Container Surfaces	HY-80	0.50	0.50	②

Notes:

① For the HAC fire event, the paint burns away and exposes the underlying steel surfaces. This surface is assumed to char to the minimum emissivity of 0.80 is required for the HAC fire in accordance with the requirement of 10 CFR §71.73(c)(4). Therefore, a value of 0.80 provides a conservative estimate for NCT conditions and meets the 10 CFR §71.73(c)(4) requirement for the HAC fire event.

② Value taken from F. F. Gubareff, J. E. Janssen, and R. H. Torborg, *Thermal Radiation Properties Survey*, Honeywell Research Center, Minneapolis, Minnesota, 1960. Emissivity increased to 0.8 for the HAC fire in accordance with 10 CFR §71.73(c)(4). Note that absorptivity is equal to emissivity for systems in thermal equilibrium and are approximately equal for nonequilibrium systems.

Table 3.2-4 Temperature-Difference (ΔT) Based Heat Transfer Convection Coefficients① for the HAC Post-Fire Condition

ΔT, °F	Vertical Surface	Horizontal Surface	
		Heated Side Up	Heated Side Down
50	0.0048	0.0058	0.0016
100	0.0058	0.0070	0.0018
150	0.0064	0.0078	0.0020
200	0.0068	0.0083	0.0021
250	0.0072	0.0087	0.0022
300	0.0074	0.0090	0.0023
500	0.0078	0.0096	0.0025
700	0.0083	0.0100	0.0026
1,375	0.0086	0.0103	0.0028

Notes:

① All convection coefficients are Btu/hr-in^2-°F, and calculated per Appendix 3-1.2, *Post-Fire Natural Convection Coefficient Calculation.*

Pathfinder Canister: The materials of construction of the Pathfinder Canister are standard materials with well-documented thermal characteristics. The Pathfinder Canister is entirely of type 304 stainless steel construction except for the Alloy 600 O-rings. These materials are not subject to ductile-to-brittle transition above –40° F, therefore it is safe from brittle fracture. Contents of the Pathfinder Canister will not contain sufficient liquids to cause the canister to expand due to freezing. The temperature limit for the fuel is the melting temperature of the stainless steel. Conservatively, 1,200° F Pathfinder fuel assembly temperature limits is established. The Alloy 600 O'ring has design temperature range of cryogenic to 1,000° F.

3.3 TECHNICAL SPECIFICATION OF COMPONENTS

None of the materials used in the construction of WE-1 package, such as HY-80 armor plating, Series 300 stainless steels bolts, and ASB-2300 ceramic fiber insulation are sensitive to temperatures within the range of -40 °F to 1,475 °F that spans the NCT and HAC environment. HY-80 steel armor plating and Series 300 bolts have a melting points

above 2,550 °F, and maximum service temperatures of 800 °F[2]. Similarly, the ASB-2300 ceramic fiber insulation has a maximum operating temperature of 2,300 °F[3]. Wooden wedges are used as dunnage in the WE-1 package to restrain the inner container within the outer container. Before being consumed in the HAC fire, the wood dunnage would insulate portions of the inner container from exposure to the flames. The HAC transient thermal analyses presented herein ignore the presence of the wood dunnage thereby conservatively neglecting its insulating effect.

The temperature limit for the BW 17x17 fuel assembly's rods is 1,200 °F, based on the pressure calculation provided in Section 3.5.4, *Maximum Internal Pressure*. The temperature limit for the Pathfinder fuel is the melting temperature of the stainless steel. Conservatively, 1,200° F Pathfinder fuel assembly temperature limits is established.

3.4 NORMAL CONDITIONS OF TRANSPORT

This section presents the results of thermal analysis of the WE-1 package for the normal conditions of transport (NCT) specified in 10 CFR §71.71.

3.4.1 Ambient Temperatures and Heat Input

Per 10 CFR §71.71(c)(1), the maximum environmental temperature is 100 °F, and per 10 CFR §71.71(c)(2), the minimum environmental temperature is -40°F.

Given the negligible decay heat of the fuel assembly, the thermal loads on the WE-1 package come solely from the environment in the form of solar radiation for NCT as prescribed by 10 CFR §71.71(c)(1). As such, the solar heat input into the package is 122.9 Btu/hr-ft^2 (400 gcal/cm^2 per 12 hours) for the cylindrical exterior surface of the WE-1 package.

3.4.2 Maximum Temperatures

For ambient conditions of 100 °F and maximum insolation, the peak temperature of the WE-1 package may be calculated using a heat balance equation for a unit area section of a horizontally oriented cylinder experiencing laminar natural convection[4]. The heat balance equation is:

---

[2] American Society of Mechanical Engineers (ASME) Boiler and Pressure Vessel Code, Section II, *Materials*, Part D, *Properties*, 1992 Edition, 1994 Addenda, United Engineering Center, 345 East 47th Street, New York, NY.

[3] Zircar Products, Inc. Product Data Sheet, *Alumina-Silica Blanket Type ASM-2300 and ASB-2600,* Florida, NY.

[4] Frank Kreith, *Principles of Heat Transfer*, 3rd Edition, Intext Educational Publishers, New York, 1973, Equation 7-27, p400.

$$\ddot{Q}_{insolation} = \ddot{Q}_{radiation} + \dot{Q}_{convection}$$

$$\ddot{Q}_{insolation} = (122.9\ \text{Btu/hr - ft}^2)\alpha = 30.73\ \text{Btu/hr - ft}^2$$

$$\ddot{Q}_{radiation} = \sigma\varepsilon(T^4_{container} - T^4_{ambient}) = (1.37(10)^{-9}\ \text{Btu/hr - ft}^2 - {}^\circ\text{R}^4)(T^4_{container} - T^4_{ambient})$$

$$\ddot{Q}_{convection} = \frac{0.27}{D^{1/4}}(T_{container} - T_{ambient})^{5/4} = (0.196\ \text{Btu/hr - ft}^2 - {}^\circ\text{F}^{4/5})(T_{container} - T_{ambient})^{5/4}$$

where the solar absorptivity of the painted outer container exterior surface is $\alpha = 0.25$, the Stefan-Boltzman constant is $\sigma = 1.714(10)^{-9}$ Btu/hr-ft^2-°R^4, the emmisivity of the painted outer container is $\varepsilon = 0.80$, the outer package diameter D = 3.583 feet (43.0 inches), and the ambient temperature is $T_{ambient}$ = 100 °F.

Solving the heat balance equation results in a maximum temperature for the outer container of 122 °F. Conservatively, the entire package and payload is assumed to reach this temperature.

Given negligible decay heat, the maximum accessible surface temperature of the WE-1 package in the shade is the maximum environment temperature of 100 °F, which is less than the 122 °F limit established in 10 CFR §71.43(g) for a non-exclusive use shipment.

3.4.3 Minimum Temperatures

The minimum environmental temperature that the WE-1 package will be subjected to is -40 °F, per 10 CFR §71.71(c)(2). Given the negligible decay heat load, the minimum temperature of the WE-1 package is -40 °F.

3.4.4 Maximum Internal Pressure

The BW 17x17 fuel rods are purged with helium gas to a pressure of 315 psig. Hence, the maximum normal operating pressure (MNOP) for BW 17x17 fuel is 315 psig. Using a maximum normal operating temperature (MNOT) of 150°F the maximum internal pressure for Pathfinder Canister would be 17 psia, well within the capabilities of the containment. Section 2.10.1.1 provides calculaion for Pathfinder Canister MNOP. A conservative 25 psia is used as a design pressure under normal condition.

3.4.5 Maximum Thermal Stress

The design of the Pathfinder Canister precludes thermal stresses. Because of construction using similar materials and appropriate clearances, differential expansion of metals is not a problem for the canister and blind flange. Due to differential thermal expansion, the Pathfinder Canister closure bolts will experience 18 lb load per bolt during MNOT of 150° F and 66 lb load per bolt during –40° F condition.

tests[6]. Due to the much higher conductive properties of the clamp frame, maximum temperatures always occur at its inside surface.

The material properties used in this analysis are included in Section 3.2, *Material Properties*. The ANSYS® input files are included in Appendix 3-2, *ANSYS® Input Files.*

The initial temperature distribution in the package prior to the HAC fire event is a uniform 122 °F per the NCT calculations.

3.5.2 Package Conditions and Environment

The hypothetical accident condition (HAC) fire event is specified per 10 CFR §71.73(c)(4) as a half-hour, 1,475 °F fire with forced convection ($h_{convection}$ = 2.5 Btu/hr-ft^2-°F per Appendix 3-1.1, *Fire Forced Convection Convection Calculation*) and an emissivity of 0.9. The environmental conditions preceding and succeeding the fire consists of an ambient temperature of 100 °F and insolation per the NCT thermal analyses.

3.5.3 Package Temperatures

The temperature response of the peak fuel rod temperature over the course of the HAC fire scenario is illustrated in Figure 3.5-2. The temperature reaches its maximum point of 792 °F at 45 minutes after the end of the fire. This peak temperature occurs on the inside surface of the support clamp, as illustrated in Figure 3.5-3.

Subsequent to the fire and post-fire cooldown period, the surface of the inner container will absorb more insolation than in the pre-fire condition, due to charring of the surface of the inner container, resulting in a higher emmisivity. As a result, the WE-1 package will have a higher post-fire steady state temperature. Using the same energy balance equation used for the NCT calculations for the outer container for an absorptivity of 0.8, the post-fire steady-state temperature is 159 °F. Conservatively, the entire package and payload is assumed to reach this temperature for post-fire, steady state conditions.

3.5.4 Maximum Internal Pressure

The maximum internal pressure of the fuel rod 1200° F was calculated using the standard gas law. The internal gas volume of the rod was corrected for the differences in thermal expansion of the U02 fuel pellets and the stainless steel plenum springs with respect to the zirconium alloy cladding. Because of the higher expansion rate of the fuel

---

[6] Actual thickness measurements of the ceramic fiber insulating material showed almost no permanent deformation; however, the HAC fire calculations conservatively assume a 3-to-2 reduction in thickness. Further, although the inner container plates separated slightly at one end (i.e., ≤1/2 inch), the three inch thickness of the ceramic fiber insulation ensures direct flame impingement inside the inner container cannot occur. See Section 2.7, *Hypothetical Accident Conditions*, in Chapter 2 for more discussion regarding the results of free drop and puncture testing.

pellets with respect to the cladding, the internal gas volume decreases slightly as temperature increases.

Pathfinder Canister: The maximum internal pressure of the Pathfinder Canister at 800° F was calculated using the standard gas law. The maximum internal pressure for the Pathfinder Canister will be 35 psia and with all fuel rod rupture will be 51.6 psia. Section 2.10.1.1 provides calculation for internal pressure. The 51.6 psia is used as a design pressure under HAC.

3.5.5 Maximum Thermal Stresses

Pathfinder Canister: The thermal stresses due to temperature gradient are calculated in Section 2.10.2.7. The resulting stresses due to hypothetical fire accident are 81 ksi and are well below secondary stress allowable of 1,416 ksi. Pathfinder Canister closure bolt preload will be reduced by 578 lb due to differential thermal expansion between bolt and the canister flange.

3.5.6 Evaluation of Package Performance for Hypothetical Accident Thermal Conditions

Pathfinder Canister: The temperature of the fuel and O'ring seal will not exceed 800° F. At this temperature the canister, the Pathfinder fuel and the O'ring seal have large safety margin against regulatory and design limits. The Pathfinder Canister will maintain containment for all hypothetical fire accident conditions of transport.

ASSUMPTIONS:

1. 0.022 in. "thin-wall" cladding represents the limiting case for all FCF fuel rod designs.

2. Alloy M5 (Zr-Nbl%) cladding in the fully recrystallized condition represents the limiting case for all FCF cladding materials.

3. The maximum as-built fuel rod pre-pressure is 315 psi.

CHAPTER 4: CONTAINMENT

4.1 CONTAINMENT BOUNDARY

The WE-1 container is limited to use for transporting slightly irradiated, low enriched uranium, nuclear reactor core assemblies. The radioactive material, bound in sintered pellets having very limited solubility, has minimal propensity to suspend in air. These pellets are further sealed into cladding, to form the fuel rod portion of each assembly. The containment boundary for the WE-1 container with BW 17x17 fuel is the fuel rod cladding. Design and fabrication details for this cladding are given in Section 1.2.3 of this application.

4.1.1 PATHFINDER CANISTER

4.1.1.1 Containment Boundary for Pathfinder Canister

The Pathfinder Canister is used for transporting unirradiated Pathfinder fuel assemblies. The radioactive material, bound in sintered pellets, is in solid form and has minimal propensity to suspend in air. The containment boundary for the Pathfinder fuel is the Pathfinder Canister. The Pathfinder Canister is 8" schedule 40 S stainless steel pipe, welded end plate at bottom, weld neck flange at top and bolted blind flange with double metallic seals (o-rings). Design and fabrication details for the Pathfinder Canister are given in Section 2.1.1.

4.1.2 PATHFINDER CANISTER PENETRATIONS

The containment boundary is closed by a bolted blind flange, which is sealed by metallic o-rings. The annulus between the o-rings has a test port. The test port is sealed with a plug and o-ring.

4.1.3 PATHFINDER CANISTER SEALS AND WELDS

Two concentric O-ring metallic seal gaskets are located in grooves machined in the blind flange. The two seals are part of the containment boundary.

The range of seal gaskets operational temperatures presented in Chapter 3 is: -40 °F to 800 °F. The metallic seals are rated for temperatures from cryogenic to 1000 °F and working pressures from vacuum to 100 psi. The seals have excellent resistance to corrosion and radiation.

The seals have a non-compressed cross sectional diameter of 0.125" (0.097"/0.101" compressed) and a wall thickness of 0.010". The inner ring seal

has a outer diameter of 9.25" while the outer ring seal has a diameter of 10.25". The grove width is 0.160" and grove depth 0.097"/0.101" for both seals.

The Pathfinder Canister will be tested leak tight (i.e., 1×10^{-7} cm^3/s, air, or better) during fabrication. All Pathfinder canister welds are full penetration welds in accordance with ASME Code, Division 1, Section III, Subsection NB. Compliance with ASME requirements is ensured by appropriate nondestructive examination methods. These methods verify weld structural and sealing integrity.

Prior to shipment of a loaded Pathfinder Canister, the closure lid and cover plate inter-seals annulus are pressurized to 15 psig of air for 10 minutes to verify sealing integrity.

4.1.4 CLOSURE OF PATHFINDER CANISTER

Eight (8) 3/4-10UNRC-2A closure lid studs provide canister closure. These studs are made of ASTM-A193-B8M Class 2 bolting material. The bolt preload reduces any gap opening (between the blind flange and upper ring flange) during regulatory conditions.

4.2 REQUIREMENTS FOR NORMAL CONDITIONS OF TRANSPORT

BW 17x17 Fuel

The nature of the contained radioactive material and the structural integrity of the fuel rod cladding and package are such that there will be no release of radioactivity under normal conditions of transport.

10CFR71.43(e) requires that a packaging valve or other device, the failure of which would allow radioactive contents to escape, must be protected against unauthorized operation and, except for a pressure relief device must be provided with an enclosure to retain any leakage. Helium leak testing of the BW 17x17 fuel rods is performed prior to shipment to demonstrate leak tight containment integrity (i.e., 1×10^{-7} cm^3/s, air, or better).

Pathfinder Canister

Chapter 2 demonstrates structural integrity of the Pathfinder Canister. The containment seal material was selected for its performance in the range of temperature including normal and hypothetical accident conditions. This canister meets 10CFR71 containment requirements under normal conditions.

4.2.1 CONTAINMENT OF RADIOACTIVE MATERIALS FOR PATHFINDER CANISTER FOR NORMAL CONDITIONS OF TRANSPORT

The Pathfinder Canister meets 10CFR71.51 containment requirements under normal conditions. The limit for the release of radioactive gases imposed by this regulation is $(1x10^{-6}) \times A_2$ per hour.

A_2 values and specific activity for 10 wt.% UO_2 are given in 10CFR71, Appendix A-1 and Appendix A-3 as A_2 = 0.027 Ci and S_A $4.8x10^{-6}$ Ci/g respectively.

The $(1x10^{-6}) \times A_2$ limit determines the maximum permissible release rate for normal transport conditions.

$R_N = (1x10^{-6}) \times 0.027$
$= 2.7x10^{-8}$ Ci/Hr
$= 7.5x10^{-12}$ Ci/s

The Pathfinder fuel rods are unirradiated (e.g. fresh) and as such do not contain any radioactive gases or byproducts. Thus using the method for dispersible radioactive solids for the dose rate is appropriate.

As stated in section 4.1.1 of NUREG/CR-6487 dispersible solid materials will tend to fracture and crumble due to handling, vibration or accident conditions. These conditions will tend to cause the radioactive solid material inside the containment vessel to produce a powder aerosol. The source term concentration (Ci/cm^3) can be expressed as the product of the aerosol mass density (g/cm^3) and the specific activity of the dispersible solid (Ci/g). A reasonable bounding value for the mass density of a powder aerosol is ρ = 9x10-6 g/cm^3 (page 17 of NUREG/CR-6487).

$C_N = \rho \times S_A$
$= (9x10^{-6}) \times (4.8x10^{-6})$
$= 4.32 \times 10^{-11}$ Ci/cm^3

Equation 3 in ANSI N14.5-1997 calculates the maximum permissible leakage rate for normal transport conditions.

$L_N = R_N/C_N$
$= (7.5x10^{-12})/(4.32x10^{-11})$
$= 0.17375$ cm^3/s

4.2.2 PRESSURIZATION OF PATHFINDER CANISTER

A maximum internal pressure of 25 psia (1.7 atm) and minimum external pressure per 10CFR71 (3.5 psia [.24 atm]) at 150 °F is considered during normal conditions.

The canister seals are leak-tested by pressure drop test of the inter-seals annulus at room temperature and with an internal air pressure of 15 psig. The leakage rate must be less than 1×10^{-3} cm^3/s for the canister seals.

The capillary diameter required to leak at a rate of LR $= 1 \times 10^{-3}$ std air cm^3/s at test conditions is found by using the leakage correlations provided in ANSI N14.5-1997.

Definitions:

a = Capillary Length = 0.125 in (diameter of Seal): a = 0.125 x 2.54 = 0.3175 cm

Pd = Downstream Pressure = 1 atm

P_U = Upstream Pressure = 15 psig = (15/14.7) + 1 atm = 2.02 atm

Pa = Average Stream Pressure = $\frac{1.0 + 2.02}{2} = 1.51$ atm.

T = Fluid Temperature, K = 298 K (assume T=Ts = 298 K)

μ = viscosity of air at 298 K = 0.0185 cP (Handbook of Chemistry and Physics)

M = 29 g/mol (Air)

Ro = Universal Gas Constant = 8.31 x 107 erg/g mol·K

Equation B.5 of ANSI N14.5-1997 gives the volume leakage rate at the upstream pressure as:

$$L_T = (F_c + F_m) \times (P_u - P_d) \times (P_a / P_u) \text{ cm}^3/\text{s}$$

where

$$F_c = \lfloor 2.49 \times 10^6 \times D^4 \rfloor / (a \times \mu) \text{ cm}^3/\text{atm-sec}$$

and

$$F_m = \lfloor 3.81 \times 10^3 \times D^3 (T/M)^{0.5} \rfloor / (a \times P_a) \text{ cm}^3/\text{atm-sec}$$

are the continuum flow and molecular flow conductance respectively (equations B.3 and B.4 in ANSI N14.5-1997) and D is the diameter of the capillary.

Using trial and error and the values for the parameters given above with equations B.3 and B.4 and B.5 of ANSI N14.5-1997, the hole size to leak at a rate of $1x10^{-3}$ std air cm^3/s at upstream pressure (pressure drop leak test conditions) is found to be

$D = 1.311x10^{-3}$ cm (13.11 μm).

Test: For $D = 1.311x10^{-3}$ yields $Fc = 1.254x10^{-3}$, $Fm = 5.745x10^{-5}$ and $L_T = ([1.254x10^{-3}]+[5.745x10^{-5}] \times (2.02-1) \times (1.51/2.02) = 1 \times 10^{-3}$ cm^3/s.

Using this diameter and plugging in the values for normal operating conditions

T = 150 °F = 339 K (65.6 °C)

P_u = 25 psia = 25 psia / 14.7 psi/atm = 1.7 atm

P_d = 3.5 psia = 3.5 psia / 14.7 psi/atm = 0.238 atm

P_a = (1.7 +0.238)/2 = 0.969 atm

μ = 0.0204 cP ; (Interpolated from Handbook of Chemistry and Physics by using values at 74 °C and 54 °C:

$$\mu_{(65.6°C)} = 195.8+\left[\frac{65.6-54}{74-54}\right]\times(210.2-195.8) = 204.15\,\mu P = 0.0204\ cP.$$

$$F_c = \lfloor 2.49\times10^6\times D^4 \rfloor / (a\times\mu)\ \ cm^3/atm\text{-}s$$

$$F_c = \lfloor 2.49\times10^6\times(0.001311)^4 \rfloor / (0.3175\times0.0204)\ \ cm^3/atm\text{-}s$$

$Fc = 1.136x10^{-3}$ cm^3/atm-s

$$F_m = \lfloor 3.81\times10^3\times D^3(T/M)^{0.5} \rfloor / (a\times P_a)\ \ cm^3/atm\text{-}s$$

$$F_m = \lfloor 3.81\times10^3\times(0.001311)^3(339/29)^{0.5} \rfloor / (0.3175\times0.969)\ \ cm^3/atm\text{-}s$$

$Fm = 9.54x10^{-5}$

$$L_{N,MAX} = (1.136\times10^{-3}+9.54\times10^{-5})\times(1.7-0.238)\times(0.969/1.7)\ \ cm^3/s$$

$L_{N,MAX} = 1.026x10^{-3}$ cm^3/s

This leakage corresponds to a R_N release of aerosol powder.

$R_N = L_{N,MAX} \times C_N$

$= 1.026 \times 10^{-3}$ cm^3/sx 0.88 x 4.32 x 10^{-11} Ci/cc (0.88 is weight fraction of U in UO_2)
$= 3.9 \times 10^{-14}$ Ci/s
$= 1.4 \times 10^{-10}$ Ci/Hr

The maximum releasable value per 10CFR71.51 of 2.7×10^{-8} Ci/Hr exceeds the above value. Thus, the Pathfinder Canister meets the requirements of 10CFR71.51

4.2.3 CONTAINMENT CRITERIA FOR PATHFINDER CANISTER

A pressure drop leak test of the inter-seals annulus is performed at room temperature and with a canister cavity test pressure of 15 psig. The maximum leakage criteria is 1×10^{-3} cm^3/s. This ensures that the Pathfinder Canister provides containment.

4.3 CONTAINMENT REQUIREMENTS FOR HYPOTHETICAL ACCIDENT CONDITIONS

BW 17x17 Fuel

The nature of the contained radioactive material and the integrity of the fuel rod cladding and containment box are such that there will be no substantial release of radioactivity under hypothetical accident conditions. Before and after container testing, the fuel rods were helium leak tested. Before testing, no indications of a leak rate greater than 3×10^{-8} atm cm^3/s(10 CFR 71.51(a)(1)) were discovered. After testing, no indications of a leak rate greater than the limit specified in 10 CFR 71.51(a)(2). 10 CFR 71.51(a)(2) states that after hypothetical accident testing, no escape of radioactive material exceeding a total amount A2 in 1 week; a typical A2 quantity for this material is 5.4 kg UO_2. Using very conservative assumptions (UO_2 leaking at the same rate of helium and a density of 1gm/cm^3) the allowable leak rate would be approximately 1×10^{-2} cm^3 UO_2/s.

Pathfinder Canister

Chapter 2 demonstrates structural integrity of the Pathfinder Canister. The containment seal material was selected for its performance in the range of temperature including normal and hypothetical accident conditions. Thus, the canister meets 10CFR71 containment requirements under hypothetical accident conditions.

4.3.1 PATHFINDER FUEL FISSION GAS PRODUCTS

The Pathfinder fuel has never been irradiated. Thus there are no fission gas products in this fuel.

4.3.2 CONTAINMENT OF RADIOACTIVE MATERIAL FOR PATHFINDER CANISTER

The Pathfinder Canister meets 10CFR71.51 containment requirements under hypothetical accident conditions. This regulation imposes a release limit of A_2 Ci per week. A_2 is 0.027 for Pathfinder type fuel.

The maximum pressure in the canister during hypothetical accident conditions is 51.6 psia (3.51 atm). The outside pressure is the atmospheric pressure (1 atm). The maximum temperature is 800 °F.

The hypothetical accident condition uses the same calculation performed in Section 4.2.2 to calculate the leakage.

T = 800 °F = 700 K (427 °C)

P_u = 51.6 psia = 51.6 psia / 14.7 psi/atm = 3.51 atm

P_d = 14.7 psia = 1 atm

P_a = (3.51 +1)/2 = 2.255 atm

μ = 0.0344 cP ; (Interpolated from Handbook of Chemistry and Physics by using values at 466 °C and 409 °C)

$$\mu_{(427°C)} = 341.3 + \left[\frac{427-409}{466-409}\right] \times (350.1-341.3) = 344.079\,\mu P = 0.0344\ cP.$$

$$F_c = \lfloor 2.49\times10^6 \times D^4 \rfloor / (a \times \mu)\ \text{cm}^3\text{/atm-s}$$

$$F_c = \lfloor 2.49\times10^6 \times (0.001311)^4 \rfloor / (0.3175\times0.0344)\ \text{cm}^3\text{/atm-s}$$

$F_c = 6.735\text{x}10^{-4}$ cm^3/atm-s

$$F_m = \lfloor 3.81\times10^3 \times D^3 (T/M)^{0.5} \rfloor / (a \times P_a)\ \text{cm}^3\text{/atm-s}$$

$$F_m = \lfloor 3.81\times10^3 \times (0.001311)^3 (700/29)^{0.5} \rfloor / (0.3175\times2.255)\ \text{cm}^3\text{/atm-s}$$

$F_m = 5.891\text{x}10^{-5}$ cm^3/atm-s

$$L_{A\,MAX} = (F_c + F_m) \times (P_u - P_d) \times (P_a / P_u)\ \text{cm}^3\text{/s}$$

$L_{A,MAX} = 1.181x10^{-3}$ cm^3/s

Thus the maximum leak rate at 800 °F temperature and 51.6 psia (internal) pressure is $1.181x10^{-3}$ cm^3/s.

This leakage corresponds to a R_A release of aerosol powder.

$R_A = L_{A, MAX} \times C_A$ ($C_A = C_N$)
$= 1.181x10^{-3}$ cm^3/sx 0.88 x 4.32 x 10^{-11} Ci/cc (0.88 is weight fraction of U in UO_2)
$= 4.49x\ 10^{-14}$ Ci/s
$= 2.72 \times 10^{-8}$ Ci/wk

The maximum releasable value per 10CFR71.51 of 0.027 Ci/wk exceeds the above value. Thus, the Pathfinder Canister meets the requirements of 10CFR71.51.

The Pathfinder Canister satisfies containment criteria for normal and hypothetical accident conditions. Section 4.2.3 defines leak test requirements for the canister seals. These tests ensure that the Pathfinder Canister meets 10CFR71.51 containment requirements.

4.4 SPECIAL REQUIREMENTS

Not applicable because WE-1 and Pathfinder Canister is not transporting Plutonium.

4.5 CALCULATION FOR PRE-SHIPMENT TEST OF SEALS

A sample calculation showing that the proposed preshipment leak test results in a sensitivity of at least $1x10^{-3}$ std cm^3/sec (Section 8.4 of ANSI N14.5 – 1997) is presented. The sketch of the experimental leak test apparatus is presented in Figure 4.5-1 and the sketch of the inter-seal region is presented in Figure 4.5-2.

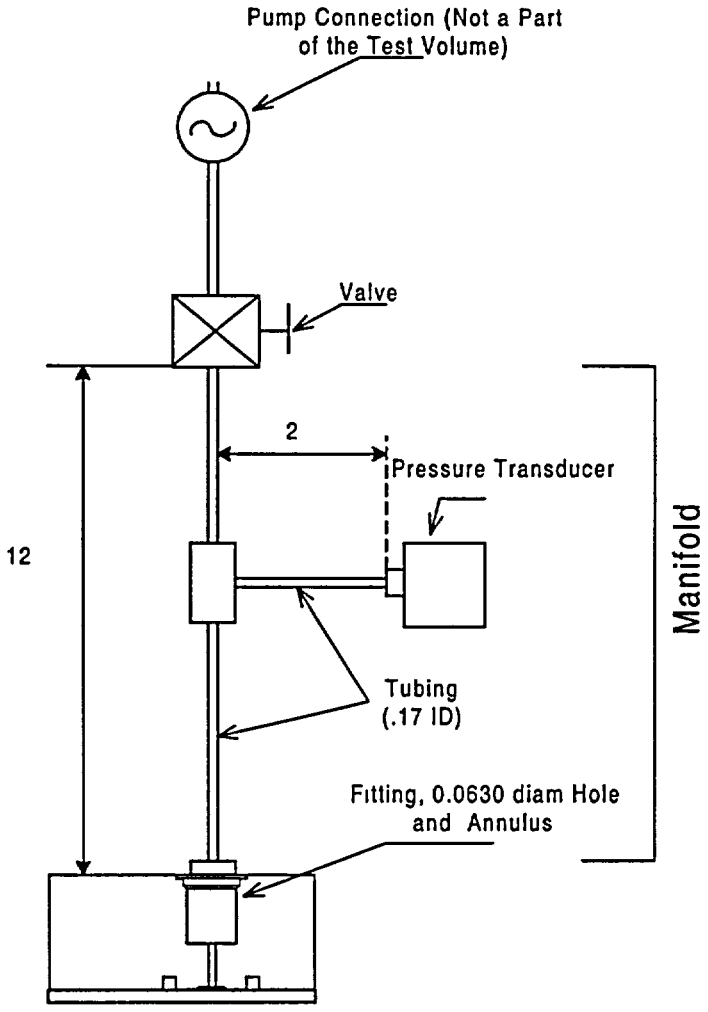

Note: Units in inches.

Figure 4.5-1 Leak Test Apparatus.

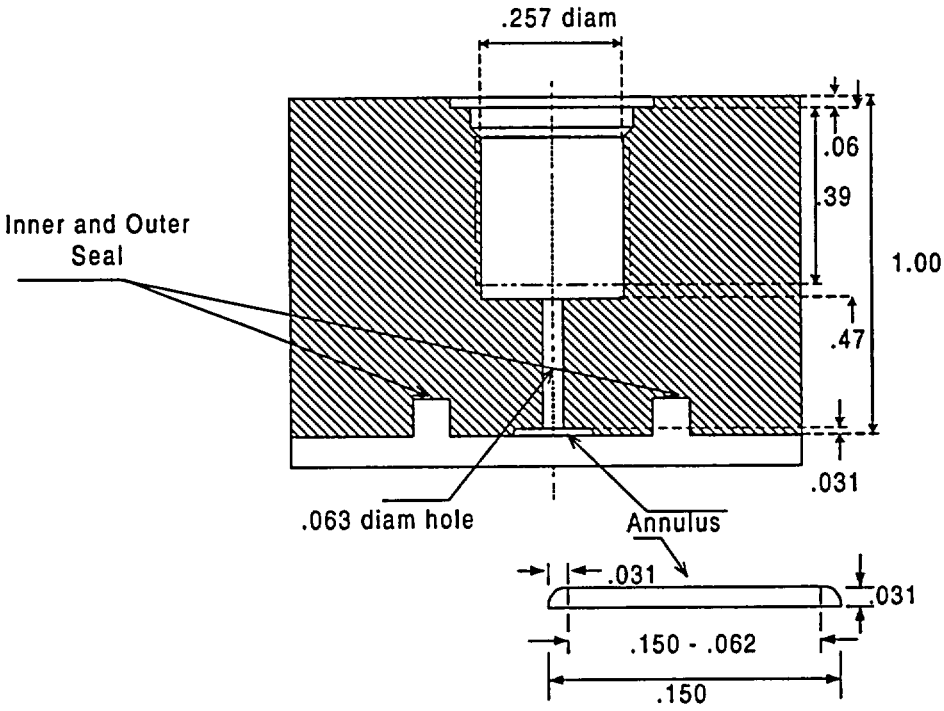

Note: Units in inches.

Figure 4.5-2 O-ring Groove and Seal Check Port Detail

The test volume is calculated for the annulus, hole, fitting, and tubing from the data shown in Figures 4.5-1 and 4.5-2. The volume of the transducer is estimated as 0.02 in^3.

ANNULUS :
Note: The annulus is around the circumference, at centerline diameter D, of the flange and located between the seals.

$$D = (9.262+9.942)/2$$
$$= 9.602 \text{ in}$$

$$A = \pi x(0.031)^2/2 + (0.031x(0.150-0.062))$$
$$= 0.00424 \text{ in}^2$$

$$V_{Annulus} = \pi xAxD$$
$$= 0.12783 \text{in}^3$$

HOLE :

$$L = 1.00-0.06-0.47-0.03$$
$$= 0.44 \text{ in}$$

$$V_{Hole} = \pi x(0.063)^2/4x0.44$$
$$= 0.00137 \text{ in}^3$$

FITTING :

$$V_{Fitting} = \pi x(0.257)^2/4x(0.47-0.39)$$
$$= 0.00415 \text{ in}^3$$

TUBING :

$$V_{Tubing} = \pi x(0.17)^2/4x(12+0.39+2)$$
$$= 0.32662 \text{ in}^3$$

TRANSDUCER (Estimated) :

$$V_{Transducer} = 0.02 \text{ in}^3$$

TOTAL VOLUME :

$$V_{Total} = V_{Annulus}+V_{Hole}+V_{Fitting}+V_{Tubing}+V_{Transducer}$$
$$V_{Total} = 0.12783 + 0.00137 + 0.00415 +0.32662 + 0.02$$
$$= 0.48 \text{ in}^3$$

Equation B.14 of ANSI N14.5 provides the leak rate equation for a pressure drop test as:

$$L_R = \frac{V \times T_S}{3600 \times H \times P_S} \times \left(\frac{P_1}{T_1} - \frac{P_2}{T_2} \right) \text{ cm}^3/\text{s}$$

where
H = time (hours)
P_S = Standard Pressure = 1 atm abs = 760000 μm Hg (1 μm Hg = $1x10^{-6}$ m Hg)
P_1 = Pressure (μm Hg) at time = 0 (start of Test)
P_2 = Pressure (μm Hg) at time = H (end of Test)
T_S = Standard Temperature (298 K)
T_1 = Temperature at time = 0 (K)
T_2 = Temperature at time = H (K)
V = Test Volume (cm^3)

The total volume calculated above need to be expressed in cm^3:

$V = 0.48\ in^3 \times (2.54\ cm/in)^3 = 7.866\ cm^3$

Let $H = t_s/3600$ where t_s is the time in seconds

$$L_R = \frac{V \times T_S}{t_S \times P_S} \times \left(\frac{P_1}{T_1} - \frac{P_2}{T_2} \right)$$ if $T_1 = T_2 = T_S$ we obtain by replacing V and P_s by above values:

$$L_R = \frac{7.866}{760000} \times \left(\frac{P_1 - P_2}{t_S} \right) cm^3/s$$

Thus the leak rate equation for pressure drop test is:

$$L_R = 1.035 \times 10^{-5} \times \left(\frac{P_1 - P_2}{t_S} \right) cm^3/s$$ with P_2 and P_1 in μm Hg.

Pressure drop in 10 minute for 12-in long tube

The pressure drop for a test of 10 minute duration and a leak rate of $1x10^{-3}$ cm^3/s for a tube length of 12 in is found by trial to be $5.8x10^4$ μm Hg or

$(5.8x10^4\ \mu m\ Hg)x(1.934x10^{-5} psi/\mu m\ Hg) = 1.12$ psi.

Test : Plug $(P_1-P_2) = 5.8x10^4$ μm Hg and t_s=600 s into above equation for L_R

$L_R=1.035x10^{-5}x(5.8x10^4/600) = 1x10^{-3}\ cm^3/s$

Pressure drop in 10 minute for 18-in long tube

A similar calculation could be performed for a test apparatus with a 18-in long tube connected to the leak test port:

$$V_{tubing} = \left(\frac{\pi \cdot 0.17^2}{4} \right) \cdot (18 + .39 + 2) in^3 = 0.46281\ in^3$$

Volume of tubing for a 12-inch long tube was calculated above = 0.32662 in^3. Thus difference = 0.46281 –0.32662 = 0.13619 in^3

Difference (in cm^3) = $(0.13619\ in^3)x(2.54\ cm/in)^3 = 2.23175\ cm^3$

Thus pressure drop equation for test apparatus with 18-in long tube becomes

$$L_R = \left(\frac{(7.866 + 2.23175)}{760000}\right) \times \left(\frac{P_1 - P_2}{t_S}\right) \text{ cm}^3/\text{s}$$

$$L_R = 1.329 \times 10^{-5} \times \left(\frac{P_1 - P_2}{t_S}\right) \text{cm}^3/\text{s}$$

The pressure drop for a test of 10 minute duration and a leak rate of 1×10^{-3} cm^3/s for a tube length of 18 in is found by trial to be 4.51×10^4 µm Hg. or

$(4.51 \times 10^4$ µm Hg)x$(1.934 \times 10^{-5}$psi/µm Hg) = 0.87 psi.

Test : Plug $(P_1\text{-}P_2) = 4.51 \times 10^4$ µm Hg and t_s=600 s into equation for L_R (18-in long tube)

$L_R = 1.329 \times 10^{-5} \times (4.51 \times 10^4/600) = 1 \times 10^{-3}$ cm^3/s

Based on the above results both variants of the test have an adequate sensitivity for determining a leak rate of 1×10^{-3} std cm^3/s

4.6 REFERENCES

Metal O-Rings, page 2 and 4; Garlock Helicoflex High Performance Seals and Sealing Systems; POB 9889; Columbia, SC 29290. Phone # 803-783-1880.

ANSI N14.5 – 1997, American National Standard for Radioactive Materials – Leakage Tests on Packages for Shipment.

Handbook of Chemistry and Physics, 60th Edition, Chemical Rubber Publishing Company, 1960.

NUREG/CR-6487, Containment Analysis for Type B Packages Used to Transport Various Contents. November 1996.

Table 6-1a
WE-1 KENO V.a Results

Condition	Model Configuration	K_{max}
Normal Single Package	Single package with a close 12" water reflector	0.156
Single Flooded	Single flooded package with a close 12" water reflector	0.943
Accident	Same as 'Single Flooded' condition	0.943

Table 6-1b
Pathfinder KENO V.a Results

Condition	Model Configuration	k_{max}
Transport	3 undamaged WE-1 packages with a close 12" reflector	0.257
Accident	single damaged package, fully flooded with a close 12" water reflector, 48 assemblies close pack	0.691
Accident	single damaged package, fully flooded with 12" water reflector, 40 assemblies optimally arranged	0.705
Accident	48 assemblies at optimal spacing, 12" water reflector (note: exceeds inner package dimensions)	0.821

The shipment of 48 Pathfinder fuel assemblies will entail shipping a smaller amount of fissile material than for the currently licensed MkBW 17x17. The current license for the WE-1 package enables shipment of up to 22.14 kg of ^{235}U in zircaloy cladding. A full shipment of 48 Pathfinder fuel assemblies will have a maximum loading of 8.1 kg of ^{235}U, well below the amount currently licensed. The cladding is Incoloy 800, a material with neutronic properties very similar to those of stainless steel, and thus with a greater neutron absorption capability than zircaloy. The Pathfinder assemblies sit inside a stainless steel cylindrical inner canister (Pathfinder Canister) with a nominal ID of 8 inches.

Table 6-2b
Pathfinder Fuel Assembly
Fuel Assembly Description

	Fabrication Specifications	**KENO Values**
Element Configuration	7-rod Cluster	7-rod Cluster
Fuel Rods	6	6
Absorber Rod	1	1 (water-filled row, no pellets or wire)
Overall element length	82.55 in. 209.68 cm	182.88 cm, Fuel only 30 cm of water at both ends
Envelope diameter	0.805 in. 2.045 cm	N/A
Fuel	Sintered UO_2 Pellet	UO_2 Pellet
UO_2 enrichment	6.95 wt% ^{235}U (415) 7.50 wt% ^{235}U (2)	7.51 wt% ^{235}U
Loading per element	2.206 kg U	2.228 kg U
UO_2 density	10.50 g/cm^3	10.61 g/cm^3
UO_2 pellet diameter	0.207 ± 0.0005 in. 0.5258 ± 0.001 cm	0.5258 cm
UO_2 pellet length	0.207 to 0.414 in. 0.526 to 1.052 cm	N/A
Active fuel length	72.0 ± 0.125 in. 182.88 ± 0.318 cm	182.88 cm
Cladding of Fuel and Absorber Rods	Free Standing Tube	Free Standing Tube
Material	Incoloy 800, mill annealed	Incoloy 800
Outside diameter	0.247 ± 0.001 in. 0.6274 ± 0.0025 cm	0.6274 cm
Inside diameter	0.211 ± 0.001 in. 0.536 ± 0.0025 cm	0.536 cm
Wall thickness	0.018 in. 0.046 cm	See OD and ID
Center-to-Center Pitch	0.289 in. 0.7341 cm	0.7341 cm

Table 6-2b (Continued)

	Fabrication Specifications	KENO Values
Poison (Absorber)	Boron-Stainless Steel Wire	N/A
Loading per element	0.978 g natural boron	N/A
Wire diameter	0.105 in. 0.267 cm	N/A
Spacer	Sintered AL_2O_3 Pellets	N/A
Spacing Arrangement	Spiral Wire, 3 per Fuel Rod	N/A
Wire diameter	0.042 in. 0.107 cm	N/A
Spiral pitch	6 in. 15.24 cm	N/A
Wire Material	Incoloy 800, mill annealed	N/A
Fission Gas Plenum Length	3 in. 7.62 cm	N/A
Sheath	Free Standing Tube	Free Standing Tube
Sheath material	Incoloy, stainless steel or inconel alloy	Incoloy (base cases) Varied (Table 6-15)
Sleeve ID	0.945 in. 2.400 cm	2.4004 cm
Sleeve OD	1.00 in. 2.54 cm	2.54 cm

Note: N/A = Not modeled for conservatism

6.3 MODEL SPECIFICATIONS

The analysis was made with the CSAS routine of the SCALE 4.2 code package[1] for the B&W MkBW 17x17, and SCALE4.4a for the Pathfinder fuel assemblies The package k_{eff} was calculated with KENO V.a using the 44-group cross section set from SCALE4.3[2] for the B&W MkBW 17x17, and using the 238-group cross section set from SCALE 4.4a for the Pathfinder fuel The detailed model of the fuel assembly and shipping container, as well as the regional number densities, are described is this section for both types of fuel.

6.3.1 Description of Calculational Model

The calculation models for the WE-1 package are described in this section. Listings of the input files for the licensing results presented in Table 6-1a and Table 6-1b are contained in Appendix 6-1.

6.3.1.1 Fuel Assembly

A. B&W MkBW 17x17

One B&W MkBW 17x17 fuel assembly can be shipped in the WE-1 package without the need for neutron absorber plates. The dimensions of the B&W assembly are listed in Table 6-3. The model values for the fuel provide an optimum fuel configuration, since 1) the fuel pellet diameter is maximized; 2) the Zr-4 tube dimensions provide a

Figure 6-1b
Pathfinder Fuel Assembly Configuration

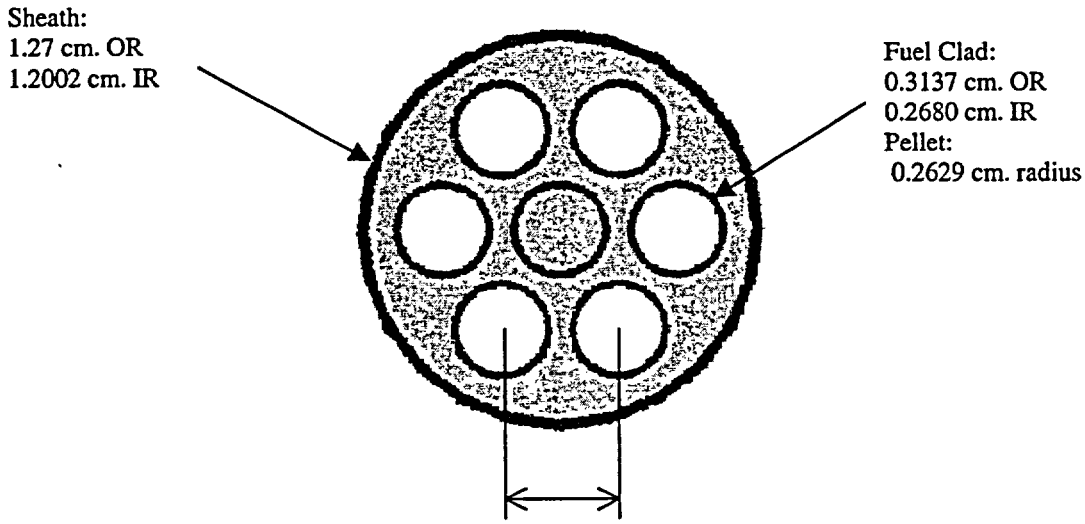

The array of 48 assemblies in a close pack triangular pitch arrangement is shown in Figure 6-2a. This array was chosen because it provides for the maximum number of assemblies that can physically fit inside an 8-inch ID Pathfinder Canister. The KENO-V.a model for the Pathfinder assemblies did not include the Pathfinder Canister or any other structural material of the WE-1 for conservatism.

B. Pathfinder Fuel Assemblies

Three WE-1 packages were assumed to be stacked in the same configuration as shown in Figure 6-6. Forty-eight Pathfinder fuel assemblies were placed inside each package. The interior of the packages were dry, but the entire configuration was surrounded by a full water reflector. The Pathfinder Canister and inner container were not explicitly included in the model.

The k_{eff} calculated by KENO-V.a for this is 0.25620 $\pm$ 0.00050. Based upon this evaluation, an array on three normal packages closely surrounded with water satisfies the criticality safety criterion.

6.3.3 Material Number Densities

A. B&W MkBW 17x17

The evaluation assumes a maximum ^{235}U enrichment of 4.6 wt. The materials used in the analysis are listed in Table 6-7a. No number densities are provided for those materials for which the SCALE standard materials specification is employed. The 4.3 weight percent fuel specifications allow a comparison between a standard LWR fuel assembly and a typical slightly irradiated fuel assembly in the package.

Table 6-7a
KENO V.a Model Material Specifications, T= 293°K

Material	KENO V.a Mat.	Density, g/cc	Weight percent or At/b-cm
Fuel (normal) ^{235}U ^{238}U	1	10.686 (0.975 TD)	 4.6 95.4
Zr (Clad)	2	default	100.0
H20	3	1.0	100.0
H20	4	1.0	100.0
H20	5	1.0	100.0
Carbonsteel	6	default	100.0
Insulation (50% Al_2O_3/50% SiO_2) Al Si O	7	0.12816 (8 lbs/cu ft)	 7.5696E-04 6.4231E-04 2.4201E-03
Insulation (50% Al_2O_3/50% SiO_2) Al Si O	8	0.09612 (6 lbs/cu ft)	 5.6772E-04 4.8173E-04 1.8150E-03
Additional Fuel Compositions for Standard/Slightly-Irradiated Fuel Comparison			
Fuel (4.385 weight percent Irradiated) ^{234}U ^{236}U ^{235}U ^{235}U	1	10.686 (0.975 TD)	 0.09 4.385 1.34 94.185
Fuel (normal) ^{235}U ^{235}U	1	10.686 (0.975 TD)	 4.385 95.615

B. Pathfinder Fuel Assemblies

To determine the atom densities for Incoloy 800, a manufacturing spec sheet that was considered representative of the material was obtained. This spec sheet gives the elemental ranges for manufacturing this metal. The weight percentages of each element that give the low nickel and chromium concentration (which are stronger neutron absorber than the primary element, iron) were assumed for the KENO-V.a

Table 6-9
KENO V.a Optimization Cases, 4.6 Weight percent ^{235}U Fuel

Description	k_{eff}	σ	K_{MAX}
Single Flooded, 12" H_2O Reflector w. Insulation	0.80817	0.00078	0.81720
Off-Centered Assembly in Inner Container	0.90076	0.00075	0.90977
0.01% Dense Water in Package	0.14761	0.00024	0.15643
5.0% Dense Water in Package	0.18187	0.00030	0.19070
10.0% Dense Water in Package	0.25077	0.00043	0.25964
Single flooded with 1-1/8" Plate Thickness	0.93416	0.00079	0.94320
Single flooded with 7/8" Plate Thickness	0.93340	0.00076	0.94242

B. Pathfinder Fuel Assemblies

KENO-V.a was used to model the shipment of the Pathfinder fuel under various normal and accident conditions. The purposes of these cases were to:

1. Determine the spacing between the assemblies that gives the maximum k_{eff} at full water moderation and reflection.
2. Determine the effect of varying moderator density from 0 g/cc to 1 g/cc, and to examine partially flooded situations.
3. Determine k_{eff} of 48 assemblies at optimal moderation and spacing
4. Determine k_{eff} for situations with fewer than 48 assemblies in the canister
5. Determine k_{eff} of 3 WE-1 packages under normal transportation conditions and full water reflection per 10CFR71.51a.

Cases were run where the spacing between the Pathfinder assemblies was varied to determine the spacing that gave the optimal moderation. Distances between adjacent assemblies varying from 0.001 inches (a small gap to prevent adjacent assembly surfaces from overlapping in KENO-Va) to 0.75 inches (distance between clad at their closest) were modeled. The results of this analysis are shown in Table 6-10 and Figure 6-7. It is seen in Figure 6-7 that the optimal spacing occurs at about 0.5 inches.

Table 6-10
Effect of Assembly Spacing on k_{eff}

Spacing (inches)	k_{eff}	σ
0.001	0.68898	0.00078
0.25	0.79041	0.00092
0.4	0.81562	0.00082
0.5	0.81966	0.00080
0.6	0.81933	0.00083
0.75	0.80344	0.00083

Figure 6-8 Optimal Moderation for 48 Pathfinder Assemblies

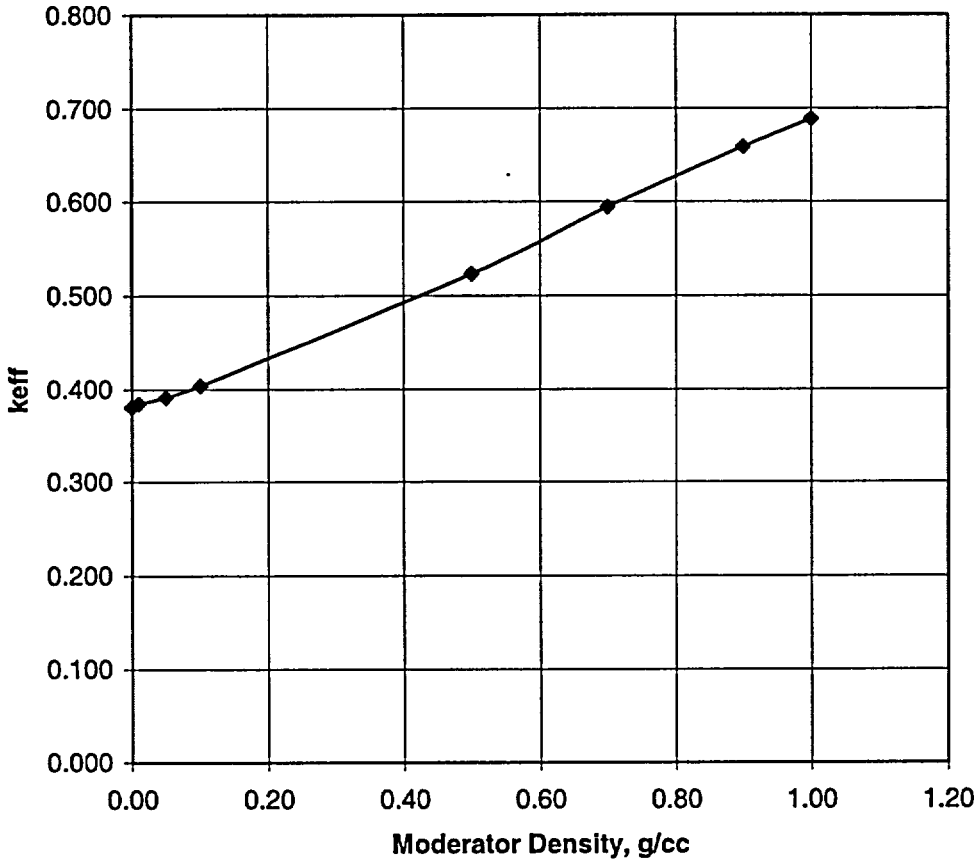

Calculations show that a fully loaded inner canister (48 assemblies) would be less than optimally moderated. KENO-V.a cases were run with 44, 40 and 36 assemblies in the canister to increase the moderator to fissile material ratio. Assemblies were removed from the model to create situations where more assemblies would be located next to water holes, and hence experience enhanced moderation.

For the 44-assembly case, assemblies in the following locations were removed (refer to Figure 6-2a, where rows are counted from the top, and locations are counted from the left most assembly):

row 4, locations 3 and 5
row 6, locations 3 and 5
For the 40 assembly case, assemblies in the following additional locations were removed:
row 2, location 3
row 5, locations 2 and 7
row 8, location 3

The preferred dunnage material for less than full loads is wood. Wood is a hydrogenous material with an overall lower density than water, and with a much lower hydrogen concentration. It is seen by the previously discussed analysis that the Pathfinder container is under-moderated, and that it achieves maximum reactivity at fully flooded conditions. The addition of wood would have the effect of decreasing the total hydrogen concentration in the container, by displacing water in the fully flooded. It can be inferred that wood would have less of an impact on reactivity than the comparable fully flooded condition. Wood then is an acceptable material with respect to criticality concerns.

Models were created that simulated situations where a flooding accident occurred and the fuel remained in the Pathfinder Canister, but part of the Incoloy 800 was released. Since Incoloy 800 is a neutron absorber, its presence acts to hold down reactivity. These cases were run to determine how much Incoloy 800 could be lost from the Pathfinder Canister, with system remaining subcritical.

The model used here blended all fuel assembly and sheath components homogeneously in the Pathfinder Canister. Fuel accounts for 16.4% of the volume and Incoloy 800 accounts for 21.7% of the volume. The remainder of the Pathfinder Canister volume (61.9%) is filled with water. A series of cases were run that maintained the fuel volume, but decreased the amount of Incoloy 800 and replaced it with water. A 30cm water reflector surrounded the entire canister.

The results are shown in Table 6-14 and Figure 6-10. It is seen that even with 80% of the Incoloy 800 lost from the package, criticality limits are still met.

Table 6-14
Effect of Loss of Incoloy 800

%Incoloy 800 Loss	k_{eff}	σ
0	0.68008	0.00073
20	0.72553	0.00073
40	0.77347	0.00078
50	0.79915	0.00084
60	0.82533	0.00082
80	0.88175	0.00090
100	0.93981	0.00099

The data shows that the fuel is more reactive when it is intact and optimally moderated, than when the assemblies do not remain intact and when the pellets are allowed to move freely in the container. This is demonstrated by comparing the calculated k_{eff} for the homogeneous case, with no Incoloy removed (0.68008 $\pm$ 0.00073), from Table 6-14, to that for the comparable heterogeneous case (0.68898 $\pm$ 0.00078), from Table 6-10. Even when half of the Incoloy clad material is removed from the canister, k_{eff} is less than when the assemblies are allowed to spread apart into an optimally moderated configuration. As such, the worst case situation for criticality is when the fuel remains intact, and is allowed to spread apart rather than collapse together. This is clearly demonstrated by comparing the k_{eff} values presented in Table 6-10 with those presented in Table 6-14.

enrichments and conditions. The third is a set of twelve mixed oxide criticals[7]. The last set comprises eight other UO_2 critical configurations that have been approved for an international database[8]. This last set includes results from the MCNP Monte Carlo code[9] and KENO V.a with the 27-group cross section set. These latter calculations provide an independent verification of the results and trends for the 44-group KENO V.a results.

The number of benchmark experiments used and, more specifically, the range of applicability of the benchmark experiments chosen for the evaluation may be questioned. Basically, the evaluation of the complete set of 51 criticals shows essentially no sensitivity relative to fuel enrichment or fuel type, i.e. uranium oxide or mixed oxide. The mixed oxide critical results from PNL experiments (cases 1 through 8 of Table 6-2.8 of Attachment 6-2) show little sensitivity to the type of material inserted between fuel assemblies, other than to suggest a trend of smaller bias with heavier absorber loading. The Boral and stainless steel plates have a bias that is equal to the bias without a plate within statistical uncertainty, i.e. 2 sigma. The cadmium and Boraflex plates with significantly more absorber show a significant reduction in bias. The B&W critical experiments listed in Table 6-2.3 of Attachment 6-2 further illustrate this trend. These experiments were performed specifically for evaluation of fuel storage arrays and form the primary basis for the determination of the 44-group cross section bias. Figure 6-2.5 of Attachment 6-2, provides a plot of the calculation bias as a function of fuel assembly spacing for the various configurations of the 21 criticals. The data suggests a trend of increasing bias with increasing spacing between assemblies for the range of spacings considered, i.e., 0 to 6.5 cm. This trend is independent of the material between the assemblies. This trend is further confirmed by the data in Table 6-2.10 that extend the spacing by use of additional experiments approved by the *International Handbook of Evaluated Criticality Safety Benchmark Experiments*. This trend is seen from both KENOV.a and MCNP calculations with completely different cross section sets. However, at present only experiments for water between assemblies are available in the Handbook. Thus, extension of the evaluations beyond the spacing and materials of the B&W critical experimental data is not yet possible.

B. Pathfinder Fuel Assemblies

This licensing evaluation was performed to support shipping ~6.95wt% to ~7.5 wt% fuel rods. In support of this effort, a validation of SCALE, i.e., KENO-V.a with the CSAS modules, was performed following the guidelines of NUREG/CR-6361. A review of the *International Handbook of Evaluated Criticality Safety Benchmark Experiments* was made and indicated several sets of experiments consisting of fuel rod arrays with enrichments between 5 and 10 wt% ^{235}U. Most of the experiments comprised hex arrays of fuel rods, although a few had square pitches. A range of H/X was represented, as were both square and triangular pitch lattice shapes. Cladding materials included stainless steel, zirconium, and aluminum. None of the experiments

had dissolved absorber material or used strong absorbers in the fuel pins or as separate rods. The experiments were at or near room temperature, except for a set of pressurized rods that ranged from 20 to 274 °C.

Forty-three experiments were selected as most appropriate for this evaluation. A description of the significant trending parameters and calculated results of the benchmark evaluation is provided in Appendix 6-2.

The benchmark evaluation provides a series of equations relating a trending parameter with the calculated k_{eff} of the benchmark. Evaluation of these equations for the range of parameters of the Pathfinder fuel within the shipping package provides the specific Upper Safety Limit (USL) to be used for this licensing evaluation. Table 6-16 lists the trending parameters for the three single package bounding conditions with the calculated USL for each parameter. The limiting USL is that derived from trending with the pitch and has a value of 0.9359. This value, 0.936, will be defined as the USL for the Pathfinder fuel licensing evaluation.

Table 6-16
Pathfinder Trending Parameter and Calculated USL Values

Parameter	48 Flooded		48 Optimum		Homogeneous	
	Value	USL	Value	USL	Value	USL
Pitch, cm						
Rod	**0.7341**	**0.9359**	**0.7341**	**0.9359**	-	-
Cell	2.5426	0.9383	3.8126	0.9383	-	-
ECF, eV	0.306251	0.9368	0.105085	0.9378	0.104816	0.9378
Enrichment, wt%	7.51	0.9377	7.51	0.9377	7.51	0.9377
H20/fuel	2.268036	0.9365	4.951	0.9378	-	-
AFG, group	195.1	0.9364	208.6	0.9380	207.3	0.9380
H/U	160.8	0.9373	289.7	0.9383	189.2	0.9376
Temperature, °C	20	0.9369	20	0.9369	20	0.9369
Minimum		**0.9359**		**0.9359**		**0.9369**